This item was submitted to Loughborough's Research Repository by the author.
Items in Figshare are protected by copyright, with all rights reserved, unless otherwise indicated.

Ion erosion in surface analysis

PLEASE CITE THE PUBLISHED VERSION

PUBLISHER

© S. Duncan

PUBLISHER STATEMENT

This work is made available according to the conditions of the Creative Commons Attribution-NonCommercial-NoDerivatives 2.5 Generic (CC BY-NC-ND 2.5) licence. Full details of this licence are available at: http://creativecommons.org/licenses/by-nc-nd/2.5/

LICENCE

CC BY-NC-ND 2.5

REPOSITORY RECORD

Duncan, S.. 2019. “Ion Erosion in Surface Analysis”. figshare. https://hdl.handle.net/2134/28023.

Loughborough University

This item was submitted to Loughborough University as a PhD thesis by the author and is made available in the Institutional Repository (https://dspace.lboro.ac.uk/) under the following Creative Commons Licence conditions.

creative commons

COMMONS DEED

Attribution-NonCommercial-NoDerivs 2.5

You are free:

- to copy, distribute, display, and perform the work

Under the following conditions:

Attribution. You must attribute the work in the manner specified by the author or licensor.

Noncommercial. You may not use this work for commercial purposes.

No Derivative Works. You may not alter, transform, or build upon this work.

- For any reuse or distribution, you must make clear to others the license terms of this work.
- Any of these conditions can be waived if you get permission from the copyright holder.

Your fair use and other rights are in no way affected by the above.

This is a human-readable summary of the Legal Code (the full license).

Disclaimer

For the full text of this licence, please go to:
http://creativecommons.org/licenses/by-nc-nd/2.5/

LOUGHBOROUGH
UNIVERSITY OF TECHNOLOGY
LIBRARY

AUTHOR/FILING TITLE
DUNCAN, S

ACCESSION/COPY NO.
010537/01

VOL. NO.

CLASS MARK
T

LOAN COPY

15 NOV 1999
13 DEC 1999
21 JAN 2000
18 FEB 2000
17 MAR 2000
31 MAR 2000
14 APR 2000
12 MAY 2000

001 0537 01

ION EROSION IN SURFACE ANALYSIS

by

S. Duncan, B.Sc.

A Doctoral Thesis submitted in partial fulfilment of the requirements for the award of Doctor of Philosophy of the Loughborough University of Technology.

© S. Duncan (1985)

Loughborough University
of Technology Library
Date June '86
Class T
Acc. No. 010537/01

CONTENTS

		Page No.
ACKNOWLEDGEMENTS		(i)
ABSTRACT		(ii)
CHAPTER 1		
INTRODUCTION		(iii)
CHAPTER 2		
2.1	Thin Film Technology	1
2.2	Depth Resolution in Sputter - Depth profiling of Thin Films	6
2.3	Depth Resolution Studies of Thin Films	14
2.3.1	Experimental	14
2.3.2	Results and Discussion	16
2.4	Conclusions	21
CHAPTER 3		
3.1	A General Theory on the Dependence of Depth Resolution on Ion and Electron Beam Geometry	
3.1.1	Introduction	24
3.1.2	The Model	29
3.1.3	Computation Results	37
3.1.4	Experimental Observations	42
3.1.5	Discussion	44
CHAPTER 4		
4.1	Ion Etching of Solid Surfaces	
4.1.1	The Physical Mechanisms of Ion Sputtering	47
4.2	The Sputtering Yield	
4.2.1	Theory	50
4.2.2	Variation of the Sputtering Yield	53
4.2.2.1	Target Material	53
4.2.2.2	Ion Species	55
4.2.2.3	Incident Ion Angle	57
4.3	The Sputtering Yield of Single Crystal Materials	
4.3.1	Physical Concepts	59
4.3.2	The Focuson Theory	62

CONTENTS

		Page No.
4.4	**Other Related Bulk and Surface Effects**	67
4.4.1	Recoil Implantation and Atomic Mixing	70
4.4.2	Temperature Effects in Sputtering	71
4.5	**The Sputtering of Alloys**	73
CHAPTER 5		
5.1	**The Development of Surfrace Topography Under Ion Erosion**	
5.1.1	Introduction	75
5.1.2	Cone Development by Particulate Contamination	77
5.1.3	Cone Development by Ion Induced Defects	82
5.1.4	The Influence of Surface Orientation and Structure on Sputtering Yield	87
5.2	**Ion Induced Morphology on Semiconductors**	
5.2.1	Cone and Pit Development	93
5.2.2	Development of Surface Faceting	98
5.3	**Sputtering Effects Using Reactive Gases**	103
5.4	**The Use of Active Gases in Surface Analysis**	108
5.5	**The Development of Surface Topography Following Active Gas Bombardment**	112
5.5.1	Experimental Method	114
5.5.2	Results (Semiconductors)	
5.5.2.1	Silicon - 5.5KeV Oxygen Ion Bombardment	116
5.5.2.2	Silicon - 10KeV Oxygen Ion Bombardment	117
5.5.2.3	Silicon - Oxygen Bombardment with No Sample Bias	119
5.5.2.4	Silicon - 5.5KeV Caesium Ion Bombardment	120
5.5.2.5	Gallium Arsenide - 5.5KeV Oxygen Ion Bombardment	121

CONTENTS

			Page No.
	5.5.2.6	Gallium Arsenide - 10KeV Oxygen Ion Bombardment	121
	5.5.2.7	Gallium Arsenide - Oxygen Bombardment with No Sample Bias	122
	5.5.2.8	Gallium Arsenide - 5.5KeV Caesium Ion Bombardment	123
	5.5.2.9	Indium Phosphide - 5.5KeV Oxygen Ion Bombardment	124
	5.5.2.10	Indium Phosphide - 10.5KeV Oxygen Ion Bombardment	125
	5.5.2.11	Indium Phosphide - Oxygen Bombardment with No Sample Bias	126
	5.5.2.12	Indium Phosphide - 5.5KeV Caesium Ion Bombardment	127
5.5.3	Discussion		129
	5.5.3.1	Oxygen Ion Bombardment	130
	5.5.3.2	Caesium Ion Bombardment	137
5.5.4	The Development of Ion Sputter Topography on Cu (11 3 1)		138
	5.5.4.1	Experimental Conditions	139
	5.5.4.2	5.5KeV Oxygen Ion Bombardment	139
	5.5.4.3	5.5KeV Caesium Ion Bombardment	141
	5.5.4.4	Discussion	142
5.5.5	Conclusions		144

CHAPTER 6

SURFACE ROUGHNESS DURING ION ETCHING: A THEORETICAL ANALYSIS

6.1	The Development of Surface Shape	148
6.2	The Influence of Surface Roughness on Depth Resolution in Surface Analysis	158

CONTENTS

			Page No.
6.3	**The Measurement of Surface Roughness Applied to Erosion Theory**		163
	6.3.1	The Model	164
	6.3.2	Computer Simulation	167
	6.3.3	Results	
		6.3.3.1 Surface Roughness of an Homogeneous Bulk Under Ion Erosion	169
		6.3.3.2 Surface Roughness of an Inhomogeneous Bulk Under Ion Erosion	172
		6.3.3.3 Discussion	175
		6.3.3.4 Conclusions	177
CONCLUSIONS			179
REFERENCES			185

ACKNOWLEDGEMENTS

There are several people to whom I would like to express my gratitude for their help in the completion of this thesis.

My thanks go to Dr Roy Blunt (Plessey Research, Caswell), Professor George Carter (University of Salford) and Professor Jim Whitton (University of Copenhagen) for supplying the semiconductor materials and the copper; Ken Topley (Loughborough University) and Leading Airman (Phot.) Clive Deer (Photographic Section, HMS Warrior, Northwood) for their excellent reproduction of SEM micrographs; the Graphics Department at the Plessey Research Centre, Caswell, for reproducing graphs and diagrams.

I would also like to express my thanks to Katherine McKay and Paula Bunting for the superb job they did in typing this thesis and in its final composition.

The experimental techniques involved in this work were a result of many useful discussions with the team of Loughborough Consultants Ltd, both past and present, including Dr Dave Sykes, Dave Hall, Dr Ian Sutherland, Dr Alec Christie and Pete Weedon. I would also like to thank my colleague Malcolm Tagg for helping with some, often very frustrating computer coding.

Finally, my thanks go to A.E.R.E. Harwell and S.E.R.C. for supplying funding for this work, and to my supervisors, Dr John Riviere (A.E.R.E. Harwell), Dr Mike Walls (V.G. Scientific Ltd) and Dr Roger Smith (Loughborough University) for their continual help and guidance throughout the course of this project.

ABSTRACT

Low energy ion bombardment is a process used in surface analysis and in the electronics and telecommunications industries. Techniques such as Auger Electron Spectroscopy (AES), X-ray Photoelectron Spectroscopy (XPS) and Secondary Ion Mass Spectroscopy (SIMS) employ ion bombardment for surface cleaning and for the provision of composition-depth profiles.

However, during ion bombardment or sputtering of solid surfaces the changes that occur are not fully understood, since in general successive atomic layers are not removed uniformly and hence the topography is uneven. This effect causes serious uncertainties in the depth resolution of sputter-depth profiles in surface analysis, and thus the work presented in this thesis is approached from two standpoints:

(i) To assess the depth resolution obtainable as a result of sputter-depth profiling thin film structures. A theoretical approach to optimising depth resolution in AES has been undertaken by considering the geometry of the ion and electron beams with respect to the sample surface. It is found that variations of 24% in the relative depth resolution ($\Delta z / z$) can be observed if the instrumental factors governing surface analyses are not optimised.

(ii) To compare the surface morphology induced by low energy ions (0→15KeV) on electronic materials (Si, GaAs, InP) and Cu(11 3 1), using reactive gas species (O_2^+, Cs^+). The topography generated by the bombardment species was found to be material and beam dependent. For these materials, Cs^+ suppressed growth over the same dose range as O_2^+. Mechanisms involved in the sputtering process are discussed since the sputtering rate ratio $Cs^+/O_2^+ \sim 5$ does not correspond to the mass ratio of the two ions.

A theoretical assessment of roughness monitored as a function of sputter time is presented where homogeneous and inhomogeneous structures have been considered.

INTRODUCTION

Ion beams have been used for a wide variety of applications for over a century, but it has only been in the last twenty years that they have been applied to products and processes in industrial and commercial environments. Perhaps the most significant effect of ion beam interaction with a solid surface is the impingement of energetic particles, and the subsequent removal of atoms from that surface, a process known as sputtering or ion erosion.

The principles of ion erosion have been known for a long time, the phenomenon first being discovered by Grove in 1853 who reported the occurrence of a metallic deposit on the glass walls of a discharge tube. Plücker (1858) noted that this process could have potential in thin-film coating, a topic later pursued by Wright (1877).

Despite initially slow progress in determining the mechanism of the sputtering effect there were several early hypotheses. Puluj (1880) and Hittorf (1883, 1884) suggested that cathode heating during discharge caused sputter removal, but this idea was subsequently made redundant when Granquist (1897, 1898) observed that the sputtering rate was insentitive to the temperature of the cathode over a wide range of temperatures.

The first experiment demonstrating ion-beam sputtering was performed by Goldstein (1902), who showed the disappearance of a gold coating on a glass wall facing an ion beam, produced by extracting canal rays through a hole in the cathode. Thus, it was deduced that the sputtering

effect was caused by positive ions of the discharge striking the cathode. In more recent times, cathode sputtering has found repeated application in the selective removal of surfaces in the investigation of materials (Pohl and Burchard, 1980) and biological substances (Orth, 1970).

Ion beam sputtering has been used extensively and in a variety of applications for more than twenty years. For example, by a method which utilises preferential erosion rates along grain boundaries and randomly orientated defect structures, the microstructure of polished specimens in metallographic studies may be revealed by ion beam etching. Indeed, metallurgists often use ion etching instead of chemical etching for a number of reasons. Padden and Cain (1964) have written a review illustrating its advantages over other classical methods, and it has since been realised that with the commercially available apparatus, ion etching is a clean, rapid and flexible means for routine metallography (Pohland and Burchard, 1980). Typically the conditions for chemical etching vary greatly for different materials but it is possible to etch all materials by ion etching under similar sputtering conditions. Chemical etching can present serious problems, for example, at the point of contact of two or more different materials, such as sandwich structures, galvanic coatings and inclusions in alloys, where to a large extent these can be overcome using ion beams.

In contrast to the apparently destructive nature of ion-surface interactions, ion beams can be used to clean and polish surfaces, a feature particularly important in surface analysis where ultra clean conditions must be maintained. Further to this, ion beams have become invaluable as a means of obtaining composition-depth profiles in

techniques such as Auger Electron Spectroscopy (AES), Secondary Ion Mass Spectrometry (SIMS), and low and high energy ion backscattering (LEIS, HEIS). Other areas involving ion-surface interaction include: the implantation of dopants and semiconductors to characterise their electrical properties; the deposition of thin films in micro-electronic circuitry; radiation blistering of structural materials and gas precipitation induced swelling, which has more recently been important in fusion device reactor physics; ion beam thinning techniques employed by electron microscopists for the preparation of electron-beam-transparent specimens.

From as early as the initial experimental observations made by Goldstein (1902) there have been several contributions relating the experimental and theoretical aspects of solid state sputtering with gas ions (Stark, 1902; Sigmund, 1969; Thompson, 1981). However, although the physical processes involving ion-surface interactions are, albeit qualitatively understood, there is still a great deal of speculation regarding the mechanisms that operate on different materials, and under different sputtering conditions as observed by experiment (Navinsek, 1976). In particular, these effects involve the way in which surface material is removed by the incident ion beam, and are dependent upon the erosion rate, the surface chemistry, and crystal orientation, and the intrinsic variable parameters such as ion incidence angle, ion energy, and the bombarding ion species. Ion bombardment of solids has been the subject of reviews by Wehner (1955), Kaminsky (1965), Carter and Colligon (1968) and Behrisch (1981), who treat in

detail the mechanisms by which ion erosion occurs. In general these authors agree qualitatively on the many different aspects involved in ion-surface erosion interaction. In particular, and with more relevance to the present work, the behaviour of surface morphology during ion erosion has a significant influence on sputtering yields, ejection patterns, cluster formation and channelling or back-scattering of ions. Recently, and as a result of earlier observations (Guentherschulze and Tollmien, 1942; Stewart and Thompson, 1969), there have been many experiments conducted illustrating the development of a variety of surface features following ion erosion (for reviews see: Navinsek, 1976; Auciello, 1982). Generally an ion eroded surface is modified in this way by differential erosion rates occurring at localized regions in the surface thus creating a macroscopic effect. This, however, can be detrimental in surface analysis studies (viz: AES, SIMS, ISS etc.) since a non-uniform surface presents a degree of uncertainty in the depth location of a particular element, thereby affecting the integrity of composition-depth profiles (Hofmann and Zalar, 1979).

The development of surface morphology under ion erosion is particularly relevant to the work presented in this thesis and the mechanisms by which these anomalous features occur will be discussed in a review section in chapter 5. It has been evident from much of the early work that the processes taking place during ion etching are difficult to interpret and some of the surface structures observed can only be explained rather speculatively. Furthermore, it has not been until recently that systematic studies have been performed on

particular materials, relating the growth of surface features under ion bombardment to the various influencing parameters mentioned previously (Navinsek, 1976; Kelly and Auciello, 1980; Lewis et al, 1982). The macroscopic effect has since been theoretically modelled, and with good agreement to experimental observation, although generally these simulations have involved comparatively simple structures (Catana et al, 1972; Barber et al, 1973). It is therefore imperative that extensions are made to existing theories, directed towards a complete description of a 'real' sputtering surface, and that experimental evidence is provided by a series of systematic approaches consistent with the current literature.

It was considered important by the present author that an investigation be carried out to observe the sputtering behaviour of some semiconductors since these materials are of ever-increasing industrial importance. Furthermore, an integral part of semiconductor dopant profiling is the employment of active gas species as a sputtering medium (viz: SIMS). The use of active gas species (O_2^+ and N_2^+ in particular), have previously been found to possess different sputtering qualities to the more frequently used inert gases (Ne^+, Ar^+, Kr^+, Xe^+), and on occasions have been reported as substantially enhancing the resolution in sputter-depth profiling (Hofer and Liebl, 1976; Blattner et al, 1979). Other studies have suggested that this is a result of a more uniform surface being produced, by the active gas (Tsunoyama et al, 1976; Katzchner et al, 1984), but in many cases although the total ion dose may be similar there is strong evidence to suggest that erosion rates are vastly different and therefore any quantitative

comparisons to inert gas sputtering should be treated with caution (Okajima, 1981).

It has previously been mentioned that the development of surface topography is an inherent effect of sputtering in surface analysis, and can seriously degrade the integrity of depth-profiles. Therefore, it is important that its growth under ion erosion is minimized, which can be achieved in several ways. By careful preparation of a surface, contamination and defect density can be reduced thereby lowering the probability of selective etching. Invariably nowadays, surface contamination is further alleviated by performing high resolution surface analysis under ultra high vacuum ($< 10^{-9}$ torr), and in situ surface cleaning using low energy defocused ion beams. The nature of the material undergoing analysis will occasionally, on some materials, initiate non-uniform erosion, for example alloys (Ho et al, 1979; Betz, 1980), but it has been shown that this problem may be overcome partially by the use of multi-directional ion beams (Sykes et al, 1980).

It is evident from the literature that ion beam sputtering plays an important part in the analysis of solid surfaces. The work presented in this thesis is therefore aimed at examining changes in surface shape following ion bombardment, where a systematic experimental approach illustrates the effects of active gas bombardment on some important semiconductor materials, and a theoretical approach to changes in surface shape uses existing theories to examine the effects of ion bombarding an inhomogeneous surface. Further, experimental and theoretical studies highlight the advantages and disadvantages

of sputter-depth profiling, where a recently developed approach is adopted to reveal the role of ion beam sputtering as an integrated part of a surface analytical system.

CHAPTER 2

2.1 Thin Film Technology

Thin films of metals, semiconductors, and insulators have found an enormous number of successful applications in modern technology. The most important of these are in the field of optics, electronics and photoconversion (photothermal and photovoltaic conversion). For example, thin films and thin film structures are used for anti-reflection coatings, beam splitters, polarizers, coatings for image forming devices, photovoltaic devices, metal-semiconductor (MS) and metal-interfacial layer-seminconductor devices (MIS), thermal absorbers and solar selective surfaces (Pandelisev and Wang, 1982). The remarkable advances that have been made over the last decade are mainly due to an increased scientific understanding of the nature of the processes used to deposit thin films. This is further complemented by new and advanced surface analytical techniques (viz: AES, ESCA, SIMS) which may be employed to determine the chemical, structural and other physical properties of the films, hence quantitative information can be obtained which indicates how the process parameters should be adjusted to suit a particular application.

There are a large number of different processes by which thin films can be produced (Maissel and Glang, 1970; Vossen and Kern, 1978), but in practice there are very few basic methods employed. Some of the deposition methods are based on purely physical processes, some

operate on physical chemical principles and others are essentially chemical in nature. Included in this category is thermal evaporation, glow discharge, ion-beam sputter-deposition, plasma anodization and gas-phase chemical formation (Vossen and Kern, 1980). These all represent generalised methods and the large variety of thin or thick film production will result largely as a hybrid process of one of the above mentioned. For example, molecular beam epitaxy (MBE) is a recently developed evaporation process, or chemical vapour deposition (CVD) is related to gas-phase formation of a film at a substrate surface and both are particularly important in the fabrication of solid-state electronic device structures.

It is essential that thin films are characterised for structure and composition in order that they perform to the specified requirements. Furthermore, a knowledge of the diffusion processes operating in thin films for applications such as microelectronic devices is important for the design, fabrication and reliability of the thin film package (Gupta and Ho, 1980). For example, in technologies utilizing flip-chip-solder interconnections and alternate wire bonding an understanding of the diffusion process is important since oxide-forming metals may be transported to the surface, making the interconnection difficult.

The tendency for discrete layers of materials to diffuse and react chemically is enhanced by the presence of a high density of defects in thin films, namely grain boundaries and dislocations in addition to vacancies present within the grains which provide fast and efficient paths for mass transport (Balluffi and Blakely, 1975).

In thin films these defects are usually in close proximity or directly connected to surfaces and interfaces, and strong electrical or temperature gradients arising during operation of thin film devices could lead to direct mass transport known as electromigration and thermomigration via the defects. The rapid nature of mass transport along grain boundaries and dislocations in polycrystalline materials is a complex process beyond the scope of the present work but has been renewed in the literature (Gleiter and Chalmers, 1972; Gjostein, 1973). Nevertheless, reliable quantitative data may be obtained on the diffusion paths in thin films through the use of sputter-depth profiling in the commercially available surface sensitive techniques (i.e. AES, ESCA, SIMS). There are, however, inherent problems associated with ion sputtering when used as a tool in depth-profile analysis such as selective sputtering (Shimizu et al, 1973), collisional mixing (McHugh, 1974), surface roughening (Holloway, 1975; Mathieu et al, 1976), and radiation enhanced diffusion (Chu et al, 1976) all of which, in addition to mass transport, cause a smearing of the depth profile. Consequently, methods must be devised by which diffusion rates can be separated from the ion bombardment induced effects.

An empirical approach was employed by Hall et al (1976(a), (b)) who measured the change in the slopes of the depth profiles between aged and unaged samples, using the latter in an overall correction procedure for the former. Adopting a similar approach to Hall et al (1976), Chuang and Wandelt (1979) have more recently performed a systematic study for the system Ni/Fe. The samples are prepared in situ and then held at temperatures ranging from -150°C - 500°C were

studied for interdiffusion by simultaneous AES and sputter profiling. By correcting the depth profiles for ion-induced effects, they were able to evaluate values of interdiffusion coefficients. At the higher temperatures (300 - 500°C) they concluded that bulk and grain boundary diffusion was the more dominant process, whereas at lower temperatures (150° - 250°C) there was a mechanism by which the metal atoms were each exchanged about the interface eliminating porosity and so reducing surface free energy. This resulted in a broadening in the depth profile at the interface, the magnitude of which dominated at the higher temperatures.

Diffusion of thin films enhanced by temperatures in the annealing process, can also result as a consequence of local temperature rises in AES analysis. Hofmann and Zalar (1979) have observed interdiffusion, evaporation and temperature enhanced sputtering in Au/Ag films which were exposed to an electron beam of either 15mW or 175mW input power, during AES profiling measurements. It was shown that the temperature rise of the sample was intrinsically dependent on the input power of the electron beam, such that for the low input power the temperature was below 150°C and between 400°C and 750°C for the high input power. These experimental observations were in excellent agreement with theoretical predictions made by Röll et al (1979, 1980) who calculated the temperature distribution in a thin metal film, exposed to an electron beam, as the balance of heat transport through film and substrate. Basing their argument on a previous relation giving the maximum temperature in a thin film (Baker and Sexton, 1975) they formulated an expression giving the central temperature T_o as:

$$T_o = \frac{\frac{\rho . r_o}{\beta}}{1 + 1.67\ (\alpha/\beta)(h/r_o)} \qquad (2.1)$$

where ρ = input power of electron beam

r_o = radius of electron beam

β = thermal conductivity of substrate

h = film thickness

α = thermal conductivity of film material

They showed that the heat distribution in metal films was not only dependent on ρ, r_o and β but more, in particular on the film thickness. This is particularly relevant to sputter profiling in AES where the film varies during analysis and in the limit, or for very thin film thickness the maximum temperature tends to (Baker and Sexton, 1975):

$$T_{max} = \frac{\rho r_o}{\beta} \qquad (2.2)$$

This prediction was substantiated by previous experimental studies (Röll et al, 1979), and showed that for a constant electron beam power on Ni - Cu films the diffusion increased rapidly when the film thickness became small during sputtering.

Diffusion phenomena have been regarded as being made up by two fundamental processes (Gupta and Ho, 1980) namely; the diffusivity and the driving force. These parameters are highly dependent on the material and the structure of the thin films, a characteristic distinguishing between kinetic reactions in thin films to bulk materials. The driving force arises from the gradient of the total free energy arising from thermal, chemical, electrical, mechanical

and other potentials, Indeed, Pandelisev and Wang (1982) have shown by AES that 'drive-out' diffusion was present as a result of interfacial reactions at room temperature for various combinations of metals and interfacial layers on different substrates. Their results showed that interfacial reactions only occurred at the metal-interfacial layer for all the combinations of structures indicating a chemical dependence on the diffusivity.

Some of the mechanisms by which diffusion operates in thin films has been discussed. The effect may be minimised by elimination of structural defects, or a compatible structure insensitive to the drive-out diffusion effect.

The theoretical understanding is not yet well understood, and only approximations of the diffusion coefficients may be made in depth profiling measurements due to the other effects inherent in sputter removal. The combination of thjs latter aspect and diffusion is more easily examined if the overall shape of the depth profile is optimised via experimental conditions, and may be quantitatively assessed by a measure of the interfacial depth resolution. In the next section it will be shown how several workers have approached this problem, and the methods employed for analysis of the data.

2.2 Depth Resolution in Sputter-Depth Profiling of Thin Films

A fundamental understanding of the structure of thin films is required before their manufacture and use, attain maximum capabilities. The variety of thin films available are variable in thickness, structure and chemical composition, and therefore a knowledge of these parameters

is essential for optimum performance.

There are presently available several high resolution surface analytical techniques (viz: AES, ESCA, SIMS) which are used for the characterisation of thin films and coatings, and the particular modes of operation, and use have been reviewed in chapter 1. Although these techniques have been refined somewhat during the last decade, it is still important to realise their capabilities and limitations. In this respect there has been much contemporary work performed to characterise the processes involved, and the influencing factors involved in surface analysis are now well documented, even if not well understood (Benninghoven, 1976; Holloway and Bhattacharya, 1981). In particular some of the most important features arising in sputter depth profiling analyses are atomic mixing effects (Schwarz and Helms, 1979), ion-induced surface roughness (Mathieu et al, 1976, Dararya et al, 1983) and surface diffusion (Ho et al, 1977), all of which limit the accuracy of measurement at interfacial regions. Another inherent phenomena limiting resolution is the escape depth of the secondary detected particles during analysis, although usually this is swamped by either one or more of the above mentioned effects.

There have been numerous studies on specially prepared thin film systems attempting to minimise the neasured depth resolution, or degree of broadening at an interface. The majority of these studies have utilised changes in precisely controlled experimental parameters namely, inert and reactive ion sputtering (Blattner et al, 1979), ion incidence angles (Sykes et al, 1980), surface roughness effects (Hofmann et al, 1977) and sputter depth (Pandelisev and Wang, 1982;

Daranya et al, 1983), to determine their relative effects on the depth resolution. It is, however, evident from the literature that the sputtering process is the most influential aspect of interface broadening and holds three major contributions: the statistics of sputtering, the roughening of the surface and knock-on damage. The following discussion will therefore be devoted to these mechanisms.

One of the first attempts to predict the sputter broadening of an interface was made by Benninghoven (1970) when he formulated a sequential layer sputtering (SLS) model associated with a statistical process. Two basic assumptions made were that (1) sputter removal will be limited to those atomic layers exposed to incident ion flux (2) the sputtering yield is constant for all layers. By considering the fraction of a layer i exposed after a sputtering time t, the constant rate of removal of the relative free part is given by (Benninghoven, 1970):

$$\frac{d\theta_i}{dt} = (\theta_{i-1} - \theta_i) \cdot \frac{1}{T} \qquad (2.3)$$

where T is the characteristic time constant required to remove the equivalent of a single monolayer and depends on the ion flux ϕ, the average total sputtering yield S and the number of atoms in $1cm^2$ N_0, such that

$$T = \frac{N_0}{S\phi}$$

The disadvantage of this model is clearly that only an element of one type can be subjected to ion bombardment and therefore preferential erosion rates, where more than one element or a change in local surface

angle is involved, are not allowed for. Nevertheless, Hofmann (1976) extended the SLS model and applied it to sputter profiling through interfaces where he predicted a square root dependence of the depth resolution Δz_s on the sputtered depth z giving

$$\Delta z_s = 2(az)^{\frac{1}{2}} \tag{2.4}$$

where a is the thickness of a monolayer.

Equation (2.4) has been found to agree well with several experimental observations (Hofmann, 1977), where a $\Delta z/z \propto z^{-\frac{1}{2}}$ dependence prevailed. Other measurements, however, indicated a $\Delta z/z \propto z^{-1}$ (Hofmann, 1980) dependence and with a smaller Δz than predicted by equation (2.4). Undoubtedly, the broadening of the depth-profile due to purely statistical sputtering Δz_s is not an adequate enough model to describe the full complementary sputtering process, such as knock-on events and cascade mixing (Andersen, 1979; Hofer and Littmark, 1979). Indeed, Hofmann (1977) has reported that for all the different contributions Δz_j causing the sputter depth-profile to broaden, a general expression relating the absolute depth resolution may be represented by a general error propagation law, whereby for mutual independence (Hofmann, 1977):

$$\Delta z = \left(\sum_{j=1}^{n} \Delta z_j^{\,2}\right)^{\frac{1}{2}} \tag{2.5}$$

It would therefore be pertinent to modify the basic definition of the SLS model and incorporate specific conditions for the variable parameters in the sputter-related process. Initially Shimizu (1979)

incorporated an additional statistical effect which accounted for fluctuations in individual sputtering events and dependent on ion energy and species, and surface conditions where:

$$\Delta z = 2\varepsilon\{az(1 + S)\}^{\frac{1}{2}} \qquad (2.6)$$

where $\varepsilon < 1$ (irradiation adjustment parameter).

Equation (2.6) is similar to an empirical relationship reported by Mathieu et al (1976) who performed AES analysis of thin gold films on nickel and found that $\Delta z \alpha zE_p^{\frac{1}{2}}$ (E_p is the primary ion energy). This analogy is valid if it is assumed that the sputtering yield S (in equation 2.6) is approximately proportional to the primary ion energy (Seah, 1981) for energies less than 5keV, thus a modification of the statistical model gives a depth resolution dependent on ion energy.

The sputtering process is governed statistically by the probability of an atomic cluster being ejected from the surface. In this respect other inherent factors contributing to the degration of sputter-depth profiling are generated, such as surface topography. Seah et al (1981) have modified SLS theory to accommodate a relative sputtering probability of exposed surface atoms which is inversely proportional to its instantaneous bonding with the matrix, rather than being constant as originally proposed (Benninghoven, 1970). The authors showed that the depth resolution altered from the typical square root dependence on sputtered depth, to a constant value at depths greater than 10nm. They were careful to note, however, that the relative effects were negligible in most instances compared to the more familiar influencing

factors such as atomic mixing, diffusional and instrumental effects.

Recently, in a series of reports by Seah et al (1983(a), (b)) studies using the basic definition of the modified SLS model represented by equation (2.4), have been performed to assess the influence of the varying parameters and surface conditions in sputter-depth profiling. For example, in a compilation of results illustrating the sputter broadening Δz_s of an interface as a function of depth (Hofmann, 1977; Honig and Magee, 1978), it was shown that for samples prepared specifically for these studies, equation (2.4) agreed well with the data. For samples that were typical of material science applications (Laty et al, 1975) a modified equation of the form $\Delta z_s = (0.16z + 36)$nm produced a more accurate representation of the data.

In further modelling, with subsequent modifications made to the SLS model, emphasis was placed on the effect of surface roughness which has been reported as being deleterious to the interface broadening on several occasions (Mathieu et al, 1976; Hofmann et al, 1977).

Seah and Lea (1981) have shown that the effect of substrate roughness can be explained through the non-cancellation of the increase in sputtering yield as $\sec^f\theta$ and the loss in flux density as $\cos\theta$ (Wehner, 1975), when the micro-regions of the surface present various angles of θ to the ion beam. The value of f for most materials occurs typically in the range 0.6 - 2.0, and for values other than $f = 1$ (where the effect disappears) a contribution to $\Delta z/z$ occurs and (Seah and Lea, 1981):

$$\frac{\Delta z}{z} = 1.66\ \alpha_o^{\ 2} f \qquad (7)$$

where α_o is the mean angular divergence of the microregions from the average surface.

It was observed that a minimum value of $\Delta z/z$ occurred for a normally incident ion beam irrespective of α_o, however, if α_o is $< 3.5^o$ the contribution to $\Delta z/z$ is $< 1\%$.

A full analysis of this particular model system was reported by Lea and Seah (1981) who considered the initial surface roughness contribution and the interface roughness contribution to be in two separate regimes where both were either correlated or uncorrelated. The latter involved a sum of the two effects in quadrature contributing to the final interface blurring. In this way the authors were able to compare the relevant advantages of ion sputtering and angle lapped compositional profiles by treating individual effects and summing them in a manner similarly described by equation (2.5). Relative contributions of each technique towards interface blurring could be assessed, and thus optimum conditions were deduced for a variety of surface conditions.

The data obtained from sputter-depth profiling through interfaces is subject to a complex variety of experimental conditions and limitations. Furthermore, for a particular selection of irradiation parameters the depth resolution at the interface often varies for materials of different structure and elemental combination. For example, it has been reported (Mathieu et al, 1976; Fine et al, 1982) that the observed interface widths are not due primarily to

cascade mixing but are related to the topography, generally associated with evaporated polycrystalline films, where the development of surface topography may be enhanced by sub-surface defects and preferential erosion of grain boundaries. The majority of work in depth-profiling has been performed on multilayer thin films developed by an evaporation process, and the broadening of the subsequent interfaces by the sputtering process has been monitored to represent a measure of the depth resolution as a function of depth (Benninghoven, 1976; Hofmann, 1977; Mathieu et al, 1977).

The present work is initially concerned that the surfaces of polycrystalline materials are unstable under ion bombardment, and that the persistence of ion induced surface topography over several layers of thin film components could lead to severe amplifications in interface widths. Furthermore, the existence of a multilayered structure may promote excess strain at elemental boundaries thereby creating extra potential sites for ion induced surface texturing. Therefore, a study has been performed using two polycrystalline materials to measure the sputter broadening of only one interfacial region which, for separate analyses, varies in depth from 250Å - 4050Å. The effect of the evaporated layer thicknesses are assessed, and the dependence of the depth resolution on ion energy is discussed. The results will be compared qualitatively to previous experiments and the SLS model, as well as investigating the possibility of improved depth profiles using two ion guns (Sykes et al, 1980).

2.3 Depth Resolution Studies of Thin Films

The physical processes affecting the depth resolution of sputter-depth profiles can be investigated by interpreting the behaviour of an interface during sputter-profiling. Ideally, a well-defined step profile should be observed, but in practice there is an inherent broadening of the profile. This can be a result of a number of effects such as ion induced surface topography, surface diffusion, atomic mixing etc., all of which have been discussed in the last section and Chapter 1. To study the combined contribution of some, or all of the effects, experiments have been performed on thin films subjected to simultaneous inert gas ion bombardment, and analysis by Auger Electron Spectroscopy (AES).

2.3.1 Experimental

A pure polycrystalline nickel substrate was prepared by a mechanical polishing procedure which included initial grinding with 300, 550, 800 and 1200 grade carbide paper, followed by a surface polish with 6μm, 1μm and $\frac{1}{4}$μm diamond lapping compound. After each step of the process the samples were ultrasonically cleaned in acetone, methanol and distilled water, in order to reduce surface particulate contamination, a well known source of sputter-induced roughness (Stewart and Thompson, 1969; Wehner and Hajicek, 1971).

The material chosen for the thin film was pure chromium since this has a similar sputtering yield to nickel (Wehner, 1962), and therefore during analysis a large contribution towards preferential sputtering will be eliminated. The chromium was thermally deposited under vacuum

($\sim 10^{-6}$ torr) onto the nickel substrate, for a range of thicknesses varying from 250Å - 4050Å. The deposited film thickness was monitored using a quartz crystal, and found to agree with stylus techniques subject to $\pm$ 10% variation.

The sample size for each film thickness was $\sim 1cm^2$ enabling several depth-profiles to be obtained from one particular sample, while varying specific irradiation parameters (namely, ion energy and number of ion guns used), thereby keeping the surface conditions constant throughout. Sputter-depth profiles were obtained in a Varian Auger electron spectrometer using 1 - 3keV Ar^+ ions as the primary sputtering source, and produced by either one or two ion guns both incident at 31.5^o to the sample normal. The current density used was $150\mu Acm^{-2}$ when one ion gun was in use, and adjusted to $75\mu Acm^{-2}$ for two ion guns. Analyses were performed in ultra high vacuum ($\sim 10^{-9}$ torr), and data acquisition was relatively fast using the systems' multiplex unit.

Contrary to previous work performed on multilayer thin film systems (Hofmann, 1977) only single layers of chromium were used in the present work since it is thought that undue stress which may be produced in multilayer films, could be reduced in single layer films. This could therefore reduce the possibility of surface roughening occurring during ion bombardment, and also create an effectively, more evenly layered structure over the depth at which analysis takes place. Sputter-depth profiling of single layered thin film structures could therefore provide a better measure of the depth resolution. Furthermore, it has been previously shown (Sykes et al, 1980, Makh et

al, 1982) that the use of two ion guns significantly suppresses the development of surface texturing, and this particular aspect will be investigated for the system described above, by using two ion guns, in comparison to only one, to obtain sputter-depth profiles.

2.3.2 Results and Discussion

The analysis of the measured data could be quantitatively obtained from multiplex probe plots of the Auger peak-to-peak heights of each element as a function of sputter time. Primarily, the data analysis was concerned with determining the relative depth resolution, and the absolute broadening at the interface as a function of depth. The depth resolution is defined as the sputter depth Δz at which the measured intensity signal of one component decreases from 86% to 14% its initial value corresponding to standard deviation limits of a normal Gaussian distribution (assuming an initially perfect interface). A measure of the relative depth resolution $\Delta z/z$ may be obtained by taking the 50% value of the intensity signal as the mean eroded depth z, which for a constant sputtering condition $z = \dot{z}t$ will be proportional to the sputter time. Therefore by taking an average of the broadening at the interface for nickel and chromium, a reasonable representation of the depth resolution can be obtained.

There have been several reports in which authors have adopted their own particular methods of illustrating the behaviour of sputter-induced interface broadening of thin films, as a function of depth. In each case, however, they are merely an arrangement suitable to expressing a particular relation to the SLS model, and in the present

work several graphical illustrations will be shown in order to clarify the processes involved in sputter-depth interface broadening, and to compare with previous observations of the same processes.

The results illustrating the relative depth resolution as a function of depth for the Cr/Ni thin films here are shown in figure (2.1(a)). The graph represents data from sputter-depth profiles obtained using one ion gun in the raster mode, and for ion energies of 1, 2 and 3keV. Clearly the ion energy difference for each set of results is not particularly significant with respect to any change in the relative depth resolution, although there is a certain amount of scatter ($\sim$ 1 - 4%). In accordance with the SLS model, equation (2.4) predicts the $\Delta z/z \propto z^{-\frac{1}{2}}$, when only the outermost surface of the sample is exposed, and for a constant sputtering probability. For visual guidance lines of z^{-1}, and $z^{-\frac{1}{2}}$ slope have been superimposed on the graph in fig. 2.1(a), and illustrate that the general nature of the dependence of relative depth resolution on depth occurs within these two bounding limits. This observation has been observed by several authors and a compilation of their results has been presented in a review by Hofmann (1980). Arguably the SLS model described by equation (2.4) therefore only represents an ideal situation in sputter-depth profiling, but with the consideration of other anomalous effects surprisingly good agreement is obtained. Fig. 2.1(b) illustrates the dependence of relative depth resolution as a function of depth using two ion guns to obtain data by depth profiling. Once again the scatter of points lie in a 1 - 3% range for any particular film thickness, and are well represented by the two limiting depth relationships

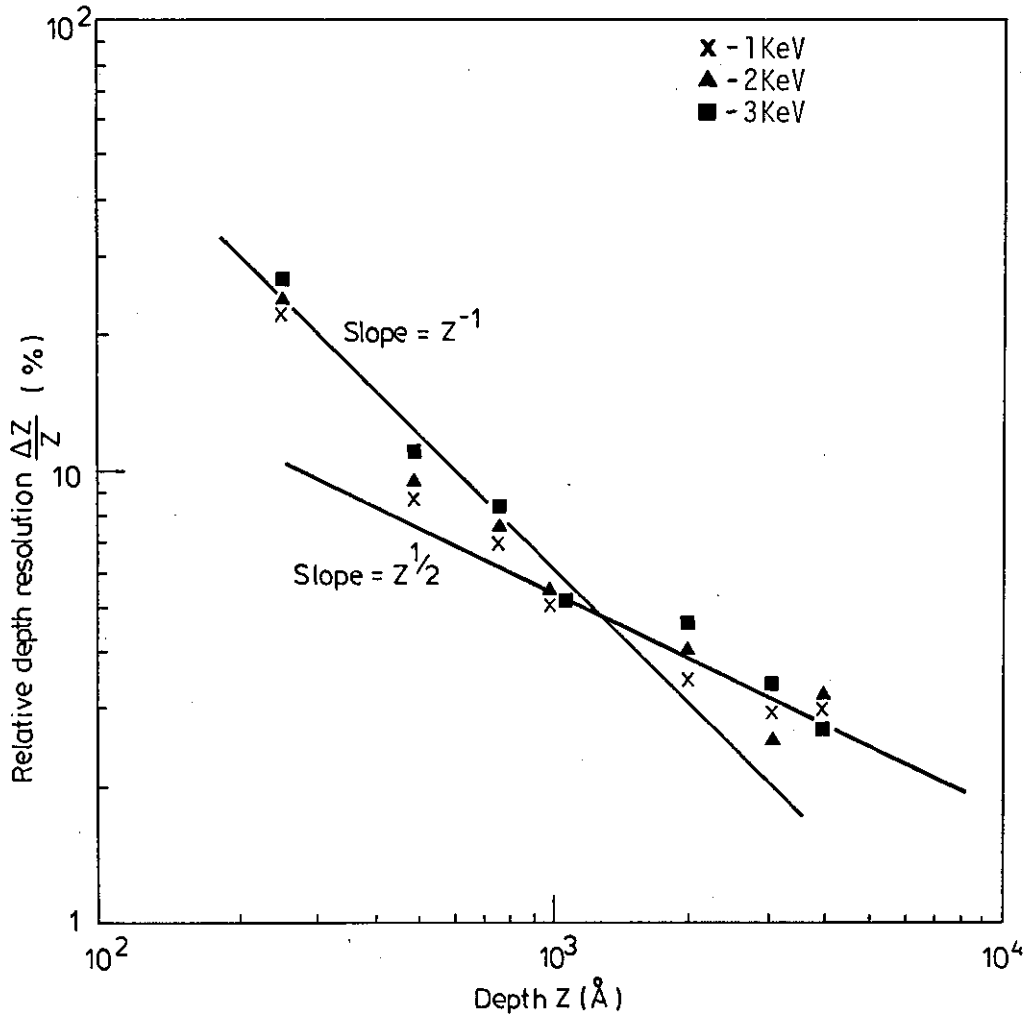

Figure 2.1(a): A measure of the relative depth resolution as a function of depth, obtained by AES depth-profiling of vacuum deposited Cr films on Ni substrates. (using one ion gun)

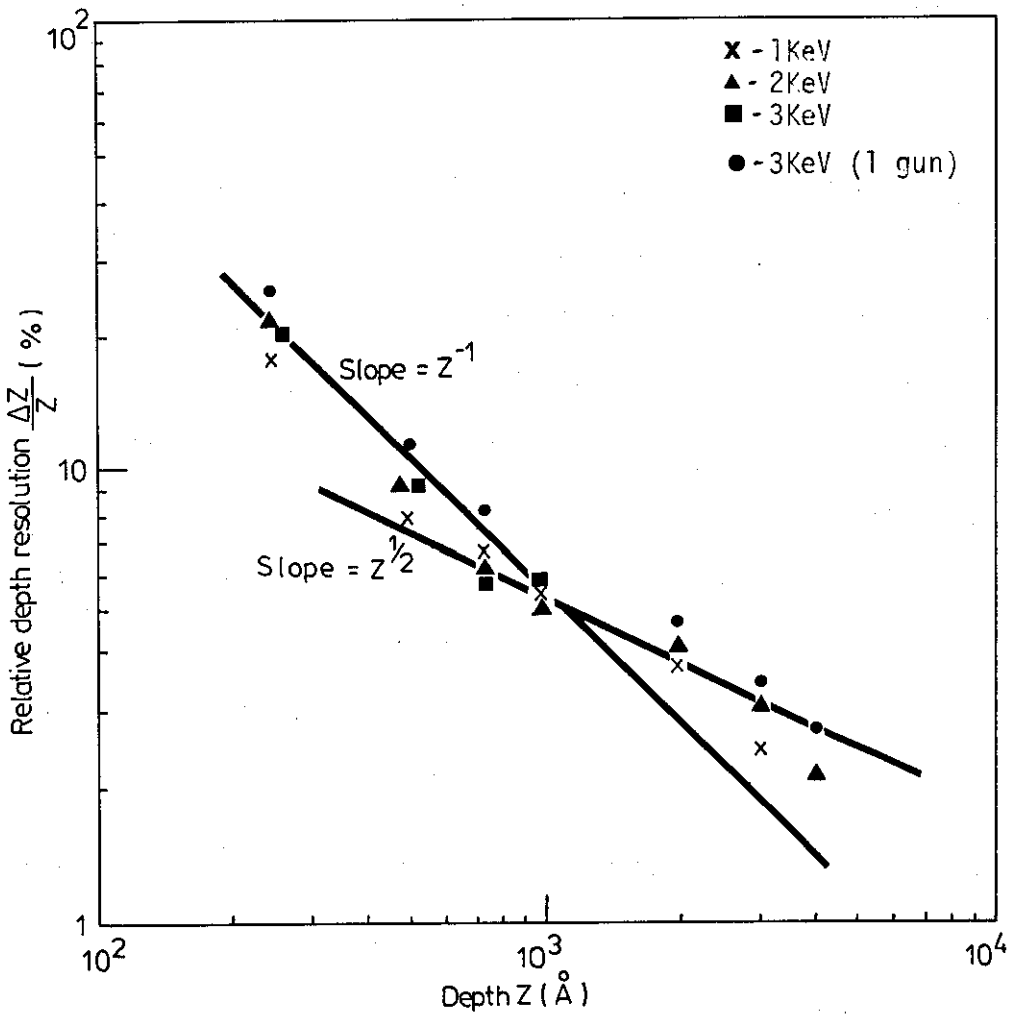

Figure 2.1(b): A measure of the relative depth resolution as a function of depth, obtained by AES depth-profiling of vacuum deposited Cr films on Ni substrates. (using two ion guns)

z^{-1} and $z^{-\frac{1}{2}}$. By comparison with figure 2.1(a) there appears to be an improvement in the overall relative depth resolution using two ion guns to sputter through the films. The data obtained for one gun at 3keV is shown in fig. 2.1(b) for comparison, where the maximum difference between the two modes is only $\sim$ 5%, however, generally the results obtained using two ion guns showed an improvement in relative depth resolution.

The results shown in figure 2.1 clearly illustrate that the relative depth resolution improves with the thickness of film, and that there appears to be an absence of ion energy dependence. Furthermore, although the results indicate that the relative depth resolution is well characterised by the limits z^{-1} and $z^{-\frac{1}{2}}$ it is conceivable that at larger sputter depths this could tend to $\Delta z/z$ = constant in agreement with other observations (Hofmann, 1980). This effect would be particularly noticeable depending on the magnitude of sputter-induced roughening at an interface as a function of depth. If the roughness was large, then even to large sputter-depths the value of $\Delta z/z$ could increase significantly (Hofmann et al, 1977).

Perhaps the ideal way to quantitatively understand the effects of sputtering on thin film interfaces is to examine the behaviour and absolute broadening at the interface, and in accordance with equation (2.4) of the SLS model, to calculate the value of 'a'. Figure 2.2(a) illustrates the interface broadening Δz as a function of depth z using only one ion gun during analysis in an energy range of 1 - 3keV Ar^+. As expected from figure 2.2(a) linear dependence prevails where to a good approximation $\Delta z \propto z^{\frac{1}{2}}$, and the effect of ion energy is

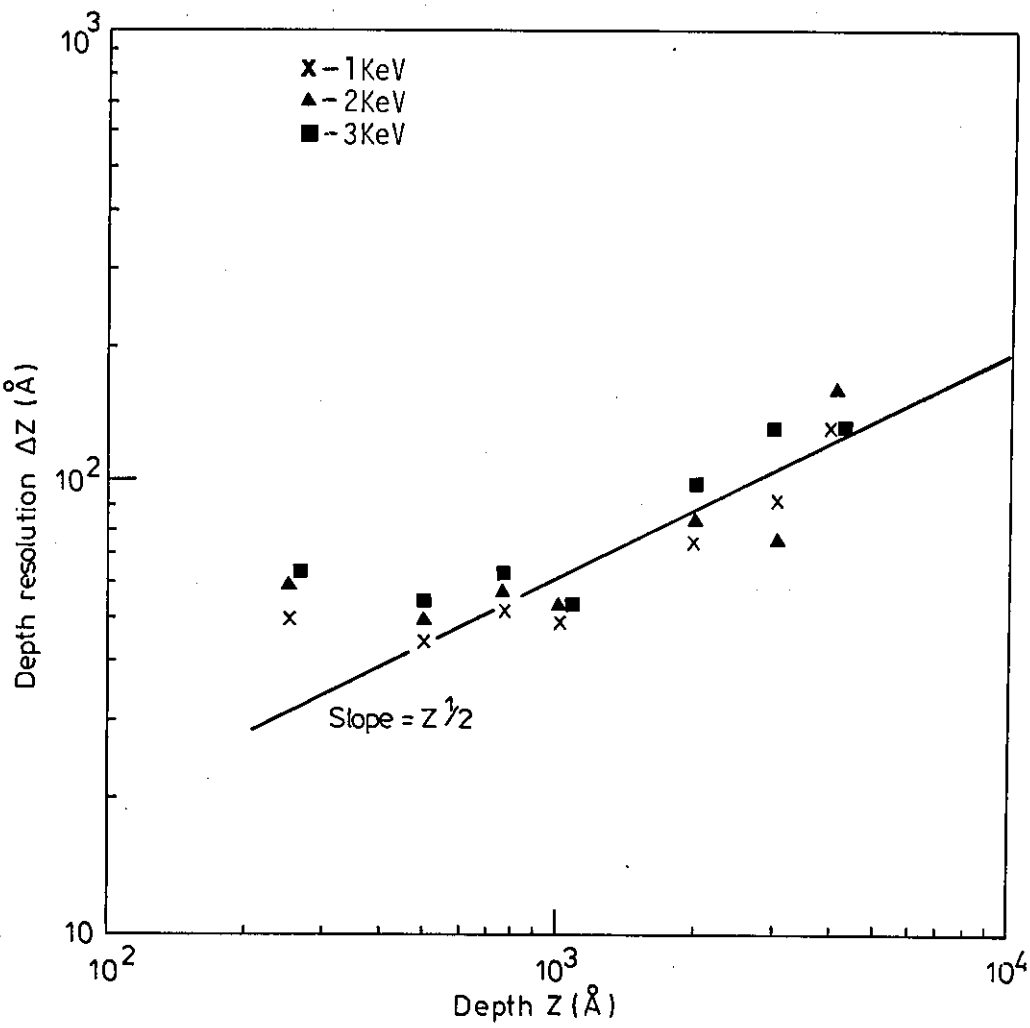

Figure 2.2(a): The depth resolution as a function of depth at the interface of Cr films on a Ni substrate obtained by depth-profiling in AES. (using one ion gun)

insignificant. The parameter 'a' in equation (2.4) has been found to correlate well with the monolayer thickness (between 2 and 3Å) in metals (Hofmann, 1977, 1980) and is found to be (6.3 ± 2)Å in fig. 2.2(a). This would normally represent several monolayers but does however agree well with previously observed values for polycrystalline multilayer thin films, for example in a report by Seah and Hunt (1983) a compilation of results determined the value of 'a' as (8.6 ± 2.2)Å. Nevertheless, the dependence of the sputtering probability on the actual site of an atom must be considered. Furthermore, due to radiation damage the event of an undisturbed monolayer is unlikely (Walls et al, 1975), and hence model calculations reveal exaggerated long tails in the depth profiles. Therefore, the value of Δz is too high or the parameter 'a' should be substantially smaller than monolayer thickness, an aspect which has been used in evidence against the SLS model (Whittmaack and Schulz, 1978). However, it is a result of several contributing factors that causes the interface broadening and therefore should not be completely dependent on the monolayer thickness. This has been confirmed by Lea and Seah (1981) who showed that the spread in values of Δz due to sputtering are related to the surface preparation and hence surface condition prior to sputtering.

In comparison to fig. 2.2(a), the results illustrating Δz vs. z obtained using two ion guns is shown in fig. 2.2(b). The same trend is evident, but the value of 'a', for the dotted line shown, is now (4.9 ± 0.7)Å. More importantly it is significant that the improvement in Δz is ∿ 10Å at a depth of 250Å in contrast to using one ion gun, and ∿ 40Å at a depth of 4050Å. Also the error in the spread of points

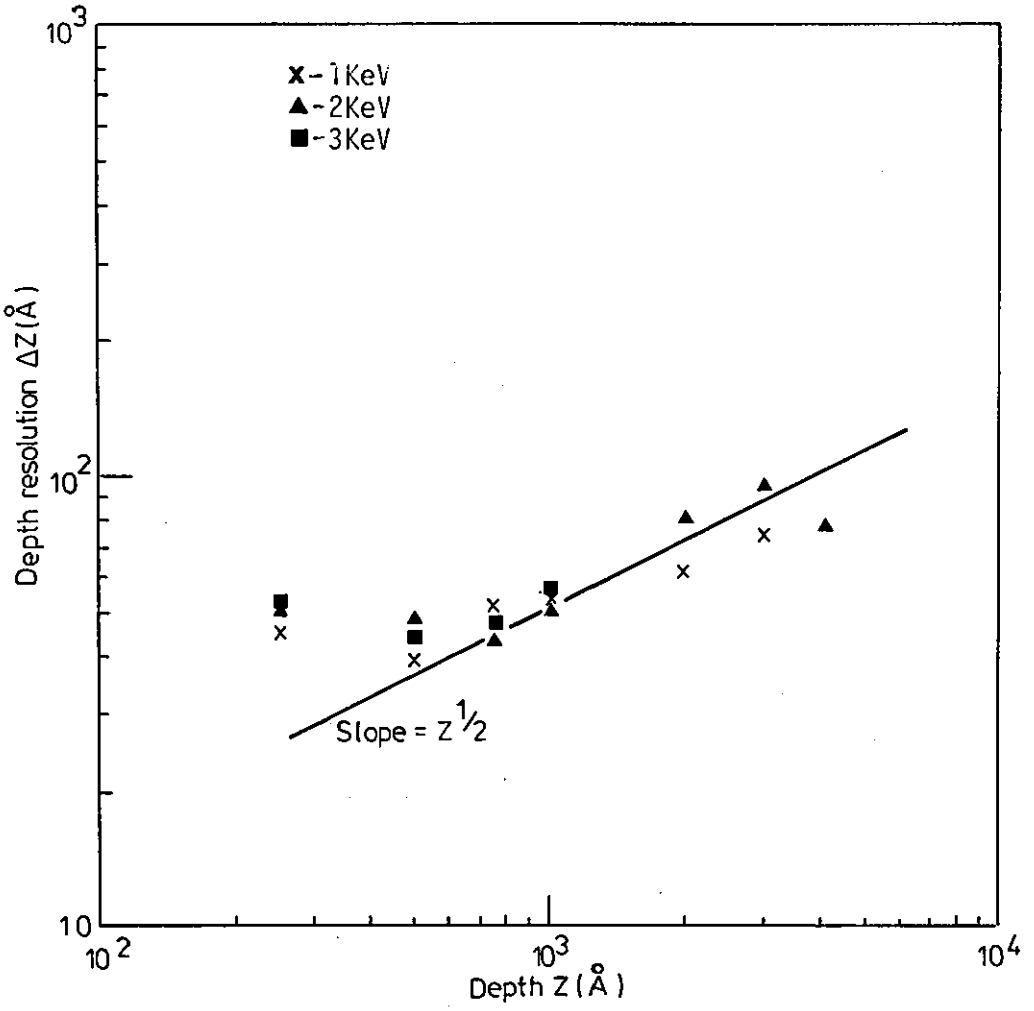

Figure 2.2(b): The depth resolution as a function of depth at the interface of Cr films on a Ni substrate obtained by depth-profiling in AES. (using two ion guns)

is significantly reduced. This illustrates two points:

i) that surface roughness increases as a function of depth, a well documented phenomenon (Stewart and Thompson, 1969; Laty et al, 1974; Navinsek, 1976).

ii) the use of two ion guns is effective in suppressing the development of surface texturing, a feature also observed elsewhere (Sykes et al, 1980, Makh et al, 1982).

The individual effects contributing to interface broadening have been discussed in detail in a series of papers by Seah et al (1981, 1983(a), (b)) where they suggest that behaviour at the interface depends upon the type of material undergoing bombardment, and thus can be represented as three separate regions of polycrystalline metals, epitaxial layers and single crystals and amorphous elements and compounds. Classically, the latter two produce singificantly less interfacial broadening than the former of these materials particularly at large sputter depths, due to an amorphization mechanism during sputtering. However, it is evident from Fig. 2.2 that the region lying between 200Å and 1000Å does not follow the same characteristic line as the results of Δz obtained for depths > 1000Å. This would suggest that in this region the predominant mechanism of broadening at the interface is due to cascade mixing, which is further substantiated by the fact that S.E.M. observations of these surfaces revealed no texturing at depths below 2050Å. However, this could feasibly be a result of a lack of contrast in the S.E.M. where slowly undulating structures might be present. Furthermore, it is thought that knock-on

processes occur over 5nm for 1keV ions, increasing to 10nm for 5keV ions (Anderson, 1979), and since the apparent independence of Δz on z in figure 2.2 occurs in the range 20 - 100nm, there could, in the event still be a contribution from surface roughening.

2.4 Conclusions

The present work has illustrated the depth dependence of the resolution during Auger sputter-profiling of polycrystalline Cr/Ni thin films. The behaviour of the interfacial distortion during sputtering is consistent with previously reported results. Fig. 2.3 illustrates many of these as compiled in a recent report by Hunt and Seah (1983), and with the results of the present work (obtained using one ion gun for sputtering) also shown. Generally, the dependence of the interface width Δz as a function of sputtered depth z is in good agreement with previously observed results for sputter-depth profiling of polycrystalline metal overlayers, shown to occur mostly within the region of the dotted lines. The points occurring outside this area, and possessing enhanced depth resolution represent the broadening of thin film interfaces for single crystals and amorphous elements and compounds (Seah and Hunt, 1983). These, however, are subject to considerable variations in resolution if experimental conditions are non-optimized. For example, it has been shown experimentally that an improved depth resolution can be obtained by using low energy ions during sputtering (Mathieu et al, 1976; Chuang and Wandelt, 1978), ion beam incident at 90^{0} to the surface, or multiple ion beams to ensure more uniform etching (Sykes et al, 1980; Keenlyside et al, 1983;

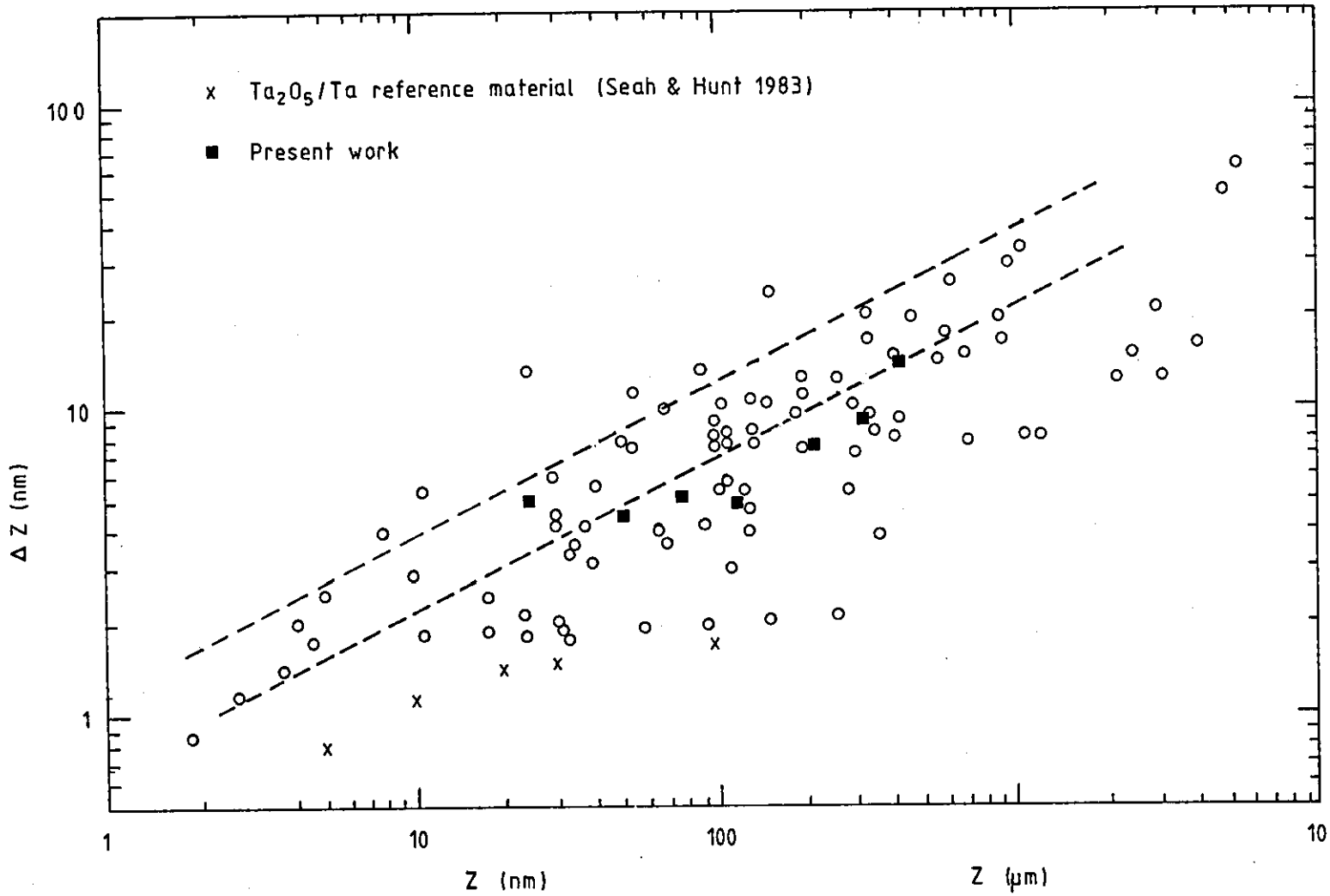

Fig. 2.3 COMPILATION BY SEAH AND HUNT (1983) OF MANY MEASUREMENTS OF DEPTH RESOLUTION IN COMPOSITION DEPTH PROFILING USING ARGON IONS. [DATA TAKEN FROM HONIG AND MAGEE (1978), HOFMANN (1980), COOK ET AL (1980), FINE ET AL (1982).]

Seah and Hunt, 1983), and well prepared surface conditions with minimal contamination and microroughness (Mathieu et al, 1976; Hofmann et al, 1977).

To quantify the results shown in Fig. 2.3, therefore, Seah and Hunt (1983) have used Ta_2O_5 as a reference material (shown by crosses) and obtained sputter-depth profiles for a well-defined set of conditions in order that subsequent experiments on different samples can be directly compared.

An attempt has been made in this present work, to improve the depth resolution by using only one overlayer thickness as opposed to a multilayer structure. Clearly, the results from Fig. 2.2(a) and Fig. 2.3 indicate that no significant improvement has been obtained. Further, the variations in the relative depth resolution (see Fig. 2.1) were small ($\sim$ 1 - 4%) with respect to ion energy and it can only tentatively be suggested that this was due to surface roughening. An improvement in relative depth resolution $\sim$ 5% was obtained using two ion guns during sputter-profiling and the variation in values was slightly less ($\sim$ 1 - 3%), which is consistent with suppression of topography development using multiple ion beams (Sykes et al, 1980; Makh et al, 1982).

The dependence of depth resolution on the sputtered depth is, in general, in accordance with the SLS model described by equation (2.4), where $\Delta z \propto z^{\frac{1}{2}}$. However, the monolayer thickness a is approximately 3 - 4 times higher than expected where for one ion gun analysis a = 6.3Å, and for two ion guns a = 4.9Å. Thus, several contributing factors,

other than purely statistical sputtering are operating and therefore the results should more adequately be described by equation (2.5). The depth resolution can never be better than the escape depth of the Auger electrons and the ion-induced atomic mixing effects. To quantitatively assess their contributions toward interface distortion it is recommended that materials with uniform sputtering properties be employed, so that a good reference may be provided for polycrystalline samples where surface roughness contributions may be significant.

CHAPTER 3

3.1 A General Theory on the Dependence of Depth Resolution on Ion and Electron Beam Geometry

3.1.1 Introduction

The in-depth distribution of atoms is crucial to the examination and chemical characterisation of thin films, metal-film interfaces and ion implanted targets. The most common method for obtaining depth profiles is by the combined use of sputter-etching and surface analysis (viz AES, ESCA, SIMS). The technique most frequently used and best suited for elemental depth profile analysis is AES, since this has a small spot size for analysis (typically 3 - 10μm in diameter), and a short data acquisition time (Mathieu and Landolt, 1979). Ideally, the depth resolution of sputter-depth profiles should be constant and should be given simply by the inelastic mean free path. In practice it is found that the depth resolution deteriorates with increasing depth (Smith and Walls, 1979; Hofmann, 1981, Seah and Hunt, 1983). Many mechanisms contribute to the deterioration of the depth resolution which are related to the sample itself and these include the effects of initial surface shape (Makh et al, 1980; Seah and Lea, 1981; Whitton and Grant, 1981; Sykes et al, 1980) and roughness (Laty et al, 1979), the movement of material to different depths by mixing (Sigmund and Gras-Marti, 1980), radiation enhanced diffusion (Webb et al, 1978) and the formation of ion-induced topography. (Mathieu et al, 1976;

Smith and Walls, 1979.) If a quantitative measure of each of these contributions can be given, the total or measured depth resolution can be calculated. Assuming that the individual contributions Δz_i are independent of each other and may be approximated by a Gaussian function, the total depth resolution Δz is given by (Hofmann, 1977):

$$\Delta z^2 = \sum_{1=1}^{N} \Delta z_i^{\,2} \qquad (1)$$

Other factors influencing depth resolution are purely instrumental and these can be controlled and optimised. For example in AES (and also ESCA), an ion beam from a hot-filament type source is often used in static mode to etch a crater in the surface. The depth profile is then obtained by using a fine electron beam to probe the base of the crater. The inherent problem in analyses such as these is the specific shape of the ion etched crater.

The radial beam intensity distribution is often represented by a Gaussian function (Hofmann, 1977, Smith and Walls, 1979), and when such a non-uniform beam is incident on a target surface, the resulting eroded crater will have a sloping cross section resembling the distribution of intensity. This can result in an edge-effect occurring, whereby a contribution is obtained from the crater walls as well as the bottom of the crater, thus a distortion in the composition-depth profile results.

There are several methods available that avoid edge-effects from the crater walls, and have been discussed in detail by Liebl (1975).

One particularly common technique used to produce a more ideally, flatter-bottomed crater is by rastering the ion-beam across the target surface (e.g. T.V. scan). This, however, due to inevitable reductions in the effective ion current density, decreases the sputtering rate which can involve long sputtering times where very deep profiles (several microns) are required.

There are techniques employed that overcome the problem of long sputtering times when investigating interfaces below several microns, and these are methods that incorporate the use of mechanical lapping. One such method involves mechanically polishing a taper section through a region of interest thereby creating a surface for analysis (Lea and Seah, 1981). By laterally scanning an electron beam across this surface the elemental composition can be monitored in the usual way. An advantage of this method is that samples with initially unknown trace impurities may be analysed over a larger sample region than would normally occur in sputter depth profiles, thereby increasing the probability of finding a trace impurity.

Fig. 3.1 illustrates schematically a taper section through two material layers A and B, and indicates how the depth resolution Δz is limited by the cross-section of the electron beam on the sloping surface. The value of α is typically in the range 0.1 - 1°. A detailed study reporting on the relative merits of ion sputtering and angle lapping for surface analysis is given elsewhere (Lea and Seah, 1981).

A similar technique that has recently been described by Thompson et al (1979) and developed for surface analysis applications by Walls et al (1979) is ball cratering. This technique uses a rotating

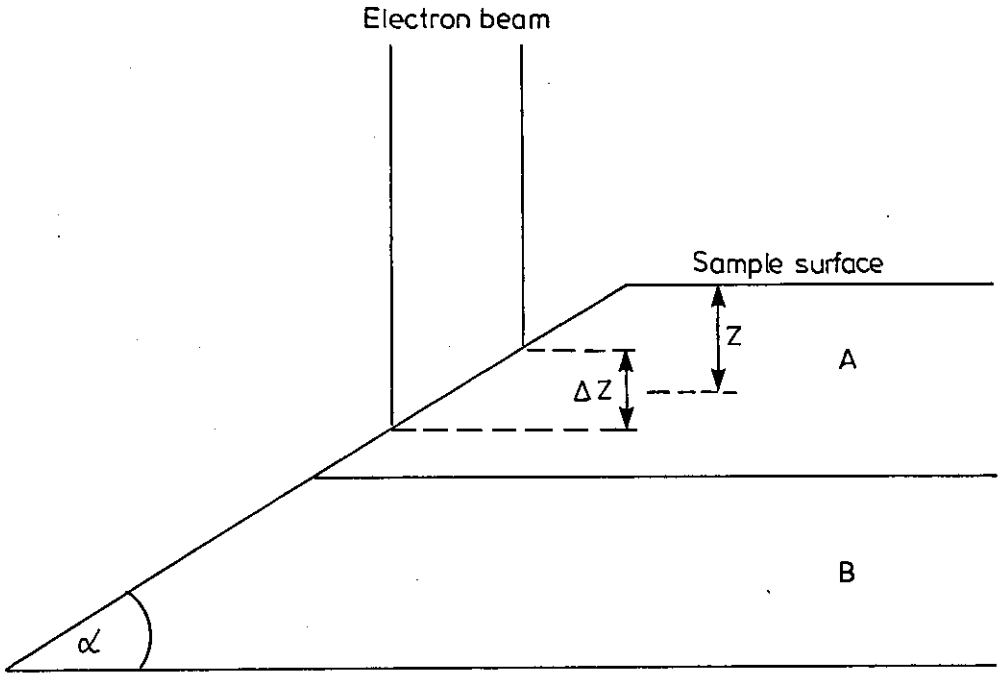

Figure 3.1: AES depth-profiling using a mechanically lapped taper angle α through an interface between two components A and B. Depth resolution Δz is limited by electron beam size.

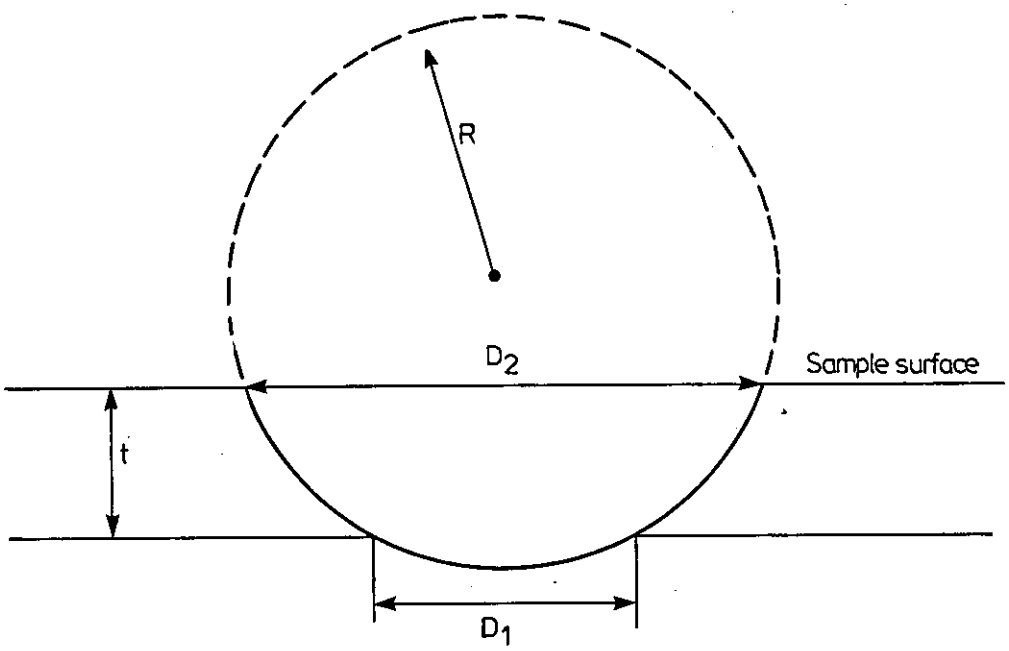

$d = D_2^2/8R$ (IF $R \gg d$)

$t = (D_2^2 - D^2)/8R$

Figure 3.2: A schematic diagram illustrating the geometry of a ball-crater through a surface coating of thickness t.

steel ball coated with fine diamond paste (0.1 - 1μm) to erode a well defined crater of spherical cross-section in the sample surface (see Fig. 3.2). Depth profiles may be obtained by point-to-point analysis down the crater walls, or by scanning the electron beam across the crater diameter to five elemental line scans. Both ball-cratering and angle lapping are the more generally preferred techniques when the depth of analysis is > 5μm. Studies on the determination of the depth resolution have been mostly concerned with the contribution of the sample roughness, the magnitude of which, being dependent on the polishing process (Lea and Seah, 1981; Brown et al, 1981).

An analogous in-depth profile technique to ball-cratering and angle lapping, is crater-edge profiling which was first described by Taylor et al (1976), in their work in Si-SiO_2 films. This method involves completely exposing the interfacial region by ion sputtering, and subsequent analysis being achieved by scanning the electron beam across the crater profile. Its major advantage over mechanical lapping techniques is that the angle subtended by the surface and the interface is generally three orders of magnitude less, thereby greatly increasing the lateral resolution (see Fig. 3.3). In a study by Zalar and Hofmann (1980) on Ni/Cr films it was deduced that lateral magnification factors of $> 10^3$ could be obtained. This was attributed to a small crater edge angle (< 5') and a small electron beam size ($\lesssim$ 10μm), normally used in the scanning mode. Their concern was also in the calculation of the relative depth resolution which, with a normally incident electron beam diameter of 100μm, and misaligned by 500μm relative to the

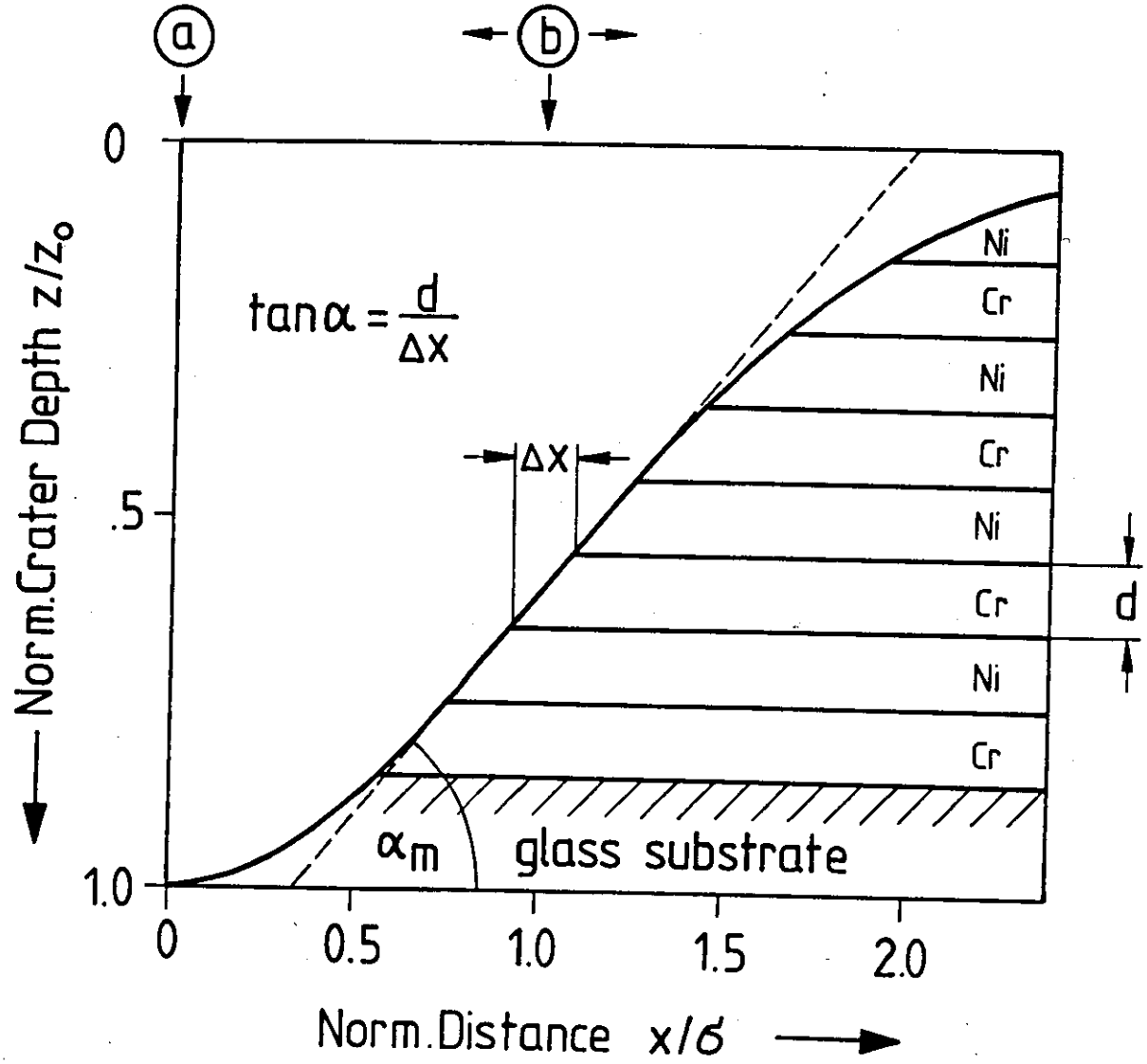

Figure 3.3: Principle of crater edge profiling: normalized crater depth z/z_0 as a function of the normalized distance x/σ from the centre if the assumed profile has a Gaussian shape with standard deviation σ. Optimum depth resolution is obtained with an electron beam at a), b) visualises the scanning position used for crater edge profiling. This particular example illustrates a crater of maximum slope α_m sectioning a multilayer Ni/Cr structure (after Zalar and Hofmann, 1980).

centre of the crater ((a) in Fig. 3.3), was found to be 5%. This value is reduced to 1% for a beam diameter of 5μm and a misalignment of $\leqslant$ 2nm. It would appear therefore, that crater-edge profiling relies on small electron beam sizes and uniformity of ion erosion for optimum depth resolution.

Crater-edge profiling requires that analysis is done at some point along the crater wall, therefore the probing electron beam is effectively misaligned from the maximum point of intensity of the ion beam ((a) in Fig. 3.3). A similar, but unintentional effect can sometimes occur in normal sputter-depth profiling. A misalignment between the electron and ion beam may be the result of machine or operator error, or by local charging effects on insulators, where the electron beam may undergo a deflection. Further, it is often necessary, particularly with insulators to increase the electron beam size in order to reduce beam damage but retain the overall signal. In both cases there is a contribution to the crater-edge effect, and it is important that they are optimised. Hoffmann (1975) developed a numerical procedure that enabled the treatment of depth profiles obtained by sputtering with an ion beam of non-uniform current density. This method, as noted in a later paper (Hoffmann et al, 1980) did not receive widespread application because of the requirement for information about the current density distribution, and also a preference by investigators for experimental remedies to the problem of edge effects. Tsong et al (1980) developed a numerical integration procedure from Hoffman's (1975) initial mathematical treatment, that corrected edge-effects in depth profiles. The procedure included a parameter characterising the ion beam and

detector, which could be determined from the depth profile of a standard sharp interface (e.g. a SiO_2 film on silicon). These studies, however, did not calculate the dependence of depth resolution on instrumental parameters.

More recently Malherbe et al (1981) have demonstrated that the depth resolution can be determined by the precise geometrical relationship between the ion and electron beams, and their relative sizes. They have, however, only considered the simple case where the ion beam is incident normal to the surface. In practice this geometry is seldom used particularly in instruments where a cylindrical mirror analyser is used with an integral electron gun.

In the following sections of this chapter, a general theoretical analysis is presented which enables the integrity of depth-profiles to be assessed as a function of several instrumental parameters. The dependence of depth resolution is determined for a range of conditions including the relative sizes of the ion and electron beams and their respective angles to the sample surface and the effect of misalignment between the two beams.

3.1.2 The Model

Consider an ion flux ψ ions cm^{-2} sec^{-1} incident on a surface in the z-direction, and at some angle ϕ to the surface normal as shown schematically in Figure 3.4. If the sputtering yield S is assumed to depend only on the angle of incidence of the ions, and the flux to depend on the x and y directions then the rate of erosion in the surface normal direction is $\psi k.n/N$, where n is the unit normal to the surface,

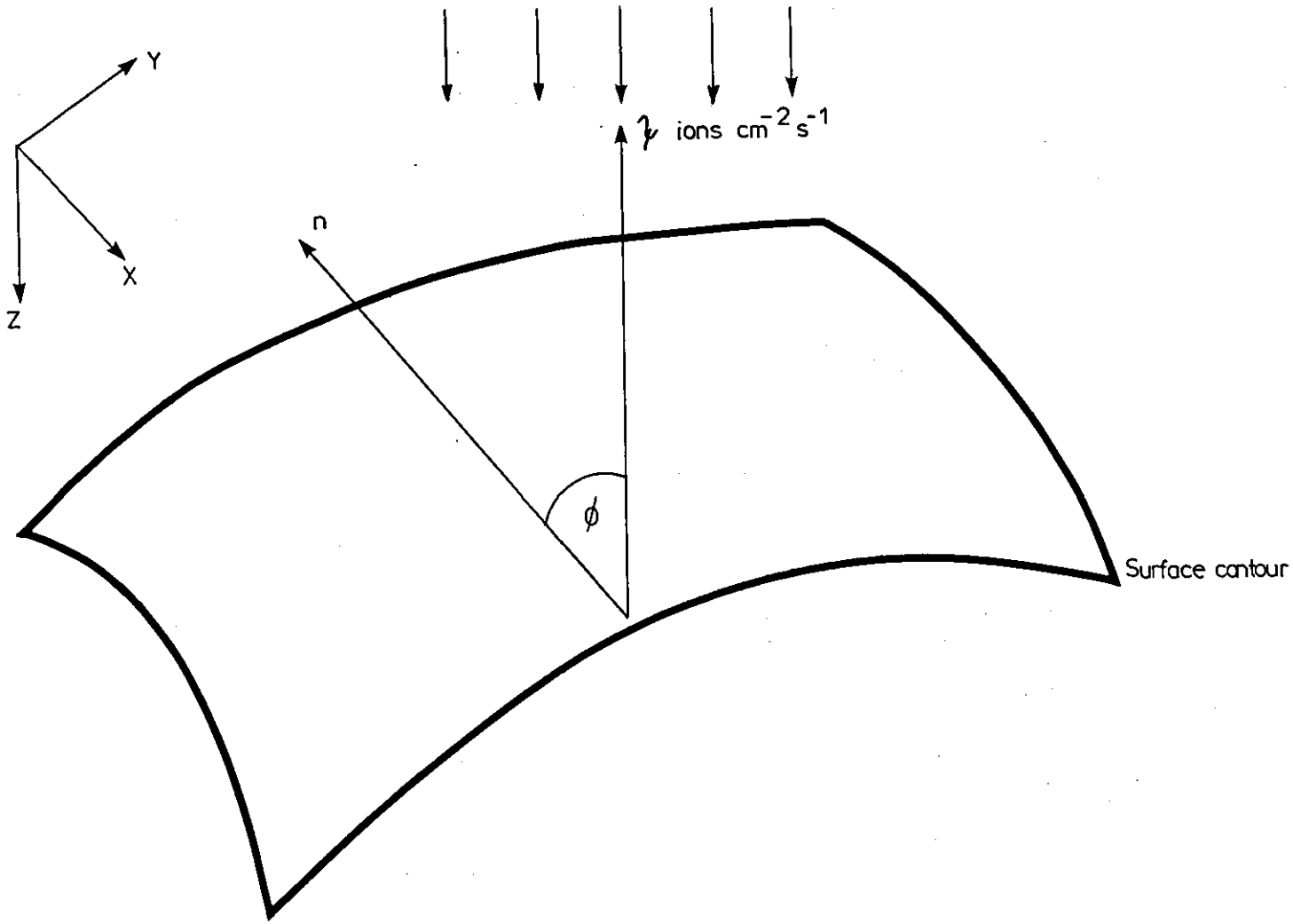

Figure 3.4. The erosion of a surface contour during ion sputtering.

k is the unit vector in the z-direction and N is the atomic density of the target. This may further be represented as a differential equation (Smith and Walls, 1979)

$$\left(\frac{\partial z}{\partial t}\right) = -(\psi/N)\ S(\phi)\ \cos\phi \qquad (3.1)$$

where t is the sputtering time.

For an initially flat surface of a pure material the sputtered crater will be Gaussian in shape (Hofmann, 1981) and extremely shallow and smooth. Thus for depths of $\leqslant$ 5μm normal to the surface the angle ϕ becomes negligible and can be considered constant to a first approximation.

For a Gaussian beam the current has spatial distributions given by:

$$J = J_0 \exp\left[-(x^2 + y^2)/\rho^2\right] \qquad (3.2)$$

where ρ is the variance of the beam.

J_0 is the maximum current density.

The contribution of this current to the unsputtered surface normal can be determined by a rotation through the angle ϕ about the y-axis, so that the z-direction is aligned with n, the unit normal to the surface. Equation (3.2) now becomes:

$$J = J_0 \exp\left\{-\left[(x\cos\phi - z\sin\phi)^2 + y^2\right]/\rho^2\right\} \qquad (3.3)$$

If z is small, and by the relation $\psi = J/e$ (where e is the electronic charge), then by integrating equation (3.2) the approximate depth of the crater

may be given by:

$$z(x,y) = -S(\phi)\cos\phi J_0 t/(qN)\exp\{-x^2/a'^2 - y^2/b'^2\} \qquad (3.5)$$

The constants a' and b' are related to the beam variance by $a' = p\sec\phi$, $b' = p$, and the co-ordinate system (x,y,z) chosen so that z is perpendicular to the surface and x and y define directions along the major and minor axes of the elliptical contours of the crater.

The analysing electron beam is assumed to have circular cross-section σ, and angle of incidence to the surface normal ϕ_1. In practice the current distribution in the electron beam is likely to be Gaussian and in this case it may be appropriate to identify σ as a characteristic dimension associated with the electron beam, for example the value of r at which the current reduces to 16% of its maximum value, where r is the radial distance from the central axis of the beam. For a shallow crater the electron beam intersects the surface in the curve

$$\frac{x'^2}{a^2} + \frac{y'^2}{b^2} = 1 \qquad (3.6)$$

The values of a and b are related to the electron beam variance by $a = \sigma\sec\phi_1$, $b = \sigma$.

Consider Figure 3.5 where the co-ordinate directions x' and y' are centred at the point of intersection of the centre of the electron beam with the surface, and incident at angle θ with respect to ion-beam co-ordinates directions (x", y"). Let a point P in electron beam space have co-ordinates (x', y'), and (x", y") in ion beam space.

Then expressing (x', y') in terms of (x'', y'') gives:

$$x' = OA + AB$$

$$= x'' \cos\theta + y'' \sin\theta \tag{3.7}$$

$$\begin{cases} AB \equiv CD \\ CD = y'' \sin\theta \\ BD \equiv AC \\ AC = x'' \sin\theta \end{cases}$$

$$y' = PD - BD$$

$$= y'' \cos\theta - x'' \cos\theta \tag{3.8}$$

Now consider the case when the electron beam is misaligned with respect to the ion beam as shown schematically in figure 3.6 (a), where

$$x'' = x - x_m \tag{3.9}$$

$$y'' = y - y_m \tag{3.10}$$

Substituting for x'', y'' from equations (3.9) and (3.10) in equations (3.7) and (3.8) gives:

$$x' = (x - x_m) \cos\theta + (y - y_m) \sin\theta \tag{3.11}$$

$$y' = (y - y_m) \cos\theta + (x - x_m) \sin\theta \tag{3.12}$$

The angle θ, cannot be measured directly but is calculated implicitly from the direction cosines (with respect to (x, y, z) co-ordinates) of the ion and electron beams. Defining these direction cosines as (l_1, m_1, n_1) and (l_2, m_2, n_2) respectively then from figure 3.6(b)

$$d.c_{(i)} = (\sin\phi, 0, \cos\phi) \tag{3.13}$$

$$d.c_{(e)} = (l_2, m_2, \cos\phi_1) \tag{3.14}$$

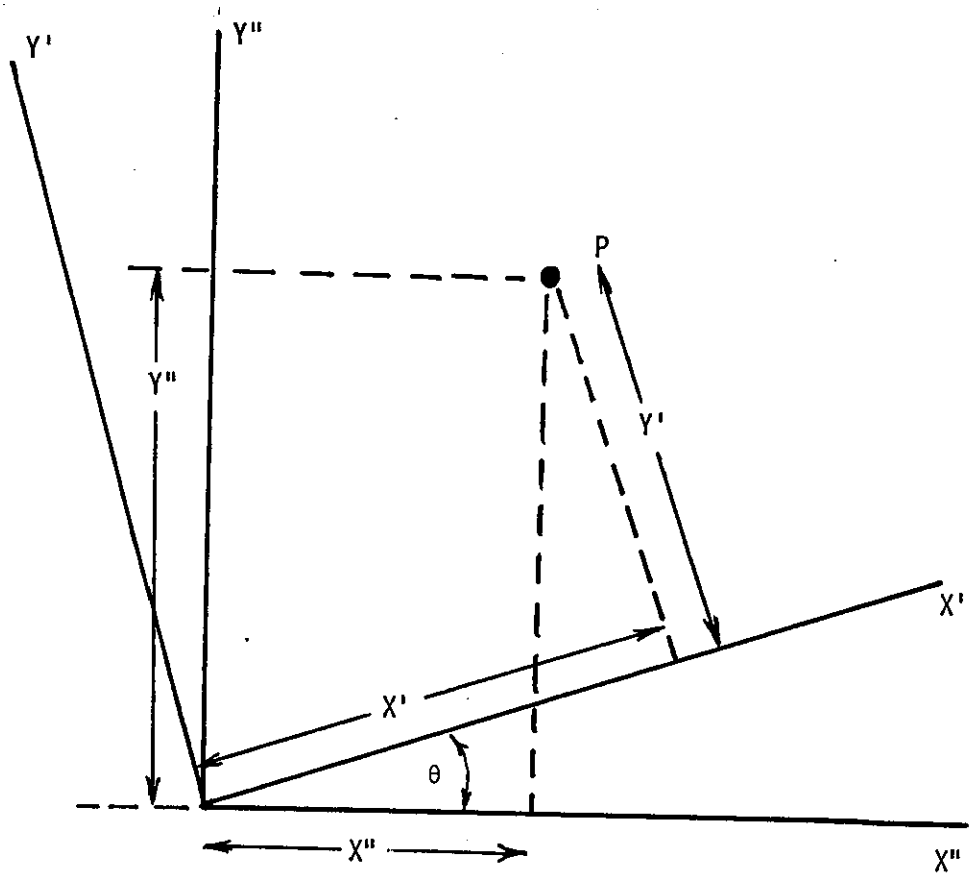

Figure 3.5 : A representation of the co-ordinate system of the ion and electron beams in an AES system.

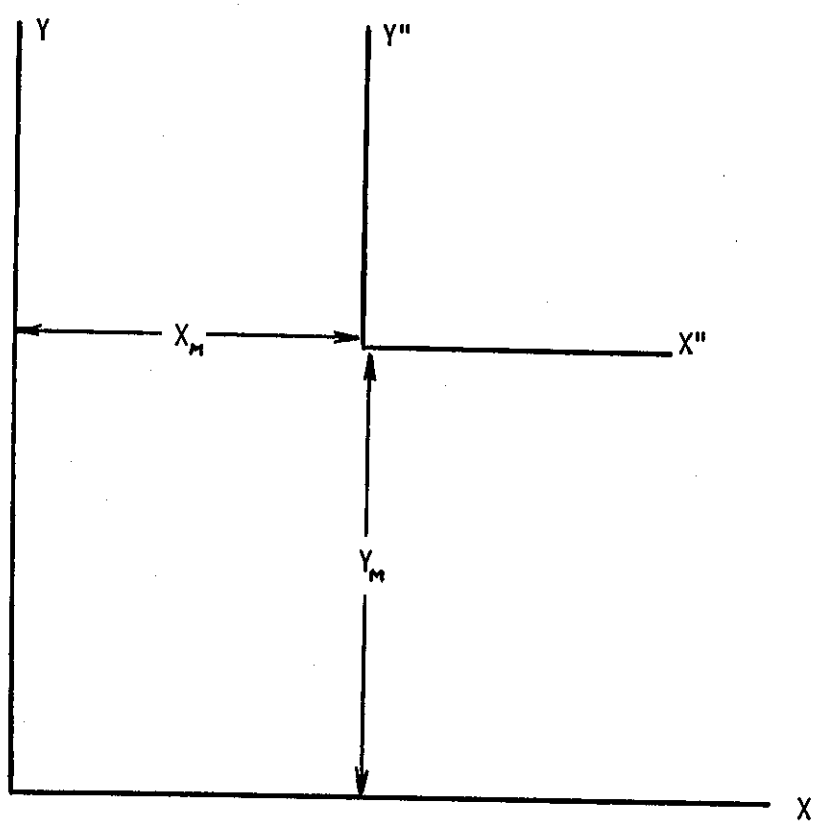

Figure 3.6(a): A diagram showing a misalignment between the ion and electron beam systems.

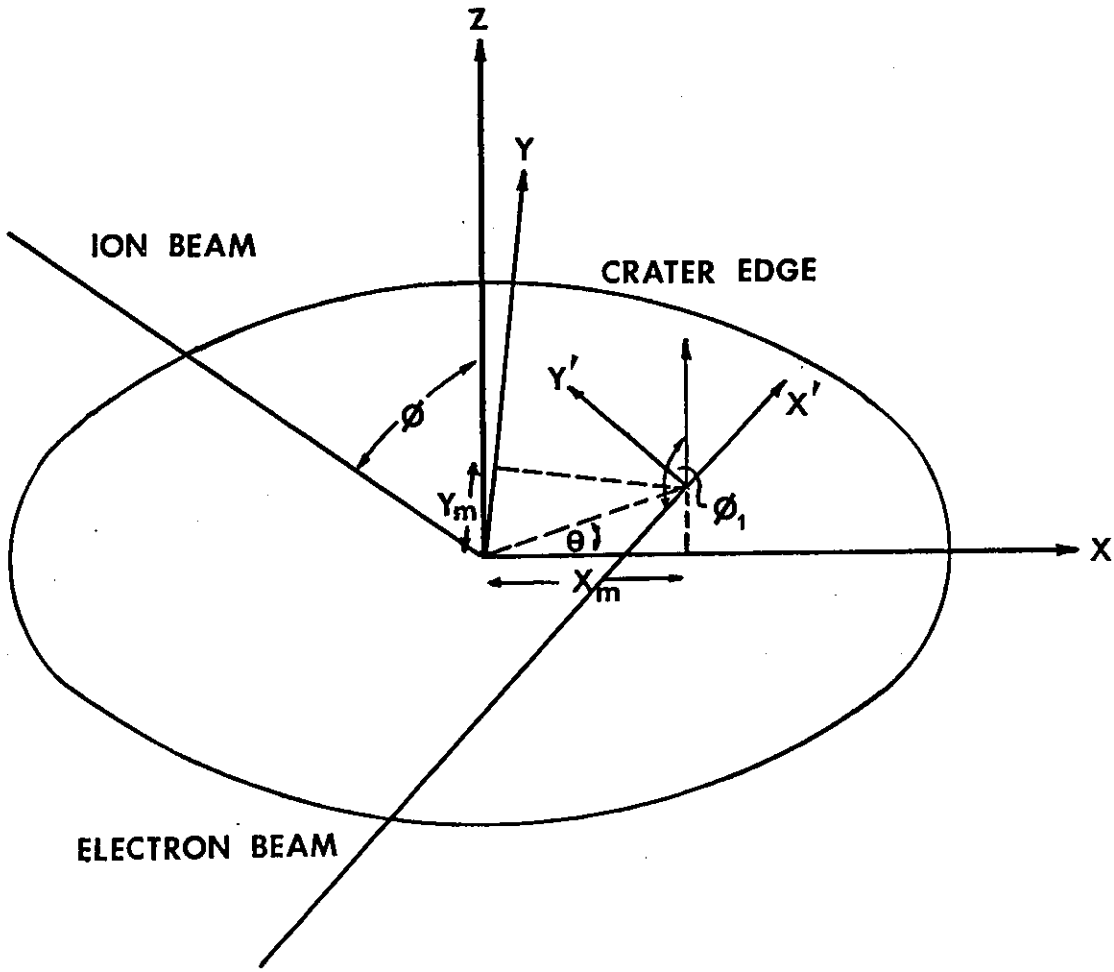

Figure 3.6(b): Co-ordinate system of an electron beam incident at angle ϕ to the normal and at a position (x_m, y_m) on the sample surface.

where the subscripts (i) and (e) represent the ion and electron beams respectively. Using the property that $l_1 l_2 + m_1 m_2 + n_1 n_2 = \cos\phi_2$ it can be shown by appropriate substitution from equations (3.13) and (3.14) that:

$$l_2 = \frac{\cos\phi_2 - \cos\phi \cos\phi_1}{\sin\phi} \tag{3.15}$$

and $l^2_2 + m^2_2 + n^2_2 = 1$ such that:

$$m_2 = (\sin^2\phi_1 - l_2^2)^{\frac{1}{2}} \tag{3.16}$$

The direction cosines of y' are ($\sin\theta$, $\cos\theta$, 0), thus using above vector analysis properties:

$$l_2 \sin\theta + m_2 \cos\theta = 0$$

$$\tan\theta = -\frac{m_2}{l_2} \tag{3.17}$$

By a substitution of equations (3.15) and (3.16) into equation (3.17) the value of θ is given by:

$$\theta = \tan^{-1}\left[\frac{-(\sin^2\phi_1 - l^2_2)^{\frac{1}{2}}}{l_2}\right] \tag{3.18}$$

In the following analysis the depth resolution is defined as the difference between the maximum and minimum z-values of equation (3.5) over the area of intersection of the electron beam on the crater surface. This is therefore a different quantity to that defined by Malherbe et al (1981) who consider an integrated signal from profiling through an interface, the depth resolution Δz being defined as the increase in sputtering depth when the signal has decreased from a value of 84.13%

to 15.87% of the original signal, and the relative depth resolution is obtained by dividing Δz by the distance z at which the signal decreases to 50% of its original value.

In the present work the maximum and minimum z-values, that occur on the line of intersection of the edge of the electron beam with the crater (shown schematically in figure 3.7), can be regarded as a decrease in signal from 100% to 0% in comparison to the work presented by Malherbe et al (1981). The stationary values of z are determined using the method of Lagrange multipliers, thus equation (3.5) is subject to a constraint described by equation (3.6) and becomes:

$$z = \frac{S(\phi)\cos\phi\, J_o}{qN}\, t \exp\{-x^2/a'^2 - y^2/b'^2\}$$

$$+ \lambda\{x'^2/a^2 + y'^2/b^2 - 1\} \qquad (3.19)$$

Letting equation (3.19) take the form $W = z + \lambda u$, and a substituting for x' and y' from equations (3.11) and (3.12) into equation (3.19), the stationary values may be found by equating the partial expressions to zero.

$$\frac{\partial W}{\partial x} = \frac{-2x}{a'^2} z + \lambda\left\{2\left[\frac{(x - x_m)\cos\theta + (y - y_m)\sin\theta}{a^2}\right]\cos\theta + 2\left[\frac{(y - y_m)\cos\theta - (x - x_m)\sin\theta}{b^2}\right] - \sin\theta\right\} = 0 \qquad (3.20)$$

$$\frac{\partial W}{\partial y} = \frac{-2y}{b'^2} z + \lambda\left\{2\left[\frac{(x - x_m)\cos\theta + (y - y_m)\sin\theta}{a^2}\right]\sin\theta + 2\left[\frac{(y - y_m)\cos\theta - (x - x_m)\sin\theta}{b^2}\right]\cos\theta\right\} = 0 \qquad (3.21)$$

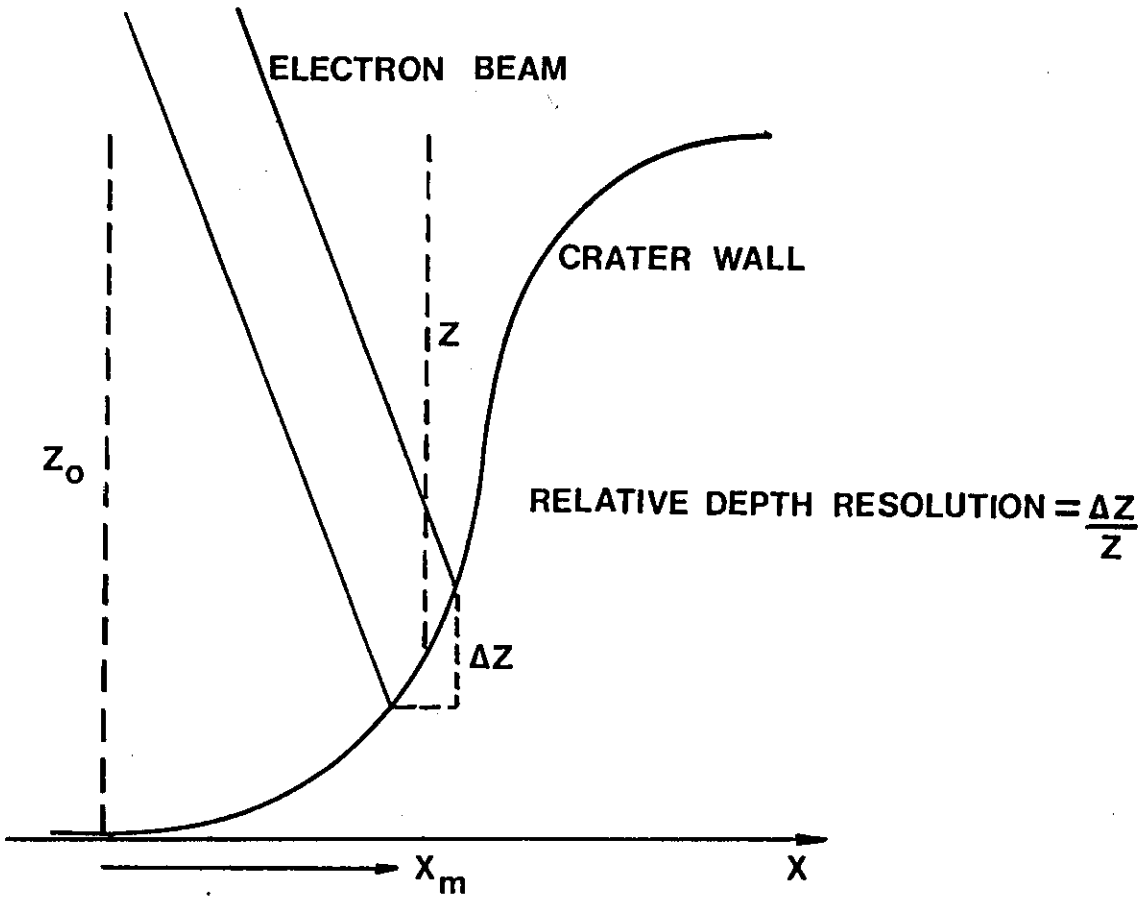

Figure 3.7: A schematic diagram illustrating the way in which depth resolution has been defined by consider a section of the sputtered crater in the x-direction.

Equations (3.20) and (3.21) reduce further, and subsequent division leads to:

$$\frac{(x - x_m)\alpha_1 + (y - y_m)\alpha_2}{(x - x_m)\alpha_2 + (y - y_m)\alpha_3} = \frac{xb'^2}{ya'^2} \tag{3.22}$$

where $\alpha_1 = \frac{\cos^2\theta}{a^2} + \frac{\sin^2\theta}{b^2}$

$$\alpha_2 = (\cos\theta \sin\theta) \left(\frac{1}{a^2} - \frac{1}{b^2}\right)$$

$$\alpha_3 = \frac{\sin^2\theta}{a^2} + \frac{\cos^2\theta}{b^2}$$

An expression describing y in terms of x may now be obtained by expanding equation (3.6) by a substitution for x' and y' from equations (3.11) and (3.12).

$$\alpha_1(x^2 + x_m^2) + \alpha_3(y^2 + y_m^2) - 2\alpha_2(xy - xy_m - x_m y + x_m y_m) - 2xx_m\alpha_1 - 2yy_m\alpha_3 = 0 \tag{3.23}$$

Secondly, equation (3.22) may be expanded to:

$$b'^2\alpha_2(x^2 - xx_m) - a'^2\alpha_2(y^2 - y_m y) + b'^2\alpha_3(xy - xy_m) - a'^2\alpha_1(xy - x_m y) = 0 \tag{3.24}$$

By multiplying equation (3.23) by $-a'^2\alpha_2$, and equation (3.24) by α_3, the terms in y^2 may be eliminated by adding the resulting

expressions hence:

$$y = (\delta_2 x - \delta_1 x^2 - \delta_5) / (\delta_4 x + \delta_3) \tag{3.25}$$

where $\delta_1 = (a'^2\alpha_1\alpha_2 + b'^2\alpha_2\alpha_3)$

$$\delta_2 = 2a'^2\alpha_2(\alpha_1 x_m + \alpha_2 y_m) + b'^2\alpha_3(\alpha_2 x_m + \alpha_3 y_m)$$

$$\delta_3 = a'^2\alpha_3(\alpha_1 x_m - \alpha_2 y_m) - 2a'^2\alpha_2^2 x_m$$

$$\delta_4 = a'^2(2\alpha_2^2 - \alpha_1\alpha_3) + b'^2\alpha_3^2$$

$$\delta_5 = a'^2\alpha_2(\alpha_1 x^2_m + \alpha_3 y^2_m + 2\alpha_2 x_m y_m - 1)$$

A substitution of y from equation (3.25) into equation (3.23) results in a quartic equation in x of the form:

$$\beta_1 x^4 + \beta_2 x^3 + \beta_3 x^2 + \beta_4 x + \beta_5 = 0 \tag{3.26}$$

where $\beta_1 = \alpha_1\delta_4^2 + \alpha_3\delta_1^2 - 2\alpha_2\delta_1\delta_4$

$$\beta_2 = 2\{\alpha_1(\delta_2\delta_3 - x_m\delta_4^2) + \alpha_2(\delta_2\delta_4 - \delta_1\delta_3 - \delta_4^2 y_m$$

$$+ x_m\delta_1\delta_4) - \alpha_3(\delta_1\delta_2 - \delta_1\delta_4 y_m)\}$$

$$\beta_3 = \alpha_1(x_m^2\delta_4^2 + \delta_3^2 - 4x_m\delta_3\delta_4) + 2\alpha_2(\delta_2\delta_3 - \delta_4\delta_5$$

$$- 2\delta_3\delta_4 y_m - \delta_2\delta_3 x_m + \delta_1\delta_3 x_m + x_m y_m\delta_4^2) + \alpha_3(2\delta_1\delta_5$$

$$+ \delta_5^2 + y_m^2\delta_4^2 - 2y_m\delta_2\delta_4 + 2y_m\delta_1\delta_3) - \delta_4^2$$

$$\beta_4 = 2\{\alpha_1(\delta_3\delta_4 x_m^2 - x_m\delta_3^2) - \alpha_2(\delta_3\delta_5 + y_m\delta_3^2 + x_m\delta_2\delta_3$$

$$- x_m\delta_4\delta_5 - 2x_m y_m\delta_3\delta_4) - \alpha_3(\delta_2\delta_5 - \delta_3\delta_4 y_m^2 + \delta_2\delta_3 y_m$$

$$- \delta_4\delta_5 y_m) - \delta_3\delta_4 \}$$

$$\beta_5 = \alpha_1(x_m{}^2\delta_3{}^2) + 2\alpha_2(x_m\delta_3\delta_5 + x_m y_m\delta_3{}^2) + \alpha_3(\delta_5{}^2$$

$$+ y_m{}^2\delta_3{}^2 + 2y_m\delta_3\delta_5) - \delta_3{}^2$$

This quartic equation for x can be solved numerically by computer, and the values of x and y and hence depth z may be calculated. The depth resolution $\Delta z/z$ is obtained by dividing Δz by the value fo z at the centre of the electron beam as illustrated in figure 3.7. However, if the electron beam intersects the centre of the crater then the maximum z value (z_{max}) will be the z-value at the crater centre. In this case the depth resolution would be defined as $\Delta z = z_{max} - z_{min}$.

The present work described here also differs from that of Malherbe et al, in considering ion-etched craters for non-normally incident ion-beams, a situation common in many commercial systems. A comparison is made between these results later in the chapter.

3.1.3 Computational Results

The method used for determining depth resolution by simulation is a very versatile one, since although the solution of equation (3.26) can be determined with a high degree of precision, approximate values can also be attained schematically. This is illustrated for two general cases in figures 3.8(a) and 3.8(b), where an ion-etched crater of elliptical cross-section is represented by a series of contours spaced at 0.5% intervals of the depths at the crater centre. Thus the depth resolution is characterised by the number of contours covering the area of incidence of the excitation beam. For example, for the excitation

beam shape (100μm radius) in figure 3.8(a) approximately twelve contours are covered giving an approximate relative depth resolution of 7%. Figure 3.8(b) illustrates the versatility of this approximation method, where for an excitation beam size of half that in figure 3.8(a), the relative depth resolution is 8.5%, at a greater misalignment from the centre of the crater.

The first variable instrument parameter convenient to examine is the electron beam diameter. Figure 3.9 shows the dependence of the relative depth resolution on the electron to ion beam diameter ratio σ' (for a normalised crater variance), and incident angle ϕ, of the electron beam to the crater surface. In this example the crater was formed by an ion beam normal (i.e. $\phi = 0^{o}$) to the surface and whose centre is coincident with that of the electron beams. The area of spread of the electron beam over the crater determines the depth resolution, and this depends on the angle of incidence and diameter of the electron beam as illustrated in figures 3.8(a) and 3.8(b). Since the area of spread varies approximately as sec ϕ, the electron beam incidence angle can be an important factor, particularly near grazing incidence. This feature may be of more significance when near-surface depth-profiles are being carried out both in AES and ESCA, and is confirmed in figure 3.9. The loss in relative depth resolution obtained by increasing σ' from 0.1 to 0.2 when $\phi = 30^{o}$ is $\sim$ 5%, whereas when $\phi = 80^{o}$ the loss over this range is $\sim$ 50%, although this is probably an extreme case for most applications.

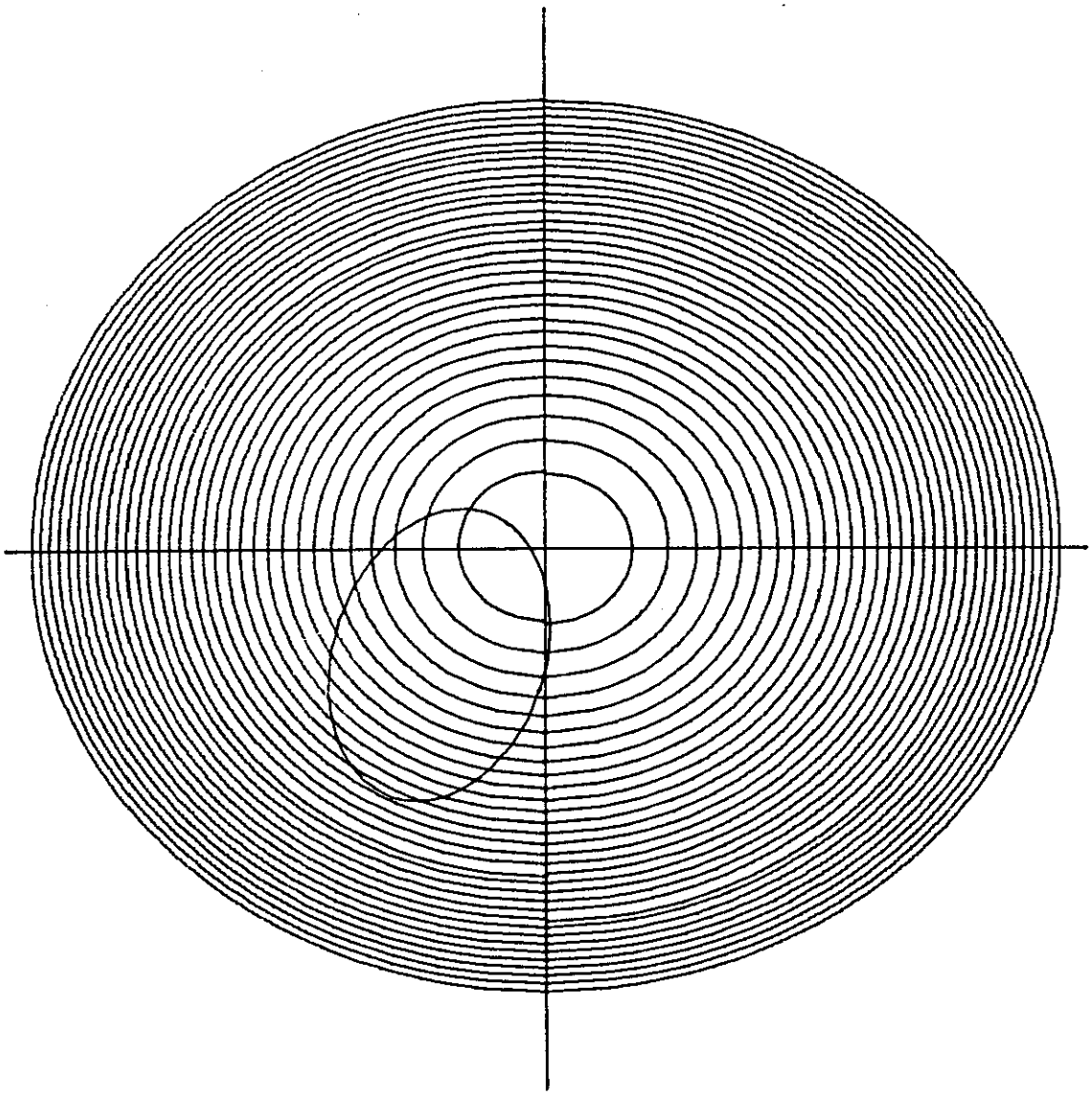

Figure 3.8(a): A relative depth contour plot of a sputtered Gaussian shaped crater formed by an ion beam incident at $\phi = 30^{o}$. Contour spacing is 0.5% of the total depth. The electron beam size is $\sigma = 50\mu m$ projected at an angle of $\phi_1 = 60^{o}$ and $\phi_2 = 60^{o}$.

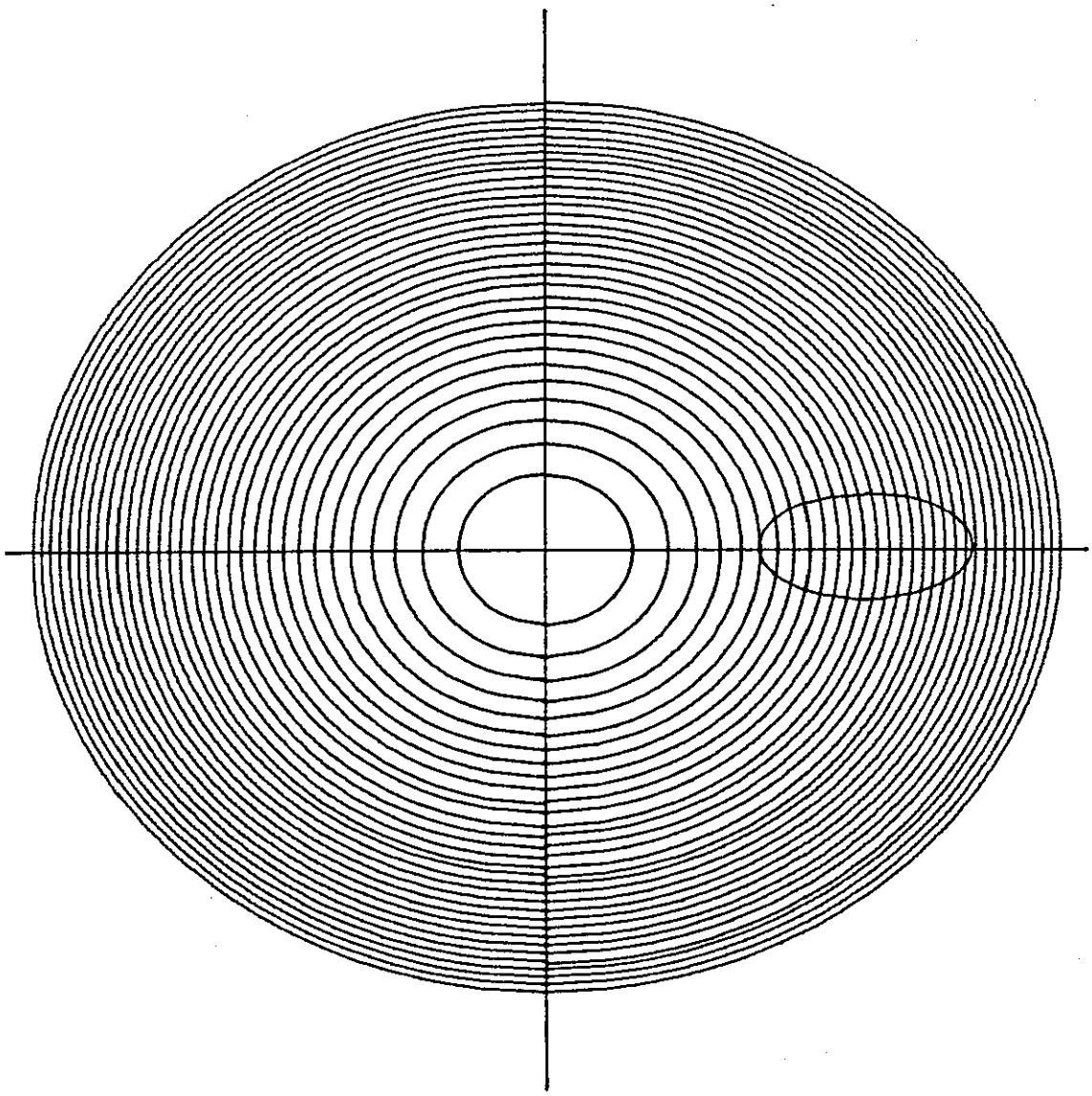

Figure 3.8(b): A relative depth contour plot showing the resolution obtained when an electron with σ = 25μm is projected at $\phi_1 = 60^o$, $\phi_2 = 90^o$ ($\phi = 30^o$).

The results shown in figure 3.9 illustrate one particular aspect of depth profiling that would contribute edge effects. Alternatively, a situation might arise where the ion and electron beams maximum intensity points do not coincide, thus the effective analysis will be a small, or total contribution from the crater walls, depending on the degree of misalignment. This effect is illustrated in figure 3.10, which shows a misalignment along the y-axis of a crater produced by a normally incident ion beam (indicated by the schematic diagram). The effect of increasing the electron to ion beam ratio is apparent from the loss in relative depth resolution. For example when $y_m/\rho = 0.4$ for $\sigma' = 0.005$ the loss is approximately five fold , whereas the degredation in depth resolution is clearly more prominent for larger σ' and in the same range of misalignment. The result obtained by Malherbe et al (1981) for $\sigma' = 0.021$ is shown to be in close agreement to the present work. Figure 3.10 considers the case of a relatively small misalignment and σ' applicable mainly in AES. It would therefore be pertinent to consider a case with larger values of σ' and misalignment, as might occur in ESCA. Figure 3.11 illustrates such a case, where the dependence of the depth resolution on larger values of misalignment and σ' is evident. Note also that in this case there is little difference between these results and those of Malherbe et al (1981) even though the definitions of depth resolution are different. In both figure 3.10 and 3.11, however, the same trends are evident.

As a complementary procedure to figure 3.9 - 3.11, it would be useful to examine the dependence of the depth resolution as a function

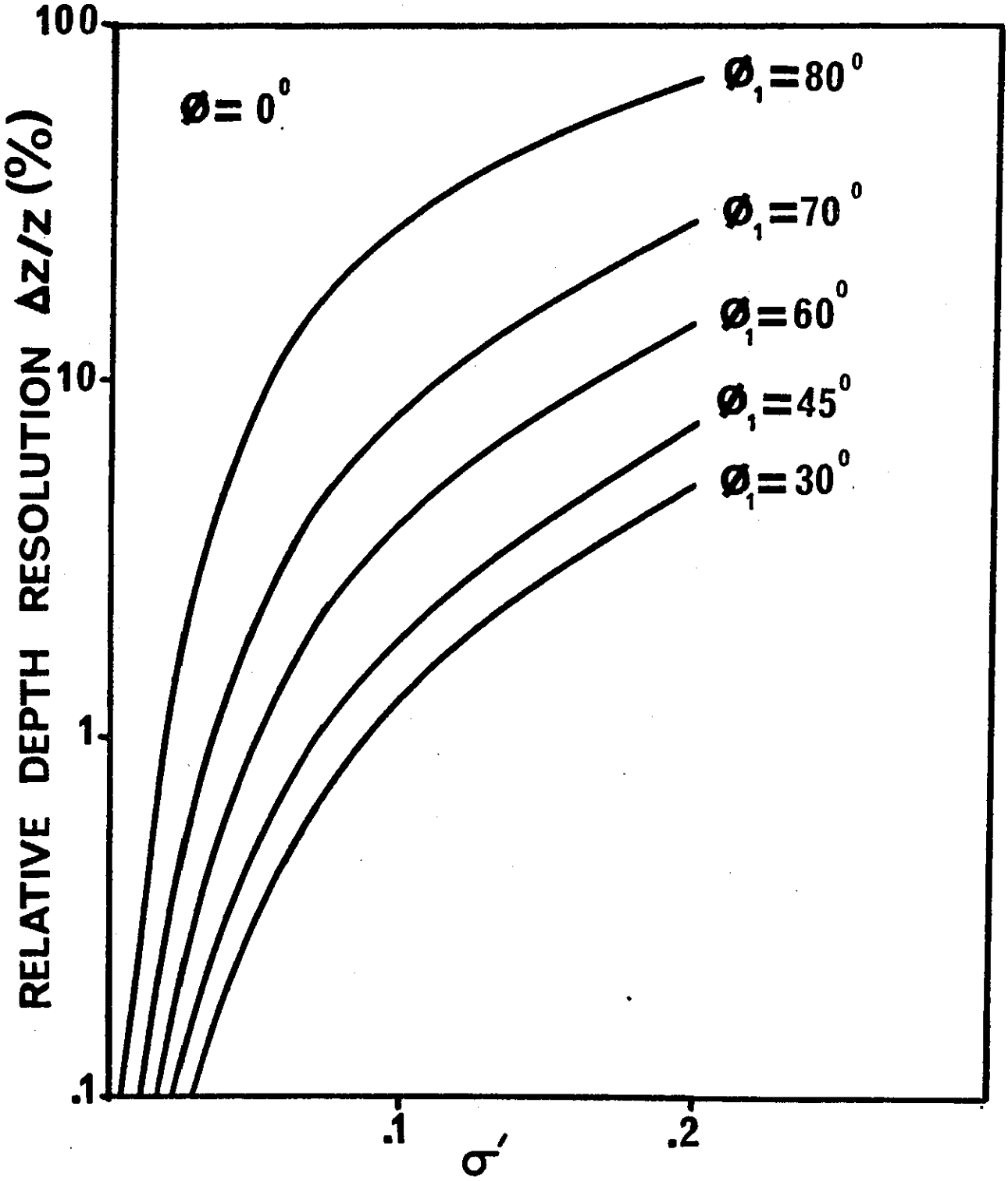

Figure 3.9: Plot of relative depth resolution as a function of σ', for various electron beam angles to the surface, and a crater formed by a normally incident ion beam.

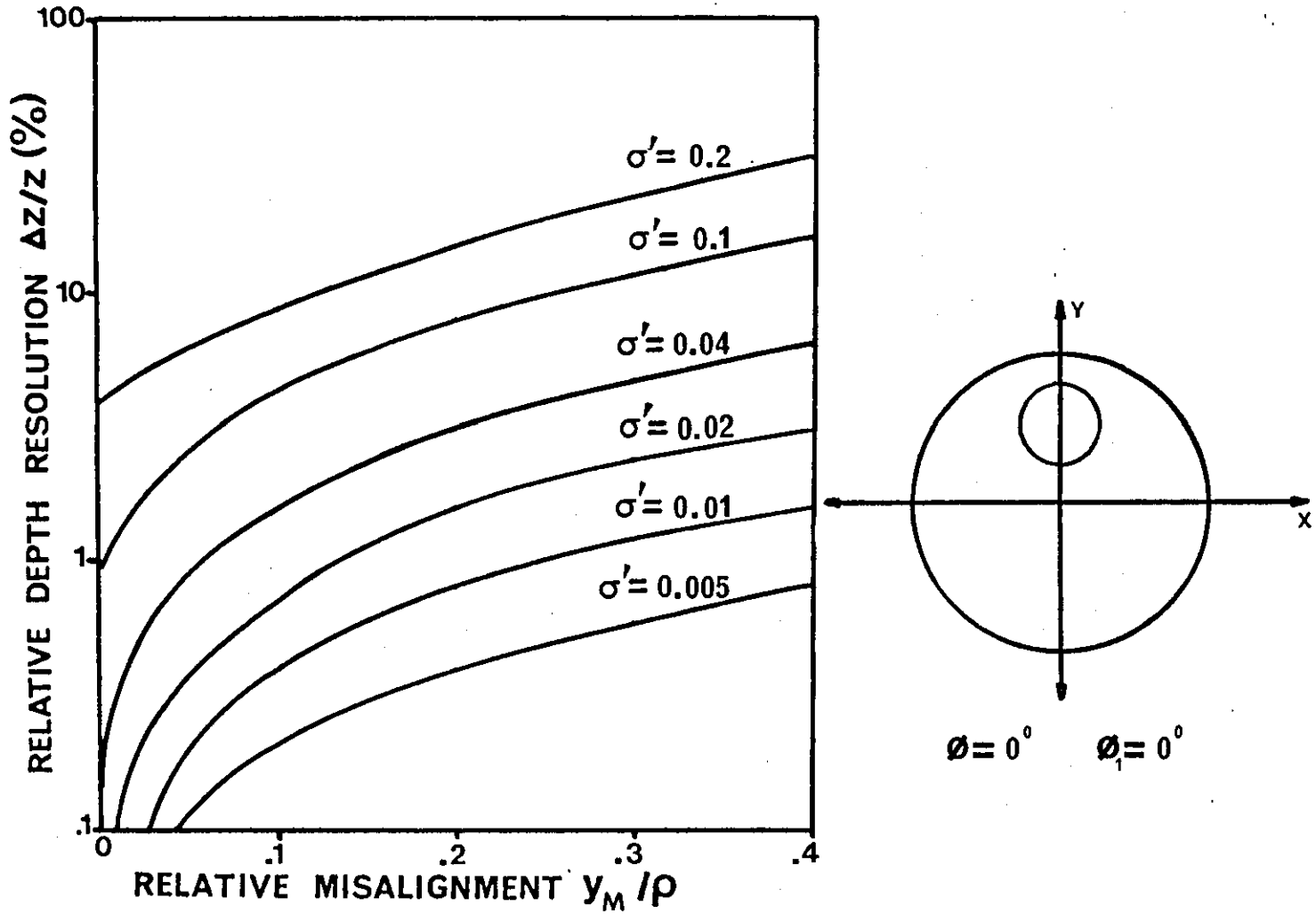

Figure 3.10: The effect of misalignment on relative depth resolution as a function of electron to ion beam ratio σ'.

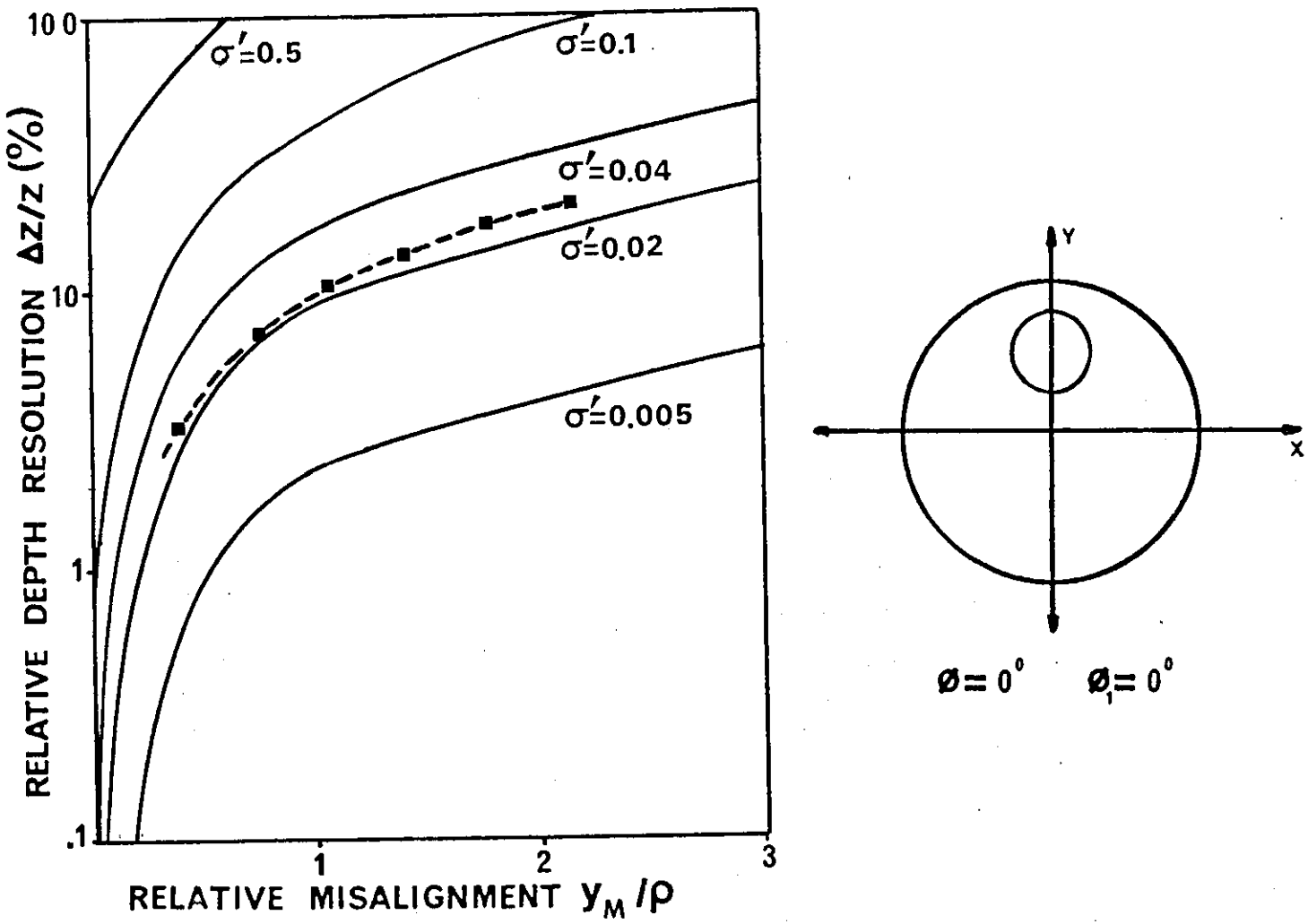

Figure 3.11: A plot of relative depth resolution against misalignment for electron to ion beam ratios (σ') more applicable to techniques such as ESCA. (----■----■Malherbe et al; result obtained for $\sigma' = 0.02$).

of misalignment and varying electron beam angles. This analysis is illustrated in figure 3.12 where for $\sigma' = 0.02$ and $\phi = 0^{o}$, the electron beam incidence angle is varied as a function of different misalignment parameters.

The results shown in figures 3.9 - 3.12 clearly indicate that the depth resolution is a sensitive function of the size of the electron beam, its angle of incidence and its position in the crater. This was also established by Malherbe et al (1981) and comparisons with their results are again in good agreement. However, the influence of the instrumental parameters on the depth resolution has so far only been examined for the case of normal incidence ($\phi = 0^{o}$). Generally, in most practical systems both the ion and electron beams are at some non-zero angle to the sample normal. Since the ion beam profile is initially circular it will etch a crater of approximately elliptical cross-section for non-normal incidence, as illustrated in figures 3.8(a) and 3.8(b). The physical significance of this is that the crater width along the axis parallel with the ion beam direction will increase, thus effectively making the crater flatter. The influence this has on the depth resolution can be demonstrated by a comparison to the $\phi = 0^{o}$ case, and the results of which are also illustrated in fig. 3.12. When the ion beam has an incident angle of 45° ($\phi = 45^{o}$), and the electron beam angle is $\phi_1 = 60^{o}$, then the degradation in relative depth resolution for a misalignment $x_m/\rho = 3$, is $\sim$ 24%, whereas for $\phi = 0^{o}$, $\phi_1 = 60^{o}$ and the same misalignment it is $\sim$ 48%. This clearly indicates that a lower profiled ion beam will cause less of a contribution from the crater walls if the misalignment takes place

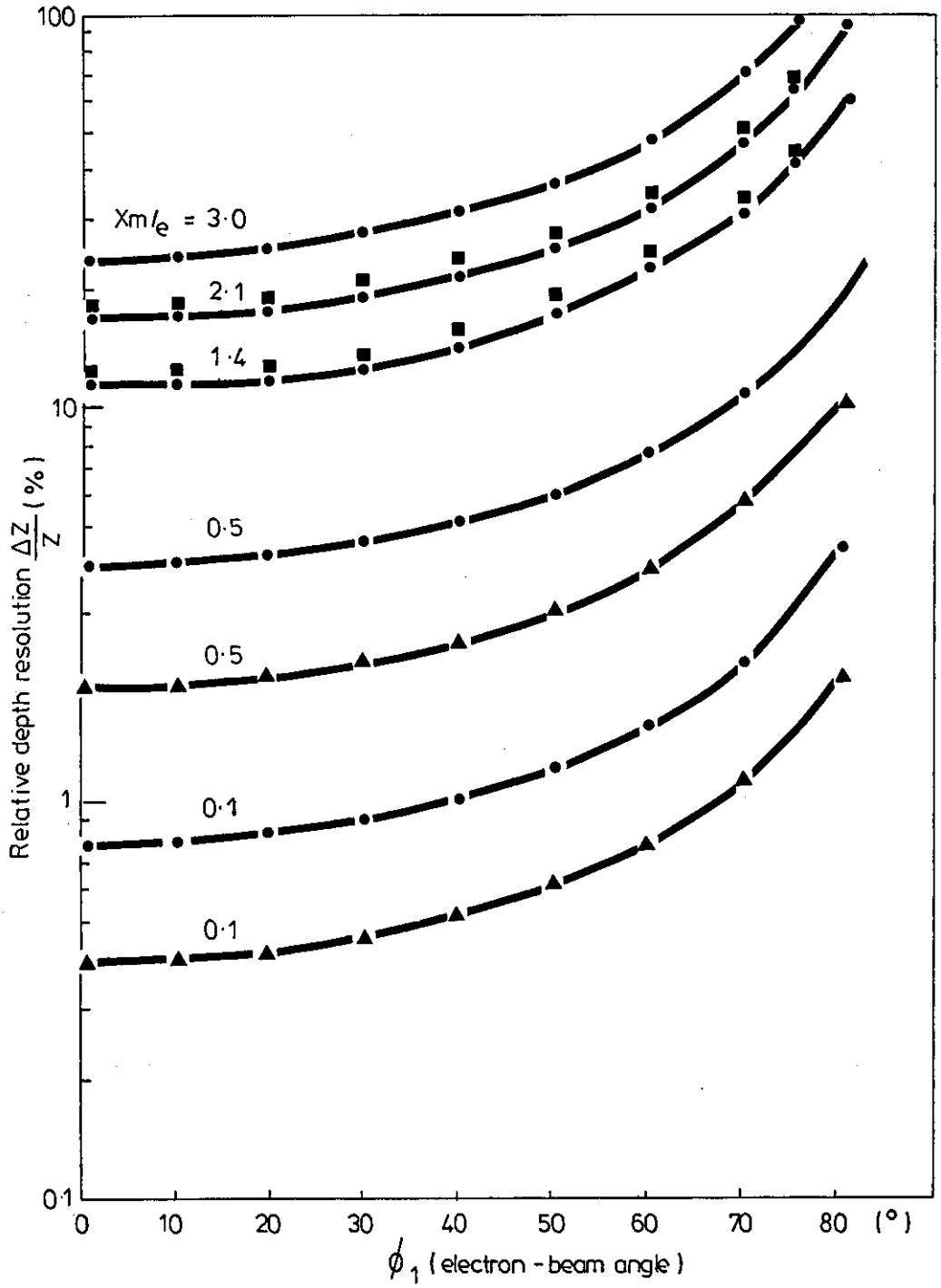

Figure 3.12: Relative depth resolution as a function of electron beam angle for various values of misalignment x_m/ρ. All data was calculated for $\sigma' = 0.02$.

- ● present work $\phi = 0^o$, $\phi_2 = \phi_1$
- ■ Malherbe et al $\phi = 0^o$, $\phi_2 = \phi_1$, $x_m/\rho = 1.41$ & 2.1
- ▲ present work $\phi = 45^o$, $\phi_2 = \phi_1$

parallel to the incident ion beam. A further example of this particular effect is illustrated in figure 3.13, showing a misalignment of the electron beam along the elongated axis of the crater for three angles of incidence of the ion beam. There is a significant improvement in the relative depth resolution as the angle ϕ increases. It should be noted that in varying ϕ, no change occurs in the width of the crater (along the y-axis) so that the depth resolution due to misalignment of beams in the y direction is independent of the ion beam angle ϕ.

One further consideration in optimizing system geometry is the orientation of the electron beam ellipse on the crater surface which is determined by the three dimensional relationship between the ion and electron beams as described by equation (18). The angle between the ion and electron guns varies for the different commercial AES systems, for example the PHI model is commonly 70° but sometimes 90° and the Kratos XSAM 800 model varies from 35° to 90°.

The geometry of a crater produced by a non-normally incident ion beam dictates that the maximum degradation of depth resolution will occur when the major axis of the electron beam ellipse is coincident with the minor axis of the crater. This is illustrated on the inset in figure 3.14 and might be achieved in practice by some common beam angles given by $\phi = 30^{o}$, $\phi_1 = 60^{o}$ and $\phi_2 = 64.34^{o}$. The results clearly show that as the electron beam ellipse rotates by increasing the angle between the ion and electron beams ϕ_2, the depth resolution is enhanced. This example is illustrated in figure

3.14 by misaligning the beams along the y direction for a beam ratio of $\sigma' = 0.05$.

Figure 3.15 shows the effects on misalignment for the same electron beam size and angle conditions as in figure 3.14 but for a misalignment in the x-direction. The value of the worst possible depth resolution now occurs when $\phi_2 = 90^0$, when the major axes of the electron and ion beam ellipses are aligned (see inset of figure 3.15). This value is a 4% improvement on the worst possible case shown in figure 3.14 ($\phi = 60^0$). Note also that in figure 3.15 a cross-over occurs in the crater region. This is attributed to the fact that when the electron beam is aligned along the y-axis ($\phi_2 = 60^0$), the contribution from the crater walls is greater than when it is aligned along the elongated x-axis of the crater ($\phi_2 = 90^0$), thus indicating the changes in crater wall slope in the central region.

3.1.4 Experimental Observations

Experiments were carried out to determine the effect of deliberately misaligning the ion and electron beams during composition-depth profiling in AES. A uniform SiO_2 layer, 1200Å thick, thermally grown on smooth silicon substrate was used as a model system. The relative effect of various misalignments was determined simply by monitoring the Auger peak intensity for oxygen as a function of sputtering time. The depth resolution was determined from the profiles by measuring the width of the SiO_2/Si interface between 0% and 100% of the peak intensity level. The experiments were conducted using a Varian 10KeV Auger electron spectrometer incorporating

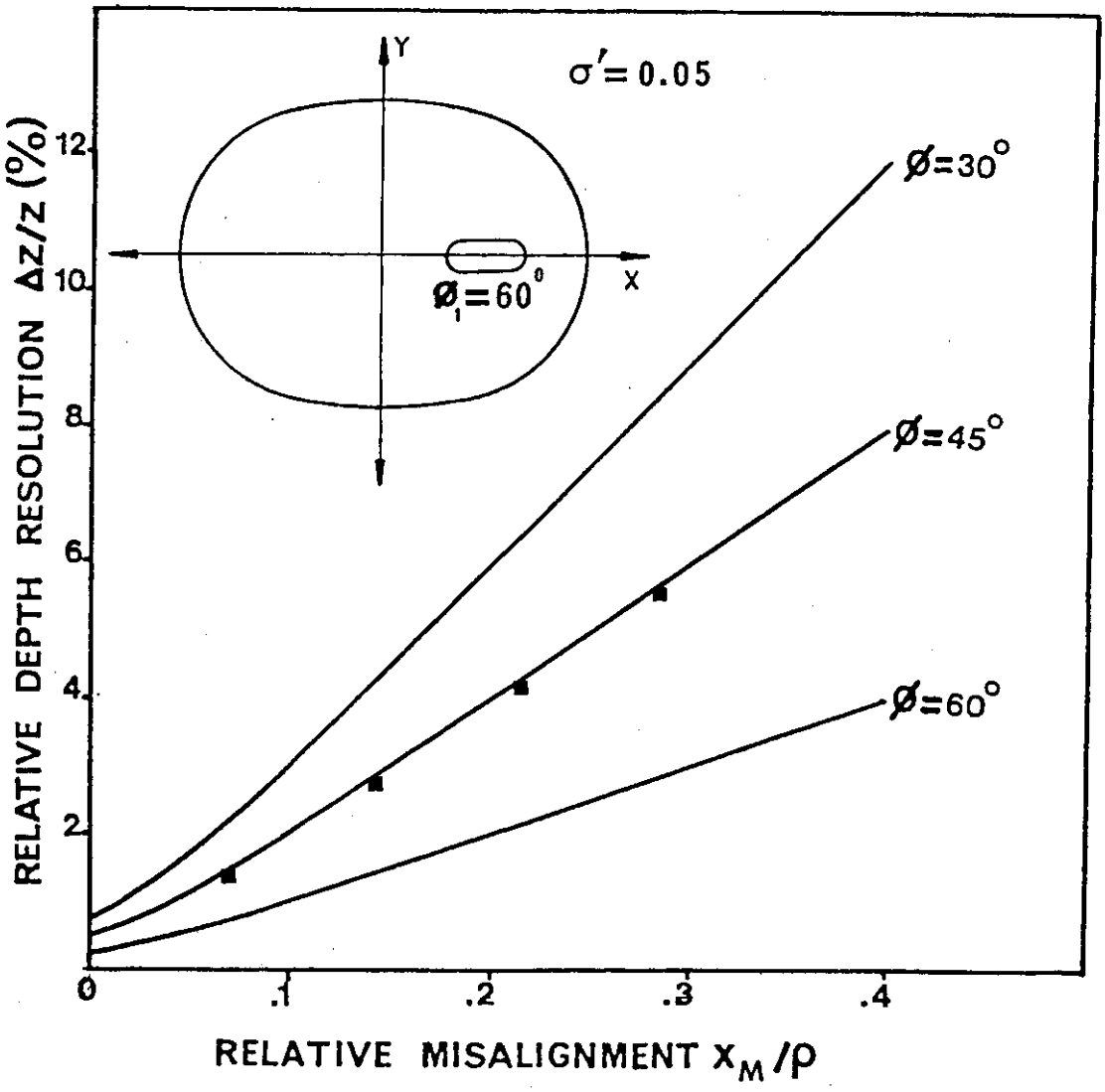

Figure 3.13: The dependence of relative depth resolution as a function of ion beam angle ϕ (Malherbe et al results for $\phi = 45^o$, $\phi_1{}^o = 60^o$, $\sigma' = 0.05$).

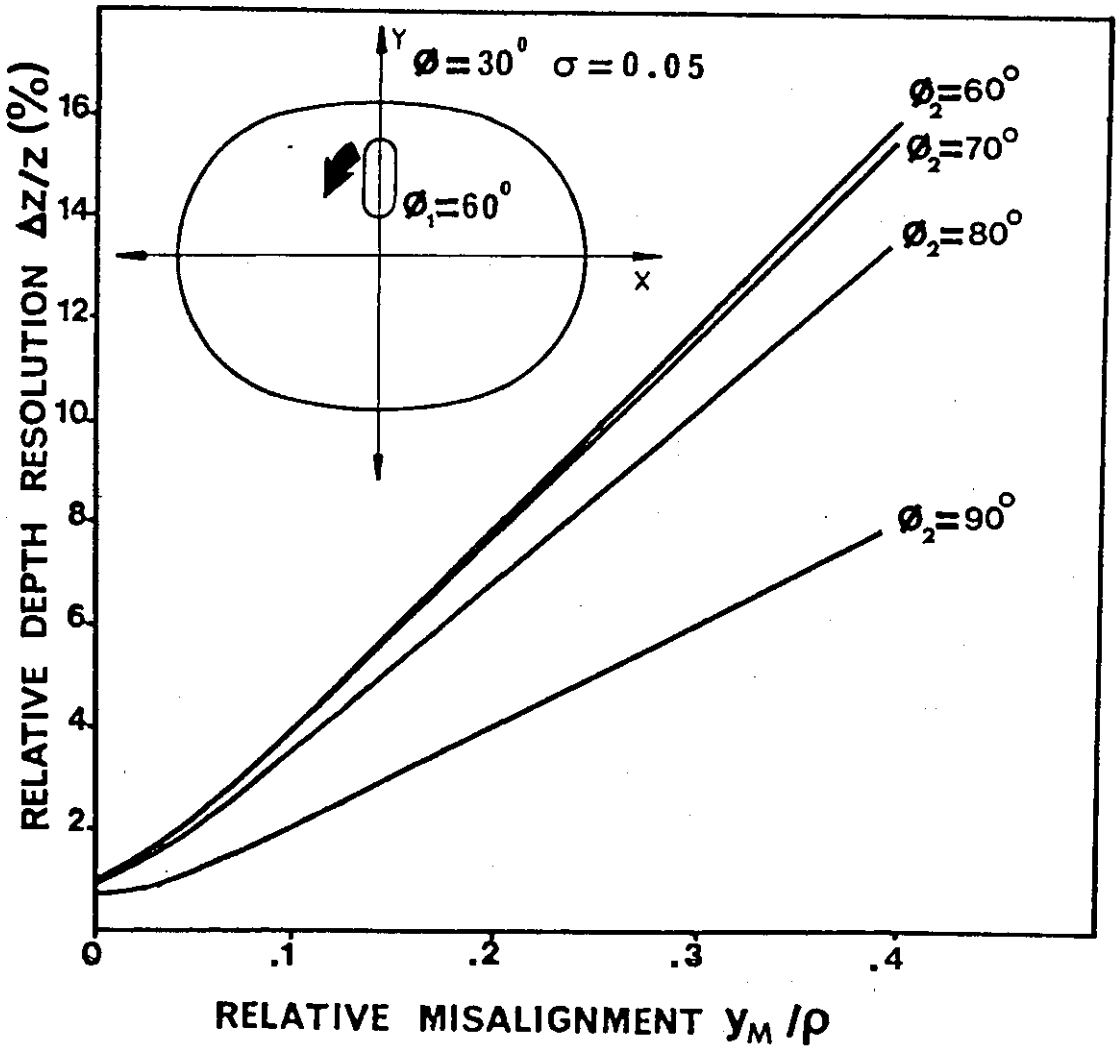

Figure 3.14: A graph showing how a variation of the angle between the ion and electron beams ϕ_2 affects relative depth resolution. A misalignment along the mirror axis of the crater is incurred for each angle of ϕ_2.

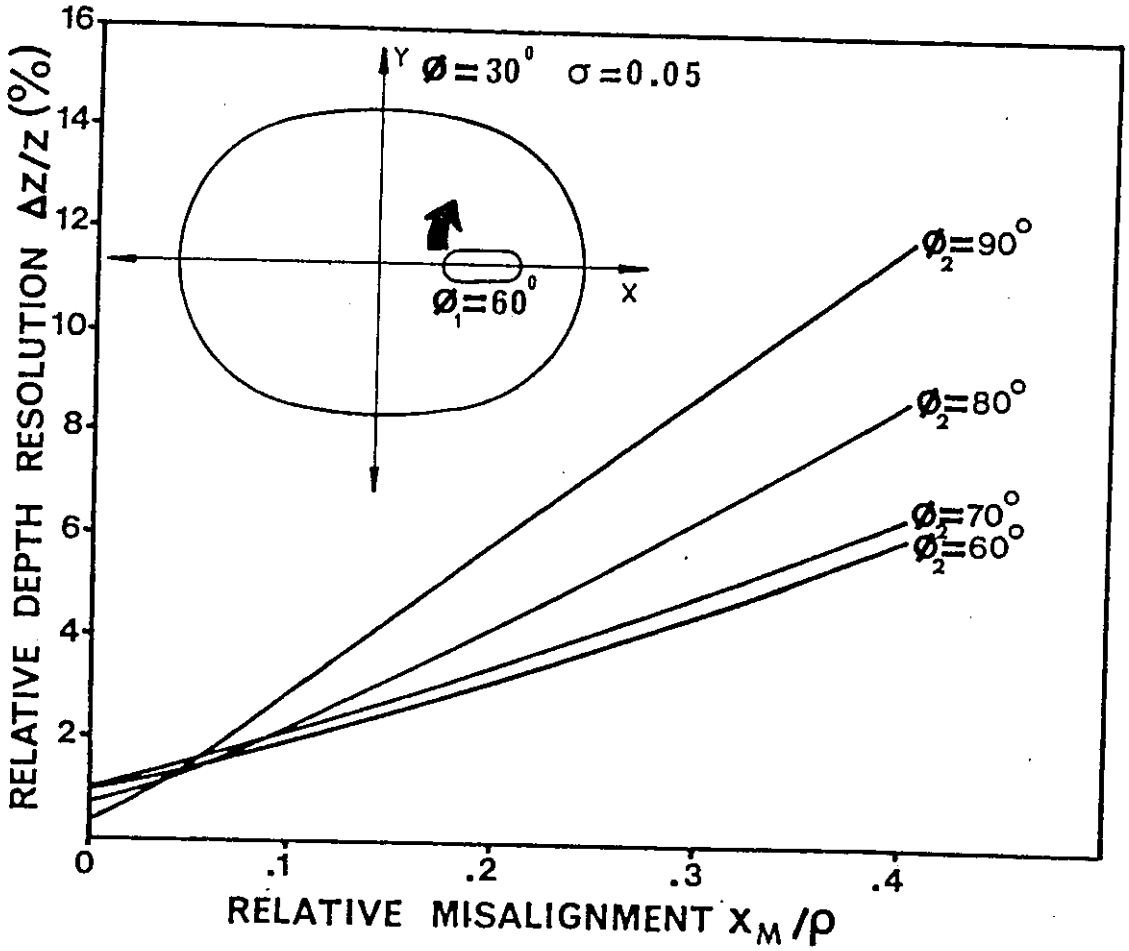

Figure 3.15: A graph illustrating the dependence of relative depth resolution on a variation in the angle ϕ_2 for a misalignment along the crater's major axis.

a cylindrical mirror analyser (CMA) with an integral electron gun. Although the system was capable of producing spot sizes < 5μm an electron beam diameter of 72μm was used in all cases since the electron current density ($24.5mAcm^{-2}$) precluded any beam effects. The ion beam diameter in all cases was 2mm. By performing a slow scan across a stainless steel knife-edge the iron Auger signal was monitored and hence by knowing the scan distance the width of the electron beam could be measured between the 84% and 16% levels of peak intensity. The ion beam diameter was measured by performing a point-by-point analyses (across the knife-edge) by monitoring the ion-induced Auger electrons (Fe signal), and in a similar manner to the electron beam the ion beam size could be calculated.

The geometry of the Varian system included an electron beam incident at 60° while the ion beam was incident at 30°, the angle between the two being 63.34^{o}. In all cases sputtering was achieved using 3KeV argon ions (current density $185\mu Acm^{-2}$) from a Varian 3KV hot-filament type ion gun. Misalignment of the electron beam was obtained by altering the astigmator control in the electron gun. In this way the electron beam was positioned at points along the major axis of the sputtering crater. The misalignment parameter in each case was measured accurately using the Vernier scale on the sample manipulator.

The effect of misalignment on the depth resolution as determined experimentally with a static ion beam is shown in figure 3.16 and is compared with the theoretically predicted values. The results illustrate

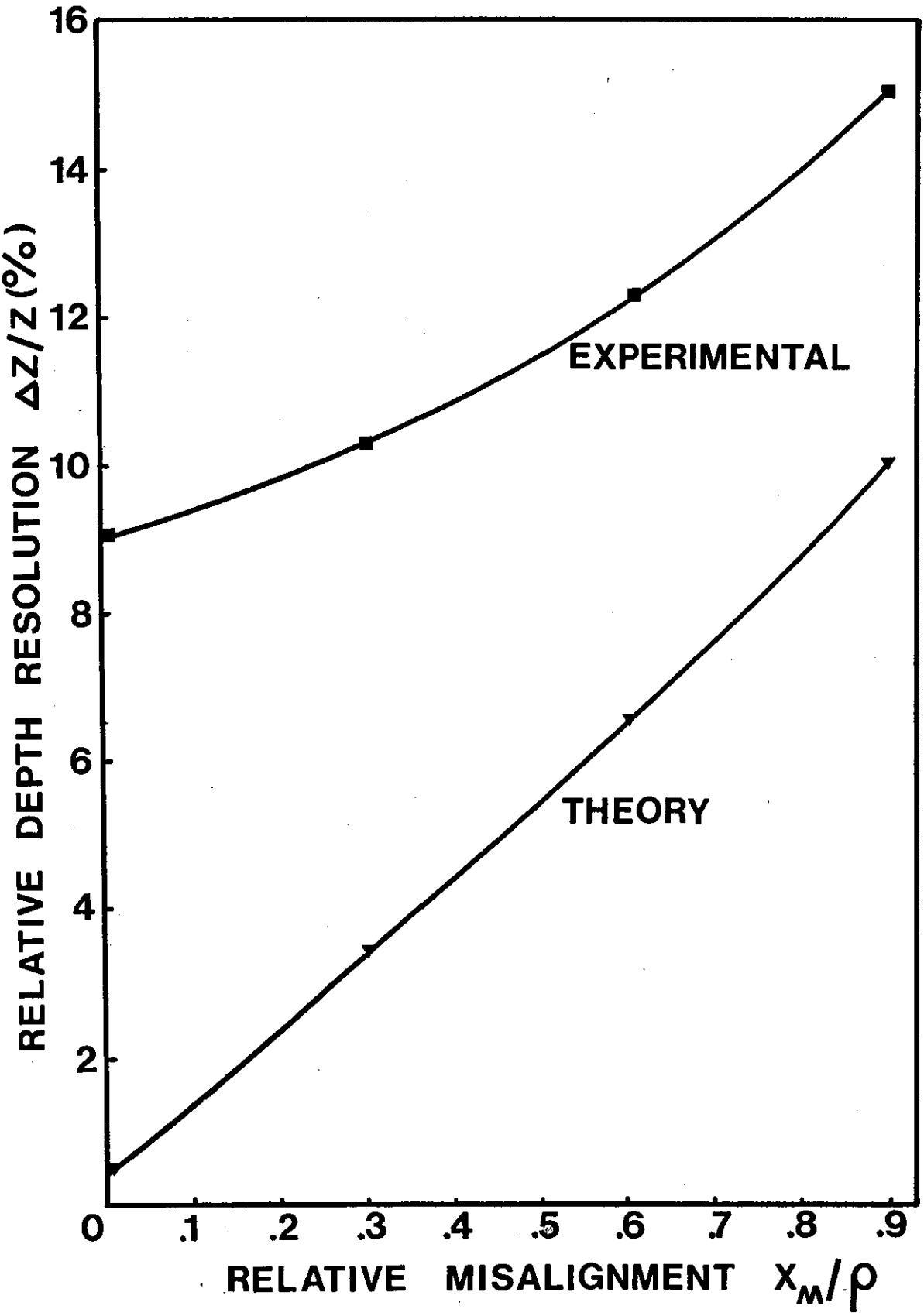

Figure 3.16: A comparison made between experiment and theory of the relative depth resolution as a function of misalignmen for an electron beam of diameter 72μm ($\sigma' = 0.036$).

that the degradation in the depth resolution obtained experimentally is generally higher than those predicted by the theory, but the two values tend to converge at high values of relative misalignment. The discrepancy between the results when the ion and electron beams are closely aligned may be accounted for by effects other than those of a geometrical nature. These include ion-induced topography (Liebl, 1975; Williams et al, 1980), atomic mixing (Schwarz and Helms, 1979; Williams, 1980), diffusion (Erlewein and Hofmann, 1980; Carter and Cruz, 1981), etc. However, at high values of misalignment ($x_m/\rho > 0.8$) the results show that the geometrical effects begin to dominate. Results obtained by rastering the ion beam ($1cm^2$) showed that misalignment of the electron beam from the centre of the crater has virtually no effect on depth resolution provided that the electron beam is incident within the rastered area of the ion beam.

3.1.5 Discussion

A general theory has been given to predict the depth resolution of composition-depth profiles achieved using a static ion beam for different system geometries. The theory accounts for various ion and electron beam diameters and all possible ion and electron beam angles of incidence. The results show that such effects can be significant particularly if either the electron or ion beam (or both) are used near grazing incidence. The best relative depth resolution obtained is in the case when $\phi = \phi_1 = 0^o$ and this is determined, for example, as 0.2% for an 80μm electron beam and an ion beam diameter of 2mm.

However, the deterioration of relative depth resolution for $\phi = 30^{o}$, $\phi_1 = 80^{o}$ and $\phi_2 = 81.35^{o}$ is 5.2% for the same size beam. Although only geometrical effects have been accounted for in this work it is of interest to note that suggestions have been made elsewhere (Lea and Seah, 1981; Keenlyside et al, 1983) that in order to produce a more uniform etch, and hence enhancement in depth resolution, the optimum position for the ion beam in sputter-depth profiling is at normal incidence.

In agreement with Malherbe et al (1981) the depth resolution $\Delta z/z$ is found to be independent of sputtering depth except for large misalignments where it depends on the ratio z/σ to a second order due to singal integration. In contrast, however, to the previous analysis shadowing is not considered important at grazing incidence for the depth of ion etched craters normally produced ($\lesssim 1\mu m$), and taper sectioning techniques are usually preferred beyond this depth (Walls et al, 1979).

In general, the depth resolution deteriorates with increasing values of the electron to ion beam diameter σ'. In practice, this is often necessary particularly with insulators since the electron beam is broadened to reduce the current density while preserving the overall signal. The depth resolution also deteriorates with increasing electron beam angle from the surface normal, although for given angles it is optimized if the electron and ion beams are in the same place such that their major axes are coincident (assuming no misalignment).

Experimental results have been presented and compared with theoretical predictions (figure 3.16). Although the absolute relative position of the ion and electron beams in experimental conditions was difficult to simulate the trend is evident. A similar result has been observed by Mathieu and Landolt (1983), who performed deliberate misalignment analyses through Ta_2O_5 films. They also substantiated the fact that the depth resolution was independent of film thickness under optimum conditions.

Misalignment of the electron and ion beams has been shown to be a serious problem in certain circumstances. This can often occur unknowingly on insulators due to local sample charging (Behrisch, 1981). In practice, this problem can be overcome by rastering the ion beam, but this leads inevitably to reduced ion current densities and longer sputtering times.

CHAPTER 4

4.1 Ion Etching of Solid Surfaces

4.1.1 The Physical Mechanisms of Ion Sputtering

When energetic particles are incident on a solid surface material is ejected, and the process is known as 'sputtering'. A sputtering coefficient S may then be defined as the mean number of emitted atoms per incident particle. In general, the magnitude of S relies on the nature and composition of the bombarded surface, the characteristics of the incident particle and the experimental geometry. However, values of S which can be reliably detected usually occur in the region $10^{-6} \lesssim S \lesssim 10^{3}$ atoms per incident particle.

From as early as 1853 (Grove) there have been many experimental and theoretical studies and reviews relating to the phenomenon of sputtering (Carter and Colligon, 1968; Sigmund, 1981; Thompson, 1981), but the large volume of work associated with its effects has failed to produce a universal theory which explains all observed events. However, the importance of particular events occurring have been widely studied and these will be discussed later in this chapter.

Primarily, sputtering measurements can be classified into three main categories: (1) those in which the yield S atoms sputtered per incident ion is measured, as a function of some variable such as ion mass, ion species or ion energy; (2) those where the angular

distribution of the sputtered atoms $dS/d\Omega$ is measured, (3) or those where the energy spectrum and angular distribution are measured $d^2S/d\Omega\ dE$. The data gained from these parameters will relate purely to the physical nature of sputtering where the most dominant process, particularly for metals, is believed to be knock-on sputtering. (Keywell, 1955.) A typical sputtering event is illustrated in Figure 4.1, whereby an incident ion knocks atoms off their equilibrium sites and causes these atoms to move through the material initiating an atomic collision cascade. Further collisions within the material eventually cause the ejection of atoms through the target surface. This,albeit simple process, can be subdivided into three qualitative regions, the single knock-on event, the linear cascade, and the spike effect. The single knock-on event (Figure 4.1(a)) is essentially described above where atoms are ejected from the surface if their energies are sufficient enough to overcome the surface binding forces. In the latter two cases, recoil atoms possess sufficient energy to generate secondary recoils, of which some may be energetic enough to be ejected from the surface. The main difference between the linear cascade and the spike-effect is the spatial density of moving atoms within the bulk, which is greater for the latter. In this case it might be exepcted that the number of atoms leaving the surface will be more than for the linear cascade regime.

Assuming that sputtered atoms originate from some well defined layer dx in the surface it would be expected that the number of particles ejected would be proportional to the number of recoil atoms generated in that layer (Sigmund, 1981). This essentially

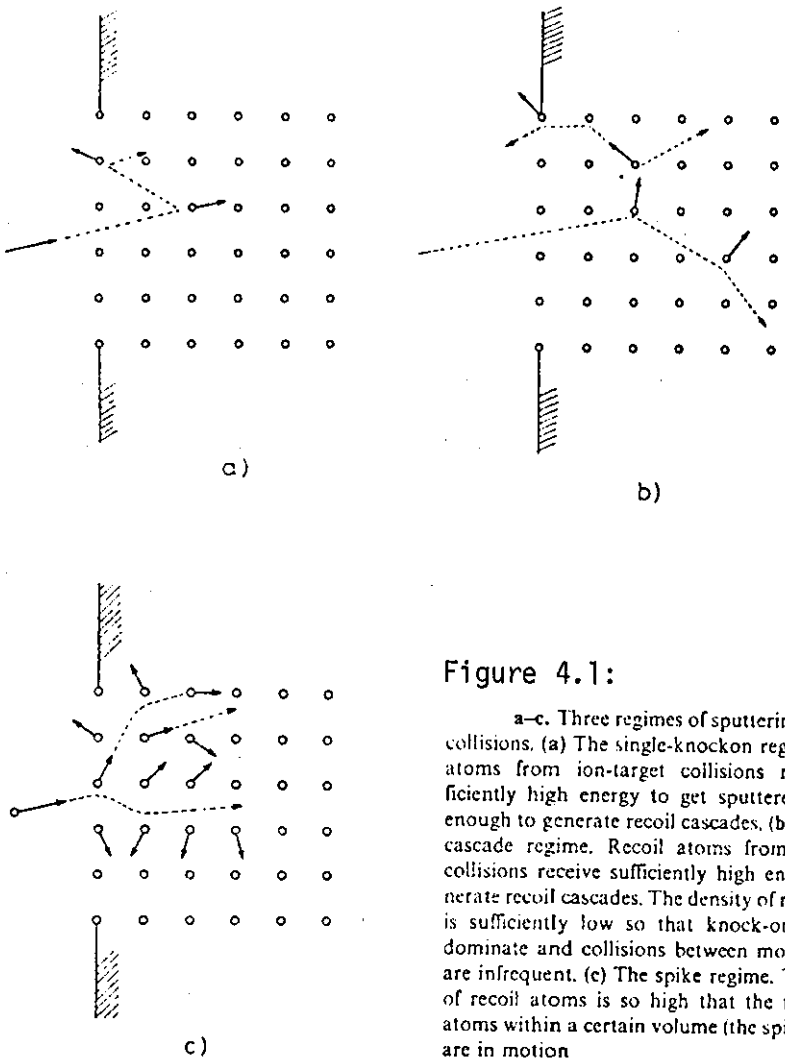

Figure 4.1:

a–c. Three regimes of sputtering by elastic collisions. (a) The single-knockon regime. Recoil atoms from ion-target collisions receive sufficiently high energy to get sputtered, but not enough to generate recoil cascades. (b) The linear cascade regime. Recoil atoms from ion-target collisions receive sufficiently high energy to generate recoil cascades. The density of recoil atoms is sufficiently low so that knock-on collisions dominate and collisions between moving atoms are infrequent. (c) The spike regime. The density of recoil atoms is so high that the majority of atoms within a certain volume (the spike volume) are in motion

(after Sigmund, 1981)

will be governed by three criteria for the processes described above. In the single knock-on regime, the number of sputtered atoms will depend on the cross-section; in the linear cascade regime it is proportional to the energy deposited per unit depth. The spike region poses a slightly different problem in that the energy deposited per unit volume is associated with local heating according to a temperature function T(r,t) of position and time, and this is known as a thermal spike. However, although this may be used to describe the eventual collision cascade Brinkman (1954) recognised an intermediate period in the dissipation of the primary energy, obeying neither binary collision theory or the thermal spike phenomenon. Thompson (1981) formulated a criterion for the occurrence of spike regions, where medium or heavy ions impinge at energies where the collisional stopping power dE/dx, is large enough to provide a threshold displacement to all the atoms neighbouring the track, and thus:

$$\frac{dE}{dx} \gtrsim \frac{E_b}{D} \tag{4.1}$$

where E is the incident particle energy

E_b is the binding energy

D is the mean interatomic distance.

There will be a critical value of the sputtering yield S_{crit}, which will be independent of ion and target and thus for spike effects the criterion for equ. (4.1) becomes $S > S_{crit}$. The cascade theory should apply when $S < S_{crit}$, where S will be proportional to equ. (4.1). However, S_{crit} may be exceeded and S may depend non-linearly on this quantity and should therefore be classed as a non-linear sputtering

effect (Sigmund, 1974).

In all the categories described above the emerging particles are of relatively low energy (few 10eV to few 100eV), compared to the normally high energy of the primary ions, due to electronic loss processes. Furthermore, the last collision encounter of a sputtered particle is with another surface atom, therefore it should be expected that excitation and ionization to be predominantly controlled by the properties of the surface atoms and to be insensitive to the nature of the primary ion (Williams, 1979). However, qualitatively the occurrence of one of the three collision events will be governed by the energy input. The single knock-on event falls into the low-medium eV region, extending to the lower KeV region for light ions because of inefficient energy transfer. The linear cascade develops for KeV and MeV ions, where for the heaviest ions, spikes are generated due to a rapid stopping of the ion.

4.2 The Sputtering Yield

4.2.1 Theory

There have been many theoretical models of sputtering based on computer simulation (Harrison et al, 1973), statistics (Schwarz and Helms, 1979) and on empirical formulas (Yamamura et al, 1983) and no attempt will be made here to compare their relative merits. Many workers have, however, adopted the classical binary collision approach which predict neutral sputtering yields (Sigmund, 1969; Oechsner, 1975; Yamamura, 1982), although other work has been performed to include ion sputtering yields (Prival, 1978; Schwarz and Helms, 1981).

The ultimate ejection of particles from a surface will depend on the spatial distribution of energy within the solid, which in turn depends on the differential cross-section. Sigmund (1972) has developed an extensive theory for the general sputtering yield formula of an amorphous target which is given by:

$$S(E,\theta) = 0.042\Lambda\alpha(\varepsilon,\theta,M_2/M_1)(dE/dx) \tag{4.2}$$

where E and θ are the energy and angle of incidence of the ion respectively, (dE/dx) the nuclear stopping cross-section, Λ a material constant and α a dimensionless function of ion and target mass M_1, M_2 and an energy parameter ε where:

$$\varepsilon = \frac{M_2E}{M_1 + M_2} \cdot \frac{a}{Z_1Z_2e^2} \tag{4.3}$$

where Z_1 and Z_2 are the atomic number for the ion and target atoms, e the electron charge and a the Thomas-Fermi screening radius of the interatomic potential. Equations (4.1) and (4.2) have been based on the assumptions that an individual ion generates a collision cascade and that the target atoms slow down randomly and independently to each other. Furthermore, only elastic collisions take place, where the cross-sections associated with equations (4.1) and (4.2) prefer small energy transfers and at high enough ion energies ($\varepsilon >> 1$) so that the nuclei approach closer to each other than the screening radius a. The energy of the ejected atoms will therefore depend on the target material parameters such as the ratio M_2/M_1, and the stopping power (dE_0/dx). The depth of origin of these atoms with energy E_0 will be given by their effective range $R(E_0)$ where (Sigmund, 1980):

$$R(E_0) = \int (dE/dx)^{-1} dE_0 \tag{4.4}$$

It would therefore be expected that the higher the energy of a sputtered atom, the deeper the depth of origin. A more specific parameter relating to the target material is the surface binding energy U_0 which governs the probability for ultimate ejection of atoms at the surface. With certain assumptions concerning Bonn-Mayer scattering the target characteristic Λ may be expressed as (Sigmund, 1969)

$$\Lambda = \left(\frac{3}{4\pi^2}\right) (1/NC_0U_0) \tag{4.5}$$

N is the atomic density of the target material where

$$C_0 \simeq (\pi/2)\lambda_0 a^2 \tag{4.6}$$

where λ_0 is a dimensionless fitting parameter dependent on energy and ion mass.

Although equations (4.1) and (4.2) predict well the dependence of the sputtering yield on ion type, energy and angle of incidence for characteristic properties of one target, in the > 1KeV medium-mass range, deviations have been observed between theory and experiment for light ion sputtering (Anderson and Bay, 1974; Littmarck, 1976), and low energies (eV region), and very heavy ions (cf. spike effects).

The discrepancy in the light ion sputtering and inelastic collision region has been shown between experimental and calculated results of the deposited energy distribution (Weissmann and Sigmund, 1973; Winterbon, 1975), which suggests the importance of a threshold energy on sputtering yields. Bohdansky (1980) has thus divided the

sputtering process into two categories: the near-threshold and the linear cascade regime; and has adjusted the Sigmund formula accordingly for both high and low energy ions and incorporated the threshold energy as some fraction of these. Recently a simplified empirical formula has been proposed by Matsunami et al (1980) more applicable to all ion-target combinations and which was developed to implicitly include the effect of inelastic stopping and the antisotropic velocity distributions of the recoil atoms (Yamamura et al, 1983).

The numerous processes involved in physical sputtering have gradually been recognised. During the development of the linear cascade theory attempts to include the spike effect (or non-linear sputtering effect) received little attention. It was not until Anderson and Bay (1975) demonstrated that the energy density promoted by heavy ion impact had significant results on the sputtering yields did several workers formulate their theories (Carter, 1979; Sigmund et al, 1980; Kitazae, 1980). Figure 4.2 illustrates Sigmund's theory for the sputtering yield as a function of energy for various ion-target combinations, highlighting some of the points discussed above.

4.2.2 Variation of Sputtering Yield

4.2.2.1 Target Material

The standard method normally adopted in sputtering yield measurements is to determine the sputter induced weight loss of the target. By utilising highly sensitive micro-balances in situ, sputtering yields of 10^{-4} atoms/ion are detectable for heavy targets (Oechsner, 1963).

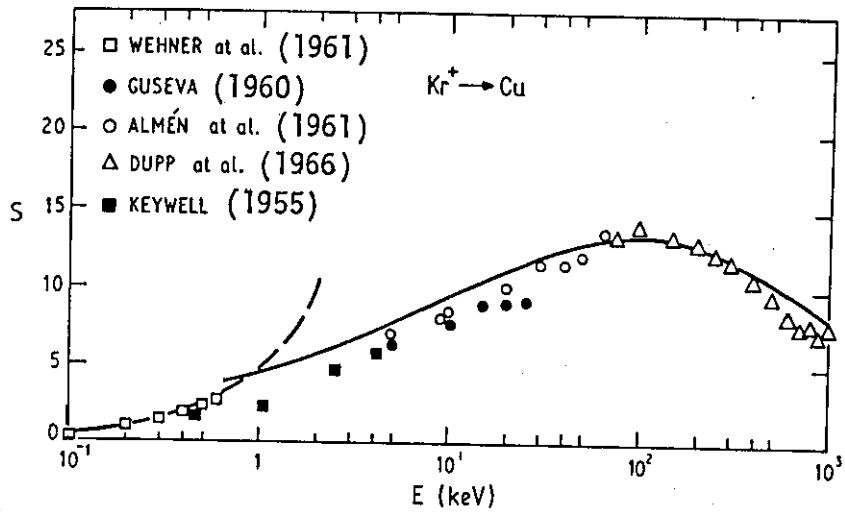

(a)

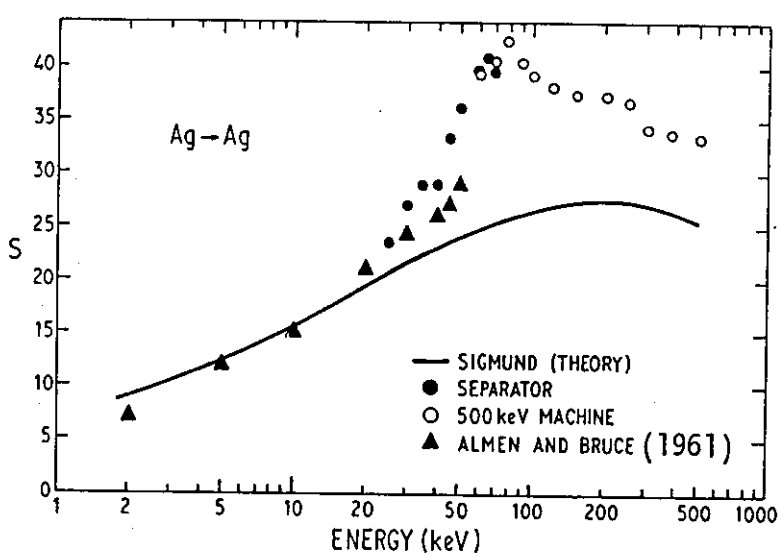

(b)

Figure 4.2: Sputtering yields for Cu and Ag calculated from equation 4.2 (solid curves) compared with experimental results.

Due to the extemely low yields obtained during light ion sputtering, Rutherford backscattering and neutron activation techniques have sometimes been employed to determine these yields (Eckstein et al, 1973; Kaminsky and Das, 1974). Wehner et al (1962) have carried out a series of experiments to determine the variation of sputtering yield with target material. They bombarded 26 metals with 400eV mercury (Wehner, 1957) and noble gas ions, and the results of their experiments are illustrated in Figure 4.3.

Essentially, the variation in sputtering yield with target materials should be characterised by the reciprocal influence of the surface binding energy U_0 (viz. equ. (4.5)), a value that can be closely associated with the heat of sublimation. Wehner suggested that the sputtering yield was related to the state of the electron concentration in the 'd' shells and also to the heats of sublimation. Carter and Colligon (1968) noted, however, that these assumptions had minor deviations but generally gave a consistent picture for all target materials even at higher energies (Almen and Bruce, 1961).

There are other significant facts underlying data obtained from experiments for sputtering yields. These include, the history of the material, the specific surface crystal orientation and the magnitude of the topography developed under ion erosion. The latter will be discussed in detail in Chapter 5. Figure 4.4(a) illustrates the variation in sputtering yields for copper, dependent on crystal orientation and in one particular case (Southern et al, 1963) on the condition of the sample, where a variation was observed from three separate sources. The results highlight the fact that data obtained

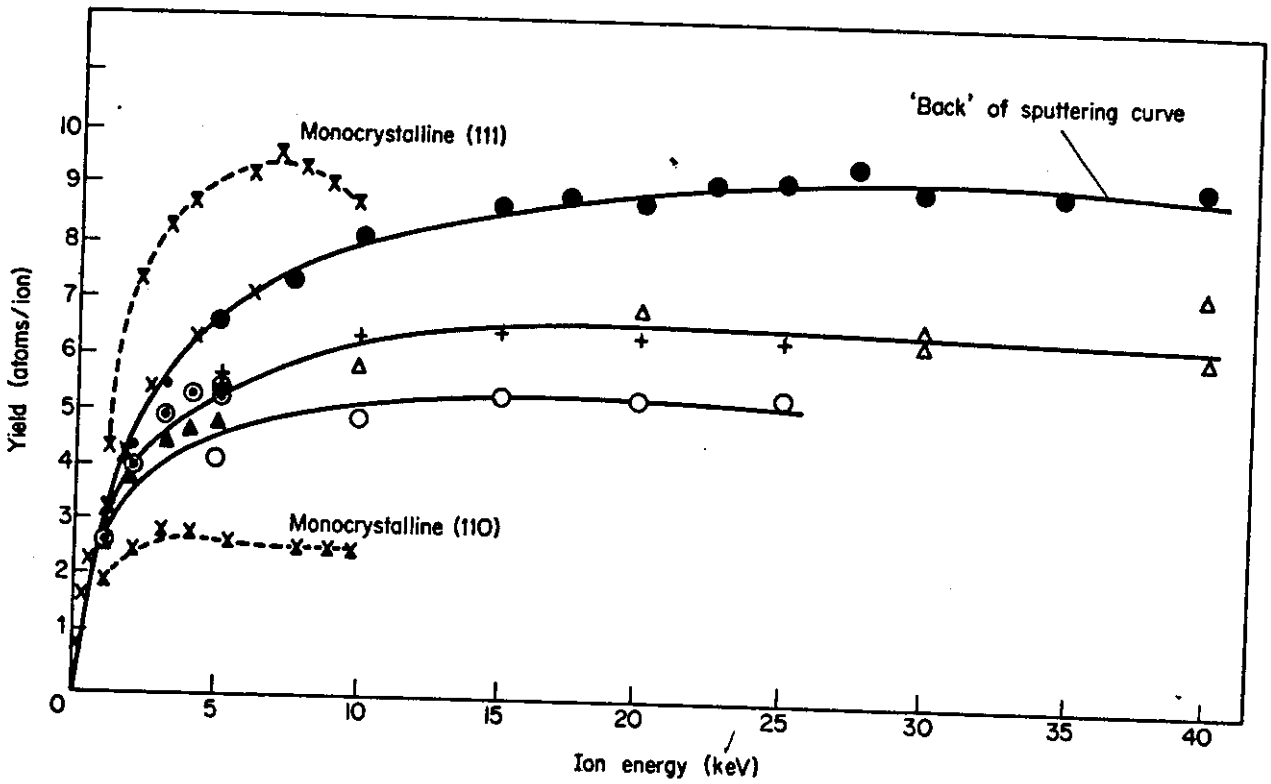

Figure 4.4(a): Variation of sputtering yield with energy for argon ion bombarding copper (high energy region) + Rol et al (1960); ⊕ Keywell (1955); X Bader et al (1961); ● Yonts et al (1960); O Guseva (1959); • ⊙ ▲ Southern et al (1963) (three different samples of copper) XX Magnuson et al (1963); Δ Almén et al (1961).

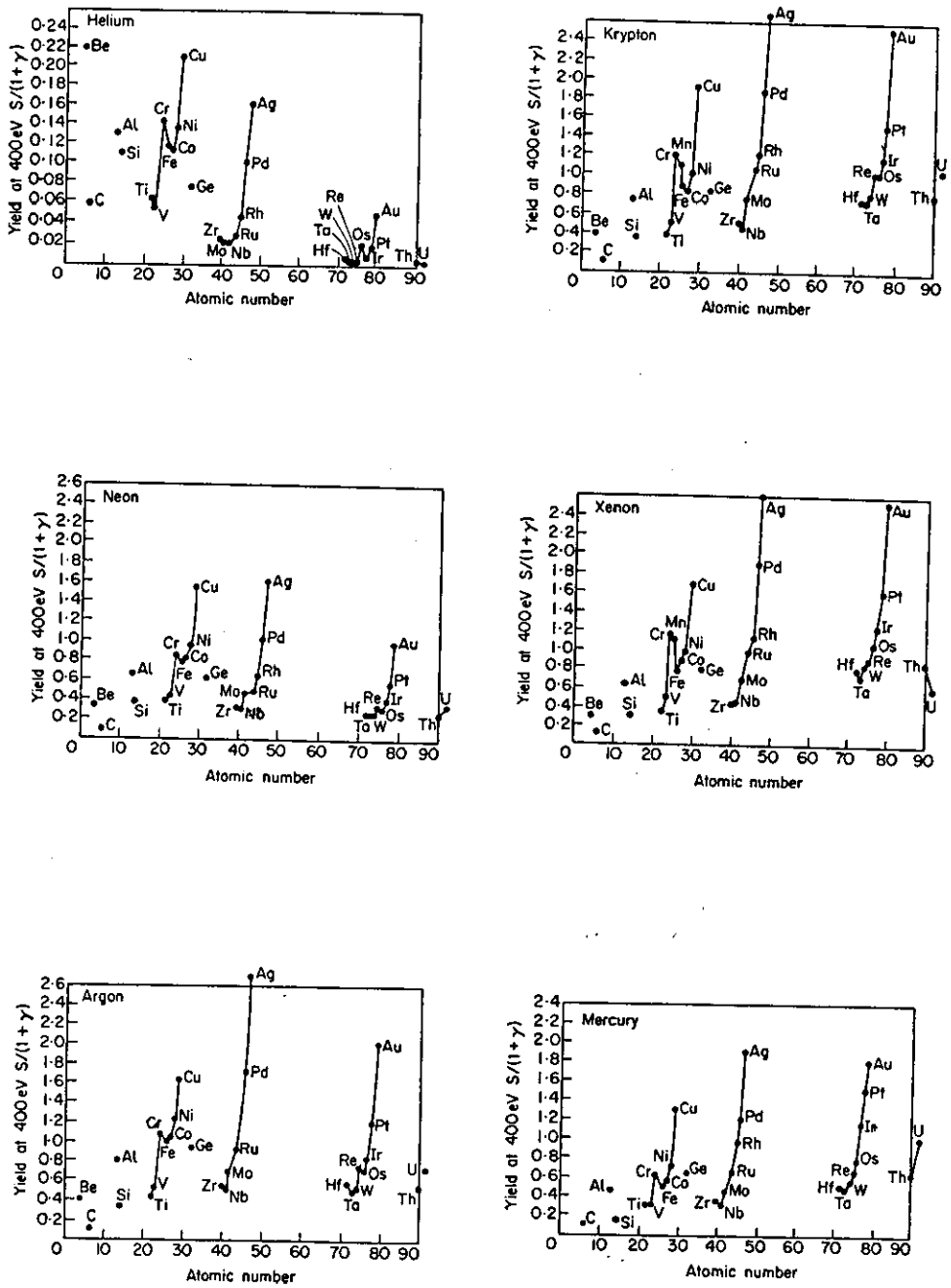

Figure 4.3:

Variation of sputtering yield with atomic number of the bombardment material for 400 eV noble gas and mercury ion bombardment (after Wehner, 1957).

from polycrystalline materials should be treated as approximations and be bounded by the data obtained from single crystals.

4.2.2.2 Ion Species

Studies indicating the influence of the primary ion on sputtering yield have been carried out by Almen and Bruce (1960) where the sputtering yields of Ag, Cu and Ta were determined as a function of primary ion mass at an energy of 45KeV. These results, illustrated in Figure 4.4(b), showed an oscillatory trend for each group of elements where the yields increased to a maximum for the inert gas species of the group and then rapidly decreased, this process being characteristic for almost every group. Rol et al (1960) did a similar study using lower energies (5 - 25KeV) although there was too little data to show any definite trend.

It would appear from more recent studies performed by Anderson and Bay (1973) that the bombarding ion mass dependence on sputtering yield shown by Almen and Bruce is incorrect. Figure 4.4(c) illustrates the results from Anderson and Bay's work when they bombarded Si, Cu and Ag with a range of primary ion species at 45KeV. Sigmund's theory is in good agreement although discrepancies arise for an increase in target mass. Since none of the yield determining quantities show corresponding fluctuations it has been suggested that the sputtering behaviour is related to the doping of the sputtered surface layer with the bombarding species (Oechsner, 1975).

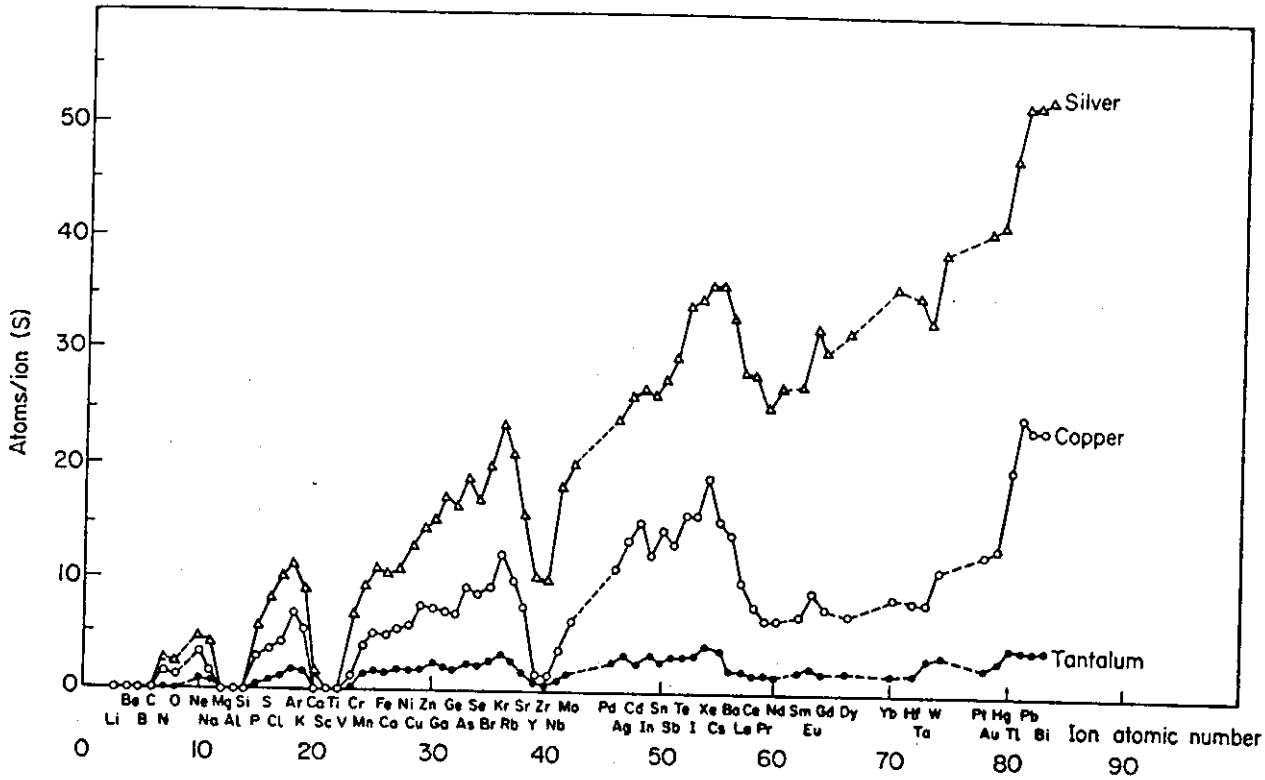

Figure 4.4(b) Variation of sputtering yield with atomic number of the bombarding ion for 45 keV bombardment of copper, silver and tantalum targets.

(After Almen and Bruce 1960)

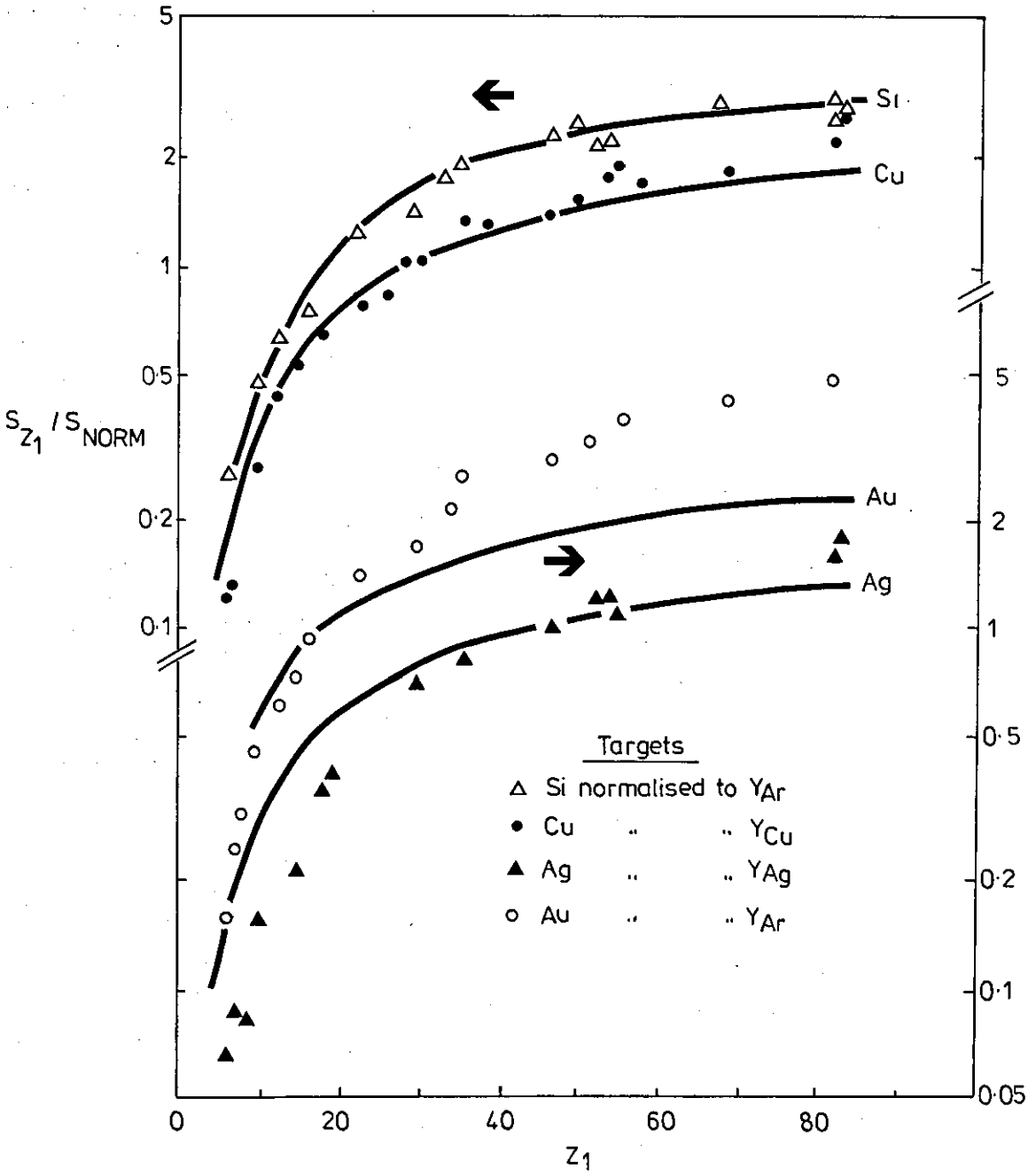

Figure 4.4(c): Relative sputtering yields for 22 different ions at 45keV for Si; Cu, Ag and An targets. To avoid influence of dose effects, the data have been obtained relative to self-sputtering (Ag, Cu) and Ar sputtering (Si, Au). Solid curves represent theoretical values according to equation 4.2 (after Anderson and Bay (1973), (1976)).

Ideally, sputtering experiments should be carried out with one single ion incident on a clean target. For practical reasons, however, several orders of magnitude of incident ions are used which penetrate the target material where they disrupt the lattice and eventually become trapped (Carter and Colligon, 1968). Consequently subsequent ions have to sputter a damaged surface and also the trapped ions, thus the sputtering yield would become dependent on the number of the ions that have previously struck the target. This effect could account for the discrepancy in Figures 4(b) and 4(c), and has been observed separately by Almen and Bruce (1962) who found silver, copper and tantalum targets to initially decrease when bombarded with carbon ions, and Anderson and Bay (1972) who bombarded copper with 45KeV V^+ ions and found continuous reduction in S with increasing bombarding dose. This has been the subject of several other studies (Nelson and Mazey, 1973; Carter et al, 1980) with a particular emphasis on its importance in irradiation effects observed on fission reactor walls.

A distinction must be made on the energy range used with different ion masses since, for example, a maximum sputtering yield is obtained for low bombarding energies ($\lesssim$ 1KeV) and nearly equal atomic masses of ion and target (Oechsner, 1973). At higher energies where the energy deposited in the surface becomes the most significant factor in the sputtering process, the high density cascades that are generated cause a decrease in the stopping power, resulting in an enhanced sputtering yield. This can be demonstrated by a comparison between the sputtering yields obtained by molecular ion and atomic ion bombardment. If the ions and molecules are of equal velocity then the effect of an

increased cascade density can be isolated with other variables remaining fixed. Sputtering yields increasing by factors of two and above can be observed (Anderson and Bay, 1974) but no quantitative explanation has been given as to the origin of the effect. Under spike conditions, the U_0^{-1} dependence (equation 4.5) of the sputtering yield changes to an exponential one (Sigmund, 1980), and hence the variation in sputtering relies on the magnitude of the surface potential and not only on the mass of the target.

These observations can be compared to experiments carried out by Bader et al (1961), who have shown that copper and nickel targets sputtered equally when they were bombarded with normally incident N_2^+ ions and two atomic N^+ at half the energy. The energies used were lower than those used by Anderson and Bay (1974) which would have eliminated non-linearity effects. This effect, however, was not duplicated when similar experiments were carried out on iron, molybdenum and tungsten targets.

4.2.2.3 Incident Ion Angle

The first observation of the dependence of the sputtering yield on incidence angle was made by Fetz (1942), who suggested that the variation in the sputtering yield of thin wires sputtered in a low pressure plasma, was due to oblique ion incidence angles caused by a spiraling motion in the accelerating field. Since then its importance has become evident in surface analysis studies as being one of the most influencing factors in surface shape development and has been the subject of many studies (Cheney et al, 1963; Littmark and Hofer, 1978; Kowalski, 1982). This particular aspect of sputtering is discussed

later in Chapters 5 and 6.

In relation to previous discussions the sputtering yield ratio predicted by Sigmund's theory may be written as:

$$S(\theta) \,/\, S(0) \;=\; \cos^{-f}\theta \qquad (4.7)$$

where the exponent f is determined elsewhere (Sigmund, 1969). Equation (4.7) is true for small angles of θ, but does not hold for low bombarding energies where the sputter yield will have a $(U_0/E)^{\frac{1}{2}}$ dependence on incidence angle. The $\cos\theta^{-1}$ dependence has been shown experimentally by Molchanov et al (1962) to be valid for $0^0 < \theta < \sim 60^0$ at intermediate bombarding energies and low energies as shown in figure 4.5. Other expressions relating to the sputtering ratio can be found elsewhere in the literature most of which are not without their limitations (Thompson, 1968; Oechsner, 1973). At angles of $0 \geqslant \sim 70^0$ the sputtering yield increases to a maximum and then decreases to zero as $0 \rightarrow \pi/2$ at grazing incidence. At these angles ion reflection is the dominating factor with little, or no ion penetration. The critical angle for ion reflection has been calculated by Lindhard (1965) as:

$$\frac{\pi}{2} - \hat{\theta} = \frac{5a_0 n^{\frac{2}{3}} Z_1 Z_2 E_R}{(Z_1^{\frac{2}{3}} + Z_2^{\frac{2}{3}})E_1} \qquad (4.8)$$

where E_R is the Rydberg constant

E_1 incident ion energy

Z_1, Z_2 atomic numbers of ion and target atoms

a_0 Bohr radius

n density of atoms per unit volume

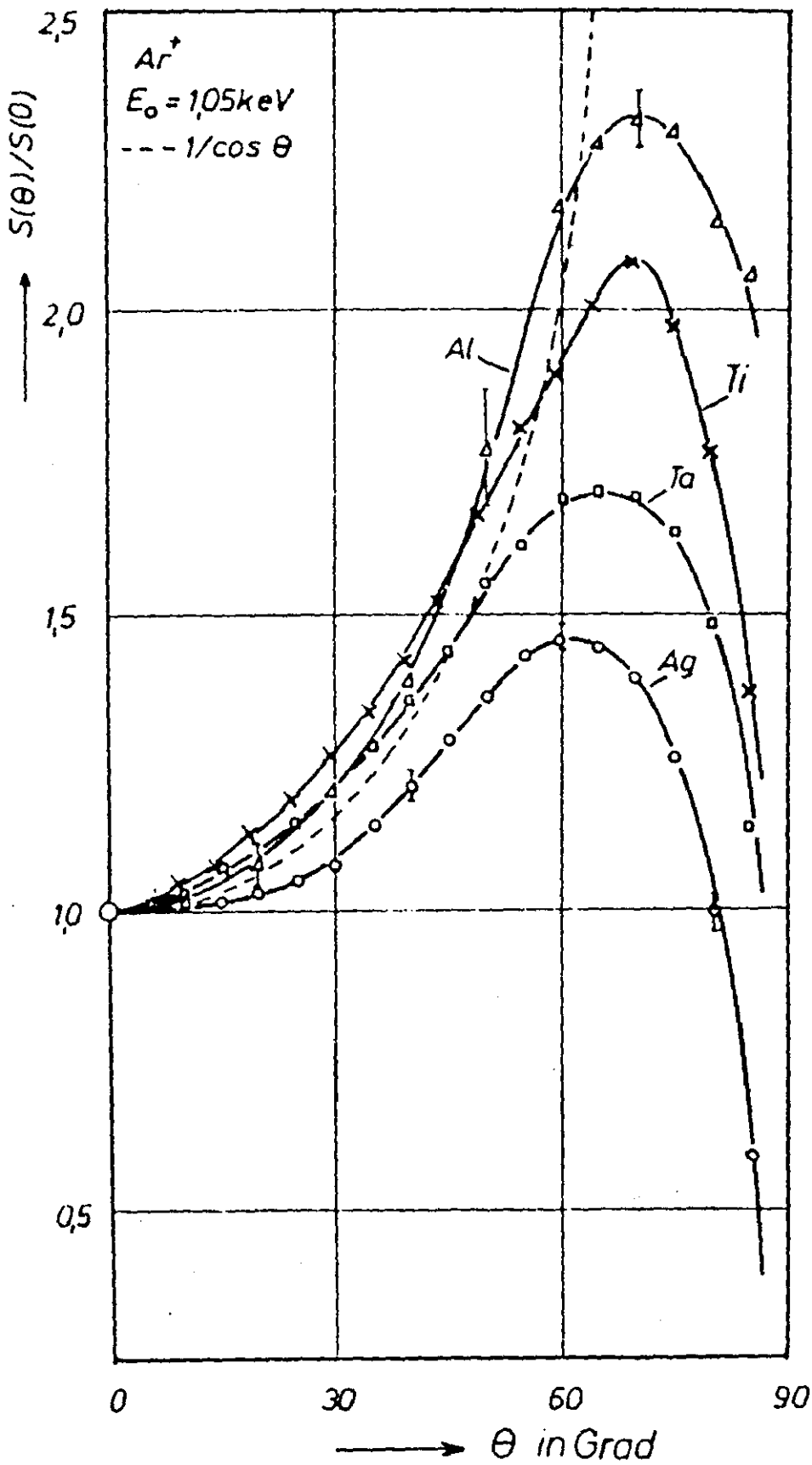

Figure 4.5: Influence of the bombarding angle θ on the normalized sputtering yield of different polycrystalline metals bombarded with Ar^+ ions of 1.05keV (After Oechsner (1975)). (--- Molchanov et al, 1962).

$\hat{\theta}$ represents the critical angle at which $S(\theta)$ reaches its maximum value and has been calculated implicitly by Firsov (1970) and more recently by Witcomb (1977). The latter utilised the planar channeling calculations of Lindhard to develop two theories describing $\hat{\theta}$ for both amorphous and crystalline targets. In general the $S(\theta)$ curves in Figure 4.5 are characteristic for most amorphous and crystalline non-metallic materials (Bach, 1970), but show vastly distinctive differences for single crystal sputtering.

4.3 The Sputtering of Single Crystal Materials

4.3.1 Physical Concepts

Collision cascades stemming from the intimate encounter of the ion with the target in sputtering will depend on the crystal structure of the material. This will, therefore, essentially be related to the sputtering yield and the discrete angle of impact of the ion with the surface. For this reason interest in single crystal sputtering has increased, and developments in the theoretical and experimental field have helped identify some of the underlying mechanisms involved in the atomic collision process.

The first observation of an influence of the monocrystalline substrate was by Stark and Wendt (1912) when they bombarded a Bismuth crystal parallel and perpendicularly to its basal plane. The result was an increase in sputtering yield by a factor of three for the latter case.

Stark (1913) then proposed a concept known as channelling which involved an energetic particle travelling through a solid between lattice rows.

For a preferred orientation the particle will travel deeper into a single crystal, than in an amorphous or polycrystalline target thus reducing the sputtering yield. One of the earliest observations of the channelling effect was made by Rol et al (1959) who bombarded a (100) Copper crystal with 20KeV Ar^+. The crystal was rotated about an axis 7° from the [011] and through an angle $0 < \theta < \sim 45^o$, and two distinct minimums were observed in the sputtering yield. Other results reported by Molchanov et al (1961) for the same material but bombarded with 27KeV Ar^+ and rotated about the $[01\bar{1}]$, axis revealed several minima. Figure 4.6 illustrates these results and for comparison includes those obtained by sputtering a polycrystalline Cu target. This curve lies between the maxima and minima of the single crystal curves which might be expected, as it should be some average governed by a contribution from all atomic planes. The strong dependence of sputtering yield on angle may cause a shift in the curve if a polycrystalline target possesses surface texture.

Other monocrystalline effects dependent on the material structure are the distinct peaks that appear for the angular distribution of particles as observed by Wehner (1956). The preferred directions of these can be characterised by low Miller indices.

The orientation effects that produced a reduction in ion ejection along a low index direction (cf. figure 4.6) were explained by 'transparency' models used by several authors (Rol et al, 1960; Southern et al, 1963; Fluit et al, 1963). Although the models differed in detail the basic assumptions were the same. They considered that each atomic site within the crystal had a specific cross-section and the collision was governed by an impact parameter. The incident

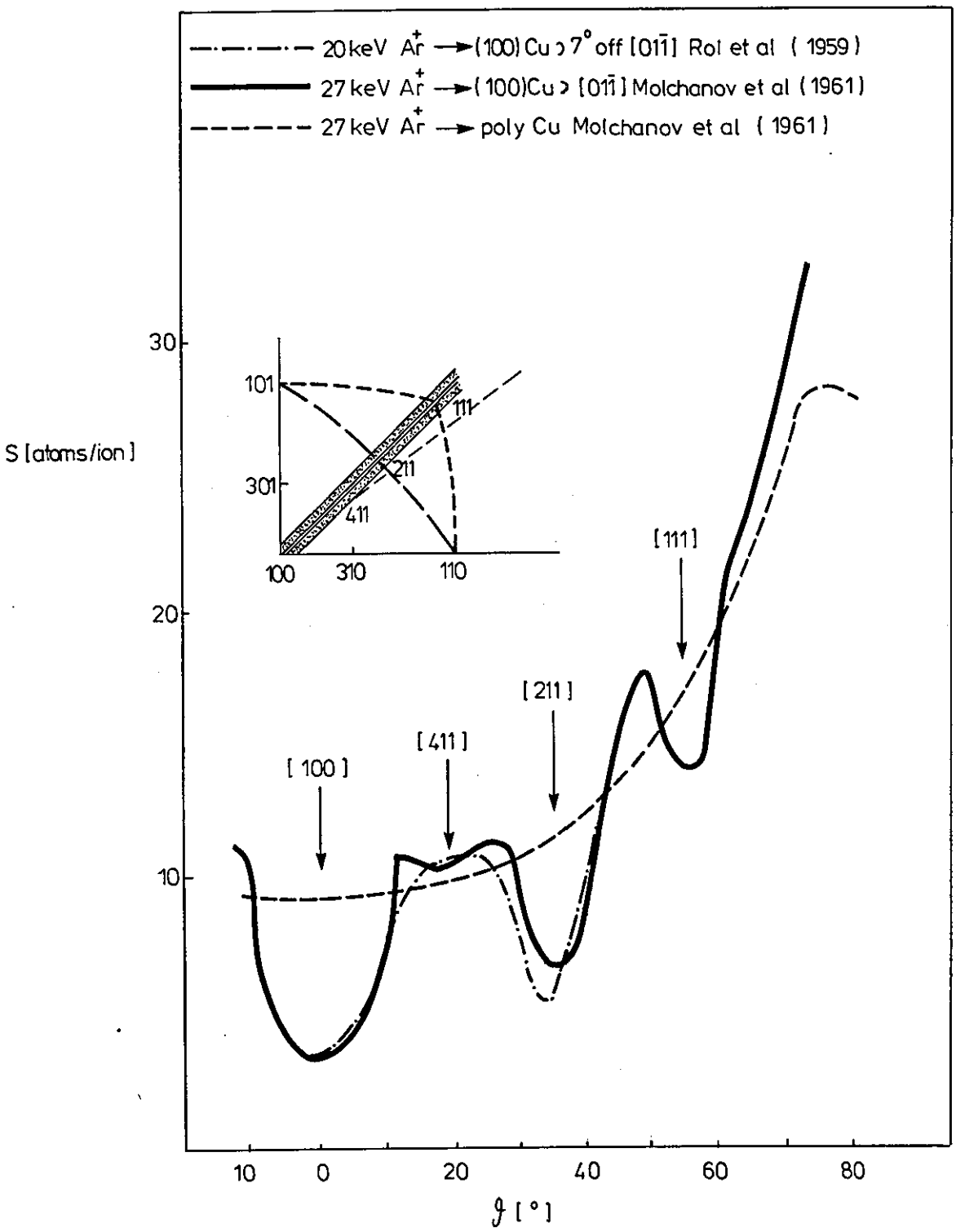

Figure 4.6: The sputtering yield as a function of the angle of incidence of Ar^+ on a (100) Cu crystal.

ions could then be divided by the lattice into two portions of colliding and non-colliding trajections and this property was responsible for the term transparency. However, difficulty in distinguishing between the two portions becomes apparent when a non-ideal situation is considered. Further work by Onderdelinden (1968) suggested that an incident beam on a crystal penetrated only a small distance into the surface approaching close to atomic sites and thus are scattered through relatively wide angles into a random beam. Alternatively, those ions that do not closely approach atomic rows constitute the axial or planar aligned beam.

This model was formulated by a consideration of Lindhard's channelling theorem (1965), and accommodates for transparency at any deviation from the ideal directions. As the angle of the ion to the crystal axis increases the fraction of the ejected atoms belonging to the random beam also increases until a critical angle is reached (viz. equ. 4.8) when the aligned beam is eliminated.

Rough approximations to the Onderdelinden model give the sputtering yield of a single crystal target as: (Onderdelinden, 1968)

$$S(\theta, E, \psi) = \eta \hat{S}(\theta, E)\ \chi\ (\psi, E) \qquad (4.9)$$

where E is the energy of the incident beam

θ is the polar angle of incidence of the beam

$\hat{S}(\theta, E)$ is the yield of the structureless medium under the same conditions of incidence.

ψ is the deviation angle of the beam from the axis of a nearby channel.

χ is the relative dechannelling yield.

η is a measure of the efficiency (Robinson, 1981)

The last parameter is dependent on the specific orientations of the crystal lattice and can reflect a range of values for different ion energies as predicted from experimental data (Elich et al, 1972). Furthermore, the dechannelling coefficient is dependent upon temperature since the thermal motion of the atoms can reduce the translational symmetry of the crystal, leading to collisions that would otherwise not occur. In this respect, the model does not given quantitative results for the dependence of the sputtering yield on energy and temperature. An attempt was made to account for dechannelling due to thermal vibrations by Elich et al (1971). Also the basic assumptions do not include the effect of focusing (see later), or contain any treatment of the way in which the energy of the incident ion reaches the surface to produce sputtering (Robinson, 1981). It does, however, describe the yield minima at, and above, $\sim$ 10KeV along low index crystallographic directions (Roosendaal, 1981).

4.3.2 The Focuson Theory

Another important idea proposed as a result of work on monocrystalline matrices was that of a focusing collision sequence between atoms. After Wehner (1955) had showed the effect of the anisotropic nature of backsputtered material from monocrystalline targets, Silsbee (1957) proposed the focusing model. This involved a collision sequence along straight rows of atoms, whereby if each particle moves at a smaller angle with the row than its predecessor it is said to be focusing. Conversely, if successive angles increase the sequence is defocusing.

The approximation that this type of collision sequence is exclusive to a single line of atoms and disregards neighbouring ones is clearly a major fault. Several workers since, however, have considered that an atom penetrating obliquely into a crystal lattice will interact with a 'ring' of neighbouring atoms about a single atomic row. As a result the atom is deflected back towards its original axis which improves focusing and a high focusing energy results. The effect of this assisted focusing has been treated numerically by Gibson et al (1960) who included studies of both the effects of neighbouring rows of atoms as well as the effect of the displacements.

Dynamical studies have been carried out (Holmes and Robinson, 1976) that show an increase in the focusing energy as a result of interactions between neighbouring rings of atoms an effect particularly emphasised for non-close-packed rows.

The sputtering of the crystal will depend on the efficiency of energy exchanges within the lattice. Energy may be lost either in an inelastic collision with a single row atom or by interaction with the neighbouring rings of atoms. Anderson and Sigmund (1966) have made detailed studies of energy losses in perfectly focused collision sequencies. However, although their results are in good agreement with classical dynamic theory involving energy losses with only ring atoms, along Cu(011) rows, there is a discrepancy with the dynamic calculation that involves both the next atom in the row as well as the ring atoms. In this event, calculations made by Gibson et al (1960) are in better agreement above about 8eV where the

energy loss is larger than in the 'ring-only' calculations (see Figure 4.7) (Robinson, 1981).

A further consideration to linear collision sequences is the real-time recording of the crystal lattice and the eventual effect on sputtering. Interstitial and replacement propagation will depend on whether atomic rows are closely, or non-closely, packed. Although defocusing collisions in closely packed planes (i.e. fcc < 001 > and < 111>) always seem to involve replacements (Robinson, 1981), an event in which a focused collision is possible that allows energy to be transmitted without the transport of matter. At the end of a focused collision an atom may be re-situated in its original lattice site by the concentrated action of the next row atom and its affiliated ring atoms, and the sequence is known as a focuson.

Conversely, a vacant site is left at the beginning of the sequence and each atomic site is successively replaced by its predecessor, resulting in an interstitial at the end of the chain, or ejection if the row intersects the surface, and the final energy exceeds the binding energy. This particular sequence is known as a dynamic crowdion. The physical aspects of both the focuson and crowdion sequences have been used recently with some success in computer simulation studies relating the bombarding angle of incidence with the sputtering yield (Shulga, 1983).

The work initiated by Silsbee (1957) on the focusing collision theory and used in different approximations by other workers, was subsequently challenged by Lehmann and Sigmund (1966). They made a

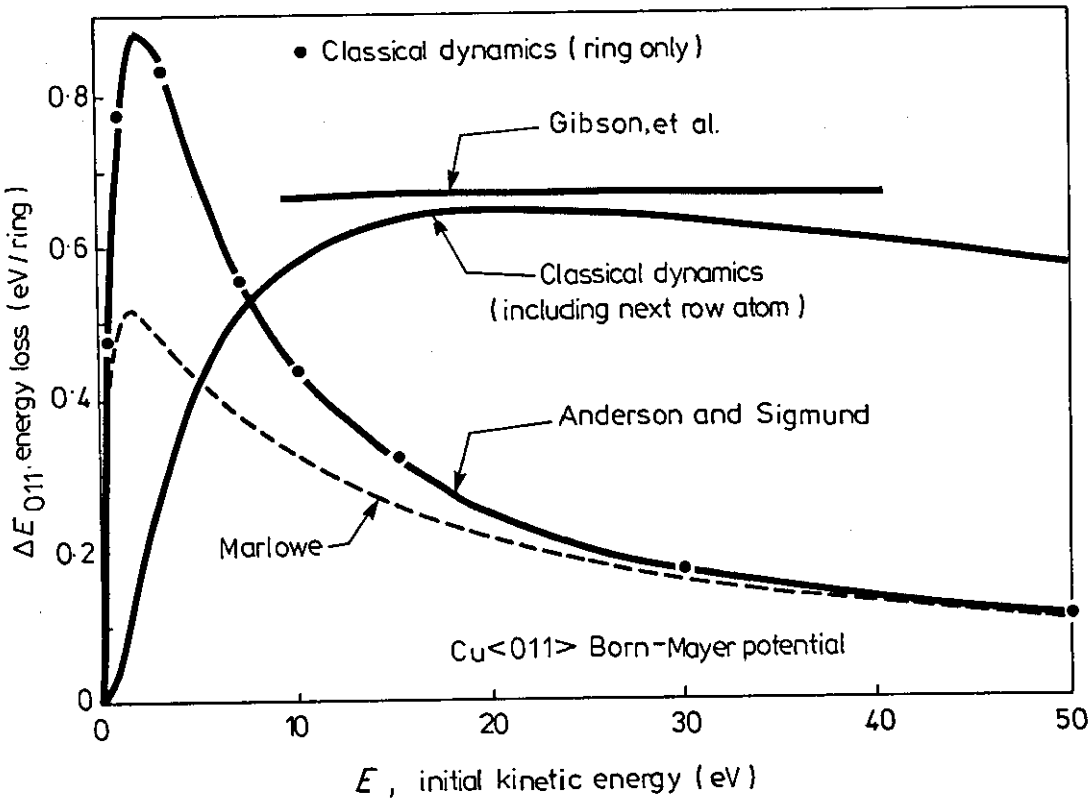

Figure 4.7: Energy losses calculated by several methods for perfectly focused linear collision sequences along Cu < 0 1 1 > rows. (After Robinson, 1981).

direct comparison of the theory with the Wehner spots produced from sputtering a crystal of tungsten with 150eV Hg^+ ions, and 50eV Hg^+ ions on a silver crystal. They deduced that the small depths of penetration of the bombarding ions could have no significant influence on the ejection patterns observed in Wehner's experiments, if collision sequences along close-packed rows were considered. Also, ejection patterns have been observed from crystal structures that possess varying atomic spacings between rows of atoms, for example diamond and zinc-blende (Wehner, 1956). The focusing idea should ideally apply only to lattice structures having short, regular interatomic spacings, which may further be complicated by radiation damage.

To avoid such difficulties, Lehmann and Sigmund (1966) formulated a model that required a target to have an ordered structure. By a consideration of the angular and energy distribution of the sputtered particles it can be shown by a simple example (Robinson, 1981) that the model exhibits spot patterns characteristic of high energies.

The previous discussion has indicated that due to approximations being made on pure dynamical theory there will always be an uncertainty between theoretical and experimental results. Neither the focuson theory nor the Lehmann and Sigmund model present the three-dimensional nature of atomic collisions, and therefore cannot be regarded as correctly predicting the origin of sputtered atoms. Because of the complex nature of sputtering, numerical calculations have until now proved too difficult and time consuming when numerous collisions are taken into account. However, recently with the aid of computer simulation and specially written programmes, studies of single crystal

sputtering have proved very promising. Many computation studies are based in the binary collision model (Schlang, 1965; Shulga, 1971; Eltekov et al, 1982), and include recoil effects and surface relaxation. They do, however, sometimes differ in detail in that they employ various approximations of collision potentials (Harrison et al, 1973). Recently, Shulga (1983) has published a computer simulation study of the sputtering yield as a function of angle of incidence for 27KeV Ar^+ ions in Cu single crystal and polycrystalline targets. The special computer package used incorporated many combinations of collision chain events including mixed focused-defocused chains, and a planar form of surface potential barrier (after Sigmund, 1969). More importantly, the simulation could distinguish the contribution to sputtering that the different collision chains produced. Figure 4.8 illustrates the good agreement between theory and experiment for 27KeV Ar^+ bombardment of Cu < 001 >.

In conclusion, the exact nature of events taking place in the sputtering of single crystal materials is not fully understood, although the implications of individual interactions and tertiary effects such as temperature rises and surface topography are slowly becoming better understood (Carter and Colligon, 1968). The sputtering yield is the most important integral characteristic of sputtering and the previous discussion has indicated the numerous studies carried out on this topic. Essentially, there is a crystallographic orientation dependence of the sputtering yield, which exhibits an increase for ions incident along a low index direction. The magnitude and angular distribution of the ejected atoms will effectively be energy dependent,

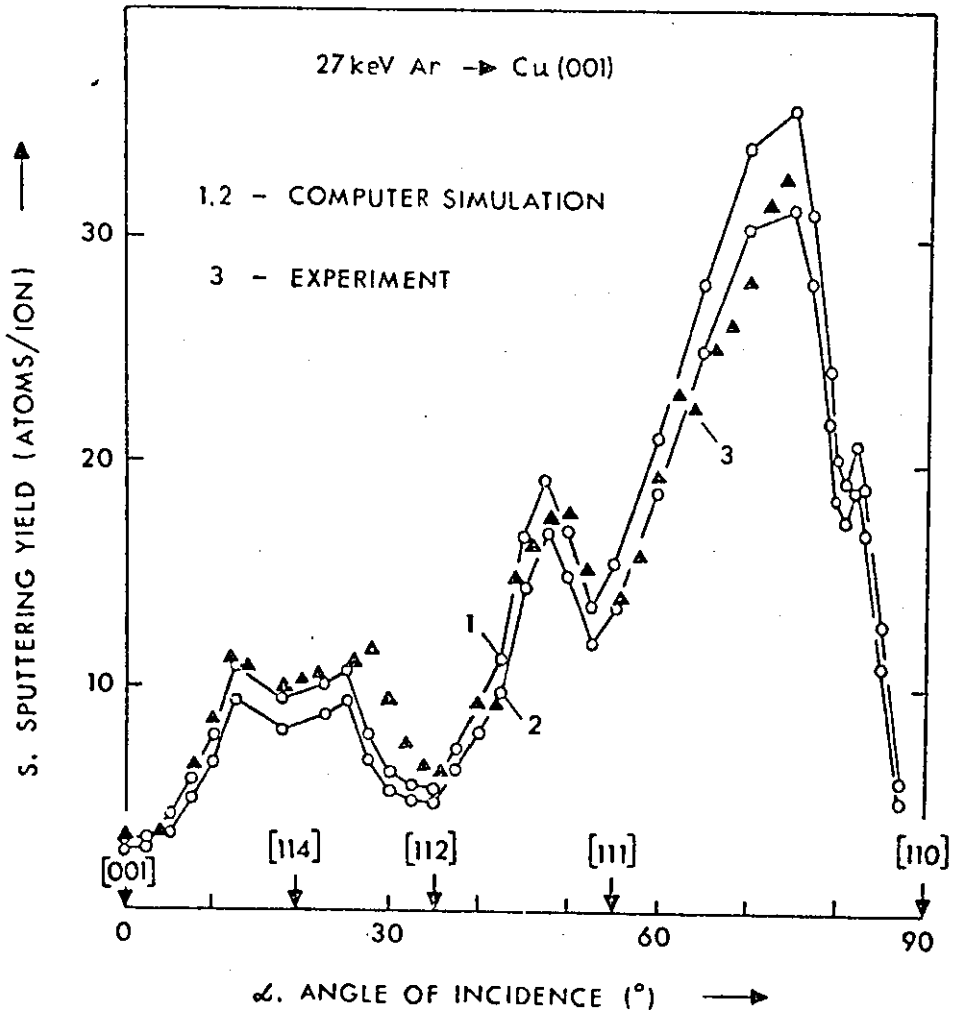

6a

Figure 4.8: Single crystal sputtering yields versus the angle of incidence. Points 1 and 2 represent a simulation for different surface barriers, and 3 is experimental data. (After Shulga, 1983).

since it is the nature of the resultant collision chain that ultimately determines the depth of origin of a sputtered particle. In this respect the transparency and focuson models are only valid for ideal ion-target combinations. A failing in the Onderdelinden model is the omission of dechannelling, an effect which may have a significant influence on the sputtering yield where high temperatures are present (e.g. thermal spike effects).

As yet, no adequate theory has been developed to account for the sputtering of single crystals in the extreme energy region due mainly to lack of knowledge of accurate surface energetics. With improving computer technology, advancement in this subject is rapidly increasing.

4.4 Other Related Bulk and Surface Effects

The previous discussion has indicated some of the physical mechanisms in sputtering, and their dependence on various ion-target parameters. Perhaps of more significance, however, is the result of these events in experimental studies. The phenomena relating to the sputtering process and which are the most widely studied include such effects as: Bulk and surface diffusion, the angular and energy distribution of sputtered atoms, and redeposition. The exact nature and occurrence of these particular effects are beyond the scope of this thesis, and will only be briefly mentioned. However, the author considers the influence of temperature, atomic mixing, preferential sputtering and surface topography, as a result of ion sputtering to be more significant to the work presented, and will be discussed in more detail in the following text.

The main difficulty in attempting to categorise the above phenomena is that in many instances two or more may be related in some way. For example, Rossnagel and Robinson (1982) have shown that by seeding a surface with impurity atoms and simultaneously ion bombarding it, specific topographical features are observed. They suggest that this results from the adatoms forming clusters by surface diffusion. Also the cone density was monitored as a function of temperature, thus a value for the activation energy of the adatoms could be determined. This type of 'surface' diffusion has been studied on a more theoretical basis elsewhere (Reed and Ehrlich, 1981) and illustrates the temperature dependence on atomic jump rates and interactions between atoms in the absorbed layer. The relevance of these studies is emphasised in surface analysis, where using a poor vacuum, effects such as surface contamination can have pronounced effects (Shimizu and Kawakatsu, 1979). Other studies of diffusion have been more concerned with impurity atoms travelling from the surface of a material into the bulk as a function of temperature (Gust et al, 1981).

Bulk diffusion phenomena becomes particularly significant in depth-profile analysis where ion beam mixing can contribute to the broadening of the profile (viz. section 1.2). This is a result of mobile defects, such as vacancies and interstitials being generated, and atomic transport occuring via local thermal effects. This process is known as radiation enhanced diffusion and has been the subject of several experimental (Biersack, 1973; Paine et al, 1981) and theoretical studies (Carter et al, 1980; Carter and Cruz, 1981).

Information on the different contributions to these effects and other sputtering phenomena can be gained from measurements of the energy and angular distribution of the sputtered particles. Calculations of the parameters rely heavily on the assumption that there is an isotropic distribution of momentum of the recoils, produced by an energetic ion in a collision cascade, and therefore will be independent of ion beam geometry (Roosendaal, 1980). This, however, has not been verified in experimental studies, where angular distributions of the sputtering yields of the targets used, had a preferred forward direction, at oblique angles of incidence (Wehner and Rosenburg, 1960; Formann et al, 1966; Hofer et al, 1978; Bay et al, 1980).

Since the early investigations, workers compared the resultant emission distribution to a cosine power law relationship. However, further study revealed that this was only approximate for intermediate energy ranges (1 - 10KeV), and tended to be over-cosine for higher energies (> 10KeV), and under-cosine for energies < 1KeV (Vossen, 1979). An example of the overall distributions at these energies; produced by normally incident ions is shown in Figure 4.9.

This aspect of sputtering is particularly relevant to ion beam etching (Miller and Czanderna, 1975), sputter deposition (Vossen, 1974), and the microelectronics industry (Smith, 1976), where a build up of sputtered material has been observed around the edges of steep surface features, and is known as redeposition. Theoretical studies have been performed by Bayly (1972), and Gloersen (1976) to examine the build-up of redeposited material, using cosine distribution (assuming an ion beam perpendicular to the surface), and by Belson and Wilson (1981) using an isotropic emission distribution for comparison. Recently, Makh (1981) and Smith et al (1983) have modelled the change in surface shape

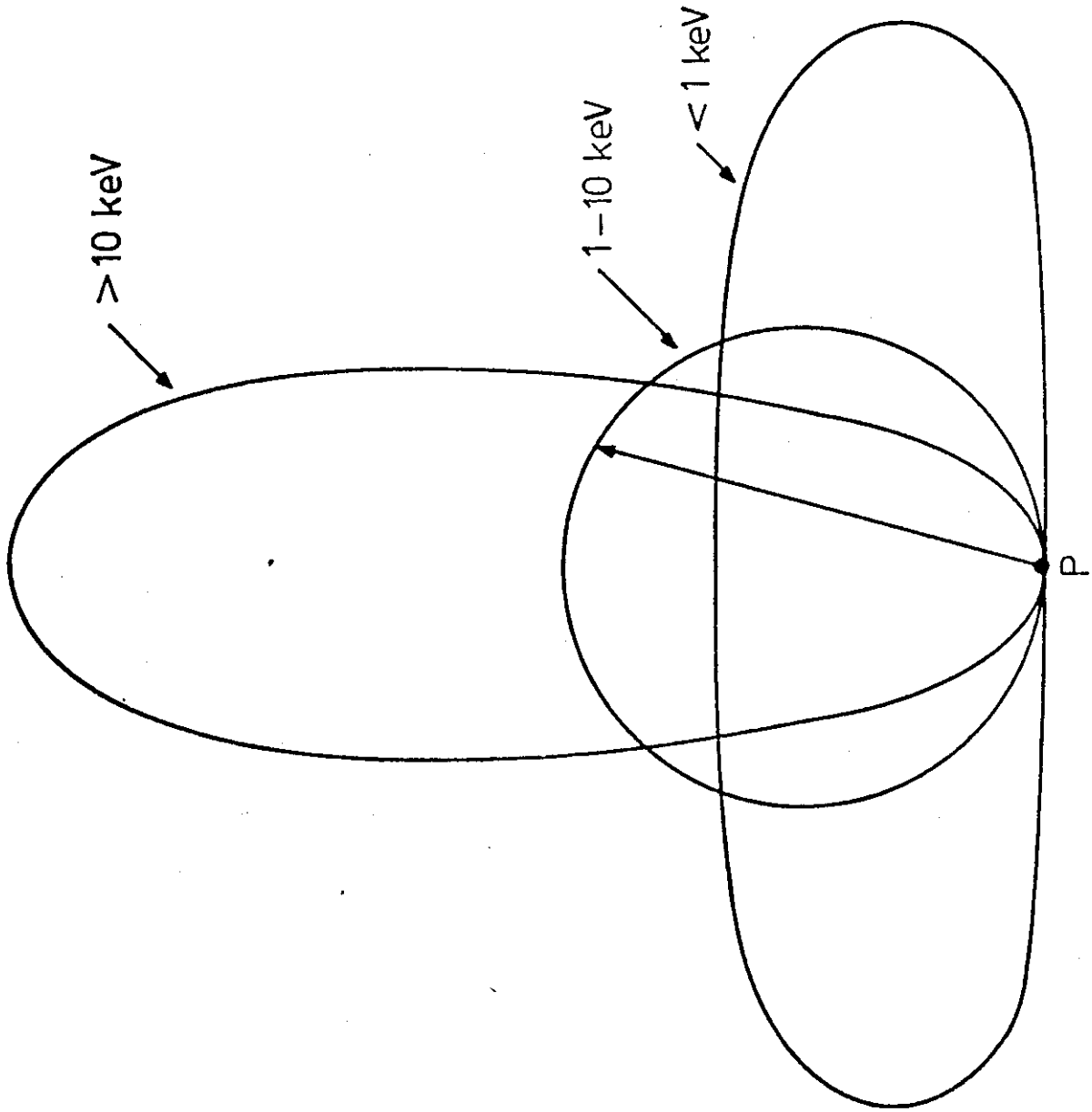

Figure 4.9: The angular distribution of material sputtered from a point P at different energy levels. The amount of material emitted in a given direction is proportional to the length of the vector from P to the distribution curve for the particular energy level of the ion incident on the sputtered surface. (After Vossen (1979)).

due to redeposition at a steep boundary, using a computer simulated anisotropic cosine distributions, similar to that depicted in Figure 4.9.

The exact nature and shape of the distribution of sputtered particles will ultimately depend on the ion target combination. Both theory and experimental studies have indicated an anisotropic emission, and in a particular paper by Rosendaal and Sanders (1980) suggests that the directional dependence implies a deviation from the E^{-2} asymptotic behaviour of the high energy collision cascade. Therefore, any such deviations cannot always be related to the different sputtering mechanisms.

4.4.1 Recoil Implantation and Atomic Mixing

The process involved in any sputtering event will inevitably lead to atomic migration or mixing, and as a consequence will be of significance in surface analysis studies. For example, the boundary layer in thin-film depth-profiling might be broadened due to the injection of one species into another (Etzkorn et al, 1973). Furthermore, bulk composition in a multicomponent target may suffer change due to an implantation of the incident ion species, or the atomic species of an absorbed layer, or by a re-ordering of the atomic structure due to mixing events.

The primary disordering mechanism is collisional mixing, which qualitatively can be classified into recoil implantation and cascade mixing (Sigmund and Gras-Marti, 1980). The distinction made here is that recoil implantation is due to direct ion-target collisions, and

cascade mixing is a result of target-target collisions.

Several experimental (Tognetti et al, 1981; Lau et al, 1981; Wittmaack, 1982), and theoretical studies (Carter et al, 1979; Winterbon, 1980; Sigmund and Gras-Marti, 1981) on collisional mixing have been published recently. The theoretical approach of these workers differ in some respects in that they adopt either the Boltzmann transport equation, and account for both cascade mixing and recoil implantation (Sigmund and Gras-Marti, 1981), or they model the mixing as a diffusional phenomenon (Carter et al, 1979). However, a general resultant effect has been observed in most cases which indicates that recoil implantation causes an anomalous shift of the depth profile, whereas cascade mixing produces primarily a broadening and its diffusion coefficient is essentially independent of temperature.

4.4.2 Temperature Effects in Sputtering

It is inevitable that an increase in a target temperature will lead to an increase in the vibrations of the atoms about their lattice sites. If a collision chain is initiated along a close-packed direction the increased vibration of the atoms will cause a less efficient momentum transfer, and hence a decrease in sputtering yield would be expected as the temperature increased. This particular effect is clearly demonstrated in Figure 4.10, which shows the results of experiments performed by Snouse and Bader (1962). They bombarded polycrystalline copper with 3KeV N_2^+ ions in the temperature region 60° - 470^oC.

Alternatively, during bombardment the damage produced by the incident ions may anneal out with a rise in temperature making the momentum transfer more efficient and thus increasing the sputtering yield.

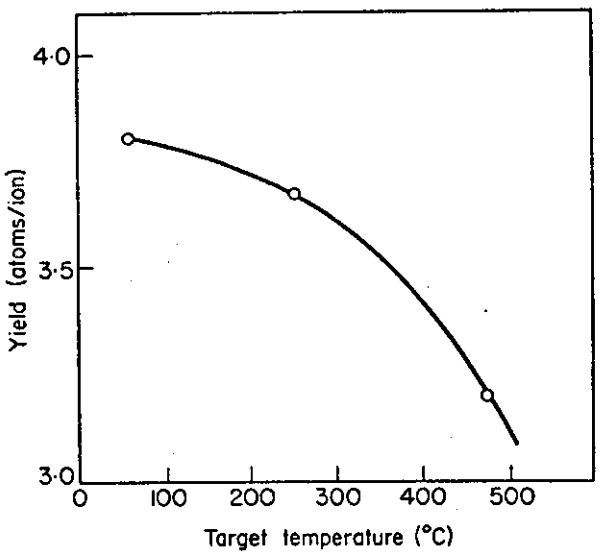

Figure 4.10: Variation of sputtering yield with target temperature for 3 keV N_2^+ ions on copper. Each point on the curve is the mean of several measurements

(After Snouse and Bader, 1962).

Another aspect to consider is that the transparency of the surface decreases due to the atoms vibrating and the sub-surface layers become more exposed. By the dechannelling (Elich et al, 1971) model an increase in temperature would lead to an increase in the sputter yield. Temperature rises have been found to cause a decrease in effective binding energy of surface atoms (Carlston et al, 1965), due to the increase in their vibrational amplitude. Therefore, it would require less energy to sputter the atoms.

A study was made by Nelson (1965) showing an increase in sputtering yields for several elements over a range of temperatures. The targets were bombarded with 45KeV Xe^+ ions, and large increases in the sputtering could be seen at just below the respective melting points. This effect, which is known as thermal sputtering, is a function of the ambient temperature of the lattice (see Figure 4.11).

Other work related to thermal effects in sputtering have been published elsewhere (Elich, 1972; Szymonski et al, 1978; Kelly, 1979) and report on the sputtering behaviour in a certain temperature range. It must be noted however that ion beams can cause the local heating of a sample surface, particularly when fluxes are in the range 1 - 10mA cm^{-2}, as sometimes do occur in dynamic SIMS. The final temperature will depend on the material and its cooling efficiency as was shown in a recent paper by Te-Chang et al (1983). Although they do not relate the temperature rise to the sputtering yield it would seem likely that a similar effect could occur to that seen in Figure 4.11.

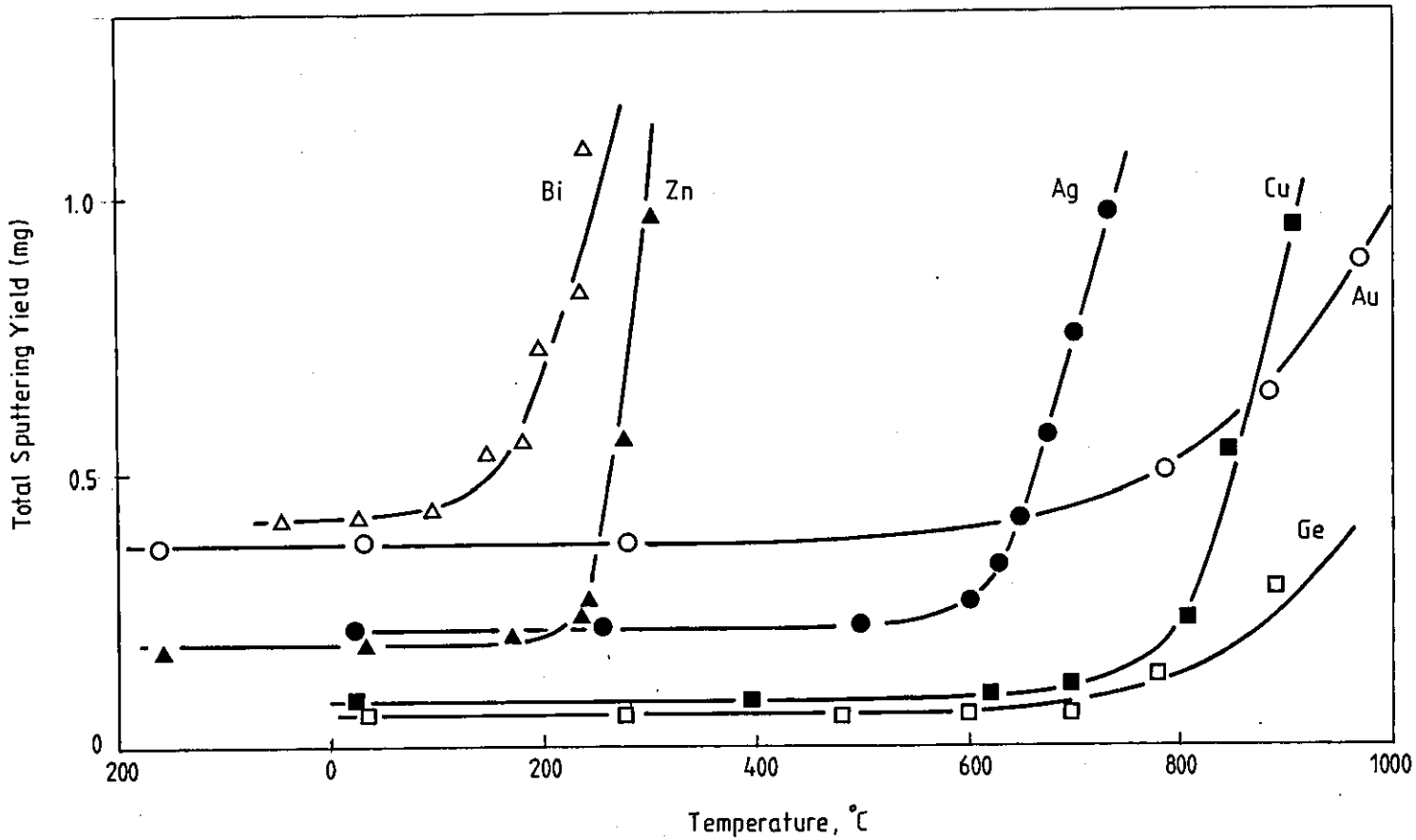

FIG. 4.11 TOTAL SPUTTERING YIELD (LOSS IN WEIGHT) VERSUS TARGET TEMPERATURE FOR BOMBARDMENTS WITH 45 keV Xe^+ TO A TOTAL DOSE OF 2.9×10^{16} IONS. Due to Nelson (1965)

4.5 The Sputtering of Alloys

It is well known that the surface composition of multi-component targets is modified under ion erosion, and with the technology now available for surface analysis there has been an increased interest in the sputtering of these materials (Rehn and Wiedersich, 1980; Betz et al, 1980; Frankenthal and Siconolfi, 1981). The mechanism by which this surface modification takes place is known as preferential sputtering, where the components in the surface layer are ejected preferentially due to their different partial sputtering yields. It is therefore necessary to gain an understanding of the sputtering behaviour of this class of materials in order to obtain quantitative information about the surface and several reasons indicate the importance of this. Following prolonged bombardment a multicomponent target is inherently created due to the incident ions becoming embedded in the surface of the material. This could have a significant influence on partial sputtering yields as a comparison between the results of Almen and Bruce (1961), and Anderson and Bay (1972) indicate. The former found yield minima for reactive ions and a maxima for noble gas ions, whereas the latter observed that these minima disappeared when the ion dose was kept extremely low. In a recent paper by Winters (1982) it is shown that the sputtering yield of nitrogen adsorbed onto W and Mo targets is dependent on both the incident ion energy and its mass, and the mass of the substrate, thus indicating the complex nature of preferential sputtering for an alloyed target in comparison.

Prolonged ion bombardment of multi-component systems requires that a steady state condition is reached due to conservation of momentum. This is a situation in which the sputtered atom flux reflects that of the bulk and has been shown theoretically by Werner and Warmoltz (1976) to be of the order of one mono-layer. Other theoretical models showing the influence of preferential sputtering assume that a steady state situation already exists (Shimizu et al, 1973; Webb et al, 1978).

On the macroscopic scale preferential sputtering manifests itself in the development of surface topography. Bibic et al (1982) have shown this experimentally by sputtering silver/copper alloys with Ar^+ ions and observed a variety of surface relief effects. An indication of how surface topography would form by this mechanism is also discussed in the paper by Werner and Warmoltz (1976). The development of rough surfaces has been shown to appreciably affect depth profiles in surface analysis (Hofmann and Erlewein, 1977), and some aspects governing its evolution will be discussed in Chapter 5.

CHAPTER 5

5.1 The Development of Surface Topography Under Ion Erosion

5.1.1 Introduction

There have been numerous studies on the development of surface topography in the last twenty years, and consequently the published results showing the specific structures formed, vary considerably due to the vast range of materials used. Furthermore, surface changes have been found to be dependent on one or more variable parameters including bombarding ion species and energy, angle of ion incidence, total dose effects and target material (Navinsek, 1976). In many of these studies observed surface features have been reported as a result of one set of conditions relating to arbitrary values of the above irradiation parameters, and if several materials are to be compared difficulty may arise interpreting the mechanisms by which different topographies are formed.

It is therefore of prime importance to know under what conditions and by which process their formation occurs. This can be achieved by adopting a systematic approach where one or more materials are chosen for ion bombardment and each of the irradiation parameters are varied over a particular range of values. Although this has only recently been achieved (Lewis et al, 1982; Auciello, 1982), the majority of the work has been concerned with commonly occuring ion induced features such as cones (Stewart and Thompson, 1969; Panitz and Sharp, 1981), pyramids (Whitton et al, 1980) and faceted step structures

(Carter et al, 1977, Littmark and Hofer, 1978), as well as other forms of undefined shape (Bibic et al, 1982).

The development of conical protrusions under ion bombardment has received particular attention since these types of surfaces have a degrading influence on depth resolution in surface analysis (Hofmann and Zalar, 1979; Williams, 1983). Generally, it has been recognised that cone formation relies on two basic processes, and the mechanisms operating in such instances will be discussed in this chapter.

The frequent use of inert gas species for much of the reported work on this topic is evident, but recently, due to improved results in micro-etching of electronic circuits, there has been an increased interest in the use of reactive ion bombardment (Gokan et al, 1984; McNevin and Becker, 1984). The work in this area is relatively new and not well understood, and it has been suggested that ion-surface reactions take place which may influence the nature of the topography developed (Tsunoyama, 1980). Therefore, to clarify the two regimes and more specifically for the purpose of this present work, surface topography development by inert and active gas bombardment, will be discussed separately. Further, due to inherently different characteristics of metals and semiconductors, a separate section will be dedicated to each, thus highlighting similarities and differences of observed topographies following ion erosion for each particular material.

5.1.2 Cone Development by Particulate Contamination

The first observation of surface erosion by ion bombardment processes was reported by Grove in 1852. Interest in the technique was not evident for almost a century when in 1949, McCutchen (1949), and McCutchen and Pahl (1949) established that for some purposes the method was superior to chemical etching. However, it is now known that there exists a close relationship between the selective etching of surfaces by chemical processes and that caused by ion beams (Barber et al, 1973).

Several years earlier to McCutchen's study, the first observation of surface texturing by erosion was made by Güentherschulze and Tollmien (1942). They hypothesised that angular variations in surface reflectivity of glow-discharge cathodes were the result of sub-microscopic conical structures. In the same year Fetz (1942) discovered that the sputter yield of atoms ejected from a surface was dependent on the angle of incidence of the impact ions.

Güentherschulze and Tollmien who initiated studies into ion induced topography also noted that the cone phenomenon occurred on a wide variety of metals, and that the cone apex angle was different for each metals. Further observations of similar structures were reported by Spivak et al (1953) who described cone development on aluminium using high ion current densities, and Wehner (1955) who found cone formation on silver (111) planes. Both these authors concurred with Güentherschulze's postulation that the cones occur where low sputtering yield particles protect the underlying material

from sputtering, initiated by a migration of condensed metal atoms on the cathode surface.

A detailed study of textured surfaces following ion bombardment was not possible until the advent of the scanning electron microscope (SEM). However, observations of cones on the sputtered surface of polycrystals were first carried out by Spivak et al (1951) using the replica technique with an electron microscope, although this was most suitable for the study of considerably rough surfaces.

The discovery of cone development, following ion bombardment of solid surfaces prompted initial suggestions that they resulted from a preferentially sputtered substrate shielded by a foreign body. An example of cone development is shown in Figure 5.1 for Ar^+ bombardment polycrystalline gold. Stewart (1962) studied ion etched (110) tungsten indicating that the resultant conical spikes could originate from either inclusions in the material or particles resting on the surface. This particular aspect was later discussed by Stewart and Thopmson (1969) who observed conical structure developed on a tin crystal following 5KeV Ar^+ bombardment. Their development was attributed to the fact that the crystal was grown in a graphite mould and was therefore expected to contain graphite and oxide particles. Small blobs appearing at the tops of the cones and then finally disappearing after prolonged ion bombardment, were considered to be foreign particles initially present as inclusions in the crystal and uncovered during the erosion of the surface. Stewart and Thompson (1969) also discussed the theoretical development of the cone by considering an intersection between two planes in motion on the surface

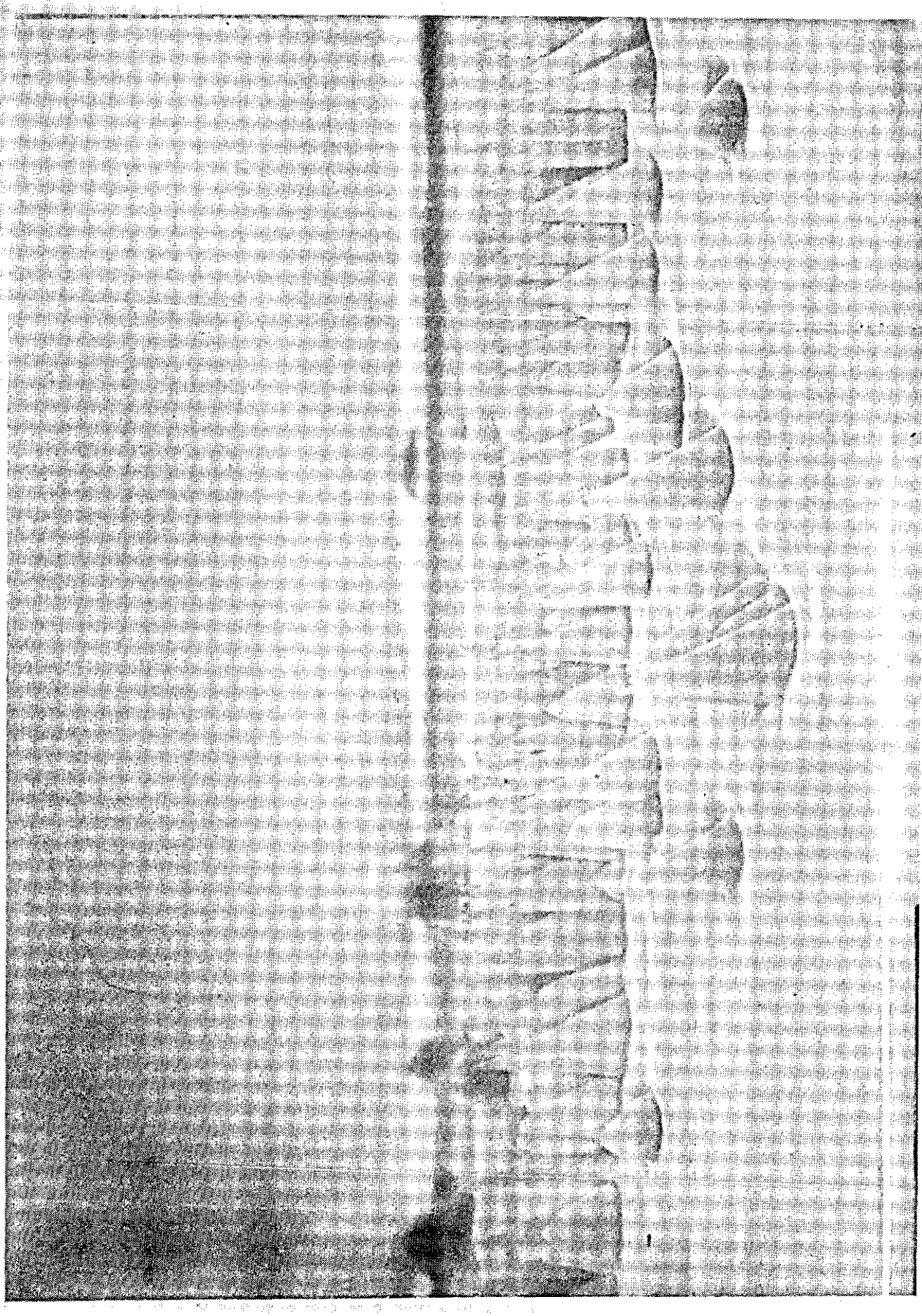

Figure 5.1: The development of conical features on polycrystalline gold following prolonged Ar^+ ion bombardment.

and showed that its angle at the tip contracts inwards to a value ($\pi - 2\hat{\theta}$) (where $\bar{\theta}$ corresponds to the maximum sputtering yield angle on the $S(\hat{\theta})$ curve), and with its axis along the direction of ion incidence.

The shielding principle for cone formation has also been substantiated by Wehner and Hajicek (1971) who studied the surface of Mo and Cu targets sputtered simultaneously in a Hg discharge tube. They arrived at several conclusions:

1. The cone density on the Cu surface was dependent on the flux of the Mo atoms, and even at low arrival rates of these atoms (1 Mo atom per 500 sputtered Cu atoms) cones were formed.

2. If the seeding with Mo atoms was stopped but sputtering of the Cu was continued the cones break up and eventually disappear.

3. By partial masking of the target it could be shown that the cones did not protrude above the original surface, hence they are a result of sputter protection at selective points.

4. The surface of the Mo target where Cu atoms arrived during sputtering showed no cone development.

5. When the Cu was replaced by Ag or Au, or when Mo is replaced by W, cones still form. However, no development of such structures took place for target combinations such as Cu-Ag or Cu-C.

6. Oblique ion incidence showed the cones to point in the direction of ion bombardment.

Further points noted by Wehner and Hajicek (1971) were that the angular distribution of sputtered particles from the textured surfaces were quite different from that of a smooth surface. Also the sputtering yield of the copper was severely reduced after dense cone coverage, attributed to sputtered material becoming trapped between the cones and therefore unable to escape the surface.

The postulation that a shielding effect took place in the development of the cones was not upheld as demonstrated in 5 above for the target combination Cu-C. Wehner and Hajicek suggested that the solubility or the activation energy for surface migration of the low-yield atoms on the high-yield material play additional roles. This has been the subject of more recent work by Kaufman and Robinson (1979) who formulated a theory based on surface diffusion predicting the variation in cone spacing with surface temperature as well as a critical temperature below which cones will not form. Qualitative agreement was shown with experimental results, and the theory was also able to predict coning of a low sputtering yield substrate seeded with a high sputtering yield material (e.g. Au on Al). For this particular case they argued that cones would form, provided that the seed material is sufficiently mobile to replenish the sputtering loss from a seed cluster. The mobility of the seed material would be dependent on activation energy and surface temperature, thus they concluded that the existence of a minimum critical temperature was important such that a sufficient reduction should suitably restrict the mobility of any seed material to avoid coning. This had previously been demonstrated by Hudson (1977) who found that if the normal coning

process of copper seeded with tantalum was interrupted after every minute of operation and allowed to cool for several minutes, no texture was created. Instead, the copper became coated with tantalum. It was also noted by Hudson (1977) in the same study that the precise structure and density of the cones formed on a particular substrate varied depending on the seed material. However, this in turn was dependent on the combination of seed-substrate materials, where for silicon textured with tantalum, molybdenum and titanium the resulting morphologies were found to be nearly identical, indicating an influencing interaction between the substrate and the seed material.

During the time devoted to work on cone generation, workers began to observe a variety of subtly different structures evolving on a surface. For example Wilson and Kidd (1971) observed faceted cones with hexagonal symmetry when they bombarded gold with Ar^+ and Xe^+, and which they attributed to crystalline effects within the lattice. Witcomb (1973, 1974) also found a similar effect on stainless steel and in accordance with Wilson and Kidd (1971) suggested that the facets formed as a result of the high sputtering yield of low index crystal planes. Further, and consistent with other hypotheses, Witcomb (1974) concluded that the types of structures he observed on stainless steel (cones and pillar protrusions) were formed from the different sputtering yields of the matrix and precipitates or fibrous inclusions within the substrate. It should be noted that the specific structure of the cones formed in this way will differ from those formed purely by initial surface contamination. This was particularly emphasised in a study by Rossnagel and Robinson

(1981, 1982) who deliberately seeded a Cu target with Mo atoms while maintaining the target temperature at 300°C. They were able to calculate activation energies of the seed material on different substrates (Rossnagel and Robinson, 1982) where they noted that many of the materials used developed intrinsic cones but at the bombardment energies used (500eV) they were found to be of different shape to the impurity induced cones. In accordance with theory (Barber et al, 1973) and experiment (Hudson, 1977) it was also shown that if there was not a sufficient cluster of seed material at the cone apex, it would eventually be eroded away.

5.1.3 Cone Development by Ion-Induced Defects

The discussion so far has presented two mechanisms for cone formation (1) that a surface impurity of a different sputtering yield than the matrix results in a discontinuity between the two media causing conical protrusions to form (2) cone growth can result from surface migration of atom clusters. Conical structures have been observed to form on single crystals, polycrystalline and multicomponent systems by these processes, however, there exists a further mechanism by which they can form. This is the initiation of surface discontinuities or ion beam induced defects followed by ion erosion to produce the final form. A necessary condition for the appearance of damage induced surface topography during ion erosion of metal single crystals was first presented by Hermanne (1973). This model proposed a mechanism of preferential erosion of parts from the sample surface due to a local increase of sputtering yield above extensive defects. These were created as a result of the migration of point defects in the near

surface, produced by collision cascades of the incident ions. The condition was in terms of experimental parameters and implied that extensive defects should have formed before the receding surface reaches them. A more recent study has been reported by Nobes et al (1983), who extended the theory of the evolution of surface shape (Barber et al, 1973; Carter et al, 1973) to include spatio-temporal variations of ion flux density, sputtering yield and substrate atomic density. This treatment was more generalised than Hermanne's (1973) since examples pertaining to polycrystalline or single crystal targets were shown.

The existence of defects within the surface, whether induced by ion bombardment or surface preparation (Turley and Samuels, 1981) has led to an even more varied development of different surface features in the form of pits (Carter et al, 1982), blisters on the surface (Erents and McCracken, 1973) and ripple topography (Nelson and Mazey, 1973). Examples of some of these are illustrated in Figure 5.2.

Perhaps one of the most widely used materials in ion-induced topography experiments is copper, in single crystal and polycrystalline form, and consequently much of the following discussion will relate specifically to this material. However, other studies have been performed on materials such as graphite, cobalt, beryllium (Paritz et al, 1981), stainless steel (Witcomb, 1974) and glass (Lukaszewicz and Kowalski, 1981) although the lack of quantitative data has restricted any definite conclusions in these areas. Controlled experimental procedures, however, have been carried out on some

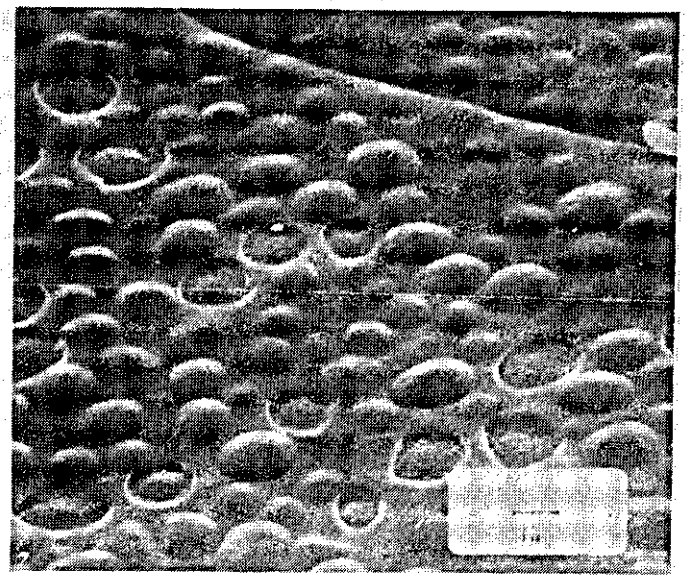

a

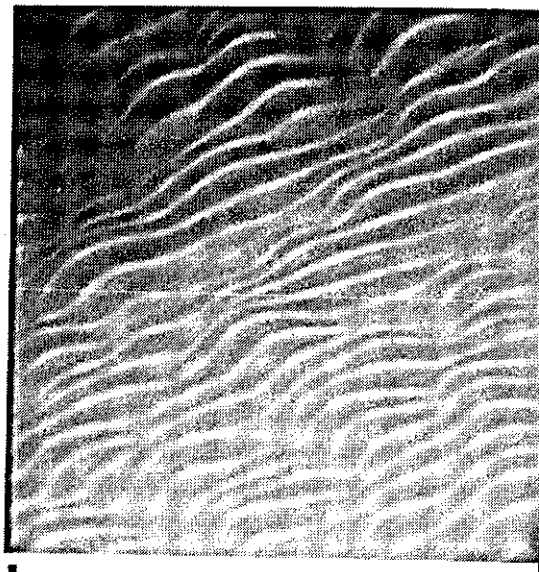

b

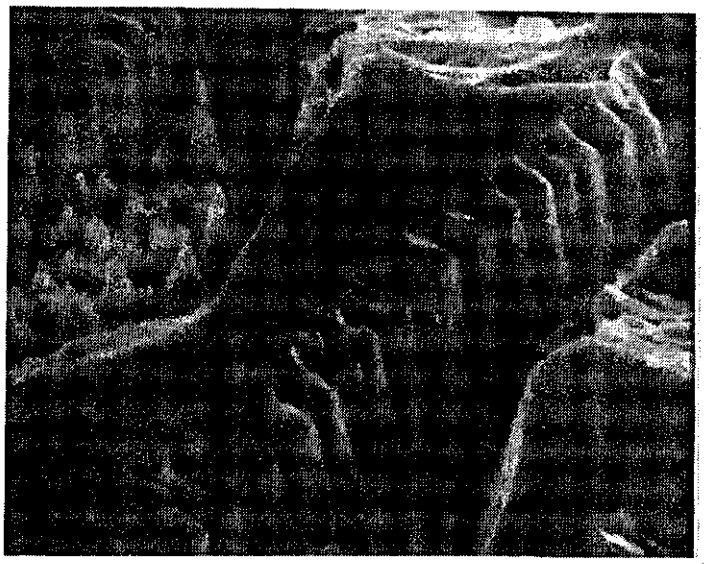

c

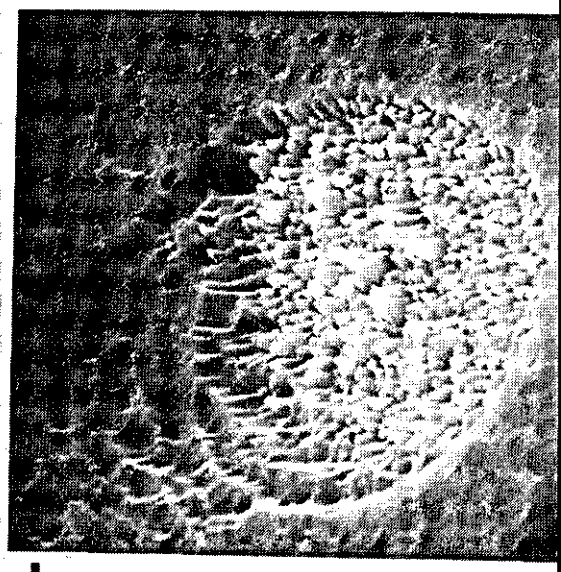

d

Figure 5.2 (a) Blistering of a Mo surface after high energy He^+ bombardment (After Erents and McCracken 1973)
(b) Ripple trains developed during O_2^+ bombardment of Si
(c) The topography of a Ag/Cu alloy bombarded with Ar^+ ions; (Bibic et al 1982)
(d) Surface topography of Cs^+ bombarded InP.

semiconductors by Wilson (1973), Nelson and Mazey (1973) and later by Carter et al (1977) and the nature of the features observed on these materials will be discussed in detail later.

Only recently have systematic studies been undertaken to examine the evolution of surface morphology with increasing ion dose and on the effect of different initial surface preparations. In a paper by Whitton et al (1977) several distinct features were observed on high purity polycrystalline copper following 40KeV argon bombardment which included:

(1) The delineation of individual-crystal grains via differential erosion processes.

(2) The formation of etch pits of density variable with grain size and with proximity to a boundary.

(3) The formation of cones located near major boundaries and within etch pits.

(4) Fine scale furrow or ripple structure.

The last feature was observed on both polycrystalline and (110) single crystal copper, and is similar to that observed in earlier studies (Nelson and Mazey, 1973), and is similar to that shown in Figure 5.2(b). Whitton et al (1977) followed suggestions made by previous workers (Nelson and Mazey, 1973; Hermanne, 1973) that the fine-scale ripple structure was associated with selective sputter etching of a dislocation network generated by the ion bombardment. The cone formation from this work could not be attributed to impurity induced

growth on the surface as had been previously reported (Stewart and Thompson, 1969), since a clean crystal surface was used. It was thus suggested that the intersection of a grain boundary and etch pit, caused by the elaboration of large defects or defect clusters was associated with the cone formation. Two micrographs illustrating this particular process are shown in Figure 5.3.

One most common observation resulting from the study described above was the production of regularly shaped faceted cones or pyramids on the copper surface. The term pyramid may be defined as a solid figure having a polygonal base with triangular sides meeting in a point, two separate examples of which can be seen in Figure 5.4. It was found on pure copper crystals that in etch pits, associated with certain grains, pyramids appeared, while in grains having other orientations pits were formed but with no associated pyramids. From Laue pattern analyses it was observed that only on grains having orientation of $\pm$ a few degrees from the (11 3 1) (which lies midway between the {100} and {110} planes) were pyramids formed. This discovery prompted a series of systematic studies to be carried out on specially prepared (11 3 1) copper, and in an initial study by Whitton et al (1980) several major conclusions were reported. The observations of dense arrays of cones and/or pyramids produced during 40KeV Ar^+ bombardment in clean conditions was clearly a result of ion bombardment induced surface defects, the most dominant experimental parameter being that of the crystal lattice and orientation. The etch pits for single crystal copper substrates were the forerunners of pyramid development (Figure 5.3) with both the etch pit base and the pyramid

Figure 5.3: The development of cones associated with the elaboration and intersection of large defect clusters and pit formation (after Whitton et al (1977)).

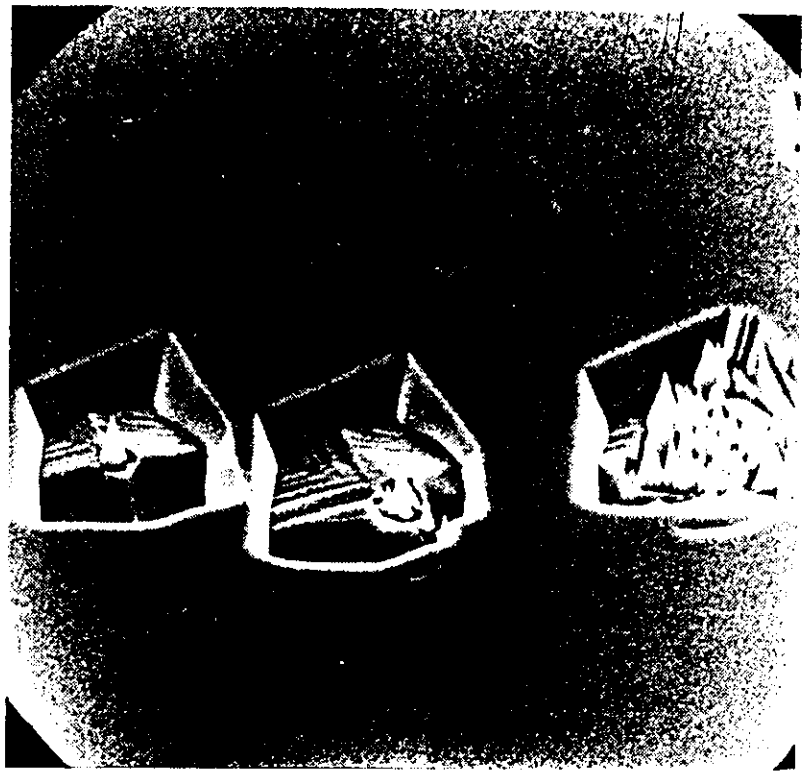

a

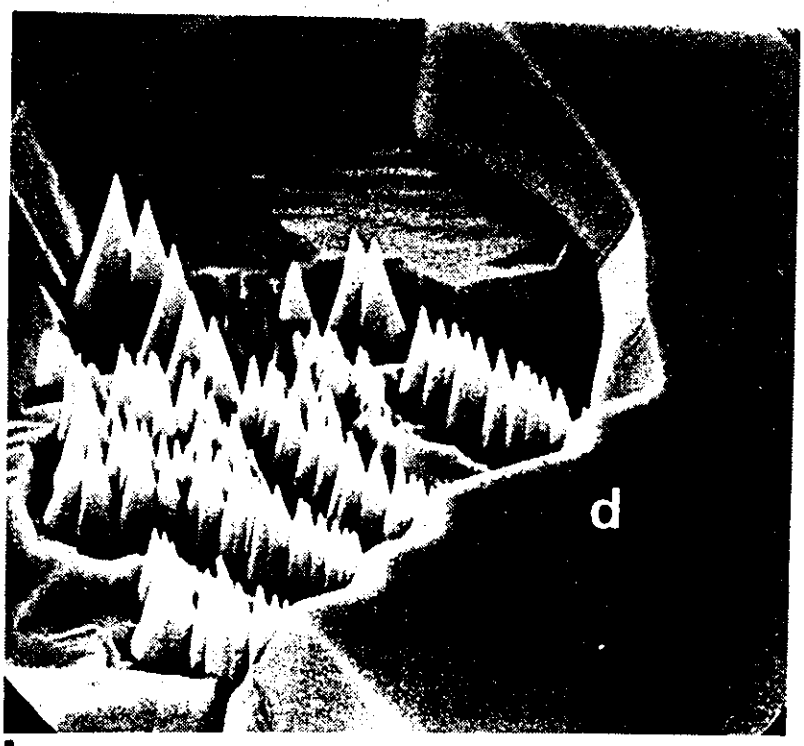

b

Figure 5.4: (a) An illustration of a pyramidal structure formed following Ar^+ bombardment of polycrystalline copper (after Whitton et al (1978)).

(b) Pyramid development following Ar^+ bombardment of Pb(111) (after Alexander et al (1980)).

a

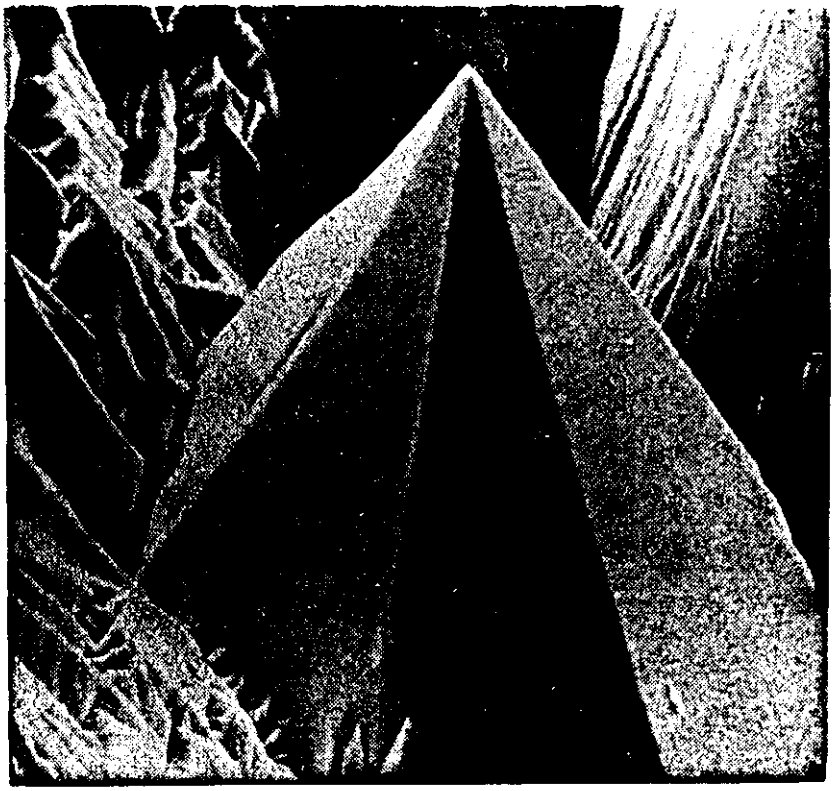

b

facets having a specific association with particular low index planes. The most significant feature of this study was the process of impurity-free formation of surface structure, characteristic of the crystal orientation and indicating a strong dependence on the history of the material and ion induced damage. This has further been substantiated by Whitton et al (1983) and Carter et al (1983) who performed ion bombardment on several (11 3 1) single crystal materials using a range of inert gases (this also included self-ion bombardment of copper). In all cases the topography formed on each material exhibited similar features, and the theories of development previously expounded (Whitton et al, 1980) were upheld. Furthermore, evidence was presented comparing impurity-induced pyramids to those produced from etch pits, the distinction being made by the fact that the former are always higher than the receding sputtered surface, while the latter are always at, or below, the level of the surface surrounding the pits.

Similar work has been performed recently by Auciello et al (1979) and Kelly and Auciello (1980) who observed pyramid formation on pure polycrystalline copper, that has been obtained by three different methods of surface preparation. All revealed an evolution of pre-existing asperities to well-defined pyramids underlain by grooves, to a later stage in which only pits were left, to a final stage having little or no relation to the initial asperities. The final stage was characterised by rippling, terracing, and preferential grain erosion. The most revealing feature of the work was that in the absence of major surface impurities, the initial surface topography was very important, and attributed convex-up irregularities as playing a major

role in pyramid development, an effect previously discussed (Carter et al, 1972; Barber et al, 1973). It was observed that pyramid density has a 1 : 1 correlation with asperities on initially rough surfaces, and that they were in general unstable and disappeared at high doses. This feature, however, should not be confused with the work performed on the (11 3 1) single crystal surface (Whitton et al, 1978, 1980) where pyramids formed on this crystallographic plane could be stable. However, separate work carried out on polycrystalline copper has confirmed the instability of conical protrusions following high dose ion bombardment (Lewis et al, 1979). Indeed, the relative stabilities under ion bombardment of surface features such as ridges, cliffs and cones (pyramids) have been regarded with some interest in recent studies on polycrystalline copper (Chadderton, 1977, 1979; Auciello et al, 1979(a)(b)).

5.1.4 The Influence of Surface Orientation and Structure on Sputtering Yield

The above discussion has introduced some vital conditions for the initiation and growth of surface topography. In much of the work performed on a large number of materials presented in the literature there has rarely been a systematic study accounting for all the different irradiation conditions, such as ion species, angle of ion bombardment, temperature and ion dose. However, it has generally been accepted that large scale surface changes induced by ion bombardment are mainly due to the fact that the sputtering yield is not constant over the whole surface (Navinsek, 1976). An investigation of the influence of this parameter was made by Teodorescu and Vasilui (1972)

who bombarded polycrystalline iron and copper at 0°, 45°, 60° to the surface normal. They explained the observed ion etching patterns on the basis of two factors (a) the surface microgeometry existing before ion bombardment (b) the angular dependence of the sputtering yield. Difficulty may be experienced in quantitatively explaining ion etched features on polycrystalline materials, since there is a relatively wide variety of structures developed due to preferential erosion of the many crystal orientations present. For this reason, experimenters generally preferred single crystal materials, where several irradiation parameters can be studied quantitatively (Gvosdover et al, 1976; Alexander et al, 1981; Lewis et al, 1982; Carter et al, 1982). Polycrystalline materials, however, have been successful for this particular investigation but only where pre-existing asperities on the surface produced well-defined features under ion bombardment, such as cones or pyramids (Lewis et al, 1979; Auciello and Kelly, 1982).

Tertiary effects in ion bombardment have been observed to influence surface structure, sometimes significantly enough so as to create large macroscopic changes in the overall surface appearance. These effects include processes such as redeposition and ion reflection, the latter of these being well illustrated in Figure 5.1, as the small pits occuring at the bases of the individual cones. The general mechanism for this process has been widely accepted as being the flux enhancement caused by ion reflection from a steep incline relating to any particular type of initial, or ion-induced topography. Figure 5.5 illustrates schematically a possible mechanism for the development of the pits occuring at cone bases during ion bombardment. Other features, such as singly expounded pits may also occur as a result of this process and

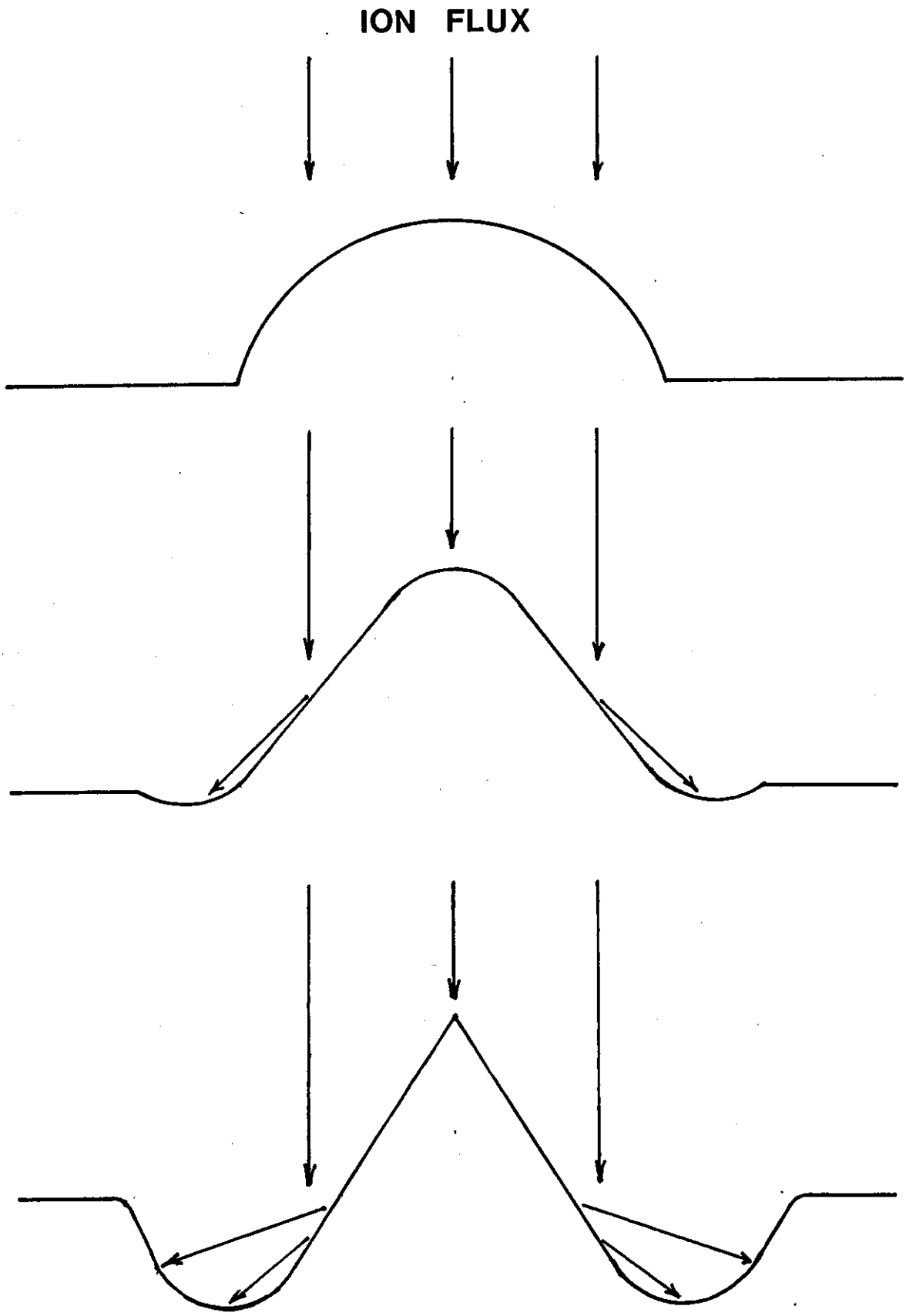

Figure 5.5: Schematic diagram showing a possible mechanism for the development of pits at cone bases.

these mechanisms have been discussed theoretically and observed experimentally elsewhere (Bayly, 1972; Vossen, 1979; Lewis et al, 1981).

Redeposition occurs when sputtered material has insufficient energy to escape into the vacuum, or it collides with a protruding part of the surface. The quantity of redeposited material would therefore depend on the energy and angular distributions of the sputtered atoms, the surface topography and the sticking coefficient. The effect of this mechanism has been shown to be significant in the fabrication of electronic device circuits where a considerable amount of redeposited material has been observed along the sidewalls of the etch patterns after the photoresist mask has been removed (Gloersen, 1975; Castellano, 1980; Makh, 1981). Subsequent theoretical considerations of this process have considered the backscattered material to be described by a cosine power law distribution for normal incidence ions, and the exact shape of the distribution to be related to the incident ion energies (Vossen, 1979; Makh, 1981). Oblique ion incidence sputtered anglular distributions have also been studied by several authors (Patterson and Tomlin, 1962; Gurmin et al, 1969; Rödelsperger et al, 1974). With decreasing bombarding energy the direction of preferential emission is observed to shift continuously from the target normal into the region of specular reflection of the incoming ions for moderate bombarding angles. The exact distribution of the sputtered particles would also be dependent on the ion species being used to bombard the surface and also on the substrate material.

The spatial distribution of sputtered particles from rough surfaces has also been considered and, for example, surface structure can

significantly influence total and differential sputtering yields. Littmark and Hofer (1978) considered regularly faceted surface (similar in structure to those shown in Figure 5.2(b)) and attributed changes in sputtering yields to two competing effects: (1) a yield-increase by an enhanced effective projectile incidence angle and (2) a yield-reduction by recapture of obliquely ejected particles. In general they concluded that the total sputtering yield was found to be enhanced by surface structures except at projectile energies near the sputtering threshold, or where the angular distribution of sputtered particles from the surface follows a cosine and inverse cosine law. The differential yield from flat surfaces was also found to be strongly distorted by surface structures particularly near grazing ejection angles. There have been several reports of reduced (Wehner and Hajicek, 1971; Mattox and Sharp, 1979; Panitz and Sharp, 1980) or increased (Elich et al, 1971; Roth et al, 1977; Emmoth et al, 1980) sputtering yields of textured surfaces relative to smooth surfaces of the same material, apparently with some discrepancies in the conclusions of parallel experiments performed by different workers. This was the subject of a critical analysis review by Auciello (1982) on related phenomena of textured surfaces. It was noted in this work that the 'apparent' discrepancy arising in a comparison of the experimental data could have been the result of a number of effects including the precise method by which the sputtering yield was measured, the particular form of topography created by ion bombardment and the irradiation parameters. The last two aspects were considered as having the most dominating influence on sputtering yields, although it was noted that in yield measurements a faceted surface would render flat collectors (used in Rutherford Backscattering

techniques) for sputtered material unsuitable if only selected deposit areas were analysed, since with these collectors the uncertainty is largest where the increasing solid angle demands higher precision. Semicircular collectors appear to be a better approach (Littmark and Hofer, 1978; Emmoth et al, 1980), but in the several communications of reduced (Mattox and Sharp, 1979; Panitz and Sharp, 1980) or enhanced (Elich et al, 1971; Roth et al, 1977) sputtering yields it was unclear as to whether weight loss measurements were performed in situ.

Although Auciello (1982) regarded the comparisons between previous experimental results as being apparently pseudo-complementary there is still a high degree of speculation involved. Ziegler et al (1977) and Panitz and Sharp (1980) attributed the lower sputtering yield of needlelike and faceted surfaces respectively, to the fact that the bombarding ions approach such structures at glancing angles of incidence, and hence the sputtered material is directed down into the valleys of the features where the probability of recapture is high. This is a conflicting view with Littmark and Hofer's (1978) mathematical predictions and other experimental observations who regard an enhanced sputtering yield on coned and faceted surfaces. However, the energy ranges reported for these observations differed significantly, where for the reduced sputtering yields the bombarding ions were between 200 - 4000eV, and for the enhanced sputtering yields they were 10KeV - 1MeV. There was an exception to this classification represented by Roth et al (1977) who reported enhanced yields for stainless steel bombarded with 2KeV H^+ ions, which correlated with the appearance of cones on the surface. However, the target temperature of the samples during

irradiation was 773 - 950K, a parameter which is known to cause an increase in sputtering yields (Nelson, 1965).

It was, therefore, concluded by Auciello (1982) that experimental results concerning the sputtering yield of some textured surfaces is related specifically by the energy of the bombarding ions. This would inherently influence the angular distribution of the sputtered atoms as shown by other authors (Snouse, 1964; Gurmin et al, 1969) which also depend on the incident angle of the bombarding ions. Therefore in order to quantitatively examine the effect of surface topography on the sputtering yield, a systematic study would need to be performed which involves ion bombardment of surfaces having the same initial texturing and/or bombardment-induced secondary texturing, the same crystallographic orientation and a full understanding of the redistribution of sputtered particles.

The nature and development of some commonly observable surface topographies produced by ion erosion, have been discussed, and other forms of surface structure produced by this method have been presented (Figure 5.2). The various forms of these structures are dependent on several main parameters which involve the initial state of the surface, the local angle of incidence of ions to the surface (dependent on the crystal structure and the initial ion beam angle), and the total ion dose and damage formation. The latter of these has become particularly significant where ultra-high vacuum conditions have been incorporated, thus heavily reducing the probability of contaminant induced artefacts. Much more experimental work will be required in well determined and widely varying sputtering conditions, especially on the correlation

between the damage in bulk and the surface topography, before the surface changes induced by ion bombardment are better understood (Navinsek, 1976; Carter et al, 1982, Auciello, 1982).

5.2 Ion Induced Morphology on Semiconductors

5.2.1 Cone and Pit Development

The rapid development of the electronics industry over the last decade has necessitated the requirement for increased sophistication in materials science, and more specifically in semiconductor technology. Equally important is the growing demand for high sensitivity analytical techniques (viz. AES, SIMS) capable of characterising sample composition at very low concentration levels with a depth resolution of a few nanometres (Liebl, 1975; Wittmaack, 1982). It is therefore important that for an electronic device to function within expected capabilities the electrical characteristics need to be determined with a high degree of accuracy.

Semiconductors are succeptible to non-uniform ion erosion during surface analysis and the subsequent development of surface topography could impair the resolution required to detect small quantities of dopant material. The surface morphology of semiconductors under ion erosion is therefore an important topic to discuss.

The mechanisms by which a variety of surface structures can be produced are still not fully understood, and more importantly may develop from initially pure and contaminant-free substrates. Some of these effects have been described previously relating more specifically to topography development on metals. Nevertheless, the formation of ion-

induced topography of semiconductors observed by several workers, indicates that similar processes are involved, and it is therefore important to expand on these initial findings in view of the high technological applications of these materials.

The volume of work performed in this area on semiconductors is relatively small compared to metals, due to their very recent development. Semiconductor surfaces must be smooth and clean if they are to be used for research or production purposes, such as electronic device fabrication, the active element in ion implantation processes or as targets in a thin film sputtering machine. It should be noted, therefore, that mainly cone formation and secondary processes have been studied on semiconductor surfaces, and it has not been until recently that a more concentrated effort has been directed towards the growth of sputter-induced surface structure. These aspects will further be discussed in this section.

Early investigations of etch effects at oblique ion incidence angles have been performed by Yurasova (1957), and Yurasova et al (1968) who observed characteristic etch pits on several materials including InSb and GaAs. The etch pits were found to differ considerably for the same material if different ion bombardment parameters were used. In other studies where the sputtering yield was measured for Ge and Si, some authors observed changes on the surfaces. Regular ion etched pits were observed on germanium (Wehner, 1958) while 'cellular structure' was typical of silicon and also some glasses (Bayly, 1972). It is now known that some semiconductors behave in a similar manner to glasses under ion bombardment, since after a certain ion dose they act as an

amorphous solid (Wilson, 1973). Low energy electron diffraction (LEED) and transmission electron microscopy (TEM) studies show how semiconductors change their crystallinity to the amorphous state down to the penetration depths of the ions (Parsons, 1965; Mayer et al, 1970). The most characteristic features are cellular structure at perpendicular ion incidence and furrows or ridges in the direction of the ion beam or parallel to its projection on the surface at different angles of ion incidence (Navinsek, 1976).

The earliest systematic study of sputtered semiconductors was by Wilson (1973) who observed surface changes using a scanning electron microscope after 40KeV Ar^+ ion bombardment at normal incidence, on the following crystals: Si(111), Ge(111), GaAs(110), InP(100), GaP(111), InSb, CdS(0001) and CdTe(111). The effects observed from this work occurred in the dose range 0.5×10^{18} - 3×10^{18} ions cm^{-2} and are too numerous to be included in this present work. However, Wilson's objective was to distinguish between the unperturbed sputtered surface and perturbation of the surface by foreign bodies. The surfaces of Si, Ge and GaAs consisted of a series of bumps approximately 0.15μm in diameter, but at doses greater than 1.5×10^{18} ions/cm^2 these disappeared. The features observed on the surfaces of these materials and InP were consistent with each other and showed the formation and eventual erosion of conical protruberances above the surface. Figure 5.6 illustrates a typical example of this process for GaAs.

There were several reasons proposed for the formation of micro-topography on the unperturbed surface based on variations in the sputtering rate possibly caused by: (a) a discontinuous oxide film (b) mechanical

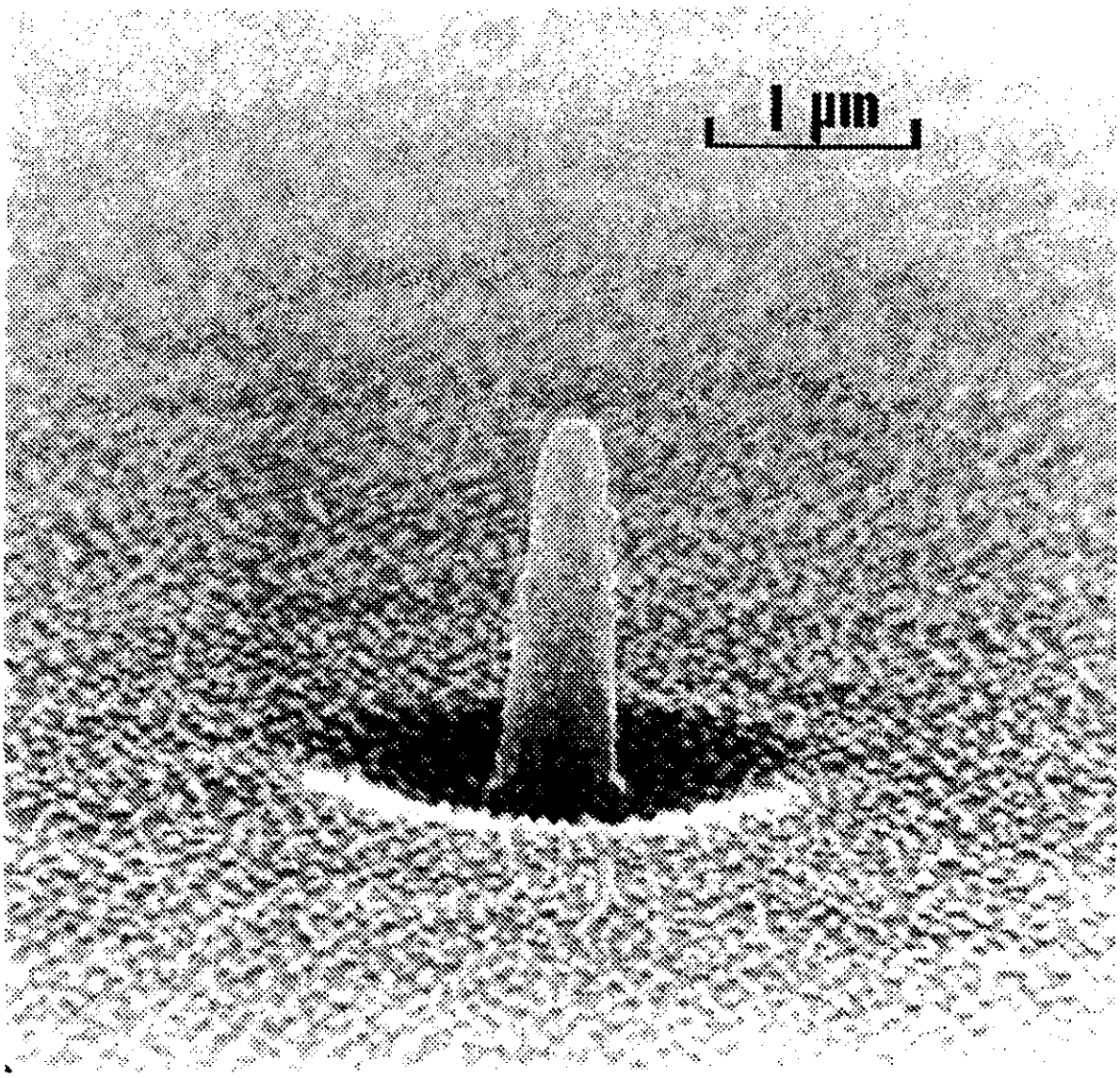

Figure 5.6: Cone development on GaAs after Ar^+ ion erosion, as a result of surface protruberances (after Wilson (1973)).

damage (c) low sputtering yield material (such as aluminium from the beam defining aperture). However, from experimental data presented none of these possibilities could either be firmly rejected or substantiated. The conclusion was that Si, Ge, GaAs and InP appraoch the behaviour consistent with a completely amorphous surface, namely formation of a flat surface normal to the ion beam.

The surface structures observed on the remaining materials (GaP, InSb, CdS, CdTe) differed significantly from the first group. The sputtered surfaces GaP and CdTe appeared to be flat after bombardment and were free of undulations, whereas CdS was very rough and exhibited facets with one plane nearly parallel to the ion beam and one perpendicular to it. It was concluded for these materials that their crystal structure was unaffected by ion bombardment and therefore the topography that develops after sputtering depends sensitively on beam orientation which made interpretation difficult. The InSb surface showed whisker formation possibly caused by preferential etching of the indium rich areas.

The work performed by Wilson (1973) on semiconductors introduced some new ideas about contaminant induced cone formation. In particular it was suggested that single cones with rounded tips observed on Ge and GaAs (Figure 5.6) were produced as a consequence of a small area ($\sim \leq$ 1μm) being masked, whereas more complex structures were developed if the masked area was larger (> 2μm) (see Chapter 6 for a detailed analysis of this). The author also pointed out that the development, and shape, of the cones formed was not consistent

with theory (Catana et al, 1972; Bayly, 1972), due mainly to increased sputtering yields at sharp points, and the influence of secondary effects such as flux enhancement and redeposition. These observations, however, should not be used as a precedent when theoretical comparisons are to be made. Experimental observations by Barber et al (1973) showed good agreement with the prediction of ion-bombarded surface topographies using Frank's (1958) kinematic theory of crystal disolution. They studied features produced by an ion beam incident at 60^0 to the normal of the surface of transparent samples of InP. Flat topped hummocks were formed at the centre of a dish in InP by ion bombardment, whereas sharply peaked cones were produced by unidirectional ion attack in the peripheral regions of the dish, and the hummocks changed into ridges or steps as the distance from the axis of rotation increased. The faceting phenomenon was discussed for the case of metal crystals.

The growth of III - V semiconductors have recently become increasingly important in the development of optoelectronic device technology, the new type materials being of a compound or superlattice nature. Inevitably the characterization of these materials is of prime importance to the understanding of their growth process, and the ultimate electrical chacteristics. Williams et al (1980) have reported that in InP and $In_x Ga_{1-x} AS_y P_{1-y}$ structures become unstable under Ar^+ sputtering conditions and cone formation severely degrades the depth resolution in subsequent Auger analysis. A similar effect was observed by Skinner et al (1983) who described cone formation on InP following Ar^+ bombardment as In coalescing to form islands while the P is preferentially etched, an interpretation previously

described in the literature (Farrow et al, 1978). An interesting aspect of this work was the improvement in depth resolution when the authors used N_2^+ (as opposed to Ar^+) to Auger depth profile through 250Å Al/InP interfaces. The use of reactive species as a sputtering agent in depth profiling has been reported on several occasions as substantially improving the in-depth resolution of Auger profiles (Hofer and Liebl, 1975; Windawi et al, 1976), and reducing the development of surface topography (Laty et al, 1976). Reports on the latter of these have been relatively sparse, and the mechanisms by which reactive species with solid surfaces are not well understood. Topography development on polycrystalline, single crystal (Lewis et al, 1982) and amorphous materials (Skinner et al, 1983) has been reported as remaining essentially the same in structure following ion bombardment under the same irradiation conditions while varying the gas species (i.e. noble gases and most commonly N_2^+ and O_2^+). Following sections in this chapter will be primarily concerned with this aspect of ion sputtering and systematic studies performed predominantly on semiconductor materials will be presented and compared to existing work. The primary aim is to distinguish between the different structures and offer some explanation for the mechanisms by which they are formed, and to assess whether sputtering with reactive gas species results in a purely physical or chemical process, or a combination of both.

5.2.2 Development of Surface Faceting

The mechanisms established for cone development have been well documented for many metals and the surface contaminant process appears

to be responsible for the development of cones on some semiconductors (Wilson, 1973). However, it has been shown that clean surfaces of Si following ion bombardment exhibit no cone formation, but show a characteristic furrow structure* across the entire surface. This was illustrated in a report by Nelson and Mazey (1973) who compared the topographies of Xe^+ bombarded polycrystalline copper, Cu (110) and Si. They examined the effects that the structure of the samples had on the phenomena occuring during ion bombardment. During ion bombardment of solids radiation damage is manifested in the form of interstitials and vacancies which may result in an agglomeration if they become mobile, initiated by some threshold temperature. Furthermore, these changes as well as crystallographic structure may give rise to enhanced local sputtering due to channelling and angle of incidence effects. Nelson and Mazey (1973) discussed the idea that dislocations may be in continuous motion during irradiation and are associated with comparatively long range elastic strain fields, and will move in such a way as to minimize the total free energy. The detailed behaviour of a particular material will depend on several parameters such as crystal structure, activation energies for defect migration, sputtering ratio and for example in a polycrystalline sample the energy deposited along certain index directions will determine the energy available for sputtering. Also the different orientated grains will have different values of binding energy and thus sputter at different rates.

* For a visual interpretation this structure compares closely to that illustrated in Figure 5.2(b).

The above hypotheses appeared to be well substantiated for Cu (110) and polycrystalline copper from the observations made by the authors, but could not be applied to the features produced on ion bombarded silicon where the structure is believed to become amorphous under ion bombardment (Morehead and Crowder, 1970; Wilson, 1973; Carter and Webb, 1979). They discovered that the 'ripple' or 'furrow' structure observed on this surface had no specific orientation relative to the original crystal structure, but depended only on the ion beam direction, where the striations were lying perpendicular to the ion beam.

Carter et al (1977) observed similar features in studies of 40KeV Ar^+ bombarded crystalline Si, and by a systematic approach illustrated several reliable and quantitative results. The angle of ion attack was varied from normal incidence to near grazing incidence (> 70°), and several significant differences in the developed topography was observed:

(1) At normal incidence ($\theta = 0^o$); a similar surface to the pre-bombarded case, but a suggestion of a random hillock and depression structure.

(2) $\theta = 30^o$, in the high fluence (of the focused ion beam), a dense array of hillocks and depressions, and in the low fluence region a whorl like structure of convoluted hillocks and depressions.

(3) $\theta = 45^o$ and $\theta = 60^o$; in the high fluence region, a continuous array of ridges and furrows across the whole bombarded zone, the direction of which lay perpendicular to the direction of the ion flux, and in the low fluence region isolated short ridges and furrow-structures lying in the same direction.

(4) $\theta = 70^{o}$; in the high fluence region, a continuous array of short ridges and furrows across the whole bombarded zone, the direction of which lay parallel to the direction of the ion flux; in the low fluence zone isolated short ridges and furrows lying in the same direction.

(5) $\theta = 75^{o}$; almost no surface features except the occasional isolated ridge, furrow-structure lying parallel to the ion flux.

These observations, as noted by the authors, were not unlike those reported by Navez et al (1962(a) (b)) who irradiated glass and silicon surfaces with air ions of several KeV and at various angles on ion incidence, and which are also consistent with the observations made by Nelson and Mazey (1973). By careful electron probe illumination Carter et al (1977) were able to relate the ripples to a form of stacked and tilted disc or cylindrical segments with plane facets approximately perpendicular to the ion flux (for $\theta = 30^{o} - 60^{o}$). For angles of $\theta > 65^{o}$ the ripple features appeared to acquire a more longitudinal appearance, but were regarded as having quasi-circular cross-section, each protruberance being a tilted cylinder with an angle similar to that of the ion flux direction. This effect is in evidence in experimental work presented in later sections of this chapter. From these observations it was deduced that with increasing θ the aspect ratio (length to height ratio) increased.

Carter et al (1977) compared these micro-structures to geomorphological erosion of sea beds and deserts, and following arguments from studies of sand blasted rock formations (Finnie and Kabil, 1965) the authors regarded the ripple structures as emanating from a surface

network of domes, which by preferential erosion and flux enhancement initially form randomly situated ridges which elaborate to ripple trains during prolonged ion bombardment.

As previously mentioned much of the work performed in the development of surface topography for many materials has described the formation of conical features produced either by contaminant induced processes (Wilson, 1973; Belson and Wilson, 1982), or by surface defect mechanisms (Whitton et al, 1978; Auciello, 1982). The former of these it would appear, only applies to semiconductor materials where cone formation is evident (Wilson, 1973). This was suitably illustrated by Carter et al (1980) who bombarded samples of Si at non-normal incidence with 8KeV Ar^+ ions. The magnitude of the characteristic ripple topography increased with higher ion dose, whereas a cone that had developed on the surface became unstable and eroded away, consistent with theory (Catana et al, 1972). The discussion of this work concentrated on the sputtering yield of Si as a function of ion incidence angle, and also on the dynamics of the cone structure, but gave us no further indication of the process involved in the ripple development.

It is evident from much of the work achieved in this area that a full understanding of the structural dependence of surface topography on ion species, ion angle and ion energy should be met by a variation over a range of values for each of these parameters. However, it is equally important to perform correct diagnostic procedures when viewing or measuring the topography using electron microscopy techniques in particular. It has been illustrated by Carter et al (1977) that

ambiguity of surface morphology can prevail if several viewing angles are not pursued. Lewis et al (1982) in an attempt to minimise the faceting observed on silicon, performed parallel experiments but with a rotating sample. The surface yielded different forms of topography from different viewing angles, and they concluded that the overall amplitude and separation of the features is less than would be found for a similar irradiation dosage without sample rotation, consistent with previous considerations (Sykes et al, 1980). A similar, but more detailed study has recently been performed by Cong-Xin et al (1983) who bombarded stationary and rotating samples of p-type < 111 > and < 100 > Si, n-type < 111 > Ge, Cr doped < 100 > GaAs, < 111 > Gd-Ga-garnet and $LiNbO_3$ single crystals for a variety of sputtering conditions which included incident angles from 0° - 80°, beam energies from 300 - 1200eV with Ar^+. They found that all the materials exhibited features whose shapes were a sensitive function of ion incidence angle and target rotation. Furthermore, the size and density of the 'hillock' type structures formed for a rotating sample increased in size and density as the ion energy and ion dose were increased. The hillock structures reduced to sharper hillock formations lying parallel to the direction of the incident ion beam, for targets remaining stationary during sputtering. The formation of all hillock structures was attributed to microscopic uneveness existing on the surface prior to bombardment, and subsequent preferential etch rates due to changing ion incident angles during the sputtering process.

5.3 Sputtering Effects Using Reactive Gases

Recently, due to accelerated advances in the electronics industry, plasma etching is frequently used in the manufacture of integrated

circuits (Poulson, 1977; Coburn and Winters, 1979; Curran, 1981), and is based on the ability to selectively etch material from, and deposit onto surfaces of suitable substrates (semiconductors or garnet wafers for example). At present there are three methods mainly employed to etch the desired surface relief structure for integrated circuits, namely (i) wet chemical etching (ii) plasma etching and (iii) ion bombardment (using well collimated ion beams). The latter two are more relevant to this particular work and a brief discussion on some processes involved in their operation will be given here.

The principle of plasma etching involves the generation of chemically reactive radicals by a d.c. or r.f. voltage-induced discharge, which interact with solid material to form volatile compounds which are then removed by the vacuum pumping system. However, in a similar process to ion bombardment, plasma etching incorporates a physical displacement of surface atoms, and these coupled mechanisms are generally very complex and still not well understood, although comprehensive explanations of the physics involved can be found elsewhere (Dimigen and Liithje, 1975). The advantage of plasma etching are that the process involves the use of relatively simple equipment where it is possible to irradiate large areas which is important in industrial applications. Furthermore, the method is suitable for etching non-conducting substrates, which cannot be achieved by d.c. sputtering due to charging. There are, however, two main disadvantages (i) the etching ions are directed towards the substrate and target mainly at right angles, due to the potential distribution around the target. This would make it practically

impossible to carry out etching at other angles of incidence (ii) the requirement for a high gas pressure can have adverse effects on the results of etching. Back diffusion, from the target to the substrate, can occur and increases as the free path of the ions becomes smaller in relation to the distance between the anode and target, which subsequently effects the etch rate.

The ion beam etching method has several advantages; (a) the substrate can be bombarded at any angle (b) the energy and current distribution can be varied independently, and the gas pressure kept low (c) insulators can be etched, provided that any positive charging effects are compensated for by a source of electrons (d) the resolution and aspect ratio of etched features is high. One of the most suitable systems for ion beam etching is based on the Kaufman type ion source (Kaufman et al, 1982).

Initially, perhaps the most significant characteristic of ion bombardment is the strong dependence of the etch rate on ion angle of incidence for most single element materials. There are exceptions, where the sputtering yield experiences only a minor increase as the ion beam angle is increased from 0^0 to 90^0 (i.e. Ti, Au - see Lee, 1979). However, significant changes in the sputter yield may occur when a reactive gas is used, or inert gas sputtering takes place in the presence of a reactive gas. This latter effect was demonstrated by Cantagrel and Marchal (1973) who bombarded various materials with Ar^+ in an oxygen ambient. The sputtering yield was observed to decrease strongly with an increase on oxygen pressure, an effect similarly noted by several other authors (Almen and Bruce, 1961;

Hofer and Martin, 1978; Wittmaack, 1978). This effect has been attributed to the sputtering ions having to eject excess oxygen atoms at the surface and overcome the binding energy of the oxygen atoms in the oxide layer (Mayer and Barker, 1982; Harper et al, 1982).

It is well known from many experimental observations that materials sputtered by inert gas atoms follow characteristic curves as a function of ion angle of incidence (Oechsner, 1973). However, instead of the well-known maximum in the sputtering yield at approximately 50° - 70°, maxima at normal incidence, and a fairly weak angular dependence is observed for etching Si, SiO_2 and InP in reactive gases (Mayer et al, 1981; Miyake et al, 1982).

A model initially proposed by Mayer et al (1981) and later discussed by Mayer and Barker (1982) hypothesized that this behaviour was based upon a contribution from a physical event (i.e. momentum transfer to the surface causes a collision cascade), and a chemical effect. They predicted that the amount of energy deposited, and the damage caused at the surface would be dependent on the angle of incidence of incoming ions. This would effectively result in chemical entities forming at the surface with a range of binding energies, thus resulting in higher or lower sputtering yields than a purely physical event. A similar view was held by Winters et al (1983) who discussed the mechanisms by which either physical or chemical sputtering dominated in a given situation. They concluded that the rate of physical sputtering drops in the presence of a chemically reactive gas, in particular an elemental material sputtered either by, or in the presence of oxygen, will form an oxide on its surface and the physical

sputtering rate will be determined by the rate that the original elemental material is sputtered from the oxide. The decrease in the number of original elemental atoms from the surface (due to the oxide layer) will cause the sputtering rate to become smaller, and hence almost always a decrease in the rate of physical sputtering (Andrews et al, 1966; Hrbek, 1977; Hofer and Martin, 1978).

In contrast to the above discussion, energetic ion bombardment may enhance the production of volatile species and their subsequent desorption depending upon the gas-substrate combination, although it must be stressed there is still a great deal of uncertainty on the behaviour of the surface chemistry. For example, Harper et al (1982) reported extremely high etch rates of polyimide with O_2^+ where for a 700eV beam at 0.7mA/cm^2, 2700Å/min was etched, and for the same conditions with an Ar^+ beam the etch rate was 450Å/min. Previous workers (Hawkins, 1979) have noted that the high etch rates of polymers in O_2^+ represent a yield of about 100Å^3 per ion impact, which is more material than can be accounted for by the two O atoms in the ion. This, therefore, suggests some additional mechanism, such as activation of adsorbed O_2 or additional decomposition in the impact region which accounts for the additional material removed. Conversely, any proposed mechanism would have to describe equally well the observed decrease in sputtering yield of many metals using O_2^+ ions (Cantagrel and Marchal, 1973; Castellano, 1977).

A brief overview has been given of some of the proposed mechanisms involved in reactive ion etching, and although the physics of the process is not yet fully understood, the applicability of the technique

to electronic device fabrication is unique and of considerable potential value. However, more particular to the present work is the use of active ion beams in the surface analysis industry. Several advantages of using active gas species have been revealed, and this coupled with implications in depth-profiling will be discussed in the next section.

5.4 The Use of Active Gases in Surface Analysis

The most commonly used surface analytical techniques (viz. AES, ESCA, SIMS) have previously been discussed in Chapter 1. The sputter-etching process is essential to all solid materials that require their elements to be characterised as a function of depth, since micro-sectioning can be achieved in a clean controllable ultra-high vacuum. However, sputter-depth profiling can often introduce ambiquities in the interpretation of analytical data, particularly concerning the elemental composition as a function of depth from the surface. This aspect is well represented in a study by Hofer and Liebl (1975) who showed that the Ni^+ secondary ion signal when profiling a Cu-Ni multilayer structure was highly distorted when Ar^+ ions were used for sputter-etching. The depth resolution was significantly improved, however, when reactive N_2^+ ions were used for etching. The degradation in depth resolution for Ar^+ ions was attributed to the development of cones on the surface, and a larger Ni signal was observed at the Cu-Ni interface as a result of these structures. Conversely, the surface was essentially featureless, within the SEM resolution, following N_2^+ ion bombardment. Cone formation has also been the result of a

degradation in depth resolution in other studies (Williams et al, 1980), and the effects of surface roughening by ion bombardment has been discussed elsewhere in this chapter. Primarily, this section is concerned with the macroscopic effect on surfaces that active gas species produce and their implications in surface analysis.

It is well established that the sputter process in surface sensitive methods such as AES or SIMS causes a broadening of depth profiles via collisional mixing (Anderson, 1979) and surface topography development (Hofer and Martin, 1975). The former of these two effects can be optimised by careful choice of irradiation parameters such as ion mass and energy, and angle of ion incidence. The latter effect, until recently, has proved in many instances to be a dominating factor in degrading depth resolution and has not been found easy to minimise (Hofman and Zalar, 1979; Williams et al, 1980).

The use of active ion bombardment is particularly relevant to surface analyses carried out using SIMS, where excitation of the sample is induced by heavy ion impact, mostly noble gas ions or O_2^+ and C_s^+ (Wittmaack, 1979). More importantly, the high degree of sensitivity attained in SIMS requires that a sufficient flux of charged secondary ions are emitted from the surface. In this respect it is known that O_2^+ and C_s^+ ion bombardment, or flooding of these gases combined with inert gas sputtering, enhances the electropositive and electronegative ion yields respectively (Simondet et al, 1980; Wittmaack, 1981). The concepts behind this effect are not yet understood since no reliable explanation exists for the problem of ion retention in the presence of sputtering (Tsai and Morabito, 1974; Wittmaack, 1981).

There have been several reports illustrating the use of active ion beams to reduce surface roughening. In a series of papers by Tsunoyama et al (1974, 1976) it was observed that conical features developed on surfaces of pure iron following Ar^+ ion bombardment, whereas the same surfaces after O_2^+ ion bombardment were comparatively smooth revealing no sharp features. The authors proposed that O_2^+ was implanted deep into the iron matrix which moderated the inhomogeneity of the surface and caused more uniform sputtering. In comparison, Ar^+ and N_2^+ ion bombardment (which also showed a rougher surface), are not retained in the surface layer and the inhomogeneity of the surface structure is not eliminated.

The use of O_2^+ for in-depth analyses, either in the form of a direct ion beam, or in the presence of an inert gas ion beam has been reported to improve experimental data on several occasions. Bernheim and Slodzian (1973) have introduced O_2 gas during Ar^+ bombardment and have shown the surface of polycrystalline Al to sputter uniformly. Their results indicated that O_2^+ ions tended to penetrate into the surface and form an oxygen enhanced layer beneficial to uniform sputtering, which was consistent with other hypotheses (Tsunoyama, 1976). A similar study was performed by Laty et al (1979) who bombarded polycrystalline Al with Ar^+ in the presence of oxygen, illustrating that the sputtering yield with oxygen flooding was reduced to approximately a half of its value without. By defining a microroughness index parameter as the standard deviation of a distribution curve of roughness as a function of depth, they were able to deduce that the presence of oxygen suppresses the development of topography.

This effect, however, cannot be related to the sputtering yield, since the initial sample surface orientation and topography will influence the rate of erosion particularly for polycrystalline substrates (Naundorf and Macht, 1980).

In response to their previous work, Tsunoyama et al (1980) bombarded surfaces of seventeen polycrystalline pure metals with 20KeV O_2^+. They classified the etch patterns produced according to the binding energy of the mono-oxide of the target atom and an oxygen atom. For low binding energies (< 2.0eV) the ion bombarded surfaces were rough (i.e. cone development), for relatively high binding energies (6.8eV - 8.3eV) the surfaces were quite uniform, for the range 4.3eV - 6.8eV only a few facets were formed mainly as a consequence of grain boundaries, and for the range 2.7eV - 3.8eV numerous pits and hillocks developed. However, for reasons unknown by the authors some materials exhibiting surface roughening did not possess binding energies that met the requirements of the above classification. An interesting comparison made by the authors was the recognition that the sputtering yield plotted as a function of atomic number, for the materials under investigation was identical to the 'd' shell pattern discovered by Laegreid and Wehner (1961) and Rosenburg and Wehner (1962) for noble gas ion bombardment. The similarity of the variation of the sputtered atom yields with target materials seemed to indicate that the total yields were more dependent on physical atomic collisions and not on the chemical interaction of the implanted oxygen atoms. They concluded, however, that the chemical affinity of the target materials for the oxygen atoms was primarily responsible for the development of ion induced surface structure.

Although many aspects of active ion bombardment remain unexplained, it is nevertheless, an important and effective surface analytical tool, and has yielded significantly improved sputter-depth profiles (Blattner et al, 1979; Naundorf and Macht, 1980). However, the development of topography induced by active ion bombardment is only suppressed, and not eliminated on most materials. Indeed, studies have been made where materials develop the same topography regardless of whether inert or active ions are used to bombard the surface (Lewis et al, 1982).

The following work represents a systematic study of active ion bombardment, normally associated with SIMS analysis (O_2^+ and C_s^+), on well prepared, pure, single crystal semiconductors (Si, GaAs, InP) and Cu (11 3 1). Strong comparisons will be made with previous work on these materials where mostly inert gas sputtering has been utilised.

5.5 The Development of Surface Topography Following Active Gas Bombardment

Low energy ion bombardment has become an important technique in the analysis of a wide range of materials (Rivière, 1982). It is frequently employed in several of the commercially available surface analytical systems such as AES, ESCA and SIMS, either to surface clean samples prior to analysis, or to act as a tool for obtaining depth information. SIMS has become increasingly important in recent years and is now a highly sensitive and versatile technique for microanalysis (Liebl, 1975; Werner, 1980; Walls and Sykes, 1982). The sensitivity of the technique lies in the ppm - ppb range and hence the provision of concentration-depth profiles of dopants (and other impurities) in

semiconductors is of obvious value in the processing and characterization of these materials. Generally depth-profiles are obtained by continuous ion erosion of the sample surface by mass filtered Ar^+, O_2^+ or Cs^+, the latter two gas species being of primary importance since they enhance the sensitivity of the electropositive and electronegative elements respectively (Magee, 1979). Although the use of SIMS in this depth profiling mode is of considerable benefit in the characterisation of dopant profiles in semiconductor materials, problems can occur which affect the apparent shape and depth resolution of the profile. This can be serious since it is the precise distribution of dopant atoms which determines the electrical characteristics of the material. The integrity of the profiles can be affected by a number of mechanisms including instrumental effects, atomic mixing, radiation enhanced diffusion and ion-induced surface topography (Liebl, 1975; Magee and Honig, 1982).

Ion erosion, however, does not always proceed uniformly, this being largely responsible for the latter of the above observed effects. Artefacts such as pits, pyramids, cones, facets and other ion-induced topographies are frequently observed. For example, Fig. 5.7 illustrates the nature of topography that may be encountered in real depth-analysis of semiconductor electronic devices. These two particular micrographs show the region where analysis was performed, and the sputter-induced topography following 5.5KeV O_2^+ bombardment.

There have been numerous reports on the characterisation of surface topography following inert gas ion bombardment for many materials (Varinsek, 1976; Auciello, 1982; Carter et al, 1982), but little is

Figure 5.7: (a) Faceted topography produced during SIMS analysis by O_2^+ bombardment of a real device structure.

(b) A micrograph showing the area of analysis.

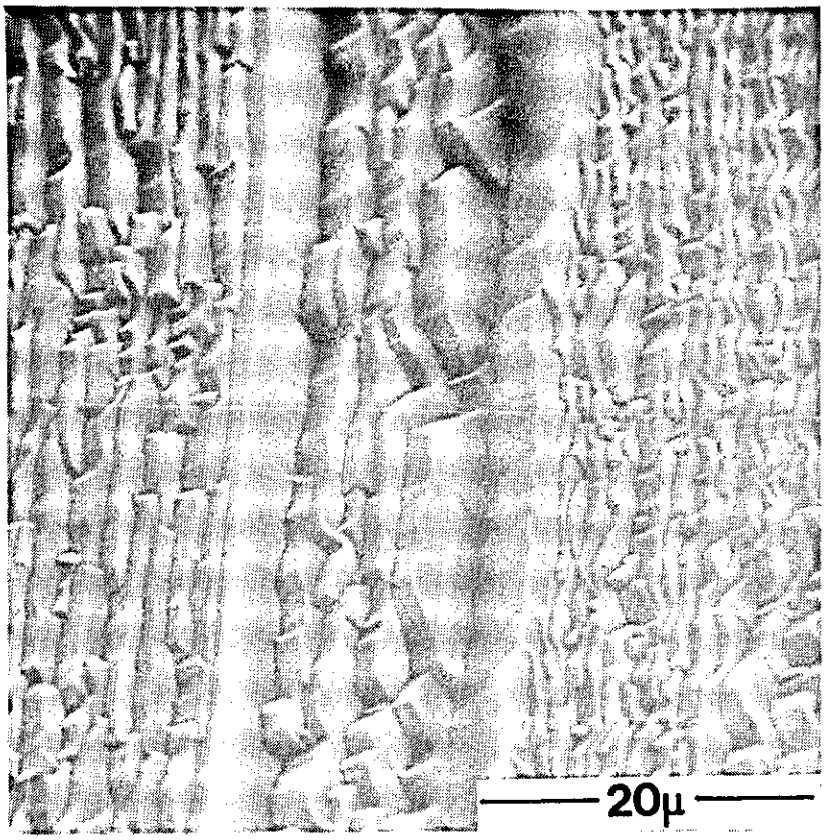

a

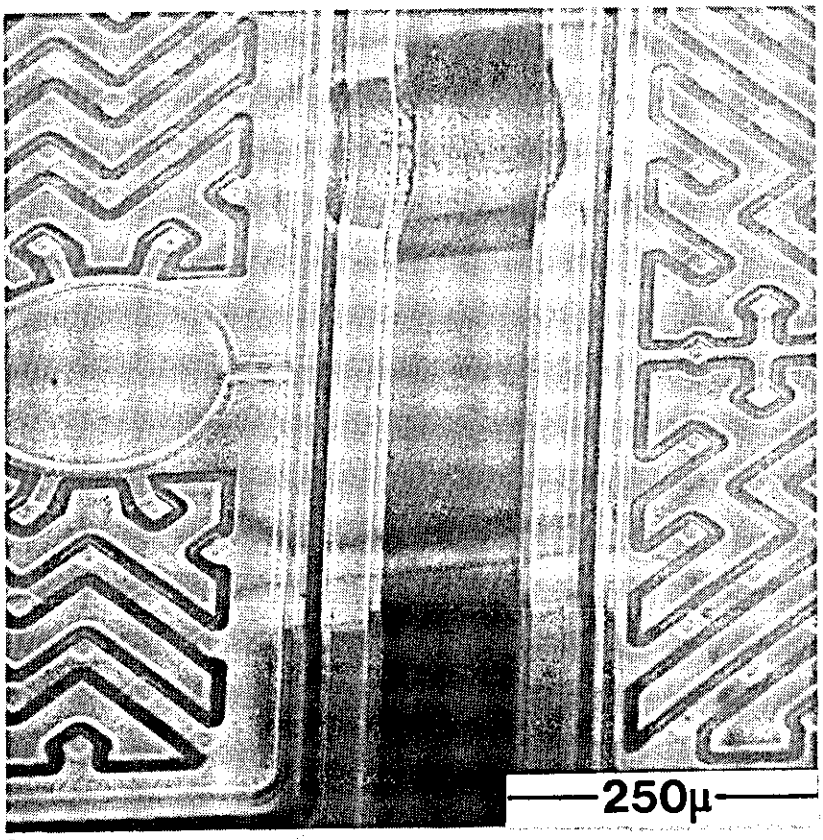

b

known about the effects of using reactive species such as O_2^+ and Cs^+, particularly on semiconductor materials. The present work reports on the nature and extent of ion-induced surface topography on some important semiconductor substrates (Si, GaAs and InP) using O_2^+ and Cs^+ as the primary bombarding gas species. Further work will extend to the material Cu (11 3 1) since this has recently held a special interest to several authors and the results from inert gas ion bombardment are well documented (Lewis et al, 1979; Whitton et al, 1980). This, therefore, allows, in many instances, direct comparisons to be made between the effects of inert gas and active gas ion bombardment.

5.5.1 Experimental Method

The samples prepared for experiment were industrially processed slices of intrinsic Si(100), Si(111), Cr doped semi-insulating GaAs(100) and Fe doped InP(100). The Cu(11 3 1) crystal was prepared by mechanical cutting and lapping methods. Due to the nature of preparation all the materials surfaces were well characterised and particular care was taken to avoid surface particulate contamination, since this is known to cause the development of cones and other surface features under ion bombardment (Wilson I.H., 1973). Consequently, ultra-clean conditions were employed during sputtering, where the sample was situated in a base vacuum of $\sim 10^{-9}$torr.

The experiments were conducted in a Cameca lms 3f microanalyser fitted with a hollow cathode duoplasmatron for O_2^+ bombardment and a general ionex Cs source. A schematic diagram illustrating the general configuration of the instrument is shown in Fig 5.8. Primary ions are accelerated to a known energy, in a primary column at 30° to the sample

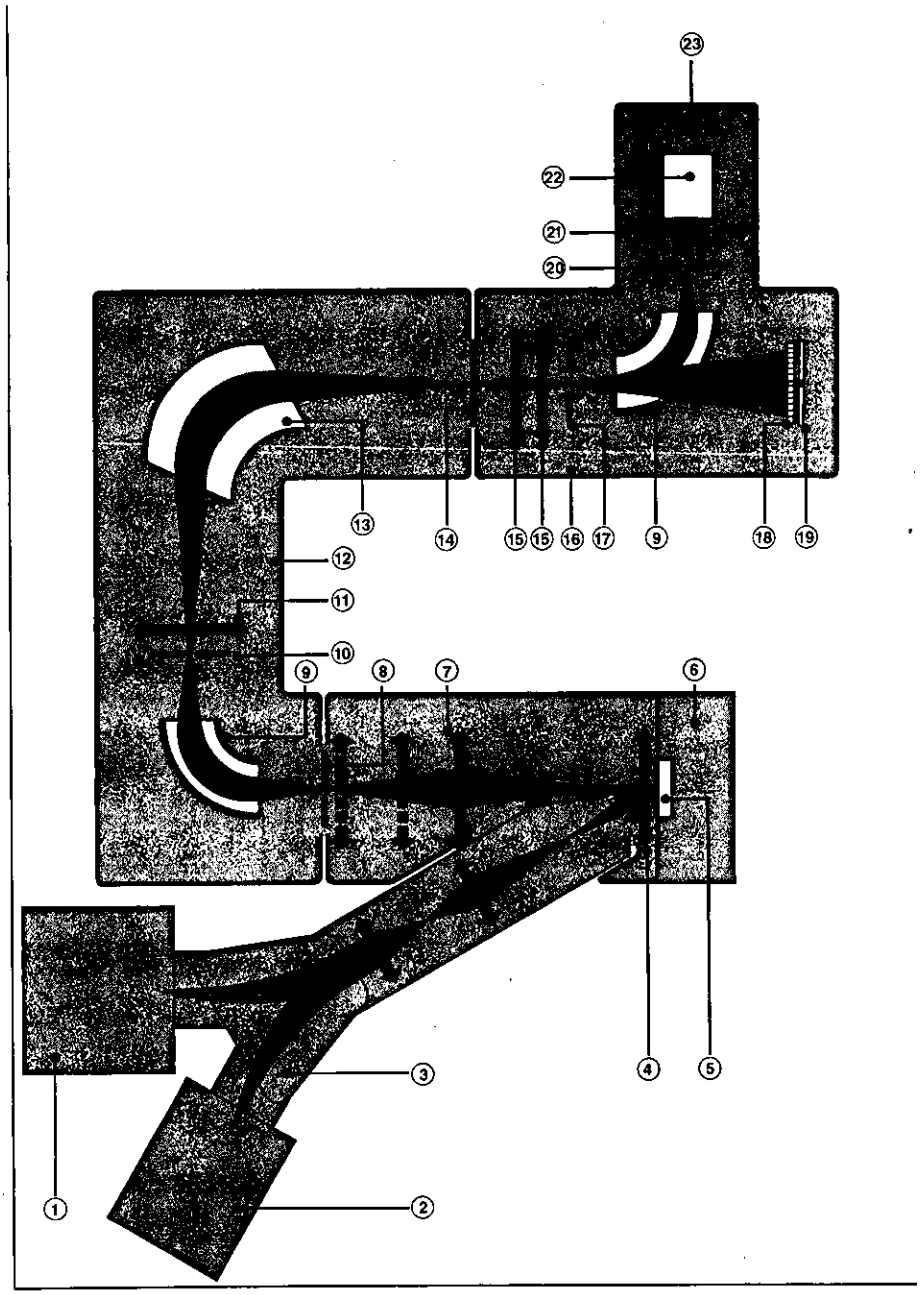

① Cesium ion source (optional)
② Duoplasmatron ion source
③ Primary beam mass filter (optional)
④ Immersion lens
⑤ Specimen
⑥ Specimen chamber
⑦ Transfer optics
⑧ Entrance slit
⑨ Electrostatic analyzer
⑩ Energy slit
⑪ Image transfer lens
⑫ Spectrometer
⑬ Electromagnet
⑭ Final slit
⑮ Projection lenses
⑯ Projection, display and detection system
⑰ Deflector
⑱ Channel-plate
⑲ Fluorescent screen
⑳ Deflector
㉑ Remote controlled Faraday cup
㉒ Electron multiplier
㉓ Detection system

Figure 5.8: A schematic representation of the Cameca ims 3f instrument

normal, and the beam was raster-scanned to erode well-defined craters 250μm square. It is required in normal SIMS analysis to have a 4.5KV secondary ion extraction field at the specimen in order to accelerate sputtered material towards the analysis chamber where a mass spectrometer is situated. This has two effects (i) to reduce the incident ion energy by 4.5KeV and (ii) to alter the angle of the incident ion dependent on the initial ion energy. The latter of these two variable parameters may be obtained from simple calculations using electrostatic theory, and Fig 5.9 illustrates the resultant effect of how the angle of incidence of bombarding ions to the sample normal varies with initial ion energy (Smith and Sykes, 1982). This feature proved useful in the experiments where combinations of energy, and the option of implementing the retarding field, provided various angles of incidence.

For reproducibility several samples were used for each material to cover the dose range 10^{18} ions cm^{-2} to 10^{20} ions cm^{-2}. The large ion dose ensured that a full development of surface topography took place, the experimental time being minimised by using current densities typically between 2 - 5mA cm^{-2}*, and for each experiment the value was kept to within 2% of its initial value.

The overall shape and depth of the craters was investigated using a Vickers M41 Photoplan light interference microscope, and a Rank Taylor Hobson Talysurf 4 instrument. The latter of these two techniques proved more useful when the floor of the crater was too rough to provide sufficient light reflectance, but generally the two methods agreed favourably to within 5% of each other for depth analyses. Fig 5.10 shows a typical interference micrograph of an O_2^+ sputtered

*It was thought that the temperature of the samples did not rise appreciably at these current densities.

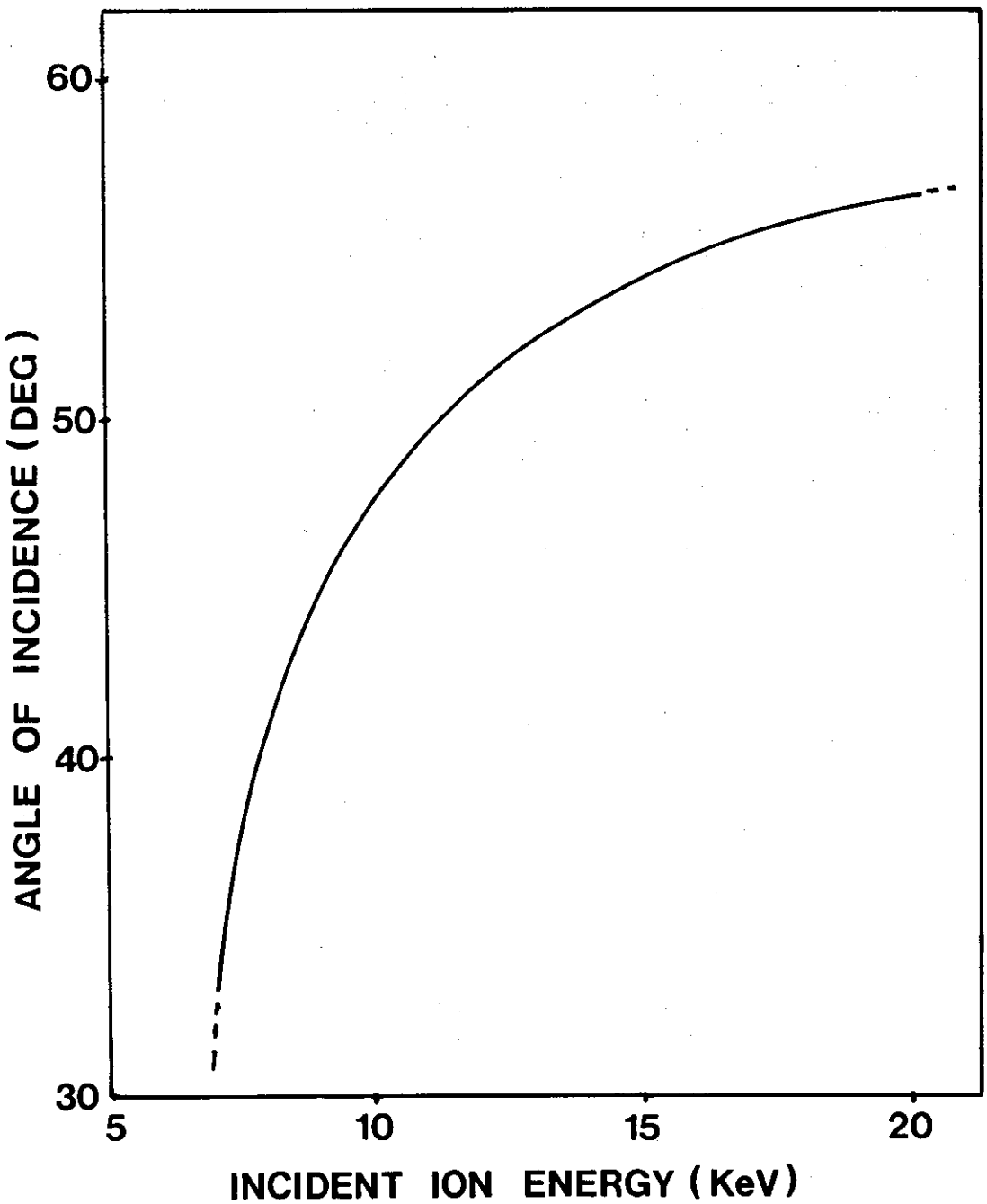

Figure 5.9: A graph illustrating the effect of a +4.5kV sample bias on the incident ion angle as a function of incident ion energy.

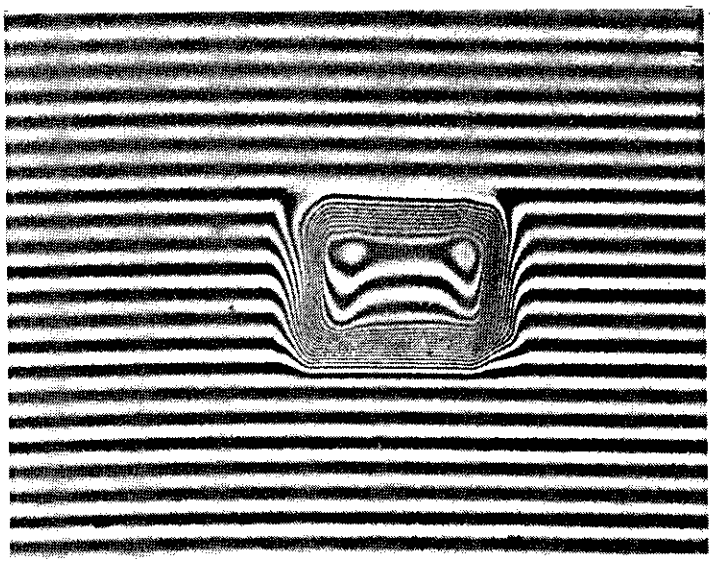

Figure 5.10: A light-field interference micrograph showing a crater formed by O_2^+ bombardment of Si. Note the sharp deviations of the interference lines at the base of the crater walls, denoting ion reflection.

crater in silicon, and highlights the well-formed shape of the crater, an added advantage over the one-dimensional Talysurf trace. Furthermore, its sensitivity to surface contour allows detection of ion reflection occuring at the base of the steep crater walls. By averaging the distance between consecutive fringes, and counting the total number of fringes n from the surface to the bottom of the sputtered crater the depth was determined simply by $n\lambda$. (λ = 270.5n.m.) All further investigations of the nature of the topography formed by ion bombardment were performed using scanning electron microscopy. It should also be noted that prior to bombardment the samples were mounted on the specimen stage at random crystal orientation with respect to the incident ion beam.

The following results sections for each particular material will firstly illustrate the topography formed by 5.5KeV O_2^+ or Cs^+ bombardment (equivalent to an initial ion energy of 10KeV), and then proceed to other effects observed with changes in ion energy and retarding field on the specimen.

5.5.2 Results (Semiconductors)

5.5.2.1 Silicon - 5.5KeV Oxygen Ion Bombardment

A sequence of SEM micrographs in Fig 5.11 illustrates the development of surface topography with increasing ion dose on Si(100) formed by 5.5KeV O_2^+ bombardment. Due to the retarding field present for these particular experiments the ion incident angle was calculated as being approximately 47° to the sample normal (see Fig 5.9). In

Note: The following series of micrographs reveal the direction of the incident ion beam as depicted by the arrows.

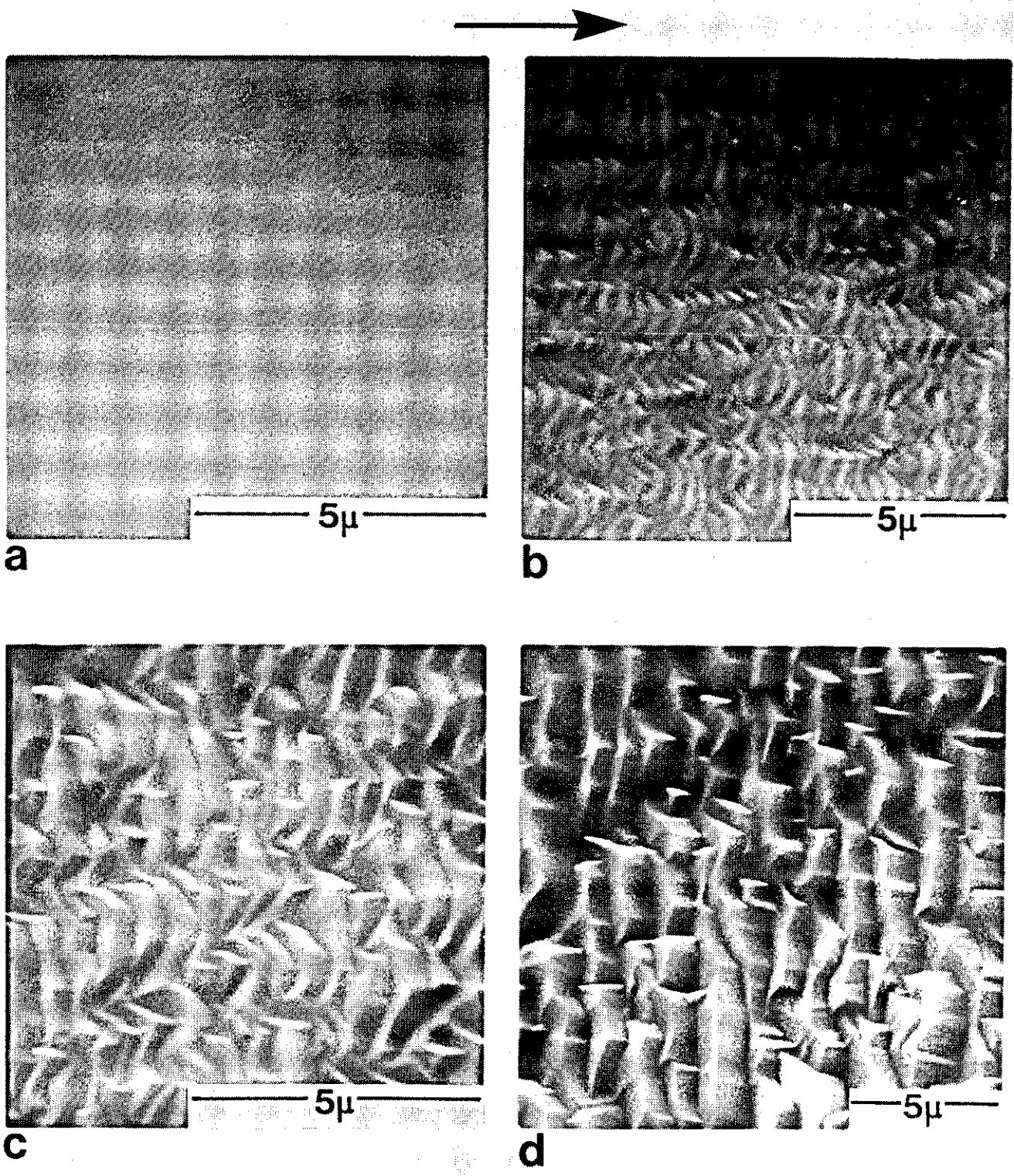

Figure 5.11: A sequence of micrographs showing the development of surface topography on Si(100) following 5.5keV O_2^+ bombardment to a depth of:

(a) 1μm (10^{19}ions cm^{-2})

(b) 4.7μm (5×10^{19}ions cm^{-2})

(c) 5.8μm (6×10^{19}ions cm^{-2})

(d) 9.2μm (10^{20}ions cm^{-2})

each case the micrograph was taken from the centre of the eroded crater where the surface was expected to be of even height. Figure 5.11(a) shows that at a dose of 2 x 10^{19} ions cm^{-2} the resultant surface is flat and featureless, and initial development of a textured surface was not observed after a total ion dose of 5 x 10^{19} ions cm^{-2}, where the surface developed a stepped and faceted morphology illustrated in Fig 5.11(b). These facets clearly propagate into and across the surface and become more distinct and greater in size as the dose increases (Figs 5.11(c) and 5.11(d)). The measured depth for each of the craters formed is shown in the figure caption.

The structure formed on Si(111) following 5.5KeV O_2^+ bombardment to a dose of 10^{20} ions cm^{-2} is shown in Fig 5.12. The faceted nature and magnitude of this topography is very similar to that seen on Si(100), although absolute confirmation of this latter aspect would require further verification by a technique such as stereo microscopy. It should also be noted that the direction of the facets differ from those shown in Fig 5.11 due to a change of illumination in the SEM.

5.5.2.2 Silicon - 10.5KeV Oxygen Ion Bombardment

In order that the effects of discrete changes in incident ion angles could be observed, two experimental parameters were varied, namely the initial ion energy and the retarding field at the specimen. Therefore by accelerating the ions to 15KeV at the source and employing a retarding field of +4.5KV, the incident ions impinged on the sample surface at an energy of 10.5KeV and at an angle of $\sim 38^{o}$ (see Fig. 5.9). By bombarding the samples under the same conditions as before and in

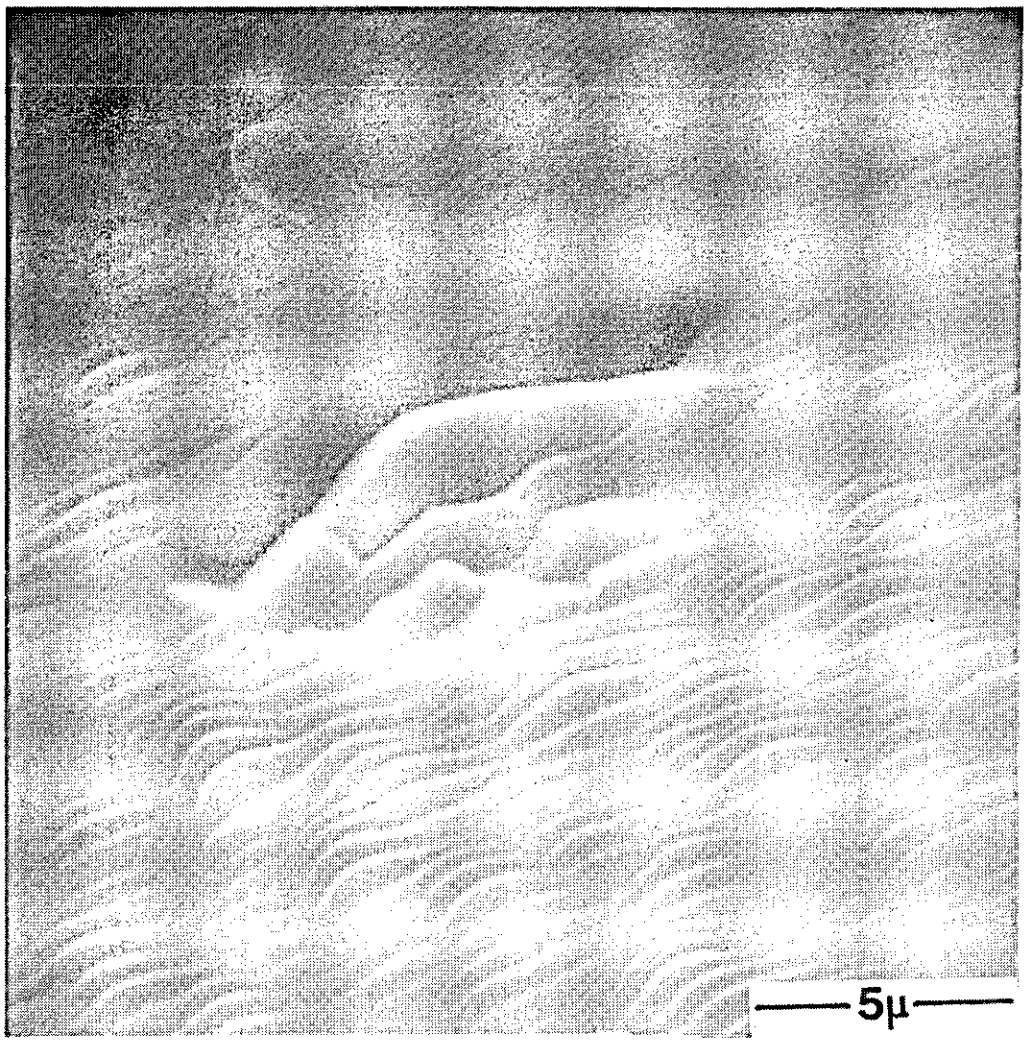

Figure 5.12 The surface of Si (111) following 5.5KeV O_2^+ bombardment to a depth of 11.1μm (10^{20} ions cm^{-2})

the same ion dose range, a direct comparison could be made. It should be noted that both the ion energy and angle have been altered in this mode, but it is initially assumed that changes in ion energy in the ranges associated in these experiments have negligible effect in the sputtering yield (Sigmund, 1969). However, there may be significant changes associated with the change in ion angle.

The effect of bombarding a Si(100) sample with 10.5KeV O_2^+ ions at $\sim 38^o$ is illustrated in the micrographs of Fig. 5:13. It is clear that to an equivalent ion dose the topography for these particular conditions appears vastly different from those observed by 5.5KeV O_2^+ bombardment. Initially pits form in small clusters on a generally featureless surface and increase both in frequency and intrinsic size as the ion dose is increased. There is, however, an important aspect to be considered, the depth of erosion after 10^{20} ions cm^{-2} is 5.4μm whereas for 5.5KeV O_2^+ bombardment to the same fluence it was 9.2μm. After further irradiation to a dose of 2.5 x 10^{20} ions cm^{-2} there is the characteristic occurence of the ripple observed previously, (see Fig 5.11)with larger outstanding pits, as illustrated in Fig. 5.13(e) (d). The eroded depth in the latter case is now 13μm which is more comparable to the depth eroded by 5.5KeV ion bombardment to a high ion dose (10^{20} ions cm^{-2}).

For a materials comparison under the same experimental conditions Fig 5.14 illustrates the developed morphology on Si(111) following 10.5KeV O_2^+ bombardment. A similar development of the "ripple train" morphology has occured and with the characteristic existence of an etch pit dominating the small scale ripple.

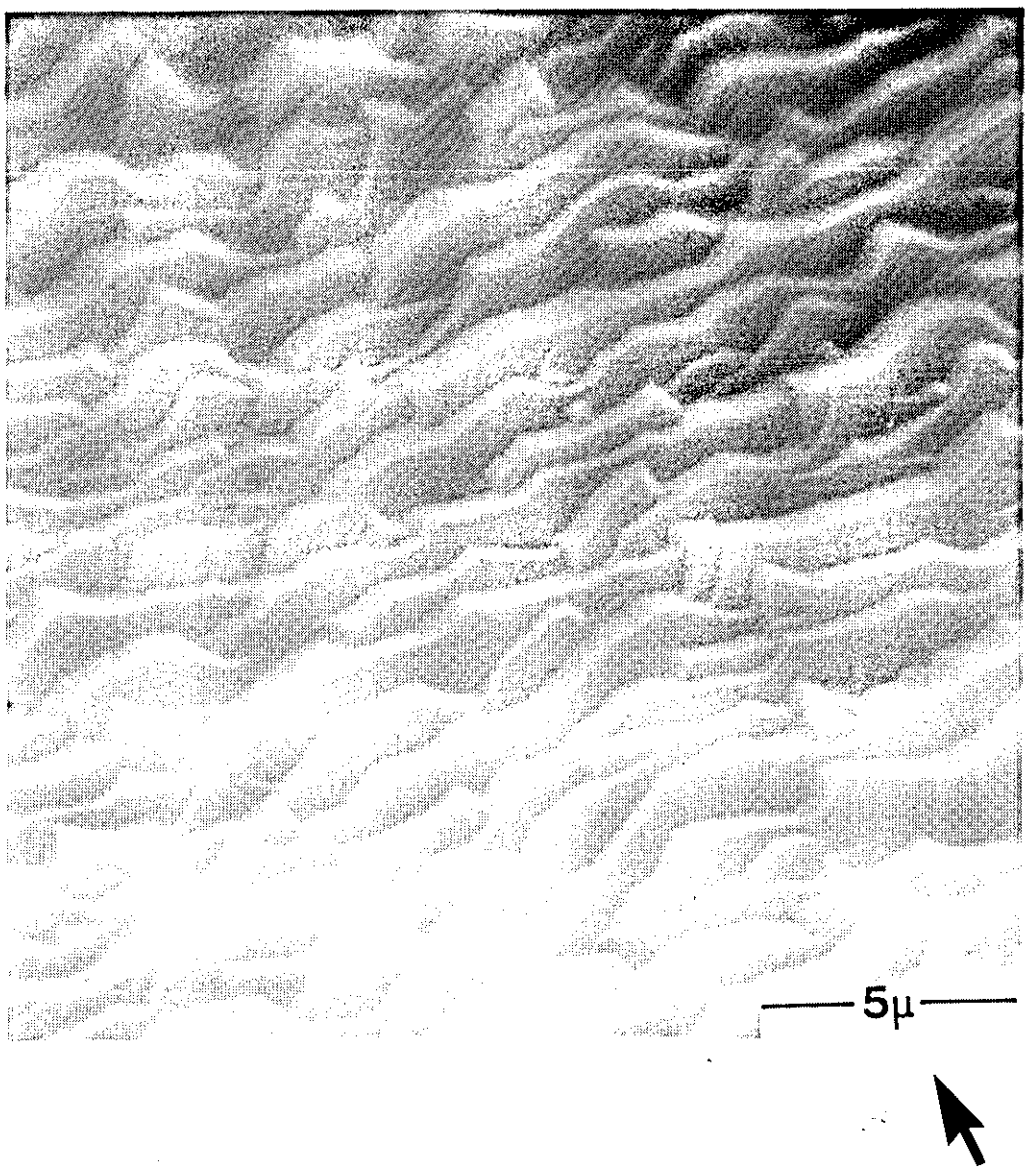

Figure 5.14: The nature of topography produced on Si(111) following 10.5keV O_2^+ bombardment to a depth of 7.6μm (10^{20}ions cm^{-2}).

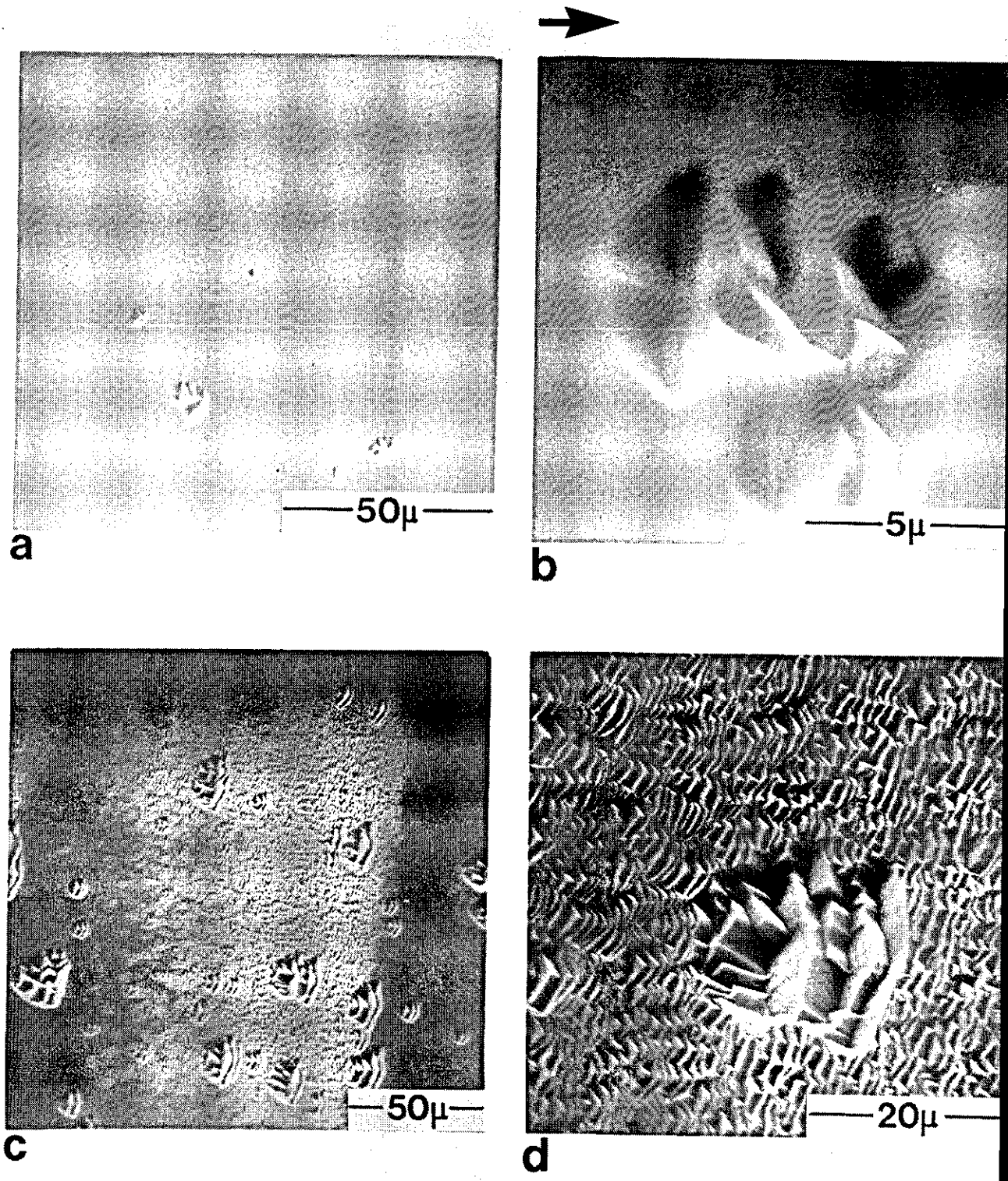

Figure 5.13: A sequence of micrographs highlighting the development of topography on Si(100) following 10.5keV O_2^+ bombardment to a depth of: (see text for details)

(a), (b) 2.8μm (6 x 10^{19}ions cm^{-2})

(c), (d) 13μm (1.9 x 10^{20}ions cm^{-2})

5.5.2.3 Silicon - Oxygen Bombardment with no Sample Bias

As previously stated the fixed sample stage in the Cameca ims 3f instrument does not allow freedom of movement to employ a variety of ion angles of incidence. A mini-matrix of experiments was, however, constructed by using the option of having the sample bias at +4.5KV or not biased (i.e. at 0V). The final results presented here therefore conclude this matrix by illustrating the effect of having a zero bias at the sample.

Figs 5.15 (a-c) and 5.16(a-d) illustrate the developed topography on Si(100), Si(111) following O_2^+ ion bombardment at 10KeV and 15KeV respectively. For these particular experiments high fluences were used since generally the resolution of the SEM was inadequate for detecting structures that may have been produced at ion doses $< 5 \times 10^{19}$ ions cm^{-2}. The micrographs, in general, have been selected to represent typical morphology changes that were observed from many experiments on separate samples, and have been varied so as to relate the general surface condition. It is clear from the micrographs presented in Figs 5.16(a) and 5.16(c)that the pits are characteristic of the previous observations made on these materials. However, it is also evident that other forms of topography can form (Figs5.16(b) and 5.16(d)) which significantly vary in appearance from the more commonly observed features. These effects may reflect the influence of the irradiating conditions or initial surface damage and will be discussed in a later section.

Figure 5.15: Two micrographs illustrating the development of surface topography after 10keV O_2^+ bombardment of Si(100) to a depth of:
(see text for details)

(a), (b) 12μm (1.1×10^{20}ions cm^{-2})

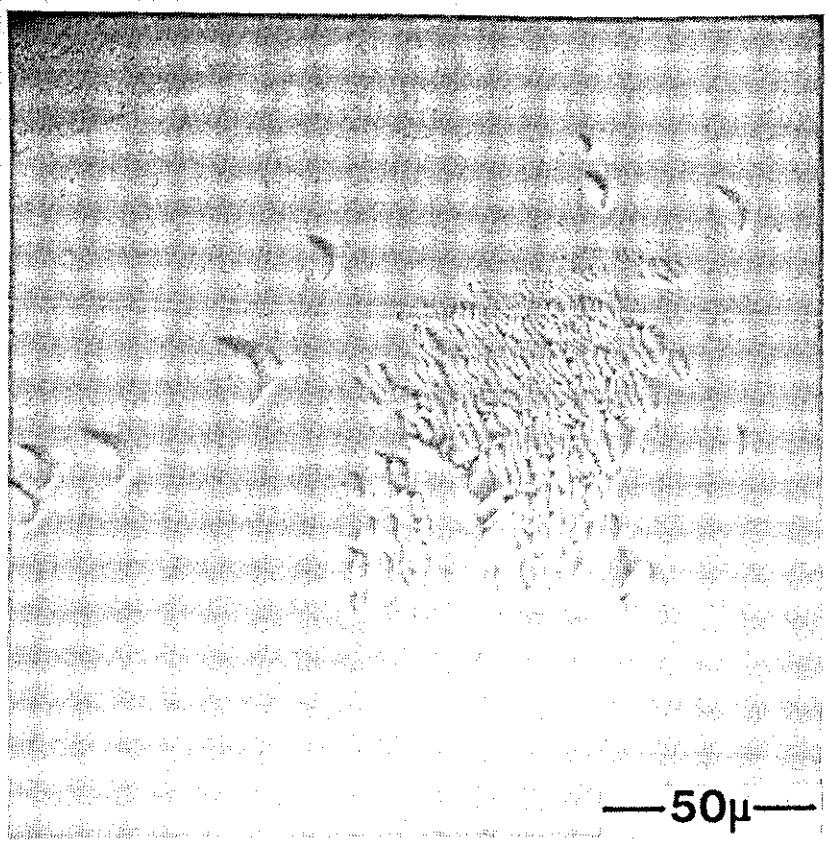

a

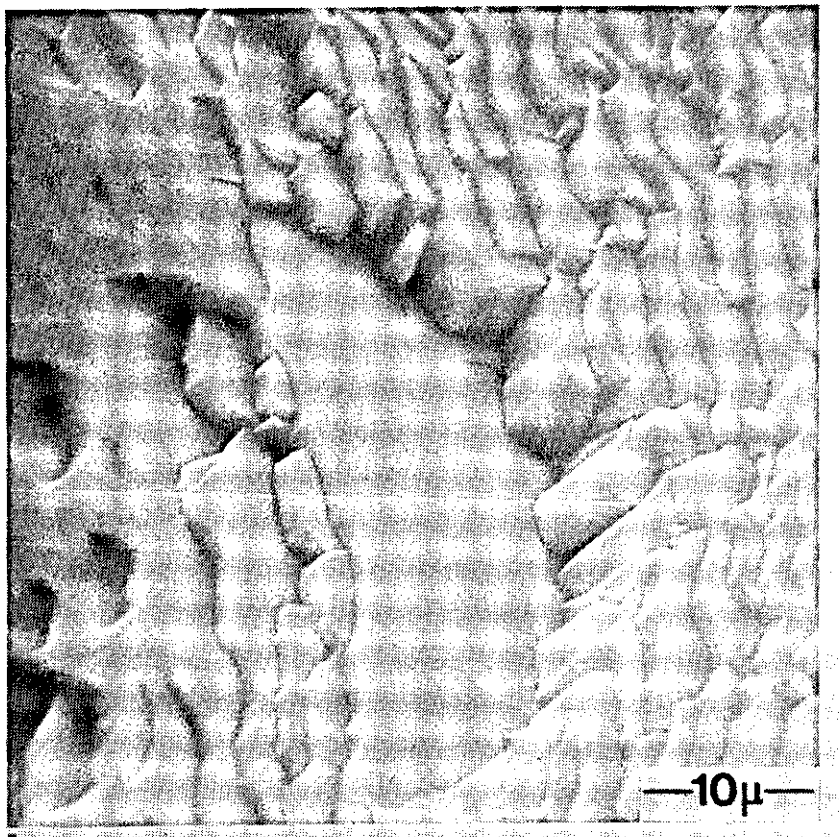

b

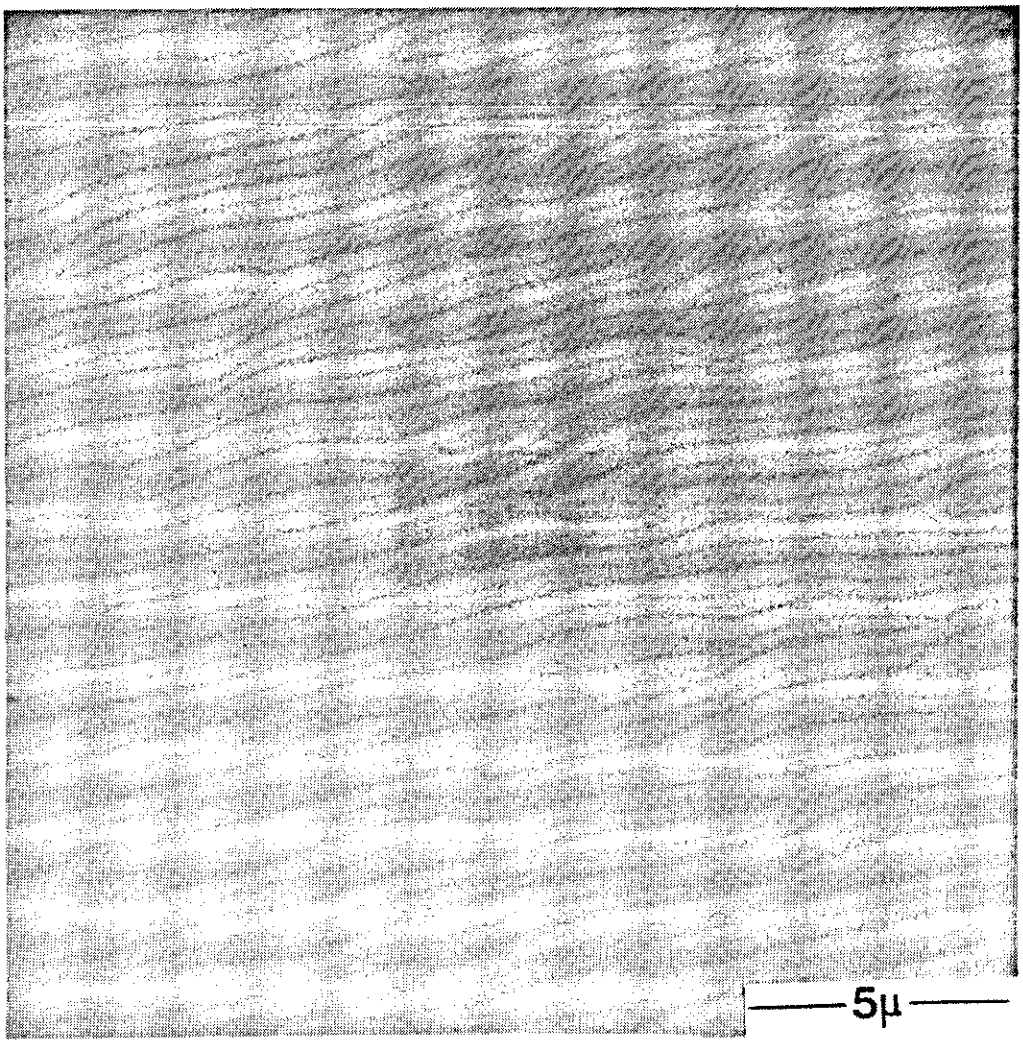

C

Figure 5.15: (c) Periodic ripple structure developed during 10keV O_2^+ bombardment of Si(111) to a depth of 9.5μm (10^{20}ions cm^{-2}).

Figure 5.16: Two micrographs illustrating the surface topography of Si(100) after 15keV O_2^+ bombardment to a depth of: (see text for details)

(a) 3.1μm (10^{20}ions cm^{-2})

(b) 10.5μm (1.1 x 10^{20}ions cm^{-2})

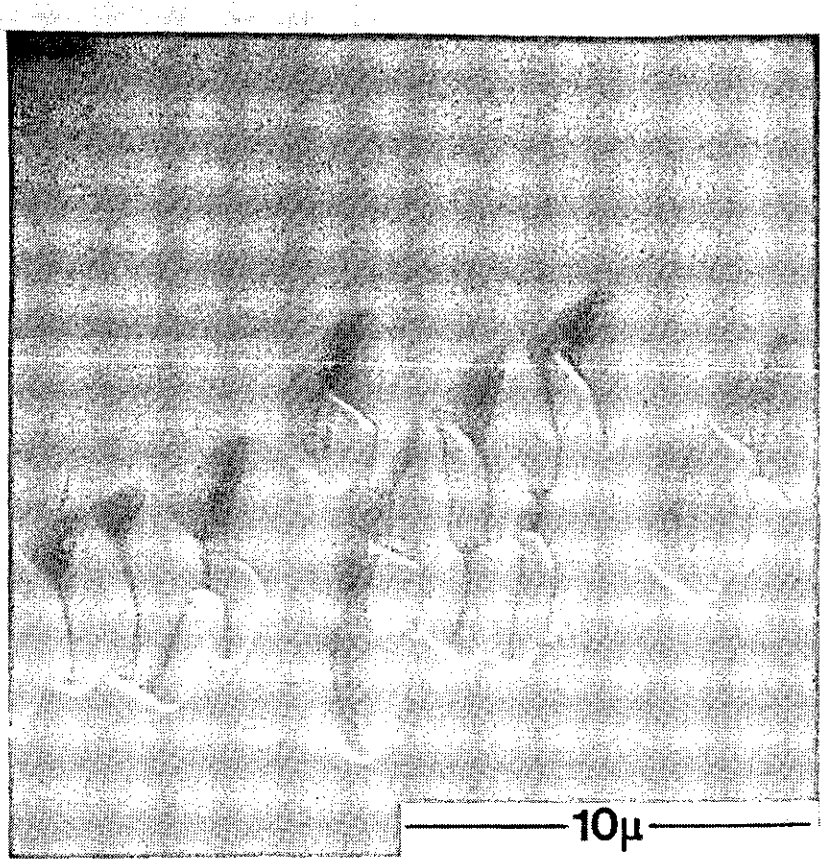

a

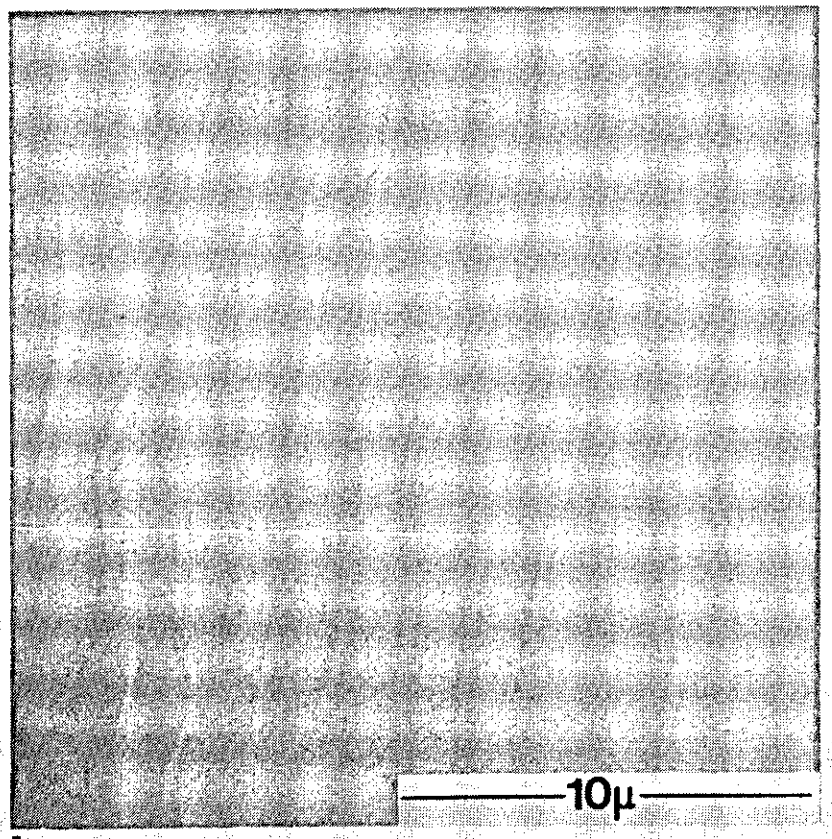

b

Figure 5.16: The general nature of topography produced on Si(111) following 15keV O_2^+ bombardment to a depth of:

(c), (d) 5.9μm (10^{20}ions cm^{-2}).

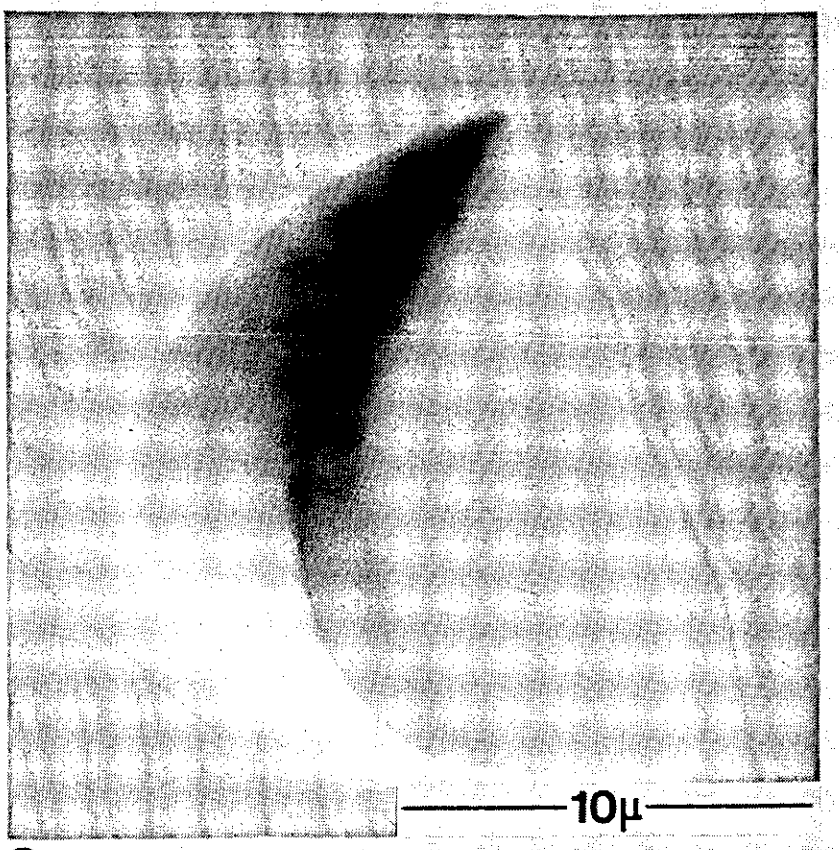

c

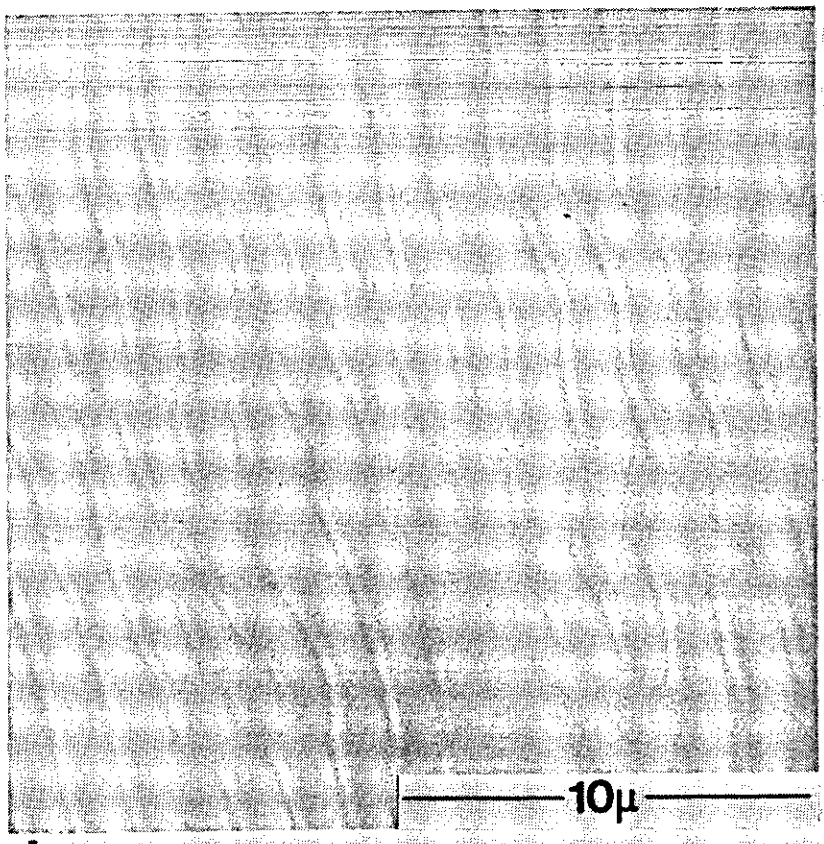

d

5.5.2.4 Silicon - 5.5KeV Caesium Ion Bombardment

The result of 5.5KeV Cs^+ ion bombardment on Si(111) following a dose of 10^{20} ions cm^{-2} is shown in Fig 5.17. The results were identical for Si(100), where in both cases the surface remained smooth and featureless even at these high doses. The sputtering yield for both materials, and under the above conditions, was much higher than for oxygen bombardment, and the depths of the eroded craters in Si(100) and Si(111) were $\sim$ 40μm and $\sim$ 43μm respectively.

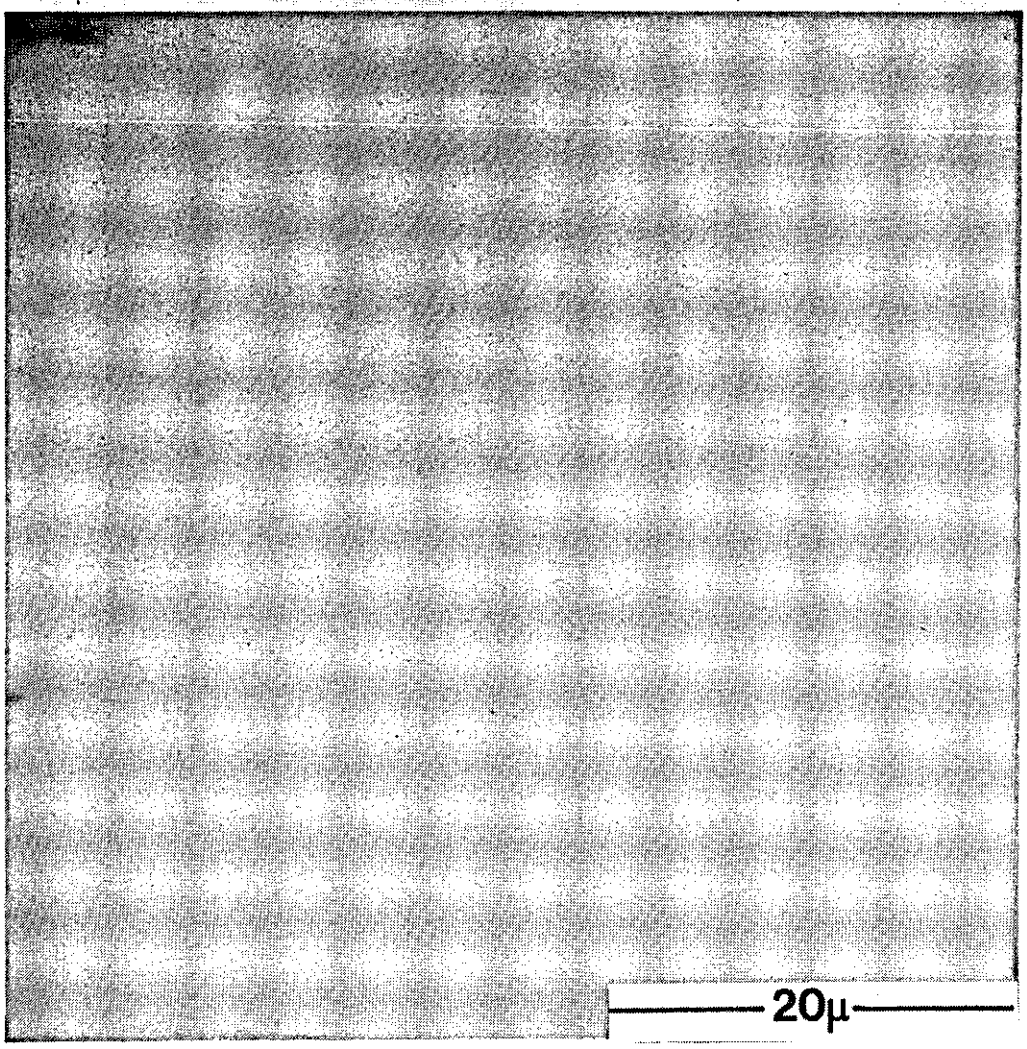

Figure 5.17: The featureless surface of Si(111) after 5.5keV Cs^+ bombardment to a depth of 43μm (10^{20} ions cm^{-2}).

5.5.2.5 GaAs - 5.5KeV Oxygen Ion Bombardment

Gallium arsenide has been utilized extensively over the last six years for low noise microwave amplification (Long et al 1981). Development of new superlattice structures is currently in progress which involves many interfacial layers (Gourly and Biefeld 1982, Kahn et al 1982).

The following study illustrates the ion induced surface topography that is likely to occur on GaAs during normal SIMS depth profiling conditions. The morphology of GaAs(100) surfaces following 5.5KeV O_2^+ bombardment is shown in Fig 5.18. A ripple topography is initially observed at 10^{19} ions cm^{-2} as illustrated in Figure 5.18(a). As the dose is increased to 5 x 10^{19} ions cm^{-2} larger pitted surface features appear and the smaller ripple becomes a sub-structure as shown in Fig 5.18(c). At higher doses, 10^{20} ions cm^{-2}, the larger ripple features tend to dominate, and from a visual comparison, it would appear that the final structure shown in Fig 5.18(d) is a result of continuous overlapping of the pitted features shown in Fig. 5.18(c) Furthermore, periodicity of both the larger and smaller features only appears to be prominent in the latter case where it remained approximately 2000Å throughout the ion dose range.

5.5.2.6 Gallium Arsenide - 10.5KeV Oxygen Ion Bombardment

The development of morphology on GaAs(100) with 10.5KeV O_2^+ ions is illustrated in Fig 5.19. Once again under these conditions the ion beam was incident at an angle of 38°, and with a source energy

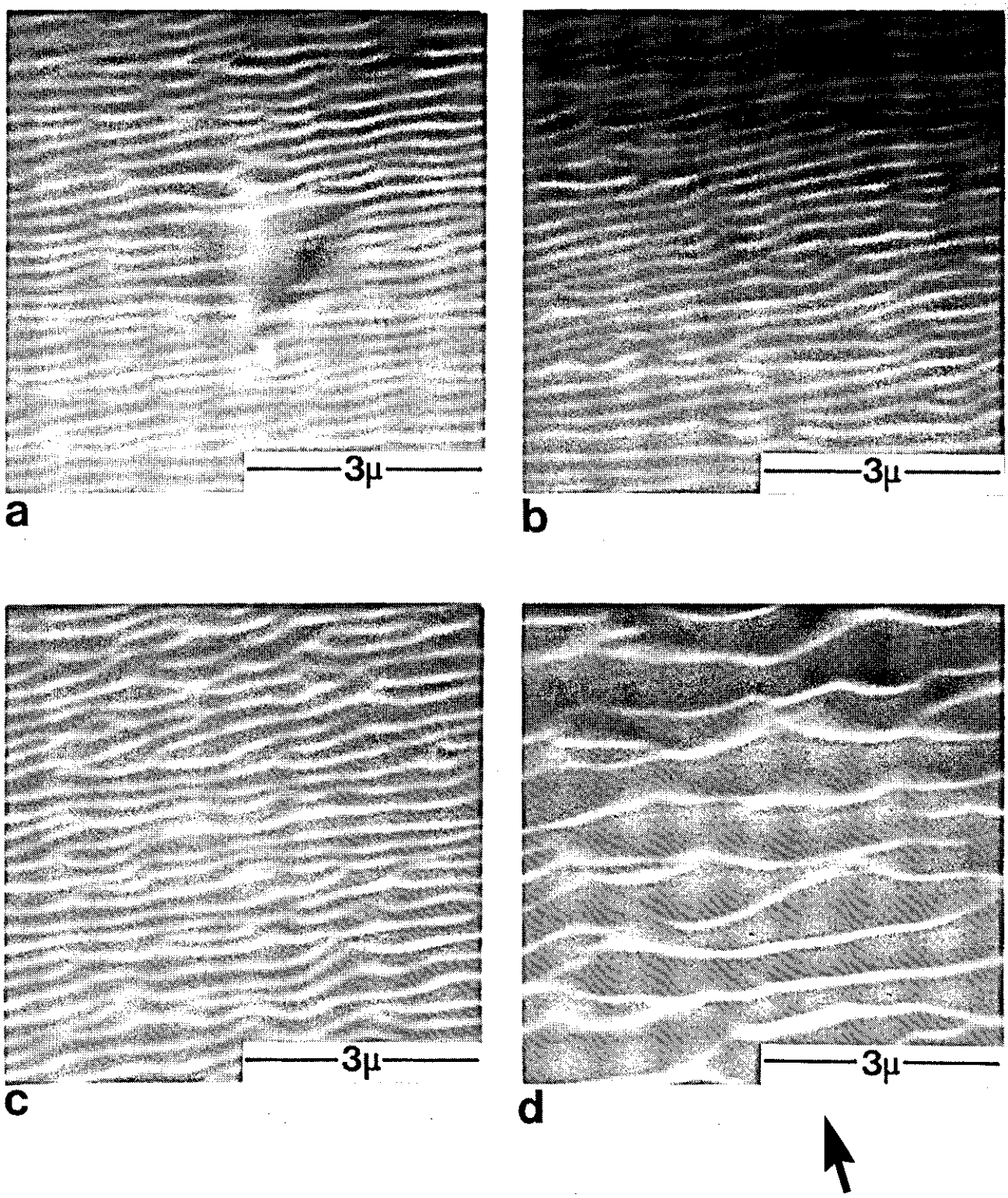

Figure 5.19: A set of micrographs showing changes in surface topography on GaAs(100) following 10.5keV O_2^+ bombardment to a depth of:

(a) 1.3μm (10^{19}ions cm^{-2})

(b) 2.5μm (2×10^{19}ions cm^{-2})

(c) 6.4μm (5×10^{19}ions cm^{-2})

(d) 12.5μm (10^{20}ions cm^{-2})

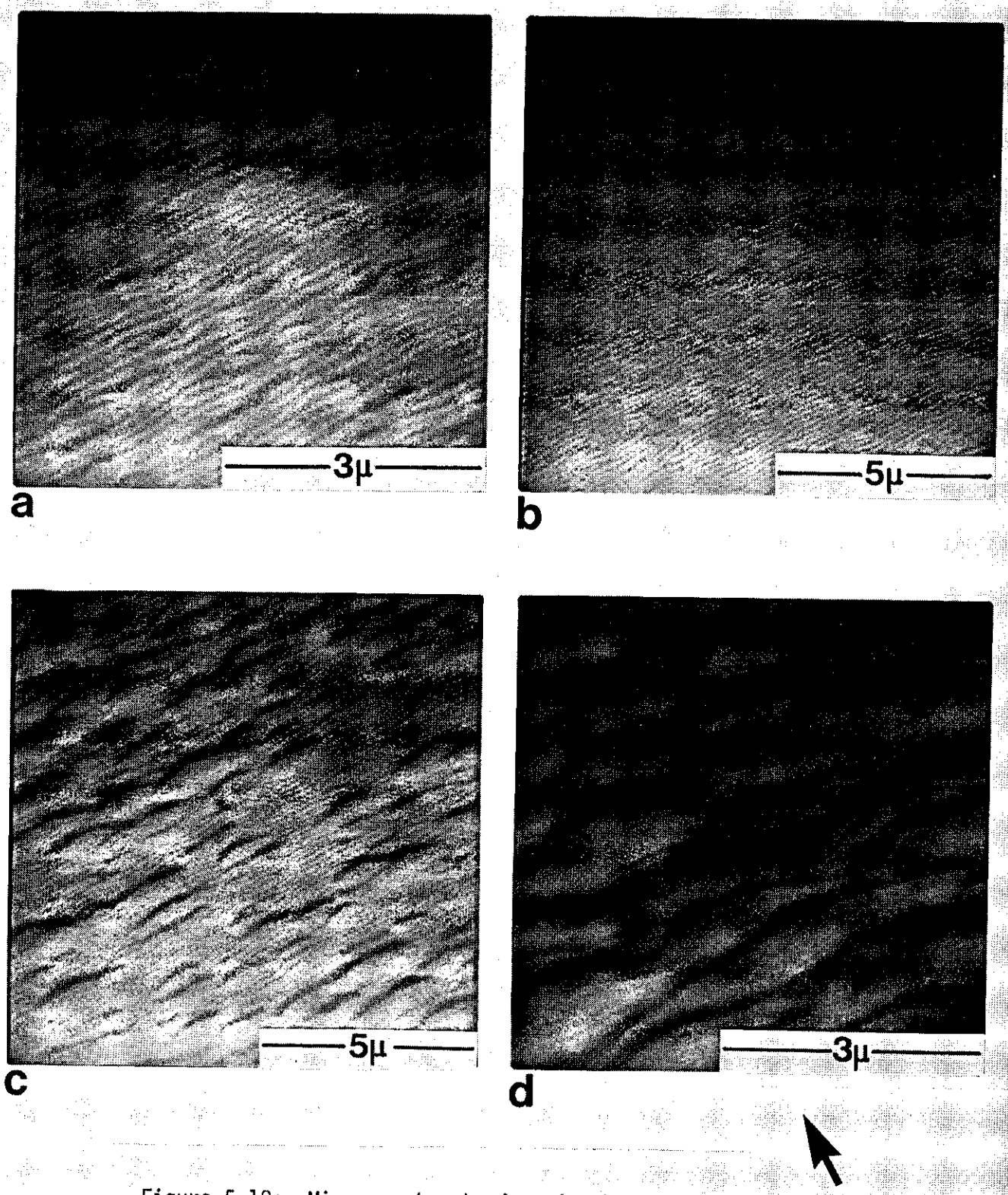

Figure 5.18: Micrographs showing the development of surface topography on GaAs(100) following 5.5keV O_2^+ bombardment to a depth of:

(a) 1.3μm (10^{19}ions cm^{-2})

(b) 2.9μm (2 x 10^{19}ions cm^{-2})

(c) 7.5μm (5 x 10^{19}ions cm^{-2})

(d) 15.5μm (10^{20}ions cm^{-2})

of 15KV. The developed features, although viewed from a different angle, are similar to those observed for 5.5KeV O_2^+ ion bombardment (Fig 5.18). The characteristic smaller ripple is initially observed at 10^{19} ions cm^{-2}, and these features increase in size with increasing ion fluence. Fig 5.19(a) also enhibits a preferentially etched sub-surface asperity which has disrupted the continuity of the ripple in that region. It can also be noted (fig.5.18) that the surface exhibits a type of "memory" effect, where after a fluence of 10^{20} ions cm^{-2} a small ripple structure appears parasitic of the larger undulating surface features. It is clear, however, from the magnifications of the different micrographs that the ripple formed at low doses (10^{19} ions cm^{-2}) is the initial stage for the larger furrows seen at the higher doses (10^{20} ions cm^{-2}), and that the parasitic ripple on these is possibly the result of a recurrence of the mechanisms initiating the surface features. It is apparent from the micrographs presented in Figure 5.18 that the periodicity of the ripple between ion fluences of 10^{19} - 2 x 10^{19} ions cm^{-2} remains relatively unchanged and is approximately 1500Å, although the amplitude increases slightly. Changes in the periodicity become more obvious at higher doses where after 5 x 10^{19} ions cm^{-2} it is $\sim$ 6000Å and after 10^{20} ions cm^{-2} is $\sim$ 20,000Å.

5.5.2.7 Gallium Arsenide - Oxygen Bombardment with no Sample Bias

The micrographs shown in Figs 5.20(a) (b) exhibit surface features resulting from 10KeV O_2^+ ion bombardment and zero sample voltage bias. Essentially, there is no significant difference in the qualitative nature of the morphology produced under these irradiation conditions

Figure 5.20: Two micrographs illustrating the details of surface topography produced on GaAs(100) after 10keV O_2^+ bombardment to a depth of: (see text for details)

(a), (b) 2.7μm (10^{20}ions cm^{-2})

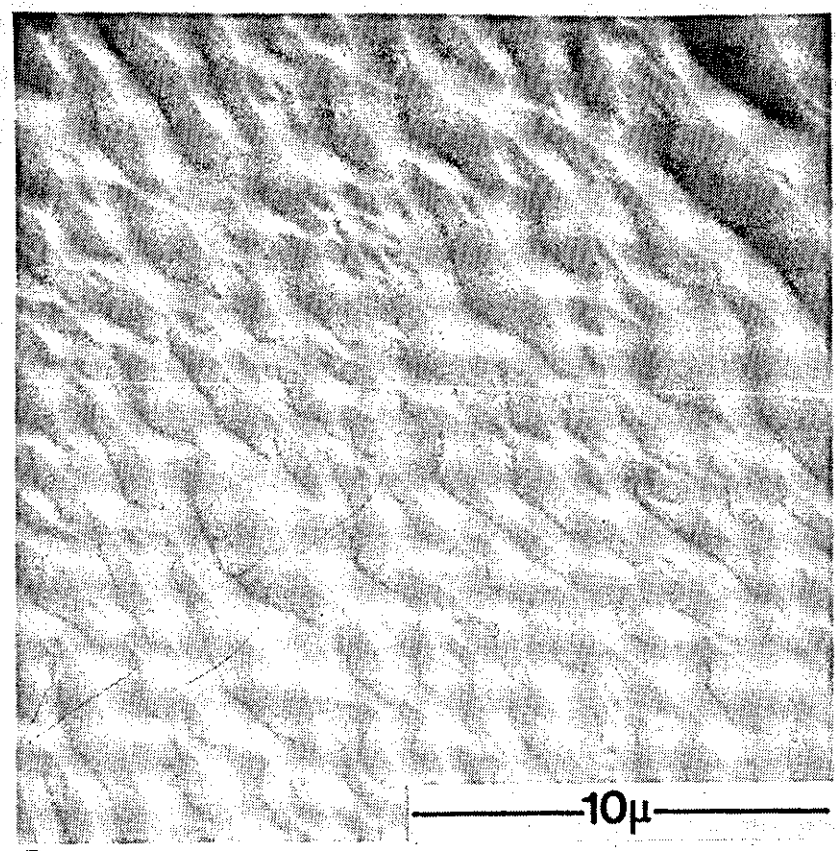

a

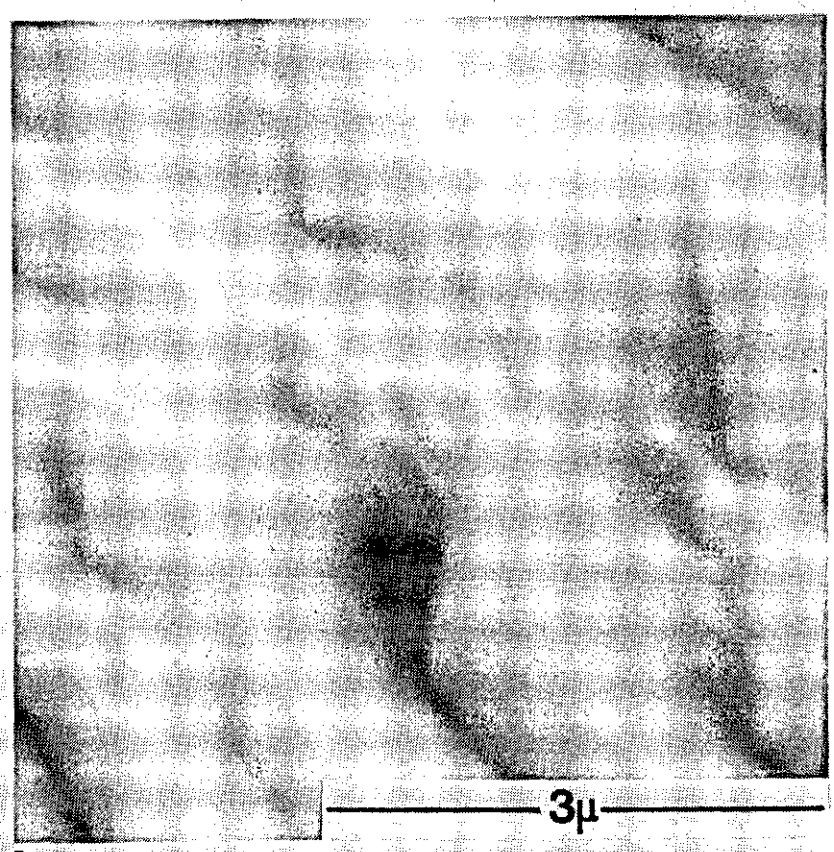

b

and the morphology observed previously, and even the parasitic small scale ripple is observable on the larger structures seen in Figure 5.20(b).

The morphology observable on GaAs following 15KeV O_2^+ bombardment to a dose of 10^{20} ions cm^{-2} is illustrated by the micrographs in Figs 5.20(c - e), which represent a sequence taken at three successive intervals from the edge of the crater to the centre. Although the same development mechanisms appear to be similar to results previously observed following O_2^+ bombardment nearer the crater walls (Figs. 5.20(c)and (d)), where dominating pits develop and overlap to create the more characteristically macroscopic structure, the fully developed topography in Fig 5.20(e) lacks the more regular periodicity and lateral continuity previously observed. This effect is possibly due to discrete parts of the surface facing the ion beam, preferentially etching during irradiation, thus swamping the smaller structure and destroying symmetry.

5.5.2.8 Gallium Arsenide - 5.5KeV Caesium Ion Bombardment

Fig 5.21(a) and (b) illustrate the surface condition of GaAs (100) following 5.5KeV Cs^+ bombardment to doses of 2 x 10^{19} ions cm^{-2} and 10^{20} ions cm^{-2} respectively. In contrast to Cs^+ ion bombardment of silicon, surface topography was developed on GaAs but only observed at high doses (10^{20} ions cm^{-2}). The nature of the ripple topography essentially remains similar to that observed in the early stages of O_2^+ bombardment (e.g. Figs 5.18 and 5.19) and has a regular periodicity of $\sim$ 12000Å. Due to the enhanced sputtering yield by Cs^+ bombardment the depth of the crater following 10^{20} ions cm^{-2} is

Figure 5.21: The surface of GaAs(100) following 5.5keV Cs^+ bombardment to a depth of

(a) 19.5μm (2×10^{19}ions cm^{-2})

(b) 82μm (10^{20}ions cm^{-2})

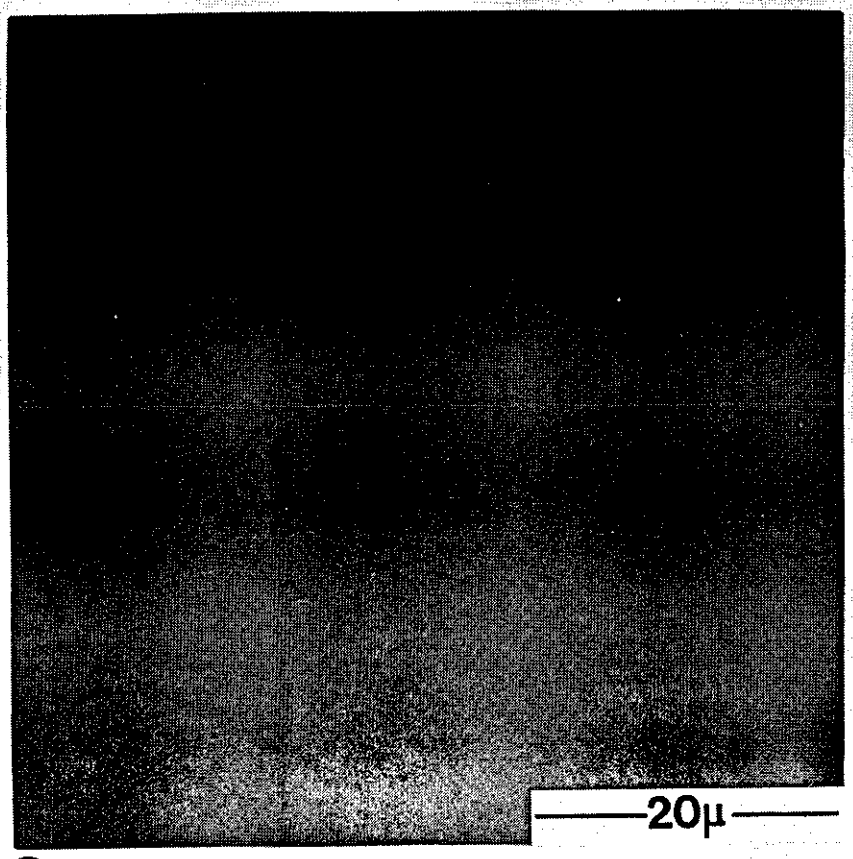

a

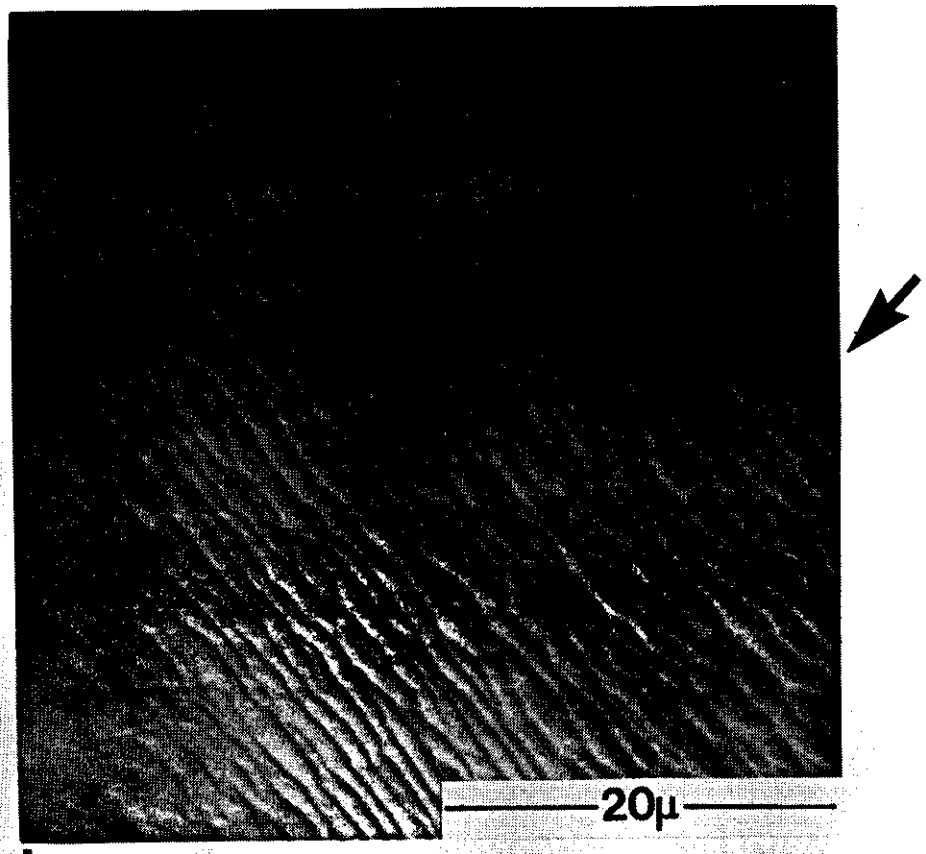

b

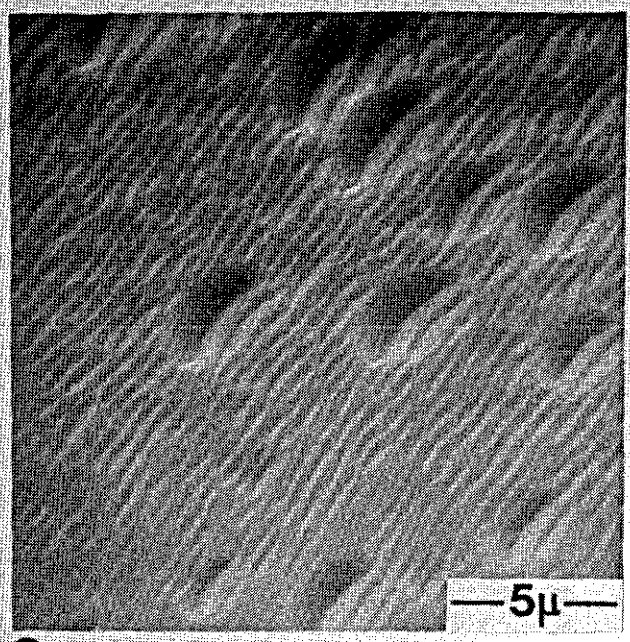

c

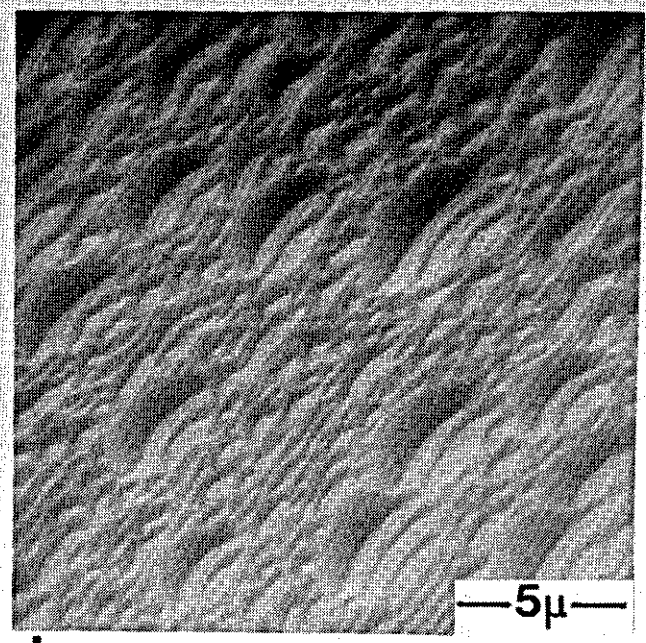

d

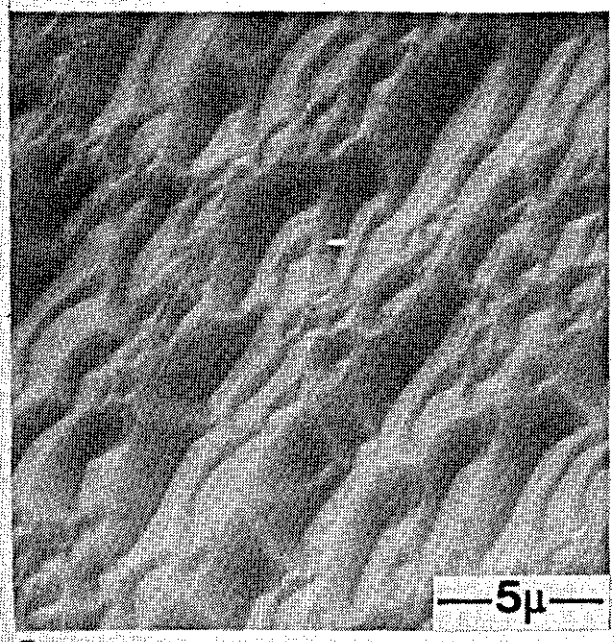

e

Figure 5.20: The surface topography of GaAs(100) following 15keV O_2^+ bombardment to a depth of:
(see text for details)

(c), (d), (e) 9.6μm (10^{20}ions cm^{-2})

82μm, compared to 15.5μm by O_2^+ bombardment to the same dose. Thus, in view of this magnitude of the ripple produced by Cs^+ bombardment is greatly reduced compared to that produced by O_2^+ bombardment.

5.5.2.9 Indium Phosphide - 5.5KeV Oxygen Ion Bombardment

The development of surface morphology on InP(100) surfaces under 5.5KeV O_2^+ bombardment with increasing ion dose (10^{19} - 10^{20} ions cm^{-2}) is shown in Fig. 5.22. The observed features were of a faceted nature, similar in structure to those developed on Si and GaAs following a similar bombardment with O_2^+ ions. The characteristic growth of the structure with increasing ion dose is evident, where the ridge to trough height, as well as the pitch increases with prolonged ion bombardment. Further to the initial observations illustrated here, experiments performed to determine the dependence of the direction of the topography indicated that the direction of the ion beam was the dominating influence, and that the crystal orientation prior to bombardment had no effect. Once the topography has been initiated, and the fine scale faceting developed into well-defined microscopic faces, the sputtering yield will be dependent on the angle of ion incidence at discrete parts on the surface, and dominate the propagation of the facets into, and across the surface consistent with erosion theory (Barber et al, 1973). This is substantiated in the knowledge that each micrograph in Fig 5.22 represents the centre of independently eroded craters, and it is clear that the morphology of the surface retains its basic appearance and only increases in magnitude with increasing dose/depth.

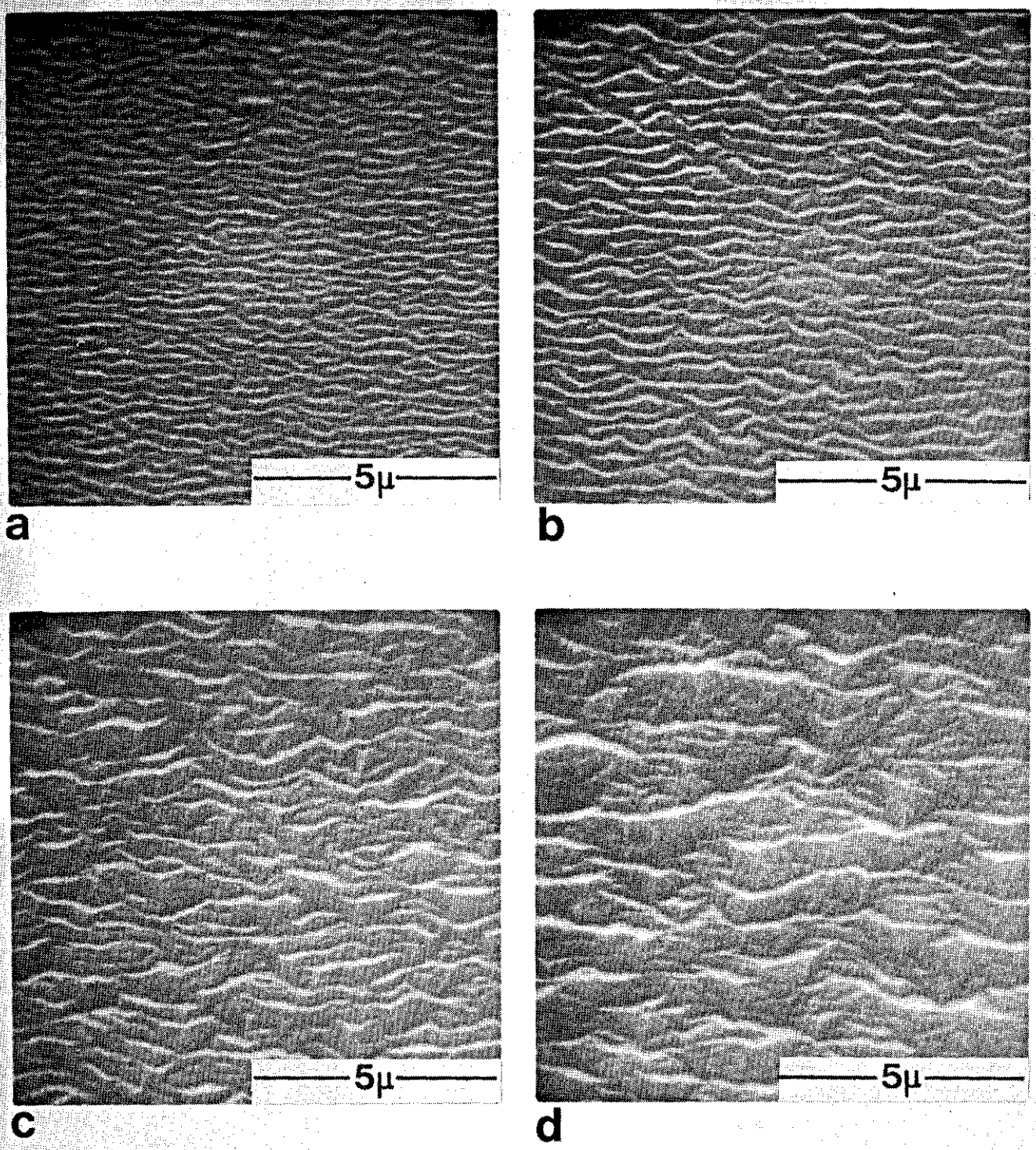

Figure 5.22: A series of micrographs illustrating surface topography development on InP(100) following 5.5keV O_2^+ bombardment to a depth of:

(a) 2.3μm (10^{19}ions cm^{-2})

(b) 5.6μm (2×10^{19}ions cm^{-2})

(c) 13.5μm (5×10^{19}ions cm^{-2})

(d) 26μm (10^{20}ions cm^{-2})

5.5.2.10 Indium Phosphide - 10.5KeV Oxygen Ion Bombardment

In comparison to the effects of 5.5KeV O_2^+ bombardment at an ion incidence angle of $\sim 47^0$, the resulting features following 10.5KeV O_2^+ bombardment at an angle of $\sim 38^0$ remain similar in appearance (see Fig 5.23). However, although the qualitative nature of the surface appears extremely similar the size of the individual facets are not as large. This is primarily a consequence of the difference in the sputtered depths. For example, after 5.5KeV and 10.5KeV ion bombardment a dose of 10^{20} ions cm^{-2} the eroded depths were $\sim 26\mu m$ and $\sim 14\mu m$ respectively, which would indicate a sensitive dependence in the change of the angle of incidence, yet having no influence on the structural shape.

At this point it is interesting to note that sometimes, depending on the illumination angle in the SEM, the surface shape can appear visually different at several orientations. To illustrate this aspect Fig 5.24 is a reproduction of the structure formed in Fig 5.23(d) when the sample has been rotated 90^0 in a clockwise direction. The ion beam was incident from the left with respect to this micrograph. This micrograph reveals that for a full realisation of a three-dimensional textured surface, careful viewing of the surface must be performed at several appropriate angles, a belief previously reported by other authors (Carter et al, 1977; Lewis et al, 1982). Comparisons made in this way with samples that had undergone 5.5KeV O_2^+ bombardment showed that the ripple trains were more segmented for 10.5KeV O_2^+ bombardment, and also possessed more well-defined facets. It is therefore conceivable that the differences observed in sputtered

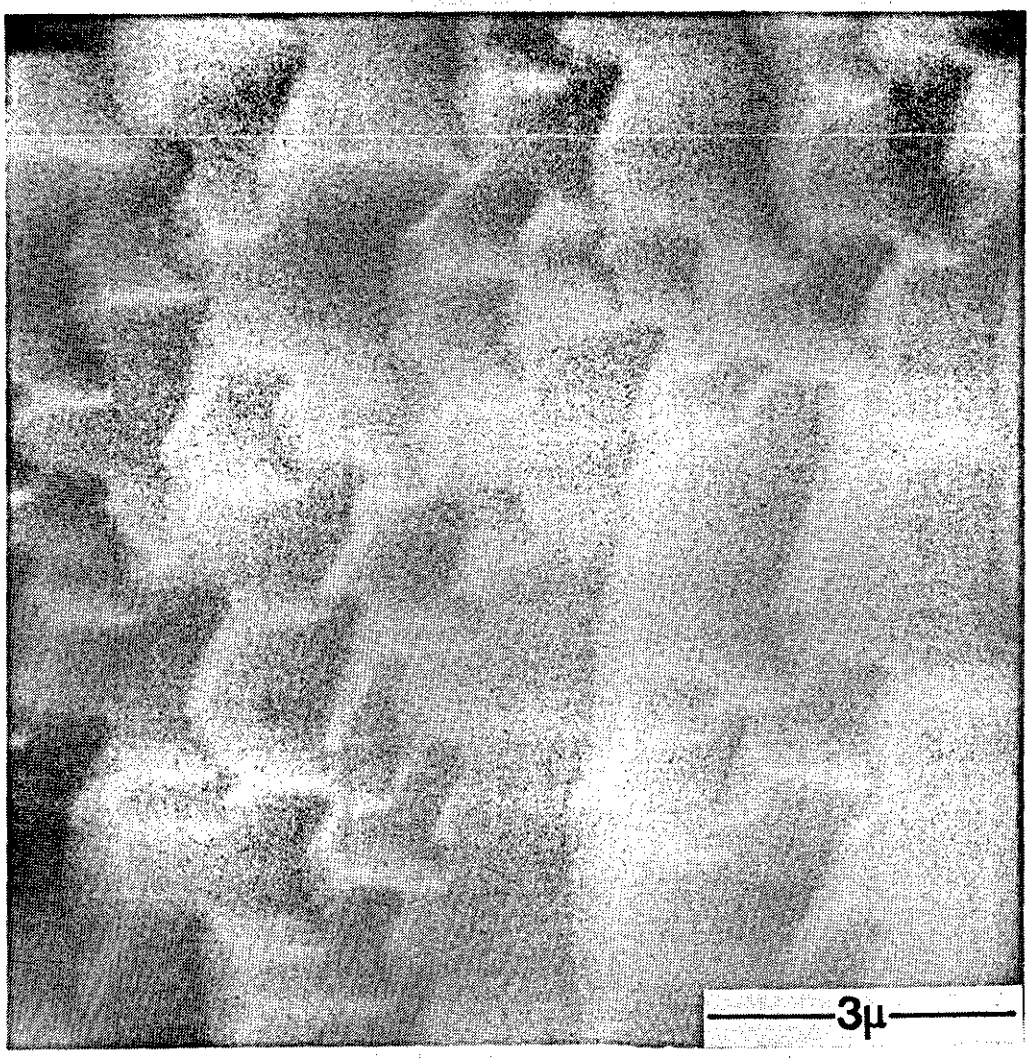

Figure 5.24: A micrograph illustrating the appearance of the topography on InP(100) after 10.5keV O_2^+ bombardment. This view is of Figure 5.23(d) rotated 90° anticlockwise.

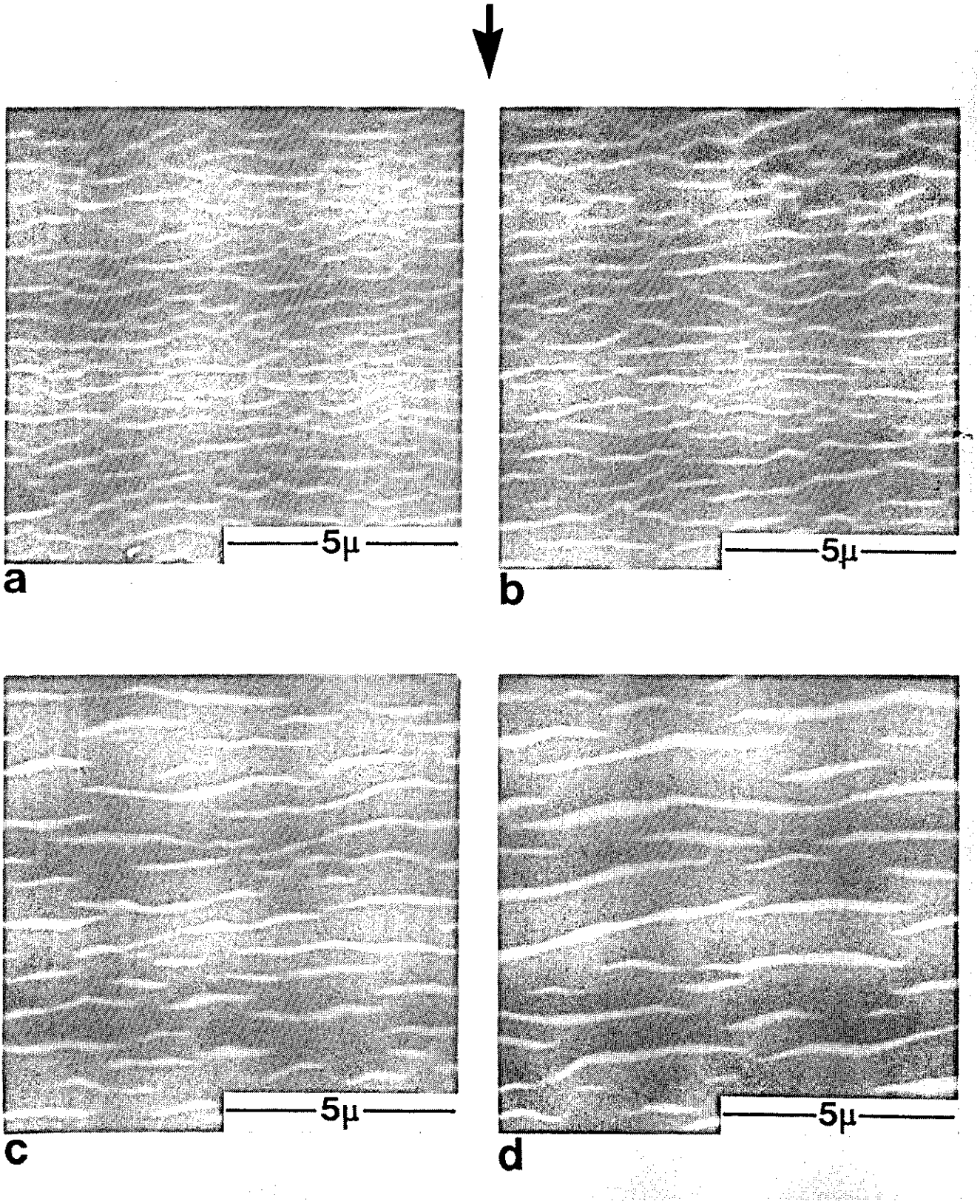

Figure 5.23: The development of surface topography on InP(100) following 10.5keV O_2^+ bombardment to a depth of:

(a) 1.6μm (10^{19}ions cm^{-2})

(b) 2.3μm (2 x 10^{19}ions cm^{-2})

(c) 6.8μm (5 x 10^{19}ions cm^{-2})

(d) 14μm (10^{20}ions cm^{-2})

depths after similar ion doses could be due to the nature of the sputter-induced structures either enhancing or decreasing sputtering yields, an effect previously reported elsewhere (Auciello, 1982).

5.5.2.11 Indium Phosphide - Oxygen Ion Bombardment with no Sample Bias

The removal of the sample bias altered the incident angle of the bombarding ions to 30°, and with an energy of 10KeV, the observed surface morphology following a total ion fluence of 5×10^{19} ions cm^{-2} and depth $14\mu m$ is shown in Fig 5.25 (a) and (b). The nature of the structures is again, similar to the morphology observed at approximately the same energy (10.5KeV) but with an incident angle of $\sim 38^{o}$ (see Fig. 5.24.

Fig 5.26 illustrates the topography occurring following 15KeV O_2^+ bombardment. Fig 5.26 (a) shows a region of facets in the crater after 10^{20} ions cm^{-2}, and Fig5.26(b) is a highly magnified view of the same structures but rotated in the SEM by 180°. These two micrographs reinforce the belief that ion-induced topography should be carefully scrutinized from all viewing angles before a realistic picture of the true profile of the features can be gained. Fig 5.26 (a) illustrates a probable source of the more densely faceted features. The surface of InP following 10^{20} ions cm^{-2} exhibits triangular shaped pits, which appear to overlap in the denser regions thus forming a continuous faceting phenomenon. The continuous faceting, in general, only occurred near the crater walls which may have been a result of enhanced etching due to ion reflection. The triangular etch pits were found to develop in groups (two or more) in the centre of the crater, where in this region there was no continuous faceting and the surface surrounding the

Figure 5.25: The surface morphology of InP(100) during 10keV O_2^+ bombardment to a depth of:
(see text for details)

(a), (b) 14μm (5×10^{19} ions cm^{-2})

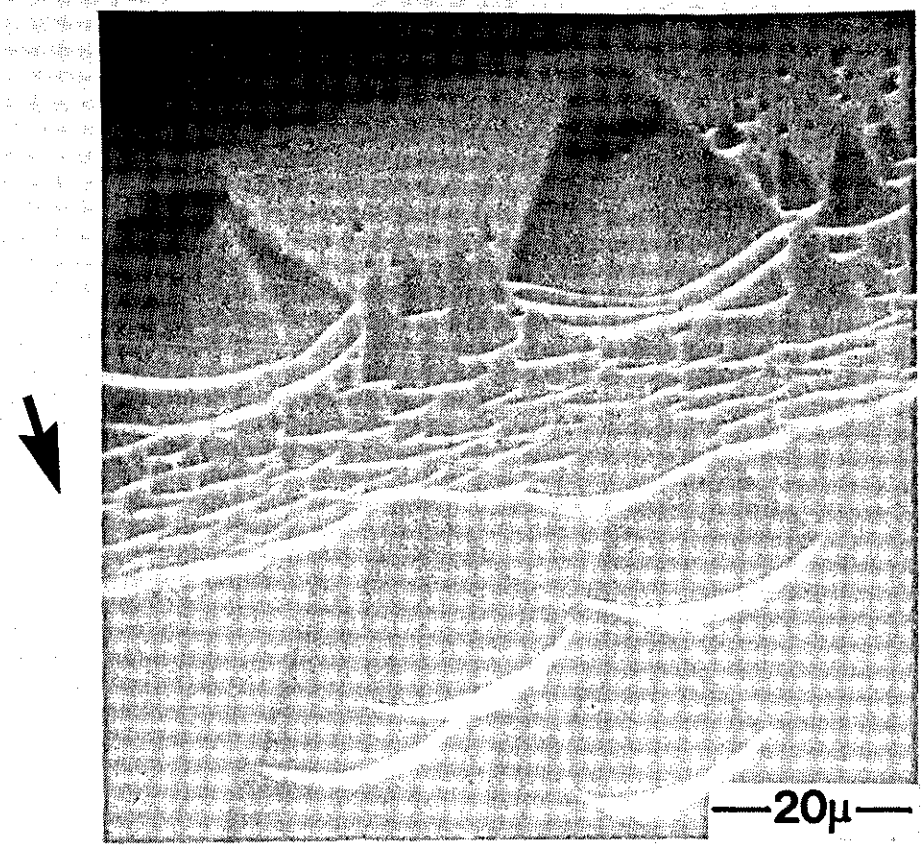

a

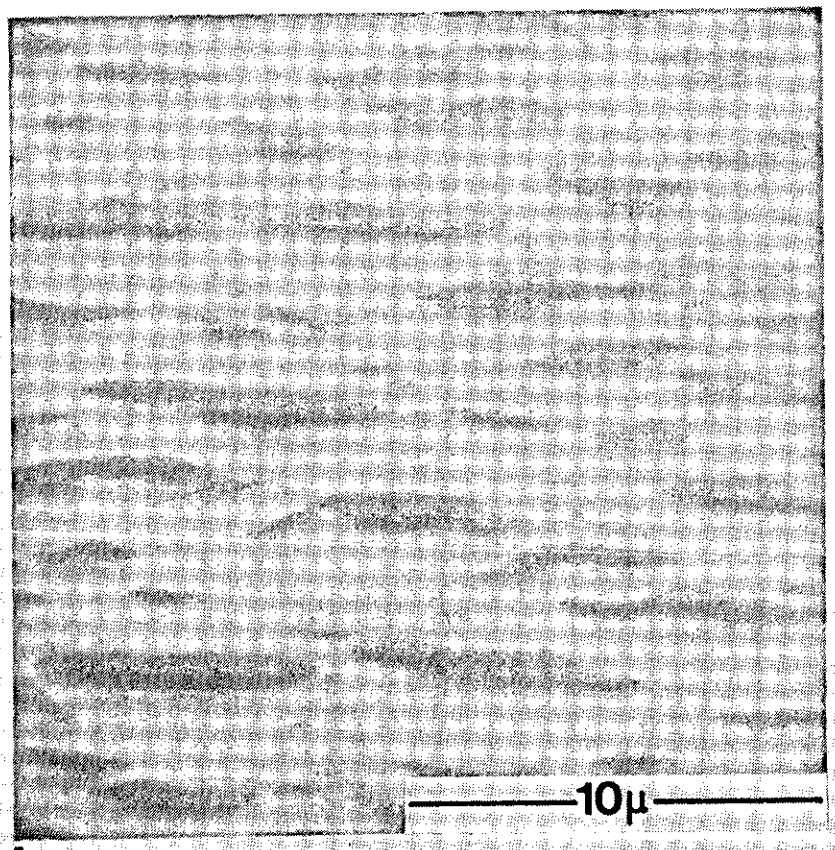

b

Figure 5.26: Two micrographs illustrating the differing appearance of surface topography produced by 15keV O_2^+ bombardment of InP(100). The eroded depths are:
(see text for details)

(a) 19μm (10^{20}ions cm^{-2})

(b) 14μm (5×10^{19}ions cm^{-2})

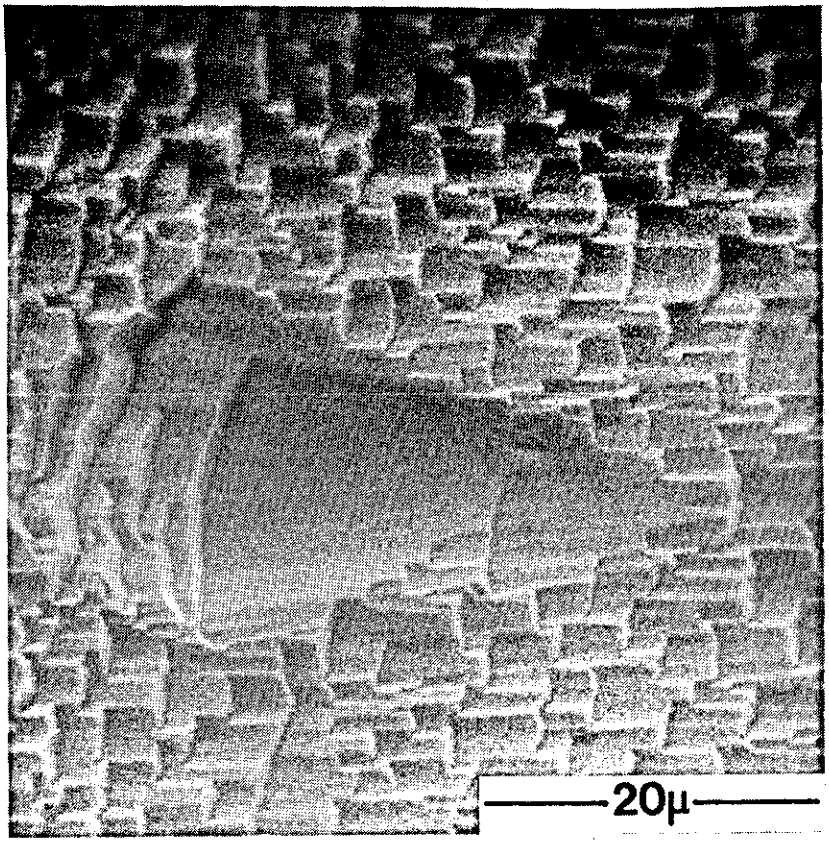

a

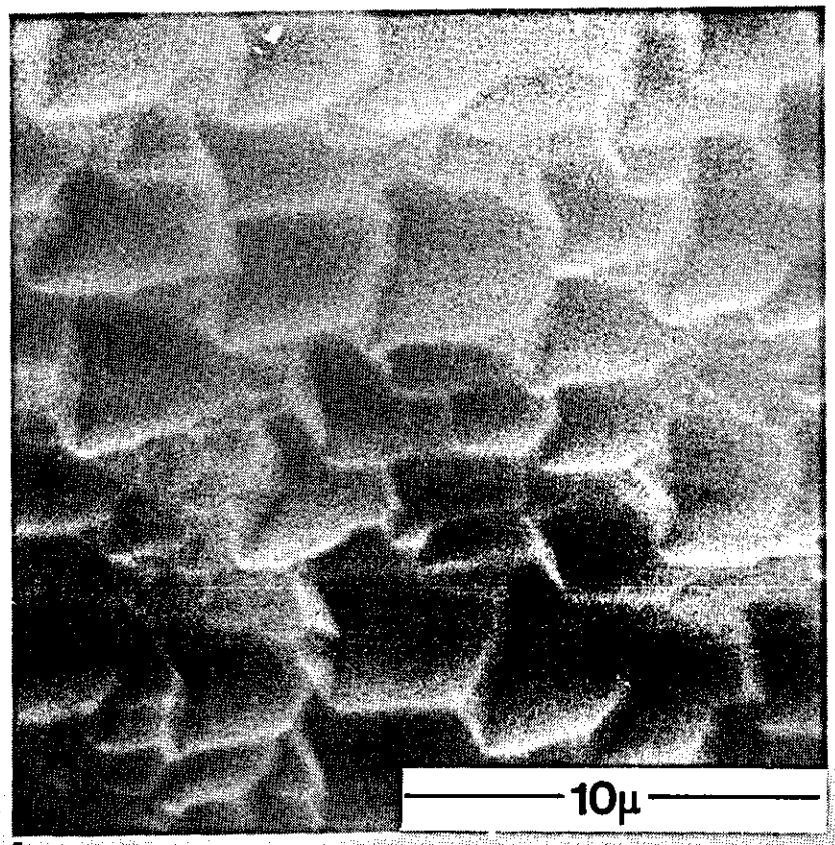

b

pits was featureless. This feature of topography development resembles the formation of continuous faceting on silicon following O_2^+ bombardment, where at the higher ion energies (> 10KeV) large pits overlapped to produce a uniformly faceted area.

5.5.2.12 Indium Phosphide - 5.5KeV Caesium Ion Bombardment

Fig 5.27 shows the effect of 5.5KeV Cs^+ ion bombardment of InP with increasing ion dose (10^{18} to 5×10^{19} ions cm^{-2}). The InP surfaces in this sequence were taken from the same slice as those used in the O_2^+ bombardment studies. In contrast to the previous experiments, cones are formed in all cases. The cones are first observed at relatively low doses (10^{18} ions cm^{-2}) which corresponds to an eroded depth of 2.1μm. They are observed to develop singly or in groups and their size and density increases with increasing ion dose. The cones point towards the axis of the primary ion beam and are accompanied in most cases by a shallow surface depression or pit, which may be formed by primary ion beam reflection from the cone as it develops.

At doses of 5×10^{19} ions cm^{-2}, corresponding to an eroded depth of 103μm, the surface is dominated by massive cone formation whose stem-to-base heights are approximately one third of the total depth of the crater.

An outstanding feature, particularly at the relatively lower doses (10^{18} ions cm^{-2} - 10^{19} ions cm^{-2}) is the mottled and slightly pitted appearance of the surface. Fig 5.28 illustrates the development of the surface specifically omitting regions of the crater floor where cones were formed. Initially, after a dose of 5×10^{18} ions cm^{-2}

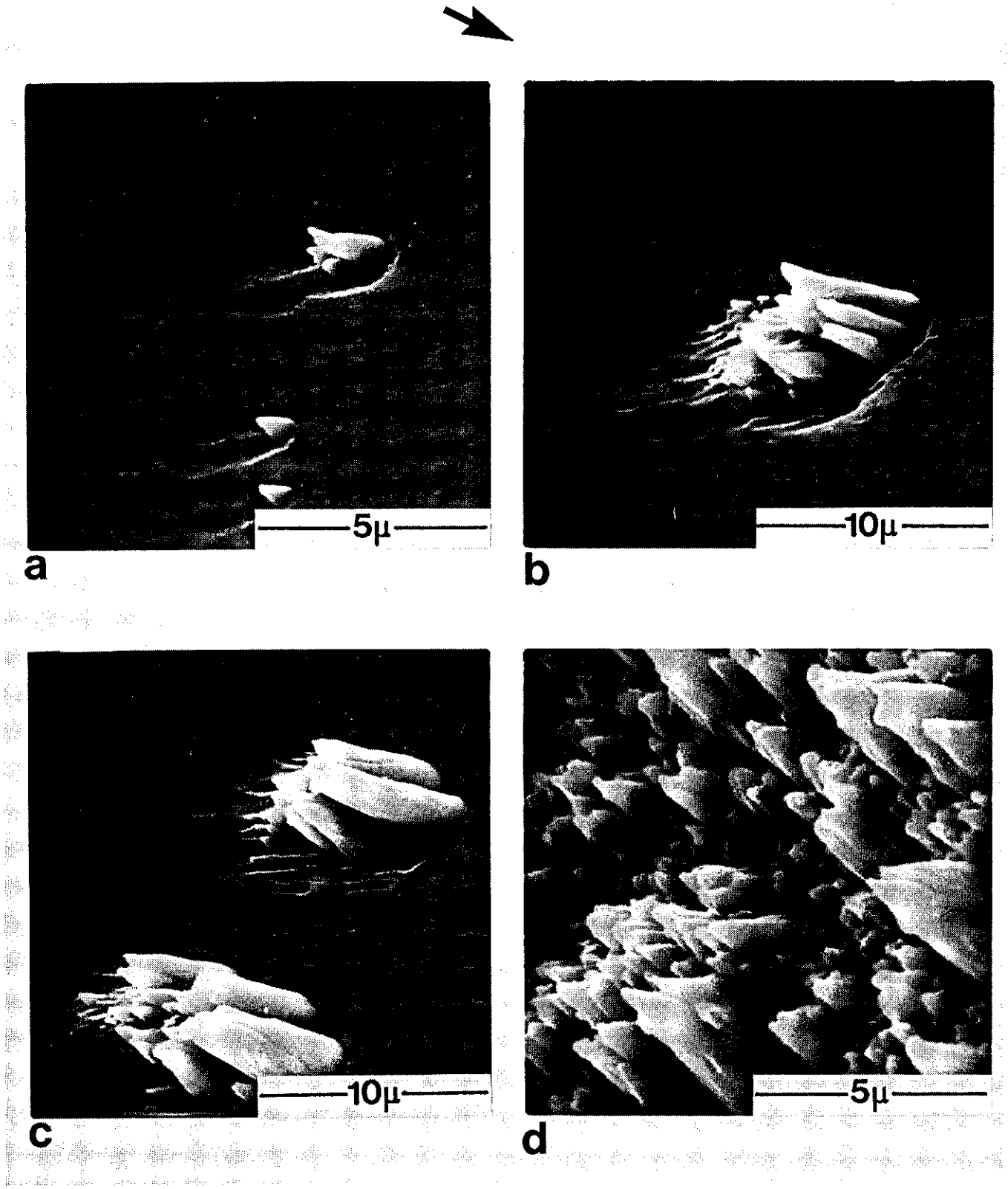

Figure 5.27: The development of surface topography of InP(100) following 5.5keV Cs^+ bombardment to a depth of:

(a) 2.1μm (10^{18}ions cm^{-2})

(b) 20μm (10^{19}ions cm^{-2})

(c) 47μm (2 x 10^{19}ions cm^{-2})

(d) 103μm (5 x 10^{19}ions cm^{-2})

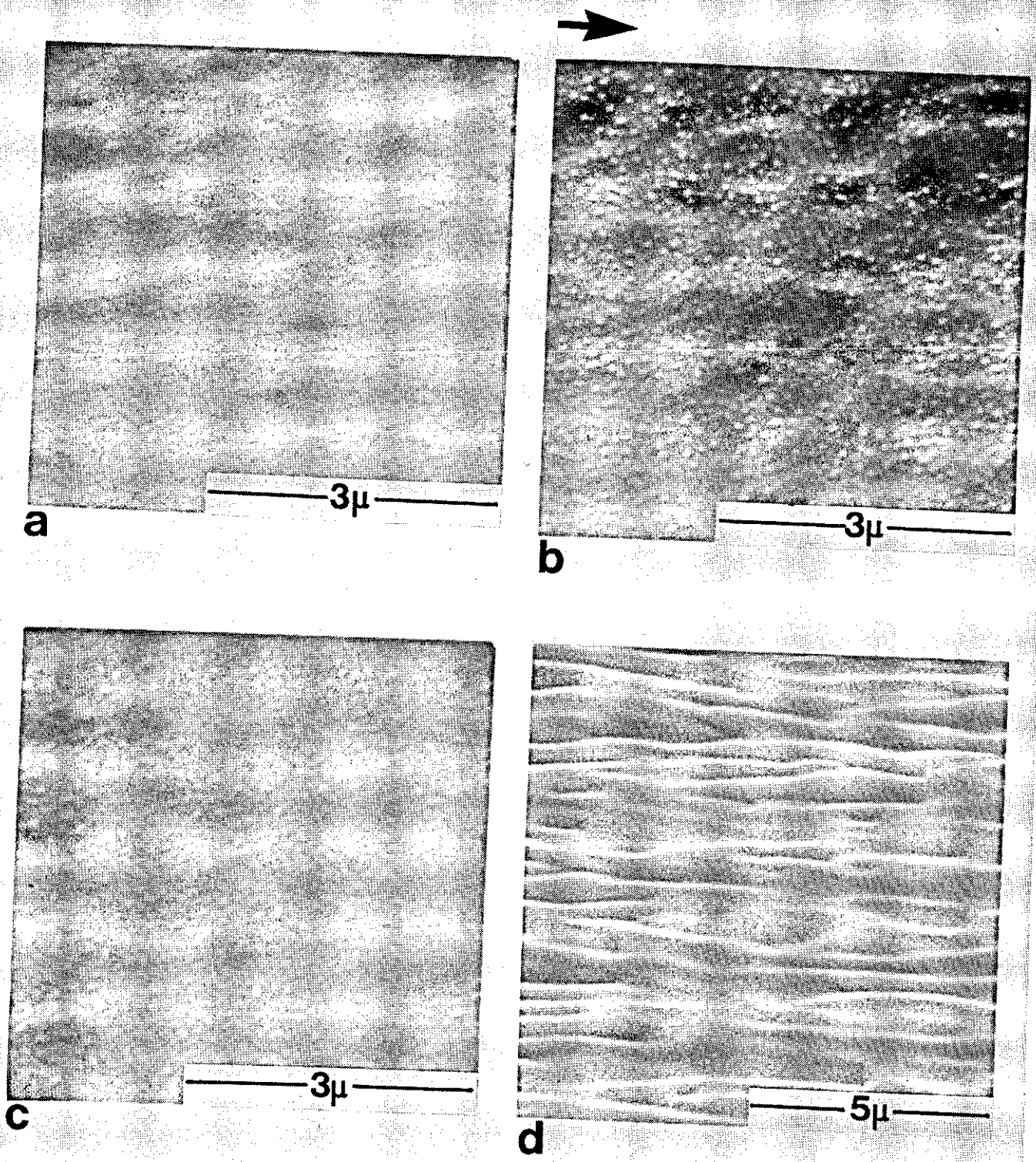

Figure 5.28: A series of micrographs illustrating the depletion of an InP(100) surface during 5.5keV Cs^+ bombardment. The eroded depths are:

(a) 11μm (5×10^{18}ions cm^{-2})

(b) 20μm (10^{19}ions cm^{-2})

(c) 47μm (2×10^{19}ions cm^{-2})

(d) 103μm (5×10^{19}ions cm^{-2})

(Fig 5.28(a)) light and dark regions can be observed highlighting a slight undulation of the surface. As the dose increases to 2 x 10^{19} ions cm^{-2} (Fig 5.28(b)(c)) these regions of light and dark contrast become more prominent, where the lighter regions emphasise the higher points of the forming structures leaving the depression depleted in the white speckle. Finally, at a dose of 5 x 10^{19} ions cm^{-2} the mottled appearance cannot be observed (see Fig 5.28(d)) and the surface existing between the cones is in the form of grooves propagating in a direction parallel to the ion beam detection.

Very similar results to those shown in Fig 5.28 have been observed by Skinner et al (1983) who bombarded single crystal surfaces of InP(110) and InP(100) with 5KeV Ar^+ ions, at 18° angle of incidence. After the sputter removal of only 200Å small spherical islands form that increase in diameter with increasing ion dose. They also indicated that these surface features form regardless of the ion species Ar^+, Xe^+, N_2^+ and O_2^+ which would appear inconsistent with the results presented for O_2^+ bombardment in the present work, but this may be a consequence of the ion angle of incidence. Interpretation of this effect is described in the literature as being a result of preferential loss of P during the sputtering process with the excess In coelescing to form islands of metallic In (Farrow et al, 1978). Skinner et al (1983) have performed energy-dispersive x-ray (EDX) analysis of the islands and found In and P in the same ratio as that in the bulk of the sample and that the surface composition was found by Auger analysis to be approximately 65% In, 35% P. Indeed, EDX analysis was performed in this present study on the mass of cones in Figure 5.27 and no differences in elemental composition were detected between these and the sample bulk.

The conclusion arrived at for this effect is that with the simultaneous action of the In forming islands and the depletion of P, a necessary condition is formed whereby the In islands act as nuclei for the familiar InP cone formation (Williams et al, 1980; Auciello, 1981). Skinner et al (1983) based these assumptions on experiments that were carried out with the sample cooled to -183°C, where with an even greater loss of P (70% In, 30% P) there were no features observed. This condition persisted even when the sample returned to room temperature, which would indicate that the surface mobility of the In depends on radiation enhanced diffusion as well as a contribution towards the activation energy at higher temperatures, in accordance with other studies (Kaufman and Robinson, 1979; Rossnagel and Robinson, 1982).

One other important aspect of this cone development to note is that the cone height is always below the unsputtered surface level indicating that initial surface contamination is not responsible for the morphological growth. The formation and subsequent development would therefore be as a result of the intrinsic behaviour of the surface during ion bombardment.

5.5.3 Discussion

The experiments described here have illustrated the development of ion-induced morphology on Si(100), GaAs(100) and InP(100) surfaces following O_2^+ and Cs^+ bombardment for various ion energies and angles of incidence. A further aim has been to assess whether the results could significantly affect the resolution of depth profiling studies, particularly in SIMS. Furthermore, by comparing these studies with

those already performed using noble gases as the primary bombarding species, qualitative comparisons can be made thus differentiating between purely physical sputtering, and sputtering with an active gas.

5.5.3.1 Oxygen Ion Bombardment

In general, the morphology observed to occur on all three semiconductor materials following O_2^+ bombardment is a stepped and regularly faceted structure. In each case the pitch and magnitude of the morphological features increase with ion dose, and hence depth erosion. Much of the previous work performed on semiconductors has mainly involved inert gas sputtering of the surfaces, and more particularly on silicon. Nelson and Mazey (1973) discussed the surface damage and topography changes produced during sputtering and generalised, from the features they observed, on the physical processes that might be associated with ion sputtering. In particular they illustrated, by SEM, the growth of surface topography on Si following Xe^+ bombardment at an angle of 45^0 the result of which is very similar to the structure shown in Figs 5.11-5.13.They tentatively suggested that the structure was associated with regions of segregated impurity within the silicon, which steadily becomes exposed as the surface is eroded. Also as amorphization of the surface took place, the density at the surface was reduced causing a strain effect which may have been significant although the authors freely admitted that these were only vague suggestions.

The physical appearance of the structures observed in Figs. 5.15 and 5.16 hold particular significance to work performed by

Mazey et al (1968) who examined thin, polycrystalline copper foils using Transmission electron microscopy, following 50 to 80KeV Xe^+, Cu^+ and Pb^+ ion bombardment. They observed that during the ion bombardment a network of dislocations was generated from the agglomeration of point defects, and that they interacted to line-up in a particular crystallographic direction. Furthermore, the perdiodicity was somewhat similar to the sputtering structure which eventually developed. Mazey et al (1968) further suggested that due to modifications in strain induced reduction of the surface binding energy in the viscinity of a dislocation, the sputtering yield could be correspondingly increased and hence small furrows could easily form. These furrows could then act as nucleation sites for the structure seen in Figs 5.15,5.16 , which have also been observed in a similar form elsewhere (Stewart and Thompson, 1969).

There is, however, a discrepancy in discrete differences in the observed structures on Si(111) and Si(100). Generally the observed features were sharp and well-defined ridges and furrows (Fig. 5.15) for Si(100), however, Fig. 5.16 illustrates the furrows having a similar appearance to those observed on Si(111). It can therefore only tentatively be suggested here that although the processes for each furrow type are essentially the same, the smoother structures may have been the result of a small amount of surface diffusion due to local heating, thereby smoothing the more characteristic stepped structure (Mazey et al, 1968). Nevertheless, these smoother furrow features have an almost regular periodicity of $\sim$ 10,000Å, which is consistent with other observations (Carter et al, 1977), and thus represent the initial stages in the full development process.

There is, at present, very little work published on the development of surface topography by active ion sputtering, and more particularly on semiconductors. Tsumoyama et al (1974, 1976) have performed Ar^+, N_2^+ and O_2^+ sputtering of metals, and some semiconductors (Tsumoyama, 1980). The etch patterns produced were classified according to the binding energy of mono-oxide B_{mo} of the target atom M and an oxygen atom, and that generally the surface became smooth as the binding energy increased. For example, the relatively high binding energies of Si and Ge with oxygen were 8.3eV and 6.8eV respectively and the post bombarded surfaces of these materials were smooth. They further found that the calculated sputtered atom yields plotted as a function of atomic number gave a periodicity similar to the 'd' shell pattern discovered by Laegreid (1961) and Rosenburg (1962) for noble gas ion bombardment. The conclusion from their study indicated that although the chemical affinity of target materials for the oxygen atoms alters the sputtered surface, the sputtered atom yield is primarily dependent on physical atomic collision.

Whether the conclusions of Tsumoyama et al (1980) can be applied directly to the present work is a matter for further study, since a variation in ion energies and ion incident angles were used. One aspect, however, is apparent by observation, that the topography developed by O_2^+ ion bombardment and Ar^+ ion bombarded (Mazey and Nelson, 1968; Carter et al, 1977) are extremely similar, strongly suggesting that the process is purely physical, and there is no dependence on the chemically active nature of the bombarding O_2^+ atoms. However, as noted by several authors, the mechanism by which oxygen affects the substrate is complex, and a need for more rigorous interpretation of

data is required (Tsumoyama et al, 1980; Wach and Wittmaack, 1981; Okajuma, 1981). For example, experiments performed by Cantagrel and Marchal (1973) have shown that the etching rates of some metals (including Si) and oxides under Ar^+ ion bombardment can be controlled by introducing a partial pressure of O_2^+. This controllable region is limited to a specific range of partial pressures of O_2^+ and is discrete for each element, where it was observed that the sputtering yield was reduced for an increased partial pressure of oxygen. The explanation of this effect, suggested by the authors was that the O_2^+ is chemisorbed onto the surface and sputtered as a normal oxide, where a variation in sputtering yield due to saturated, or doped layers of O_2^+ can be realised.

The concept of an amorphous layer developing during ion bombardment of semiconductors has been widely adopted (Wilson, 1973; Carter and Webb, 1979), as a result of irradiation damage produced as the energetic projectile comes to rest. Inert gas ions will penetrate the crystal lattice and create local dilute regions of point defects and dislocations, and for this reason it has been assumed that semiconductors will sputter uniformly due to the destruction of crystallinity in the near surface. This has clearly been shown otherwise (Mazey and Nelson, 1968; Carter et al, 1977) and the results presented here indicate that beyond specific ion doses (or depths) for each material, either some crystallinity is retained or the observed features are a direct result of ion bombardment in the form of dislocations and structural damage. Although there is a close similarity in features developed by Ar^+ and O_2^+ ion bombardment on silicon, careful interpretation of all the experimental parameters must be made, and apparent minor

discrepancies in comparisons approached with caution. For example, Okajima (1981) reported that single crystal Si(111) sputtered $\sim$ 5 times faster under Ar^+ bombardment in comparison to O_2^+ bombardment. Furthermore, it was suggested that the sputtering of pure materials following O_2^+ bombardment is attended by oxidation with reactive ions during the atomic collision processes.

The observations of Okajima (1981) would indicate that experiments illustrating the development of ion-induced surface topography should display not only the usual experimental parameters (i.e., ion energy, ion incident angle etc.), but also the specific ion dose and the depth of the topography resulting from bombardment. The results presented in this work are purely observatory and indicate the depth of erosion and at which stage in the process a particular surface feature has developed. Although a specific total ion dose was kept to within 2% of its normal value, variations in crater depth of $\sim$ 50% were sometimes observed, usually due to a non-uniform raster of the ion beam resulting in some badly formed craters. Therefore the depths of erosion shown in the results should not be interpreted as the absolute yield of the materials, but only as an indication of the depths at which the illustrated features develop. Furthermore, it has been reported that heavily faceted surfaces exhibit accelerated sputtering yields compared to smooth surfaces due to an enhanced effective projectile incidence angle (Elich et al, 1971; Roth et al, 1977; Rödelsperger and Scharmann, 1976; Littmark and Hofer, 1978). Ultimately, this effect will be limited by the incident ion beam angle and energy, and the formation of densely populated structures having a large peak-to-valley ratio (i.e., cones, pyramids etc.) where the probability of

secondary particle recapture is high (Blank and Wittmaack, 1977; Auciello, 1982).

One of the most outstanding features observed on all three semiconductors was the occurrence of pits, developing during the ion bombardment process. This effect is more noticeable on Si and InP following irradiation at relatively high ion energies (15KeV), where the surface is generally featureless but with the occasional etch pit. It is evident from Fig 5.13that the occurrence of etch pits inevitably leads to their grouping and subsequent overlapping, after high irradiation fluences to form the well-developed characteristic faceted structure seen in Fig 5.11. The phenomenon of these etch pits has been observed under similar experimental conditions with Ar^+ bombardment by other workers. From the observations of Carter et al (1977) and Lewis et al (1982) it would appear that the macroscopic development of these well-characterised features is independent of ion energy, but shows a correlation with ion angle. Thus at an incident ion angle of 50° a stepped faceted structure is observed, whereas for an angle of 30° to a similar ion dose only pits are observed.

It became evident during the course of many experiments that the surfaces developing singular pits and remaining relatively texture-free (Figs 5.13(a-d), 5.14) tended to erode more slowly than the surfaces exhibiting continuous faceting (Fig 5.11, 5.22). It is well known that the sputtering yield is a sensitive function of ion incidence angle (Bach, 1970; Vossen, 1979) and therefore it is expected that the observed eroded depth differences of surfaces possessing either pits or continuous faceting would be due to the discrete change in angle with ion energy. However, the implications of anomalous effects occurring

in sputtering yields due to textured surfaces suggest other mechanisms. For example, large pits observed on Si(100) following 10.5KeV O_2^+ bombardment at an angle of $\sim 38^0$ (Figs 5.13) were not observed following 5.5KeV O_2^+ bombardment at $\sim 47^0$, and to the same ion dose.

The difference in the eroded depths is 3.8μm where in the latter case it was 9.2μm, which is approximately 2μm greater than would be expected from purely angle of incidence effect. A complex situation arises in predicting which experimental parameter has the most significant effect on topography development. Depending on the structure of the sputtered surface local elements will present different angles of incidence to the incoming ion beam. It is conceivable that by parametric averaging a completely faceted surface could have an enhanced differential sputtering yield compared to a relatively featureless surface. Quite clearly, the initial formation and subsequent growth of various surface topographies will implicitly affect the sputtering yields.

It follows from the above discussion that the nature of the topography produced in the early stages of ion bombardment will determine the final stable form of the surface. If the mechanism of formation is by irradiation induced defects then it is expected that the incident ion energy would play a significant role. Certainly, in the range used for these present experiments there would be no significant effect on the sputtering yield (Sigmund, 1969), but the initial damage condition may be enhanced by combinations of the ion energy and its angle of incidence where channelling effects could play an integral part in contributing towards a lesser, or more deeply damaged region.

In comparison to previous studies performed with Ar^+ bombardment the nature of the morphology formed on Si(100), GaAs(100) and InP(100) by O_2^+ bombardment is consistent with purely physical sputtering, although no indication can be given here as to whether there was chemical interaction between the O_2^+ and the substrate atoms. ESCA studies have shown that an oxide layer is formed in the early stages of ion bombardment, the total depth of which is ~~possibly~~ impact angle dependent for single crystal materials. The mechanism by which the oxygen moderates the inhomogeneity of the surface structure is complex and needs more investigation.

5.5.3.2 Caesium Ion Bombardment

In contrast to O_2^+ bombardment, the results presented here illustrate that Cs^+ bombardment produces an overall smoother surface on Si(100) and GaAs(100) both at comparable doses and more particularly at comparable depths. The surfaces of Si(100) were observed to be smooth and featureless even after total ion doses of 10^{20} ions cm^{-2}, corresponding to an eroded depth of 40μm. The ripple topography evident in Fig 5.21 on GaAs(100) is first observed at a dose of 10^{20} ions cm^{-2} which corresponds to an eroded depth of 82μm, and it is fully expected that further erosion of this surface will produce the stepped faceted structure in Fig 5.18 and 5.19.

The occurrence of cone development on InP(100) surfaces is in complete contrast to all other morphologies observed here. However, it is consistent with work performed by other workers using inert gas ion bombardment (Williams et al, 1980; Skinner et al, 1983) which would indicate that purely physical processes were responsible for the

observed topography. However, implantation of the primary ions into the target may influence the chemical state of the surface (Tsumoyama et al, 1980) where binding energies between substrate and bombarding atoms would modify activation energies. During bombardment an amorphous layer will develop (Wilson, 1973) and reach a supersaturated level where steady state conditions govern the rate of implantation and sputtering yield. The depth of the amorphous layer formed and its chemical and physical qualities will be based on a complex dependence of primary ion mass, and charge state, and will be responsible for the differences in etch rates.

In general, the etch rate of the three semiconductors used in this work was enhanced by a factor of five under caesium ion bombardment corresponding to similar ion doses following oxygen bombardment. Quite clearly, since the mass ratio of Cs/O_2 is ~ 3 the sputtering yield of the materials is not totally dependent on ion mass.

5.5.4 The Development of Ion Sputter Topography of Cu(11 3 1)

The vast amount of work reporting on the development of surface morphological features under ion erosion, has in the past predominantly included pure, single crystal, and polycrystalline copper as a main source of observation (Mazey and Nelson, 1968; Wehner and Hajicek, 1971; Berg and Kominiak, 1976; Naundorf and Macht, 1980; Rossnagel and Robinson, 1981). However, in spite of the large amount of work done with this material, not until recently have systematic studies been undertaken on the evolution of morphology with increasing dose, surface preparation, and subsequent time dependent erosion of the observed features (Grosdover et al, 1976; Whitton et al, 1977; Auciello et al,

1979, 1980). The various mechanisms by which the various topographical features can originate are described at the beginning of this chapter. This study seeks to examine the topography formed on Cu (11 3 1) by O_2^+ and Cs^+ bombardment.

5.5.4.1 Experimental Conditions

A Cu(11 3 1) single crystal target carefully prepared using mechanical lapping and chemical etching techniques (Carter et al, 1981), was mounted in a Cameca ims 3f microanalyser for subsequent O_2^+ and Cs^+ ion bombardment. Examination of the polished surface of the target prior to bombardment revealed little evidence of surface damage (e.g. scratches) or surface contaminants. However, post bombardment observations suggested that surface defects had initially existed by some of the distinguishing characteristic features observed, such as parasitic rows of faceted features forming on ion etched scratch marks.

The following descriptions represent the surface of (11 3 1) copper following 5.5KeV O_2^+ and Cs^+ ion bombardment at various energies and angles of incidence, the latter being dependent on the retarding electric field at the sample (see Fig 5.9) for one particular energy.

5.5.4.2 5.5KeV Oxygen Ion Bombardment

The initial irradiation parameter specifications required that the ions had a source energy of 10KeV, which on impact with the sample surface was reduced to 5.5KeV due to a +4.5KV retarding electric field. For these particular conditions the ion incident angle was $\sim 47^{o}$, and Fig 5.29 illustrates the subsequent development of surface features

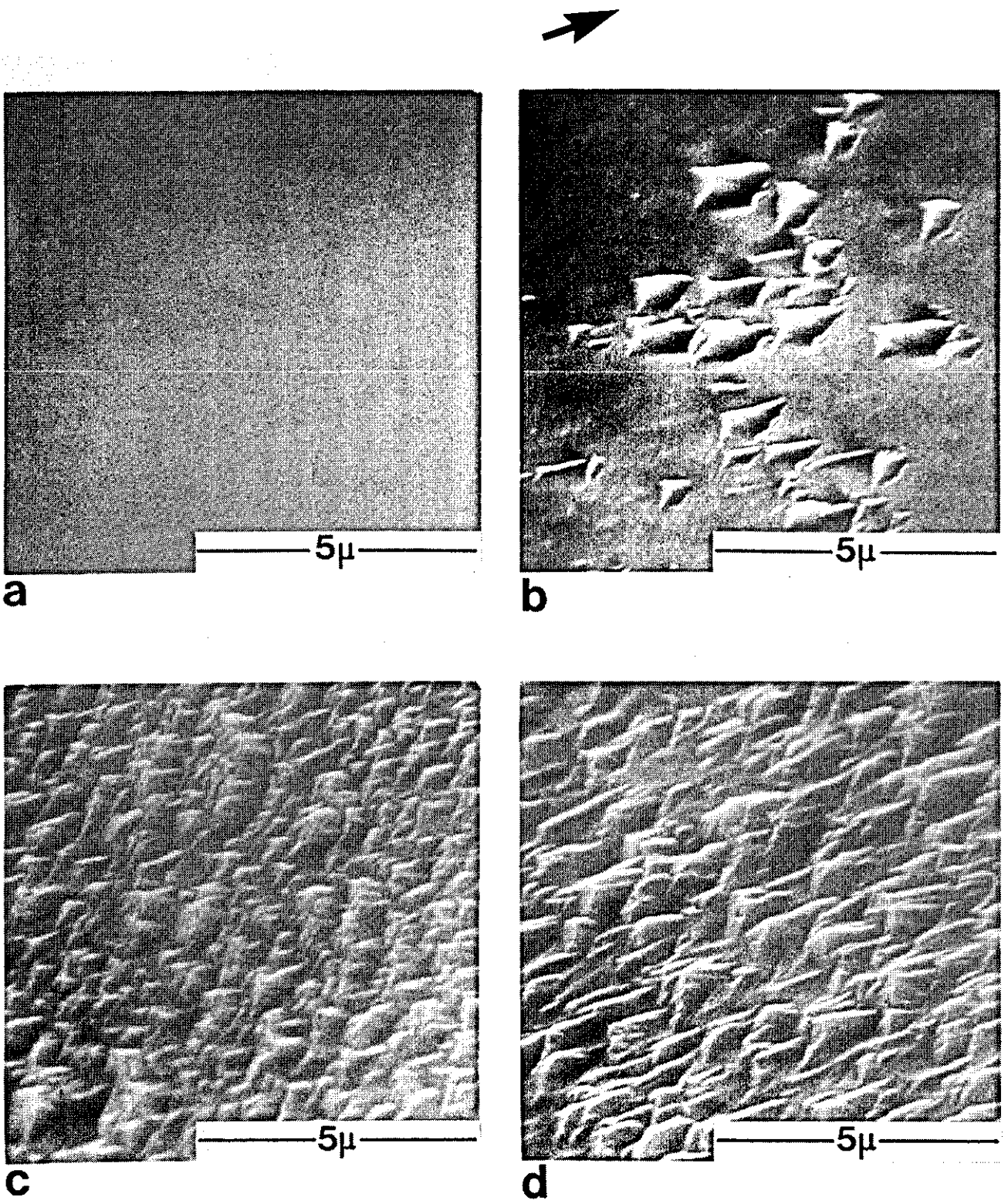

Figure 5.29: The development of surface topography on Cu(11 3 1) following 5.5keV O_2^+ bombardment to a depth of:

(a) 1.1μm (2 x 10^{19}ions cm^{-2})

(b) 3.2μm (6 x 10^{19}ions cm^{-2})

(c) 5.5μm (10^{20}ions cm^{-2})

(d) 11.1μm (2 x 10^{20}ions cm^{-2})

on Cu(11 3 1) as a function of increasing ion fluence. Careful observation of Figure 5.29 reveals the existence of minute ripples propagating across the central bombarded area of the crater, and the absence of surface contamination at this stage is clear. Following a total dose of 6 x 10^{19} ions cm^{-2} (Fig. 5.29), well-defined faceted, and elongated ridge structures develop randomly, but in clusters on the surface, and the evidence of underlying ripple trains is more prominent. After higher doses of 10^{20} ions cm^{-2} and 2 x 10^{20} ions cm^{-2} the faceted protrusions tend to dominate the surface, and it is interesting to note that the absolute size of these structures does not increase with increasing dose. Moreover, their general shape tends to adopt a more elongated appearance, where a faceted side facing the incident ion wind protects a trailing ridge.

The retention of physical size with increasing ion dose of these faceted features suggests that they are largely stable under ion erosion, or certainly within the range of ion fluence used here. Panoramic views of the surface following high dose irradiation ($\geqslant 10^{20}$ ions cm^{-2}) indicated that generally prolonged ion bombardment modified the macroscopic surface such that as the density of individual features increased the surface appeared to be composed of stepped facet trains similar in appearance to those observed on silicon (see Fig 5.11). The mechanisms operating under the present conditions are extremely complex and would be difficult to explain from the observations made here. However, following previous experimentation on semiconductors the observations presented here for (11 3 1) copper are consistent with the suggested mechanisms of ion erosion. For example, it is evident from Figure 5.30 that the ridged structure possesses an opposing face to the ion beam,

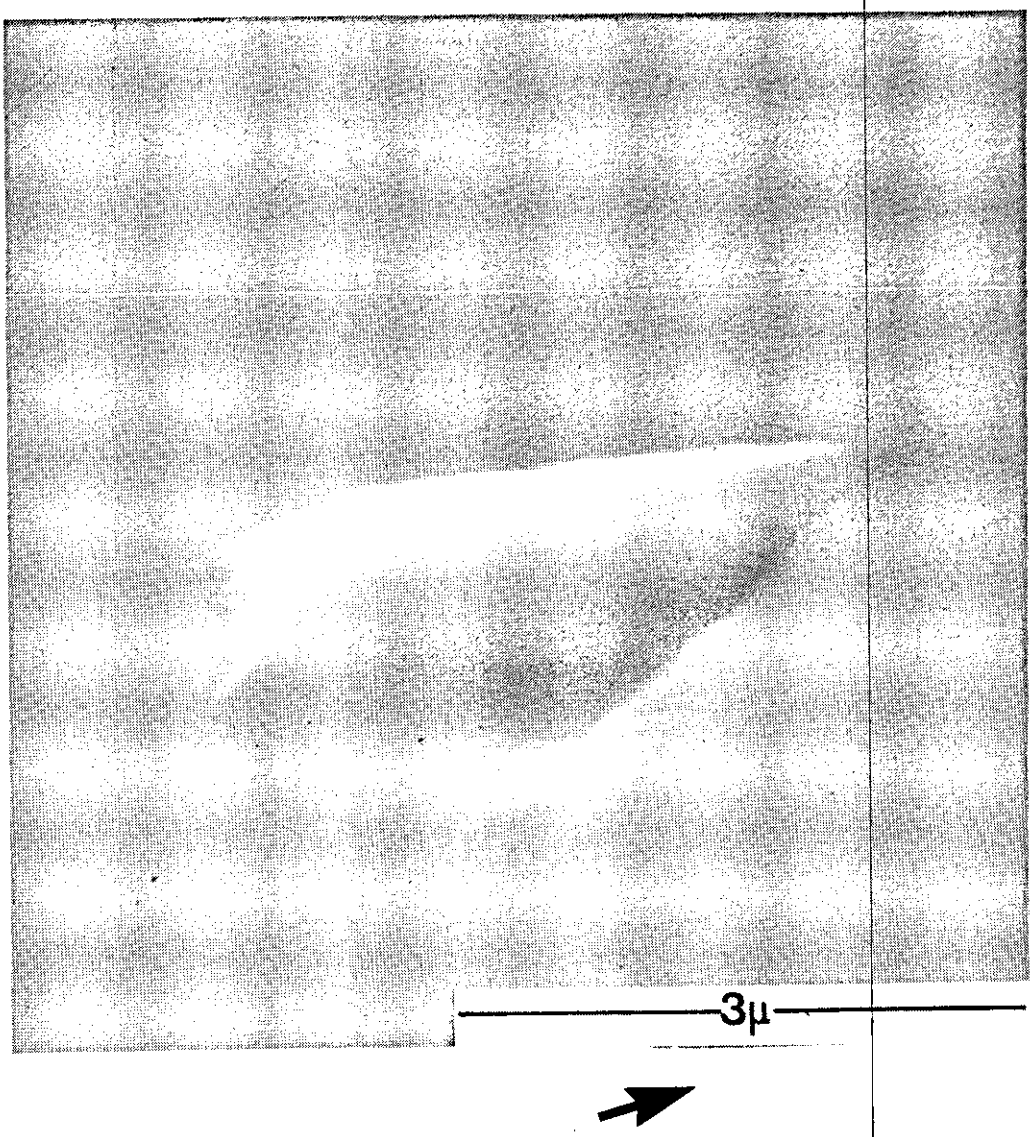

Figure 5.30: A micrograph showing a single structure developed after 5.5keV O_2^+ bombardment of Cu(11 3 1) which comprises the dense array of similar structures shown in Figure 5.29. The eroded depth is 1.1μm (2×10^{19}ions cm^{-2}).

which effectively acts as a protection against complete erosion of the structure, thereby creating the trailing ridge. Striations occurring along the sides of the trailing ridge, and the prominent pedal depressions associated with it are ample evidence for ion reflection, and clearly indicate the incident ion direction. Furthermore, the underlying ripple structure running perpendicular to the faceted protrusion reinforces the belief that the development of the morphology is dependent upon incident ion beam direction, and is consistent with the observations made on ion bombarded semiconductors. Generally, careful examinations of the well-developed ion bombarded surfaces revealed that the topography was composed of dense populations of structures similar to that shown in Fig. 5.30. This particular aspect of the eroding surface is largely consistent with the earlier observations of topography on the semiconductor materials. During the relatively early stages of ion bombardment, when topography is first observed, it is generally true that a characteristic feature is predominant, and prior to extended ion bombardment occurs only in small densities on the surface. However, as the ion dose is increased these primary features totally dominate the surface to form a characteristic macroscopic structure composed of larger densities and overlap of the primary structure.

5.5.4.3 5.5KeV Caesium Ion Bombardment

The micrographs illustrated in Fig 5.31 represent the surface of Cu(11 3 1) following 5.5KeV Cs^+ ion bombardment over a dose range of $5 \times 10^{18} - 10^{20}$ ions cm^{-2}. In contrast to O_2^+ ion bombardment

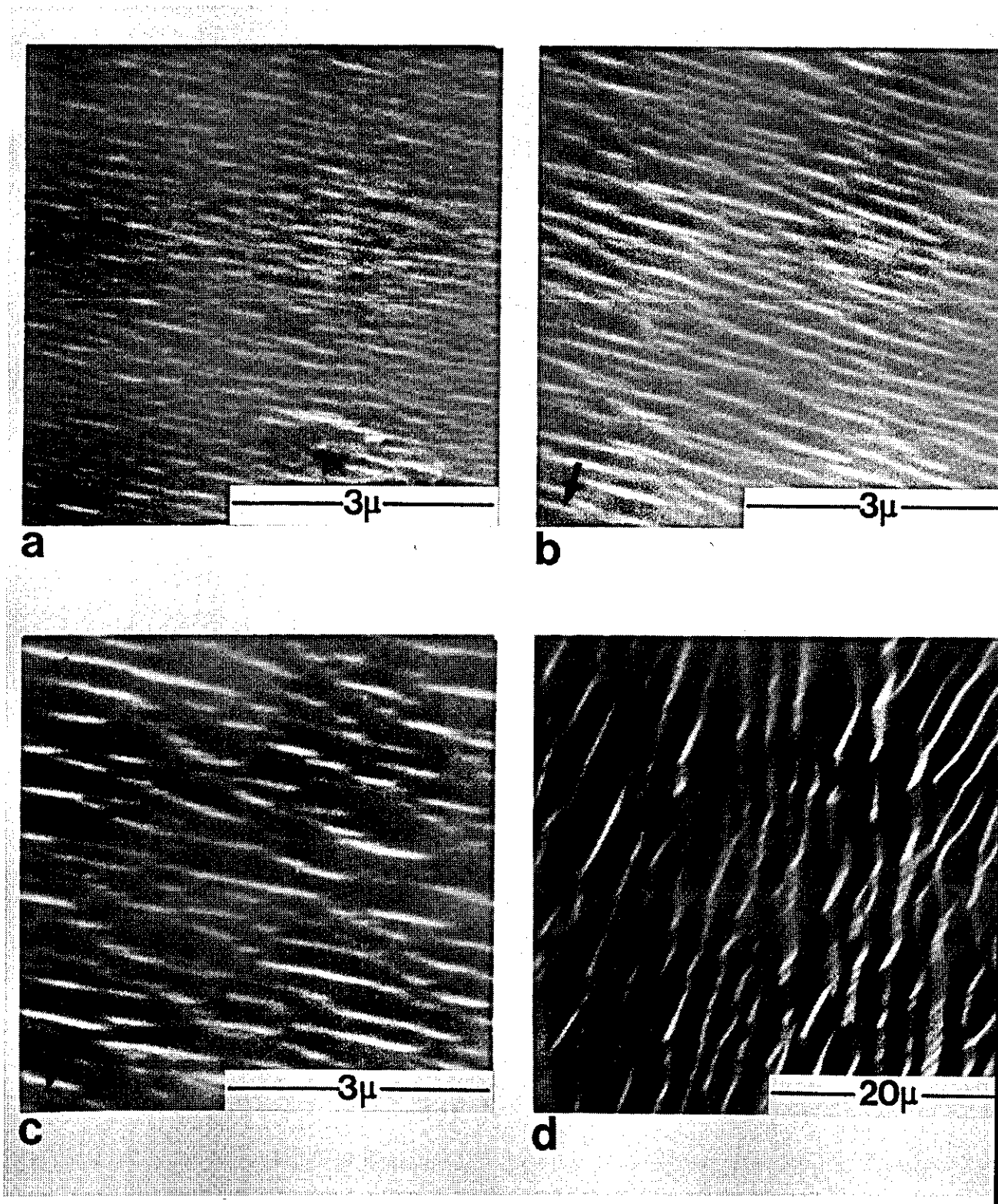

Figure 5.31: A sequence of micrographs illustrating the change in surface topography on Cu(11 3 1) following 5.5keV Cs^+ bombardment. The eroded depths are:

(a) 1.2μm (5 x 10^{18}ions cm^{-2})

(b) 5.4μm (10^{19}ions cm^{-2})

(c) 10.5μm (2 x 10^{19}ions cm^{-2})

(d) 16μm (10^{20}ions cm^{-2})

the topography produced by Cs^+ bombardment is a more well-defined faceted structure which exists as a series of stepped ripple trains, very similar in nature to the ion eroded surfaces of the semiconductors following O_2^+ bombardment. Also, consistent with erosion theory and all previous observations, the ripple increases in magnitude, both in the vertical and horizontal directions. Fig 5.31(d) is a micrograph of the copper surface following a total ion fluence of 10^{20} ions cm^{-2}, and viewed perpendicular to the incident ion beam directions. It should be noted that due to the faster etching rate with Cs^+ it appears there is some discrepancy in the correlation between total ion dose and depth of erosion. This may have been a result of areas of the sample surface having either enhanced or reduced sputtering rates depending on the nature and density of the topography formed. The recorded depths indicate the deepest eroded point in any one particular crater.

5.5.4.4 Discussion

The lack of sharp features such as cones and pyramids on the copper surface following O_2^+ and Cs^+ ion bombardment strongly suggests that mechanisms other than surface contamination are operating to produce the observed effects. It is arguable, however, that the individual features illustrated in Fig 5.29, 5.30 possess pyramidal qualities due to their faceted faces meeting at a point or forming a ridge. Even if this were true it has previously been suggested that the formation of dense arrays of cones and pyramids on Ar^+ bombarded Cu(11 3 1), (Whitton et al, 1978) are associated only with major defect elaboration and periodic discontinuation on the crystal surface,

and are not a result of surface protection by contaminant species. Under the present circumstances this latter effect does seem unlikely following careful preparation of the pre-ion bombarded surface and the UHV conditons employed during sputtering.

The topographies produced by O_2^+ and Cs^+ ion bombardment are clearly different in their overall structure, as illustrated in Figs 5.29, 5.31. Quantitatively, the measured depths of the ion eroded craters indicate that the erosion rate for Cs^+ is $\sim$ 3 times faster than for O_2^+ bombardment. Also, the initially observable features that are predominant in the early stages of development are significantly different for the two bombarding gas species used, which may imply that a chemical dependence is in evidence on the structure of the morphology formed. However, although singley faceted protrusions develop during the early stages under O_2^+ bombardment there is evidence of a small scale ripple structure underlying these larger, more predominant features (Figure 5.29). These tend to dominate most of the development process and continue to cover the surface, where at high doses (10^{20} ions cm^{-2}, Figure 5.29) their density is such that the macroscopic appearance resembles the faceted ripple trains seen following Cs^+ bombardment although slightly more segmented in nature. A dilemma occurs here, since in many respects the topographies developed by O_2^+ and Cs^+ on Cu(11 3 1) are characteristic of one another macroscopically, but are generally, quantitatively different on a smaller scale. Furthermore, similar effects to these have previously been observed by Lewis et al (1982) for 9KeV Ar^+, Ne^+, N^+, O^+ and Xe^+ at 45^0 incidence angle, which effectively eliminates

the possibility that a chemical effect, due to the reactive nature of the ions used here, is responsible for the observed effects. Nevertheless, it is conceivable that the initial stages of topography development are influenced mainly by the extent of the amorphous region governed by the ion mass, and a chemical effect. After prolonged ion bombardment macroscopic effects such as ion incidence angle and surface stress* may tend to dominate and the morphologies produced by two different bombarding gas species will physically become more characteristic of each other.

5.5.5 Conclusions

The nature of the morphologies produced by prolonged O_2^+ and Cs^+ bombardment are of a similar type to those observed in inert gas sputtering, and would indicate that its development is independent of gas species. However, quantitative aspects regarding the etch rates, sputtering yield and size of the topography at various eroded depths could give some insight into the necessary conditions initiating the growth of ion induced features, where the reactive element of O_2^+ and Cs^+ may play an important role. Therefore it is essential that the mechanisms occurring immediately implantation of the bombarding ion takes place are understood in order that a quantitative assessment of the growth of morphology can be realised.

The results presented here indicate that the ion induced surface features could potentially lead to poor depth resolution in SIMS depth profiles of important semiconductor materials (Williams et al, 1980). However, the use of reactive species such as O_2^+ and Cs^+ tends

*Surface stress is produced by the expansion of the lattice due to implantation.

to produce more uniform surface erosion than those reported for argon ion bombardment (Tsumoyama et al, 1974; Katzchner et al, 1984). Indeed, the high etch rate and smooth featureless surfaces produced by Cs^+ bombardment (on Si and GaAs in particular) could provide a useful combination for depth profiling to large depths (> 10μm) in a regime where angle lapping (Lea and Seah, 1981) and ball-cratering (Brown et al, 1981) techniques are normally employed. This would inevitably depend on the behaviour of polycrystalline surfaces under caesium ion bombardment. Generally, the formation of surface topography should not seriously impair the depth resolution of SIMS depth profiles over the depths usually associated with ion implants (< 2μm), although the present work has been performed exclusively with unprocessed material.

The experimental results presented here have provided extra data, albeit qualitative, towards understanding the influence that specific irradiation parameters have on the nature of ion-induced topographies. The provision of well-defined experimental conditions and subsequent observations, enables analogies to be drawn, and comparisons to be made from other areas of work. For example, it is evident from the literature that the formation of the ripple-faceted structures observed on all the semiconductor materials here following O_2^+ bombardment has frequently occurred on a variety of materials (Stewart and Thompson, 1969; Littmark and Hofer, 1978; Elich et al, 1971; Carter et al, 1977). Further, similar structures have been observed by the present author on mechanically polished polycrystalline aluminium following O_2^+ bombardment, and elsewhere even on lunar crystal (Zinner, 1980). Indeed, formations of similar nature in

geomorphological erosion (Navez et al, 1962) and wet chemical etching of surfaces (Tuck and Baker, 1973) present some interesting parallels.

Finally, although the observations in this work present only an imformative and qualitative assessment of ion-induced topography following O_2^+ and Cs^+ bombardment it is hoped that they provide a good database for further, and more detailed material studies. The modification of the surface by an amorphous layer developed during the early stages of ion bombardment may be responsible for the similar topographies seen on many different materials. Examinations of these ion-surface interactions occurring on the microscopic scale should adopt techniques whereby in situ sputtering and STEM (Scanning Transmission Electron Microscopy) can be performed to evaluate the effect of individual processes.

An outstanding feature particularly noticeable in the early stages of topography development on silicon and gallium arsenide was the fine ripple structure which persisted throughout the development process. Furthermore, the stable form of the topography observed at high doses ($> 10^{20}$ ions cm^{-2}) appeared to result from an overlapping and aglomeration of etch pits formed at lower doses ($\sim 10^{19}$ ions cm^{-2}). The increasing frequency of these features with ion dose would lead to two possible explanations, assuming purely physical mechanisms operate: (i) that the layers of material exposed to irradiation were previously stressed and possessed intrinsic defects (ii) that during irradiation ion-induced defects formed in the near surface were subsequently preferentially eroded during the bombardment process. Although both these explanations are possible causes for the observed features the latter would seem more probable since from the many

experiments performed on separate samples the same trends were evident. In all cases the topography of individual features within a crater was of the same characteristic structure as its neighbours, and the number of which increased in frequency during extended irradiation. If the features were formed purely by intrinsic defects it would be expected that a variety of structures would be observed.

CHAPTER 6

Surface Roughness during Ion Etching: A Theoretical Analysis

6.1 The Development of Surface Shape

It has been well established over many years of experimental observation that during ion etching of solids certain well-defined structures such as cones and pits can be formed. (Wehner and Hajicek 1971, Wilson 1973, Lewis et al 1981). The implications of the development of these features have been discussed in the previous sections. However, there was a period of 27 years before any workers attempted to relate aspects of surface topography development to theoretical interpretation.

In a paper by Stewart and Thompson (1969) cones were observed to form on tin and silicon crystals following 5keV Ar^+ bombardment and were attributed to surface contamination. Their theoretical description of this process involved a study of the intersection between two plane surfaces during ion erosion. By formulating equations describing the sideways movement of the intersection they were able to predict its movement and position during erosion of the surface. The method provided a qualitative explanation for 'edge' formation in two dimensions, and also indicated a strong dependence of surface erosion on the sputtering yield as a function of angle $S(\theta)$. However, their model did not account for secondary and tertiary effects such as surface diffusion, redeposition of sputtered material, the constantly changing gradient of the eroded surface or ion reflection.

Nobes et al (1969) have studied the motion of individual points on a general two dimensional surface, and since this theory has found useful applicability it will be described here.

Consider Figure 6.1 which shows the basic geometry and evolution of a surface contour. AB represents a surface profile of length ΔZ bombarded in the negative y direction by a uniform flux of ϕ ions per unit area. In a time δt let the surface erode a depth δr, in a direction perpendicular to the surface. Therefore the velocity of a surface point along the normal to surface at that point is (Carter et al 1971)

$$\frac{\partial r}{\partial t} = - \frac{\phi}{N} S(\psi) \cos\psi \qquad (6.1)$$

where N is the atomic density,

ψ is the angle subtended by the surface normal and the direction of the ion flux.

Note that if the angle subtended at A is θ, then the equivalent angle at B is $(\theta + \delta\theta/\delta x.\delta x)$, and using equation (6.1) the distance AA' and BB' may be calculated,

$$AA' = \frac{\phi}{N} S(\theta) \cos\theta \, \delta t$$

$$BB' = \frac{\phi}{N} S(\theta + \frac{\partial\theta}{\partial x} \delta x) \cos (\theta + \frac{\partial\theta}{\partial x} \delta x) \, \delta t \qquad (6.2)$$

If A'C is drawn parallel to AB, then an expansion to a first order using Taylor's Theorem gives:

$$CB' = BB' - AA' = \frac{\phi}{N} \frac{d}{d\theta} \left[S(\theta) \cos\theta \right] \frac{\partial\theta}{\partial x} \delta x \, \delta t$$

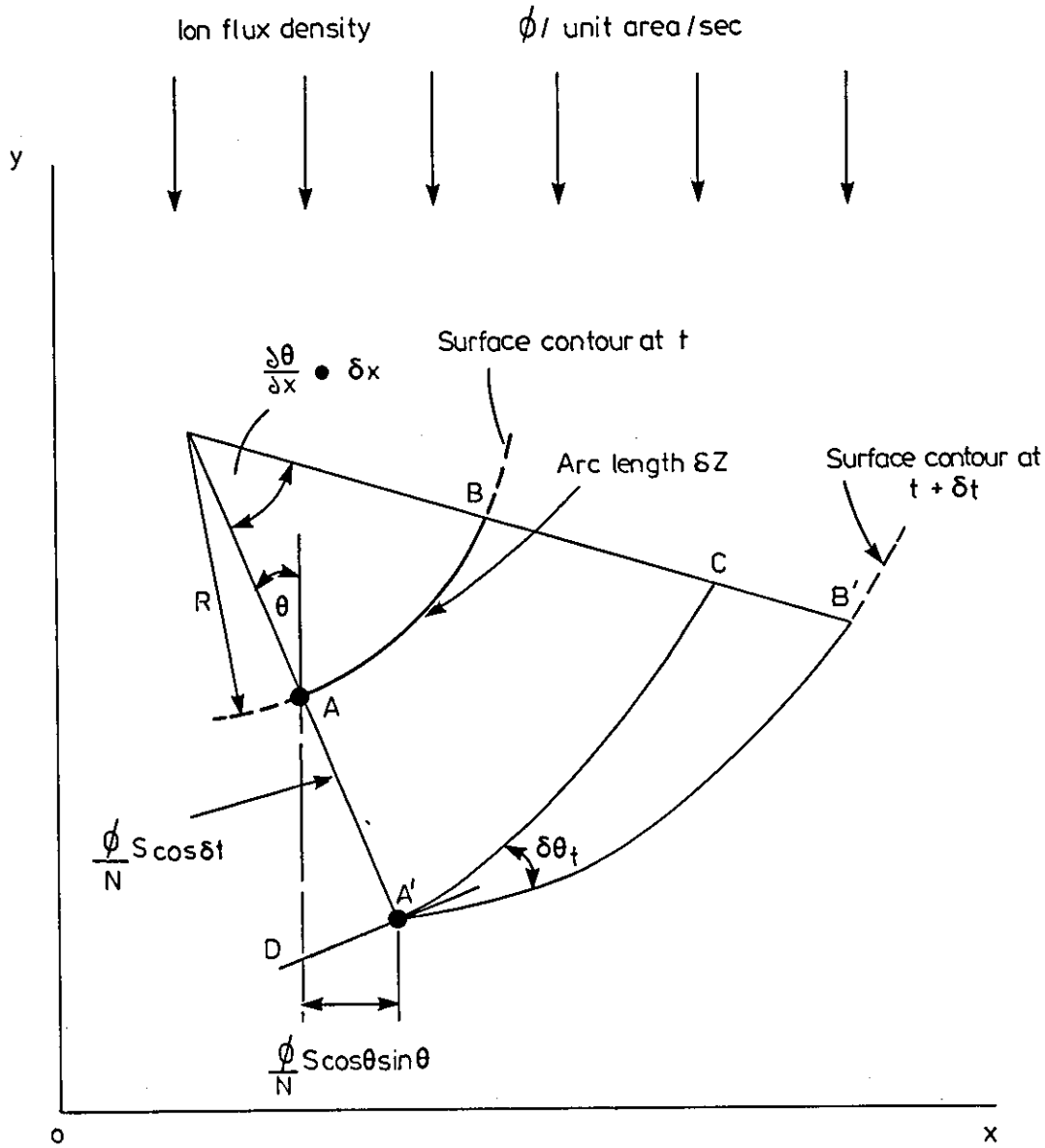

Figure 6.1: Erosion of a surface generator by an ion flux (after Carter et al (1971)).

and

$$A'C = \frac{R\partial\theta}{\partial x}\,\delta x$$

The rate of change of tangential angle in the direction of the surface normal can be expressed as:

$$\frac{\partial\,\theta_t}{\partial t} = -\frac{\phi}{NR}\,\frac{d}{d\theta}\left[\,S(\theta)\,\cos\theta\,\right] \qquad (6.3)$$

where $\delta\theta_t$ is the change in tangential angle from A to A' in time δt.

If θ is now considered to be a function of only x and time t then the rate of change of θ in any direction is:

$$\delta\theta = \left(\frac{\partial\theta}{\partial x}\right)_t \delta x + \left(\frac{\partial\theta}{\partial t}\right)_x \delta t$$

$$\frac{\delta\theta}{\delta t} = \left(\frac{\partial\theta}{\partial x}\right)_t \frac{\delta x}{\delta t} + \left(\frac{\partial\theta}{\partial t}\right)_x$$

If this direction is chosen to be a normal direction then using equation (6.3) gives:

$$\frac{\phi}{NR}\,\frac{d}{d\theta}\left[S(\theta)\,\cos\theta\right] = \left(\frac{\partial\theta}{\partial x}\right)_t \left(\frac{\partial x}{\partial t}\right)_n + \left(\frac{\partial\theta}{\partial t}\right)_x$$

The rate of change in the x co-ordinate of the point A from equation (6.1) is $\frac{\phi}{N}$ S $\cos\theta$ $\sin\theta$ and since

$$\left(\frac{\partial\theta}{\partial x}\right)_t = \frac{1}{R\cos\theta}$$

it can be shown that:

$$\left(\frac{\partial\theta}{\partial t}\right)_x = \left(\frac{\partial x}{\partial t}\right)_\theta = -\left[\frac{\phi}{N}\cos^2\theta\,\frac{dS}{d\theta}\left(\frac{\partial\theta}{\partial x}\right)_t\right] \qquad (6.4)$$

Alternatively if θ is a function of only y and time then:

$$\frac{\delta\theta}{\delta t} = \left(\frac{\partial\theta}{\partial y}\right)_t \frac{\delta y}{\delta t} + \left(\frac{\partial\theta}{\partial t}\right)_y$$

where

$$\left(\frac{\partial\theta}{\partial y}\right)_t = -\frac{1}{R\sin\theta}$$

and hence

$$\left(\frac{\partial\theta}{\partial t}\right)_y = \left(\frac{\partial y}{\delta t}\right)_\theta = -\frac{\phi}{N}\left[\sin\theta\cos\theta\frac{dS}{d\theta} - S\right]\left(\frac{\partial\theta}{\partial y}\right)_t \qquad (6.5)$$

Carter et al (1971) recognised equations (6.4) and (6.5) as a wave motion defining variations of θ with x and y as a function of time. Prompted by the work of Barber et al (1973), they associated this with earlier complementary theories of topograhic development. Barber et al (1973) applied two kinematic theorems of crystal dissolution, first expounded by Frank (1958) to surfaces undergoing ion erosion. Frank's earlier treatment of the problem used the work of Lighthill and Whitham (1955 (a) (b)) who studied the kinematic wave equation relating flux and concentration of a quantity when there exists a functional relation between these parameters. Frank (1958) studied the spatial and temporal motion of points of constant orientation relative to the ion flux and showed that the loci or trajectories of these points on the real surface could be constructed through use of an 'erosion slowness curve', which is a polar plot of $1/s(\theta)\cos\theta$ as a function of θ. In the case of crystal dissolution, the motion of discrete surface steps past a fixed point in space is shown to obey the equation of motion of kinematic waves. By considering the local slope and the rate of dissolution of these discrete surface steps in two dimensions, Frank (1958) was able to formulate expressions describing the movement of single points in

the (x,y) plane whose trajectories were straight lines known as 'characteristics'.

Barber et al (1973) realising that the erosion rate of a given element of specimen surface due to sputtering depends on the orientation of that element, related the similarity to chemical etching. They were primarily concerned with the depth d, sputtered from a plane surface which they took to be (cf. equation 6.1)

$$d = \frac{\phi t}{N} S(\theta) \cos\theta \qquad (6.6)$$

where ϕ, t, N, S and θ retain their previous definitions. Since only the thickness of material removed was of interest it was convenient to plot $S(\theta) \cos\theta / S(o)$ against θ, a case which is adequately demonstrated in Figure 6.2, showing the results of Bach (1970) for Ar^+ bombardment of silica glass. In accordance with Frank's second theorem, Barber et al (1973) plotted the reciprocal of the ratio $S(\theta) \cos\theta / S(o)$ in polar co-ordinates and designated the resulting curve 'the erosion slowness' polar diagram. This is illustrated in Figure 6.3, which shows the erosion of a silica glass sphere for a normally incident ion beam. The dissolution trajectories, obeying Frank's theorems are drawn parallel to the direction of the normals to the slowness curve at corresponding orientations. The interpretation made by Frank (1958) of these trajectories was that in terms of the crystal surface when two trajectories representing different orientations meet in space then a discontinuity or edge is produced. Thus, past this meeting point the trajectories have no physical significance to the eroded profile. Barber et al (1973) applied this technique to several different surface profiles, and for example showed the development of a conical protrusion from a

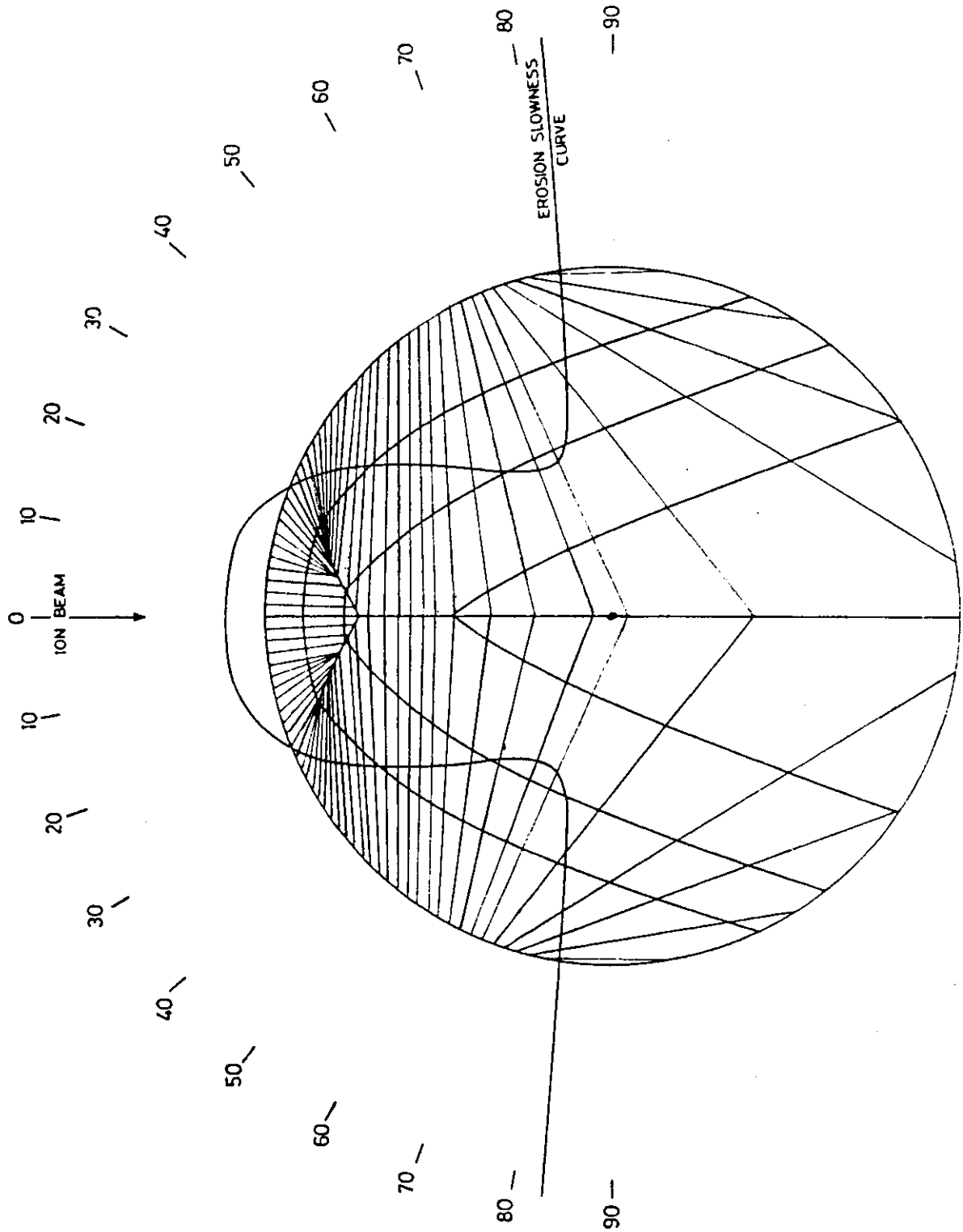

Figure 6.3: Polar diagram of the reciprocal sputtering ratio for silica (erosion slowness curve) and the 'dissolution' trajectories and derived profiles for the sputtering of a silica glass sphere (After Barber et al (1973)).

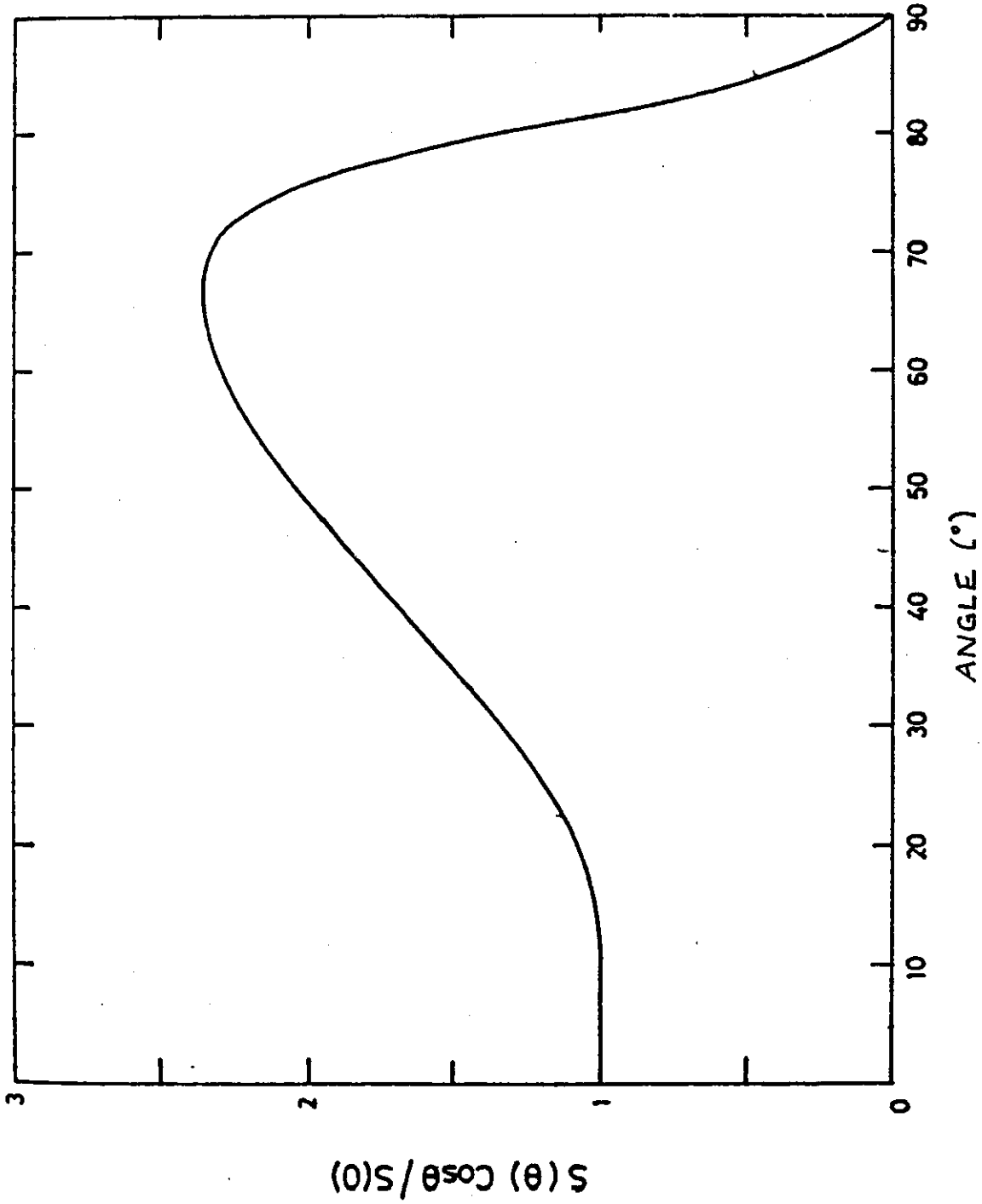

Fig. 6.2: Variation of sputtering ratio with angle of incidence for Ar^+ ions on silica glass, derived from experimental results of Bach (1970).

sinusoidal curve. The theory was further extended to show erosion by an ion beam incident at 60^0 to the surface, a case applicable to ion thinning.

A further theory complementary to the two described previously was presented by Ducommun et al (1974,1975) who considered the erosion of a surface contour as an envelope of a family of straight lines. The erosion of any point along the profile thus proceeded along straight line trajectories of constant gradient, and depended upon the initial geometrical form of the surface and the sputtered material. During subsequent computer simulations they encountered a crossing of the trajectories in a similar fashion to the crossings of the dissolution trajectories derived by Barber et al (1973). Since these points had no physical significance they were duly eliminated. Figure 6.4 shows an eroded profile of the form $y = a \sin x$ for $a = 0.1$, 1.0 and 5.0, and is consistent with work performed by previous authors (Catana et al, 1972; Ishitani et al, 1974; Barber et al, 1973).

In further work by Ducommun et al (1975) the theory was extended to incorporate the erosion of angular points on profiles. Verification of the theory was done by comparing computed results with experimental profiles showing the erosion of a step etched in silicon. An attempt has been made to outline some of the more common theories used for two dimensional ion erosion. All of them however neglect secondary effects such as ion reflection, diffusion and redeposition, and such processes were evident in the experimental work presented by Ducommun et al (1975). Bayly (1972) has discussed various mechanisms which might influence the topography development and has formulated an integral representation using a cosine spatial

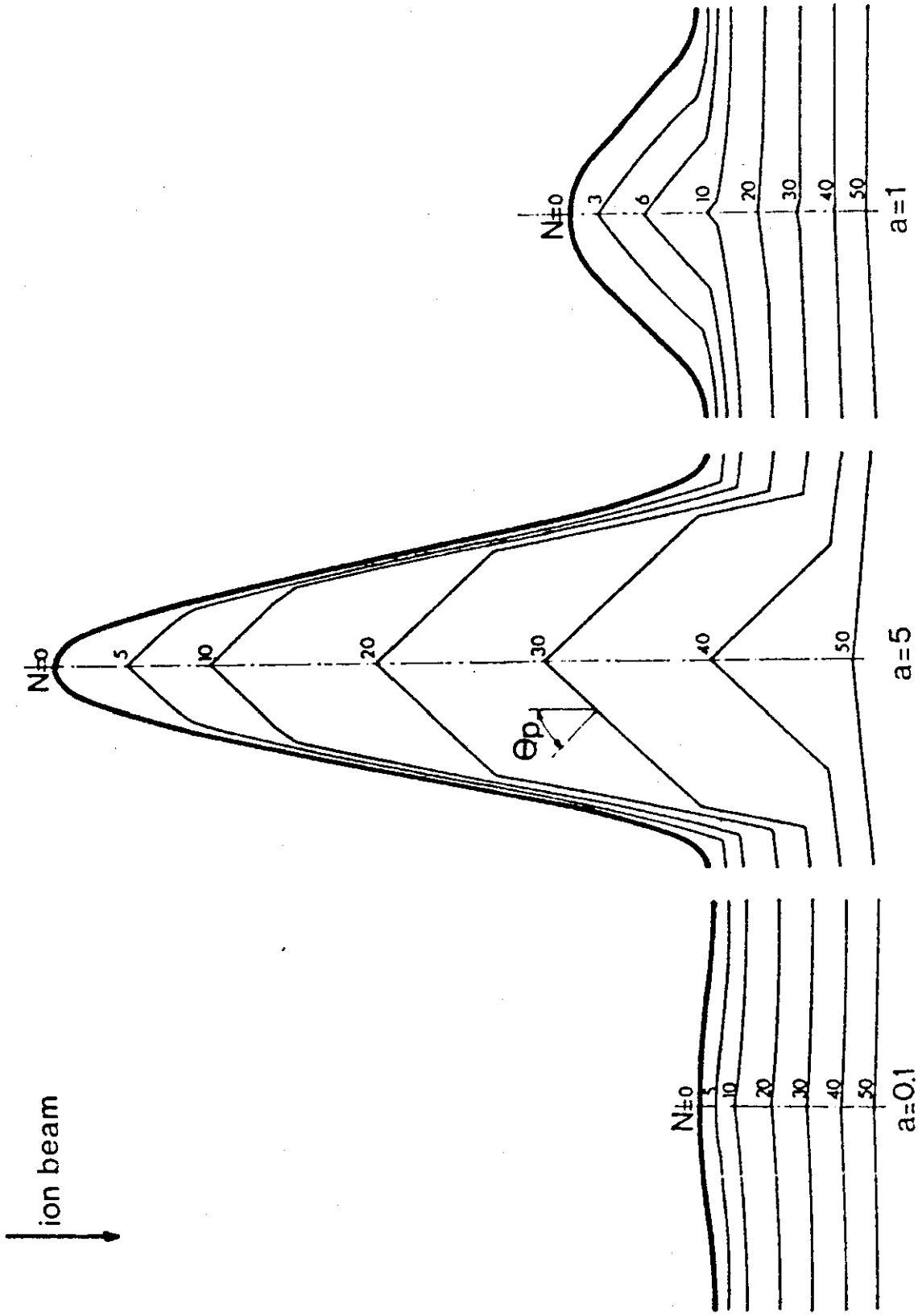

Figure 6.4: Evolution of profiles defined by the function y = a sin x (After Ducommun et al (1974)).

distribution for redeposition of sputtered material. Other secondary effects have been discussed by Belson and Wilson (1980) who derived two dimensional flux density equations to predict changes in shape due to redeposition of sputtered material onto features standing proud of a planar surface during ion bombardment. More recently Smith et al (1983) have presented a continuum model in two dimensions for the redeposition of sputtered material. The work was particularly relevant to ion etching processes in the electronics industry.

Limitations of the previously described theories are their 2-D nature, uniform ion flux and their restriction to amorphous or polycrystalline materials. The crystal dissolution theory as originally outlined by Frank (1958) was presented in three dimensions, but its practical application to the sputtering case was not clear. However, recently, Smith and Walls (1979, 1980) have formulated a general three-dimensional theory based on the method of characteristics, as in the theory of non-linear waves. By this method expressions are obtained which can be utilised in two and three dimensions, and the work presents graphic visualisations of profiles eroded with a uniform and non-uniform ion flux.

Recently Smith et al (1983) have applied the three dimensional theory of erosion to show how initial protrusions on the surface can erode to sharper conical features. This is illustrated in Figures 6.5(a)-(c), which shows time-dependent ion eroded profiles of an initially smooth-top protrusion, developing to the characteristic

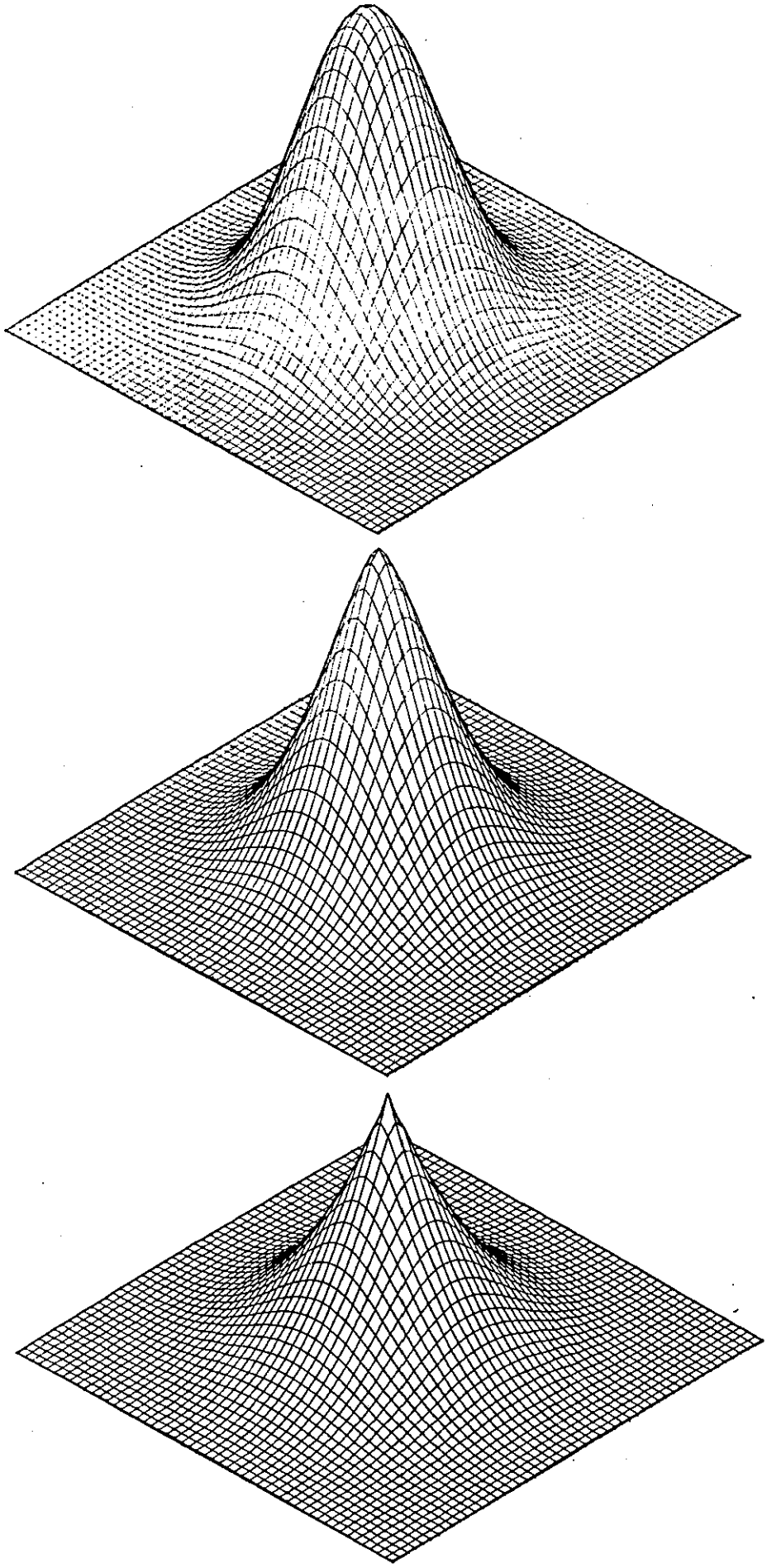

Figure 6.5: A three dimensional representation of an eroding surface protruberance (after Tagg et al (1983)).

sharp-top case.

The versatility of the method of characteristics has allowed many aspects of surface erosion by ion bombardment to be analysed. In a series of papers by Walls et al such topics covered include quantitative analysis of depth resolution degradation dependent on the shape of the eroded surfaces (Makh et al (1980)). Other work involves a study of the evolution of the surface shape of crystalline materials, and strong comparisons are made with amorphous material erosion (Smith et al (1980, 1981)). More recent work performed by Makh et al (1982) has shown that if two ion guns are used to erode a surface the formation of conical structures is suppressed thereby tending to suppress the initial surface shape. This was also supported by an experimental comparison in the same work, which illustrated a relative lack of cones on an ion bombarded stainless steel surface using two guns. The particular relevance of this is in depth profiling, and is complementary work to that done by Sykes et al (1980a) who showed that a depth profile through Ag/Cu multilayer thin films was improved using two ion guns rather than one.

Many of the theories previously described are primarily concerned with the macroscopic effect of ion erosion on surface shape. In most cases, despite the varying theoretical methods, the studies have been shown to be consistent with each other. This is also true for a recent study by Rangelow (1983) who presented computer simulations of line edge profiles undergoing ion bombardment. By dividing the initial surface into segment lengths and using a cosine expression to

describe the etch rate as a function of incident ion angle, he determined the evolving surface shape, which he noted was consistent with Barber et al (1973), Carter et al (1972) and Ducommun et al (1974).

At present there does not exist a universal theory describing evolving surface shape under ion erosion which includes all secondary effects, and substrate inhomogenity. However, some of these effects have been individually considered and have been previously discussed. Further to these it should be noted that other tertiary effects inclusive of surface diffusion and ion reflection have been discussed elsewhere (Mullins (1983), Carter et al (1981), Makh (1981), Wilson (1973), Bayly (1972)). In recent work by Nobes et al (1983) the surface morphology resulting from ion bombardment has been studied using a description of spatio-temporally variable ion flux and substrate inhomogenity. This latter aspect has particular relevance to polycrystalline or single crystal targets where there may be extensive defects. The work is particularly relevant to effects associated with rotated or translated ion beams, and allows a discussion of the erosion of polycrystalline samples where differently oriented individual grains possess different sputtering yields. Specific examples are also given for the development of a surface under ion erosion, containing dislocations.

The development and the macroscopic change in surface shape has, in the past, been the primary concern of work done in this field. However there have been considerations to effects occurring on a much smaller scale. Sigmund (1973) formulated a mechanism of surface micro-roughening by ion bombardment by considering the spatial

distribution of atomic sputtering ejection relative to the position of ion impingement on a surface. He suggested that a microscopically flat surface could become unstable under ion bombardment unless atom migration acted as a dominating smoothing effect. By considering the volume spatial distribution of the energy deposition based on a previous treatment (Sigmund (1969), Sigmund (1973)) he could predict the local erosion rates on the surface.

The conclusion of the work was that the erosion rates of corners and edges would be different from the erosion rate of the bounding planes, and would be either enhanced or reduced depending on the local incident ion flux. An example of an eroded conical structure showed some degree of stability under ion bombardment, where the apex eroded more slowly than the intersection of the base and the surface. It should be noted, however, that to quantify the development of the structure it should be of the same order, or less than, the penetration of the ions.

A more recent study of this nature has been performed by Carter et al (1981) who followed Sigmund's (1973) theory to present an approximate analysis on the local erosion rate of a non-uniform surface. They modified the erosion slowness theory to include not only surface orientation dependent erosion, but also curvature dependent erosion, in a similar manner to that of spatially variable, incidence flux erosion slowness theory (Nobes et al (1980)). By investigating both transient and steady-state morphologies they deduced that local environment effects on sputtering yield could generate transient structures of similar dimensions to the cascade volume

spatial distribution. For example, the generation of large cones could be initiated by a transient stage where small conical protrusions are formed on a macroscopically flat surface and their eventual evolution determined solely by the angular dependence of the sputtering yield. Such features, however, are unlikely to represent time-independent stable end forms since the probability that all surface points erode parallel and with equal velocity to each other is expected to be low (Carter et al (1981)).

In conclusion, the evolution of macroscopic surface shape as a function of ion impact angle is now well understood for amorphous materials. Although the theories involve a variety of different mathematical approaches to surface erosion, they are all consistent with each other. Their limitations are that they are unable to represent a surface undergoing erosion inclusive of all the secondary effects, although these may be quantitatively assessed from their individual contributions. Relatively little work has been done to examine overall effects of impurity inclusions or inhomogeneous materials under ion erosion. Furthermore it would appear from recent theoretical studies (Shulga (1983)) of ion bombarded single crystal targets, that any surface shape modelling of these materials should be accompanied by an appropriate redefinition of the $S(\theta)$ curve.

6.2 The Influence of Surface Roughness on Depth Resolution in Surface Analysis

The various mechanisms governing the development of surface topography during ion erosion have been discussed previously. Theoretical models were presented for the evolution of surface shape,

consistent with experimental observations. The influence of surface asperities on depth resolution during surface analysis was shown in a theoretical study by Makh et al (1980), who predicted that if the analysing beam diameter was compatible with the dimension of the surface inclusion then the depth resolution was degraded to a lesser or greater degree depending on the angle of the excitation beam. Their conclusion was that this could be optimised by using an excitation beam diameter as fine as possible consistent with any beam damage effects and to analyse at normal incidence to the surface. It is therefore the purpose of this section to introduce the effects of surface roughness on the depth resolution in experimental studies.

It is well established that during composition-depth profiling of a thin film on a substrate the resulting profile is broadened at the boundary between two elements. A convention for measuring the depth resolution Δz defined by the broadened profile has been adopted by several workers (Hofmann (1980), Seah and Hunt (1983)), and is the depth over which the signal intensity from a particular element at an interface drops from 84% to 16% of its maximum value. This particular definition arises from correlation between experimental observations and error functions, and that these points represent the standard deviation of a Gaussian fitted curve generally involved in the error function. Although the distinctive broadening of a depth profile can be a result of several factors such as bulk and surface diffusion effects, cascade mixing, and surface roughness, this discussion will be primarily concerned with the latter.

To determine absolute depth resolution as a function of depth in depth profiling, evaporated or grown films have generally been used.

This allows a distinction between the film A and the substrate B, as noted in a review of Auger Electron Spectroscopy (AES) by Chang (1974) that the depth profile of a sharp interface between materials A and B will show that B is detected before the interface is reached, and A will still be detected after the nominal sputtered surface has passed the interface, due to a non-uniform surface. Chang (1974) also illustrated broadened depth profiles taken of a 9Å SiO_2 film deposited between a 100Å Cu film and a Si substrate. He concluded that although the mean roughness was estimated to be ≃ 20Å, the local depth resolution was much better, as attested by the fact that the 9Å SiO_2 film was easily detected. This was attributed to the fact that ion bombardment tends to homogenise the surface, and also the development of surface roughness, possibly caused by preferential sputtering of the different component atoms, could give erroneous results near an interface.

In general, microtopographical structures are believed to be accountable for a reduction in signal intensity in either AES or ESCA and causing the profile to broaden which could significantly influence quantitative analysis. For this reason the effects of surface roughness on ESCA and AES have been the subject of several experimental and theoretical investigations.

Fadley (1974) and Fadley et al (1974) in their study on XPS angular distributions considered specific areas on a rough surface that effectively contributed to the ESCA spectrum. Thus by considering the angles involved in X-ray illumination and subsequent electron escape, they were able to predict the variation of angular distributions for varying degrees of roughness and could calculate

the intensity of the detected photoelectrons. Clearly this would highlight the sensitivity of the technique to the magnitude of surface roughness where shadowing effects would dominate. The angular distributions of emitted electrons quantified surface roughness effects by comparing variations in analyses of flat and rough surfaces as a function of their height to wavelength ratio. In a similar, although more experimentally biased manner, Holloway (1975) performed AES on gold films deposited on glass (smooth surface) and ceramic (rough surface) substrates. Although trends were similar between theory and experiment, a larger error was observed for rough substrates, attributed to profilometer traces (used for surface characterisation) of the surface not accurately representing the surface, and also shadowing effects being neglected during excitation and detection.

Holloway's study nevertheless illustrated that surface roughness does affect AES analyses regardless of whether absolute peak magnitudes or relative (ratio) peak magnitudes are used. Its existence may be a result of either the initial surface as observed on engineering samples (Keenlyside et al (1983)), or as a result of ion sputtering by ion induced enhancement of the initial roughness, or by preferential sputtering as in alloys (Werner and Warmoltz (1976)). These aspects have been widely assessed in many experimental studies on thin films (viz. Chapter 3) where it has been observed that the degree of roughness development during depth-profiling can be suppressed using active gas species (Hofer and Liebl (1975), Blattner (1979), Naundorf and Macht (1980)), reducing ion energy (Hofmann et al (1977), Mathieu et al (1976), Blattner et al (1979)), or using multiple ion guns (Sykes et al (1980)).

In contrast to many of the studies performed on multilayer depth-profiling, other techniques such as angle lapping, angle lapping with sputtering and ball-cratering have been assessed for the nature of roughness produced in preparation or during subsequent analysis (Seah and Lea (1981), Brown et al (1981)). In particular Brown et al (1981) attempted to correlate the resolution obtained in Auger analysis with the magnitude of the roughness produced by the varying sizes of diamond particles used in the wear process. They were also able to predict the depth resolution as a linear square sum of the individual contributions of the root-mean-square roughness, the interface roughness and the diameter of the electron beam. Although trends were evident, they were always lower than the experimental values, attributed to an underestimation of the roughness by profilometry.

The necessity to characterise thin films has become more important in the last five years due to the rapid development of the micro-electronics industry. It has been reported recently (Williams (1980), Adachi (1981)) that even materials of this calibre cannot always escape texturing produced by ion sputtering in surface analysis. Furthermore in order that surface texture can be fully characterised for comparison to surface analytical data it is often necessary to perform profilometry on the surface of the specimen. This technique is often unreliable due to large dimensional differences between the stylus and the peak-trough ratio of the roughness (Laty (1979)). Thus serious concern with the correct measurement of surface topography has led this present study to be primarily involved with its development during ion erosion, and the following sections will introduce a new concept to assess its evolution on a theoretical basis.

6.3 The Measurement of Surface Roughness Applied to Erosion Theory

Several techniques are available for recording the texture of rough surfaces (see Kane (1974), Welford (1977)). These may conveniently be distinguished as destructive and non-destructive methods. The latter is generally associated with light microscopy and relies on the discrete specular and diffuse properties of the surfaces under examination. The use of specular reflection measurements for determination of surface roughness has been investigated by Davies (1954) and Bennett and Porteus (1961) and experimentally verified by a number of authors whose results are all summarised by Birkebak (1971). Although these results show a significant correlation of specular reflectance with roughness, the method is limited by the assumptions that the roughness must be a small fraction of a wavelength in height (< 15% of the illuminating wavelength) and the surface height distribution must be Gaussian. Other non-destructive methods of determining surface roughness include laser speckle contrasting (Spragne (1972), Wykes (1977), Welford (1980), multiple beam interferometry (Bennett (1976), Hartman et al (1979)) and electron microscopy, all of which depend implicitly on sufficient surface height variation for quantitative analysis.

By far the more commonly used technique for direct measurement of surface roughness is the stylus method (Cripps (1975), Laty et al (1979), Thomas (1981)). A diamond tip generally pyramidal or conical in shape, and typically 5-12.5μm in radius is traversed across a surface, where the height modulations are recorded relative to some datum point and amplified electronically. Generally, the

very nature of the traversing action of the fine stylus tip leaves scratches on the surfaces, and this becomes inherently worse for soft materials. Furthermore, the accuracy of the profilometer depends upon the relative size of the stylus tip to the height and spatial variation in surface texture. If the diameter of the tip exceeds the distance between two surface peaks, then in one dimension the tip will never reach the 'trough' therefore giving a false reading of the surface height. Also singular points on the surface may be exaggerated in width due to the surface area associated with the stylus (Laty et al (1979)). Nevertheless, for typical engineering surfaces, this method is generally adopted for one dimensional trace profiles.

The development of surface roughness during ion sputtering can be particularly significant to the accuracy of results obtained in surface analysis. It would therefore be advantageous if a prior knowledge of its evolution and magnitude were known. Using the method of characteristics applied to erosion theory, the following work attempts to model the behaviour of the roughness for various initial simple surface profiles. Further, by allowing discrete parts of the profile to have different sputtering yields than the bulk, a study of contaminated surfaces are qualitatively simulated. These will also be compared to previous experimental observations.

6.3.1 The Model

Consider a surface undergoing ion bombardment with a uniform

flux along the negative y-direction. It has been shown that the equation governing the time dependence of the surface angle to the beam has the form in (x,t) space of: (Carter et al (1973), Smith and Walls (1979), Makh et al (1980))

$$\left(\frac{\partial\theta}{\partial t}\right)_x = -\frac{\phi}{N}\frac{dS}{d\theta}\cos^2\theta\left(\frac{\partial\theta}{\partial x}\right)_t \qquad (6.7)$$

and in (y,t) space

$$\left(\frac{\partial\theta}{\partial t}\right)_y = -\frac{\phi}{N}\left(\sin\theta\cos\theta\frac{dS}{d\theta} - S\right)\left(\frac{\partial\theta}{\partial y}\right)_t \qquad (6.8)$$

where ϕ is the uniform ion flux

θ is the angle subtended by the incident ion beam to the normal at any point on the surface

N is the atomic density

S is the sputtering yield

Equations (6.7) and (6.8) represent standard partial differential equations which can be solved to give the co-ordinates of a new point (x_1', y_1') from a previous point on the profile (x_1, y_1). Thus

$$x_1' = x_1 + \frac{\phi t}{N}\frac{dS}{d\theta}\cos^2\theta \qquad (6.9)$$

$$y_1' = y_1 + \frac{\phi t}{N}\left(\cos\theta\sin\theta\frac{dS}{d\theta} - S\right) \qquad (6.10)$$

(cf. equations 6.4 and 6.5).

These equations represent the loci of points that are straight lines and of constant surface orientation. It can be seen from equations (6.9) and (6.10) that any one particular characteristic

line is implicitly determined by its angular orientation and the sputtering yield of the material. It is interesting to examine the effect of allowing discrete parts of a surface to have a different sputtering yield from other regions. This has been studied experimentally by several workers in order to explain a mechanism for the growth of some topographic structures under ion erosion, namely cones, pyramids, etc. Thus, in order to model a surface undergoing ion erosion which allows regions of the surface to have varying sputter yields, a system needs to be accurately defined and modifications to equations (6.9) and (6.10) are necessary.

Consider a simple system shown in Figure 6.6 which illustrates part of a rough surface undulating about a mean surface level. Further, the system for this particular example specifies that all points above the mean surface level have a sputtering yield varying by some constant value K_S, (where $K_S = S \times K$, and K describes either a fraction or multiple of the bulk sputtering yield S), compared to points below the mean surface level with a sputtering yield S. For a pre-selected erosion time t the new points of (x_1, y_1) would normally be calculated from equations (6.9) and (6.10). However, in order that different sputtering yields corresponding to the respective regions of the structure be accounted for, each part of the structure must have its own erosion term. Thus, equations (6.9) and (6.10) are modified accordingly to:

$$x_1' = x_1 + K_S \frac{\phi}{N} \cos^2\theta_1 \, S'(\theta_1) t_1' + (t-t_1') \cos^2\theta_1 \, S'(\theta_1) S \qquad (6.11)$$

$$y_1' = y_1 + \frac{\phi}{N} K_S \, t_1' \left[\cos\theta_1 \sin\theta_1 S'(\theta_1)\right] + S(t-t_1') \ldots$$

$$\ldots \left[\cos\theta_1 \sin\theta_1 S'(\theta_1) - S(\theta)\right] \qquad (6.12)$$

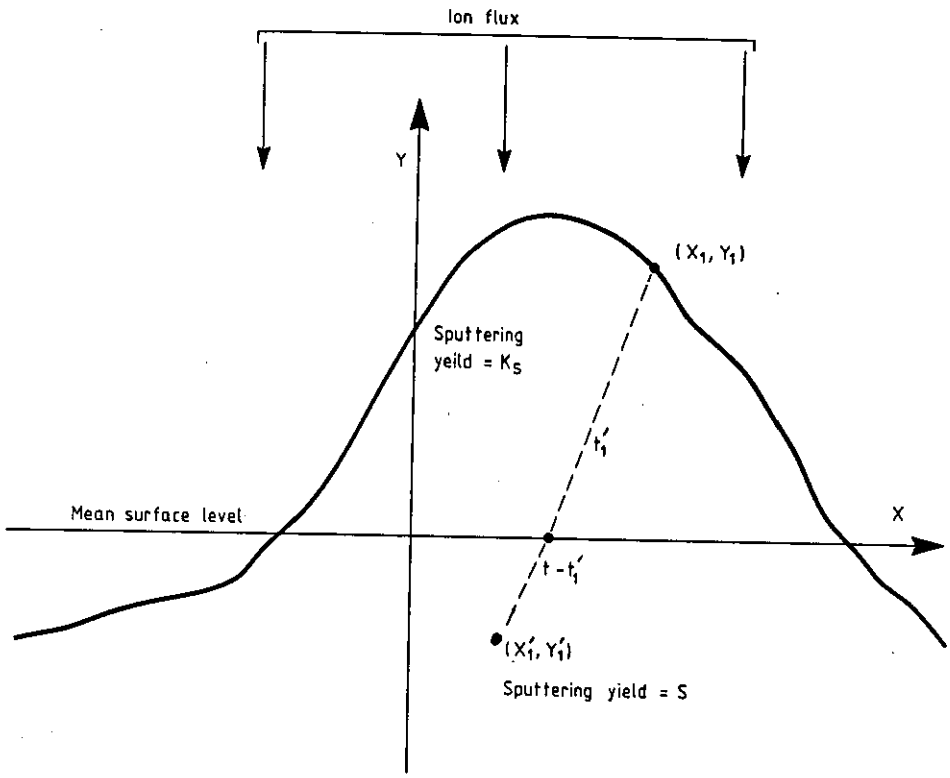

Figure 6.6: Diagram illustrating the erosion of a surface containing two elements of varying sputtering yield. (N.B. K_S = K x S where K represents a number greater than zero).

where (x_1', y_1') are the new points on the profile following erosion, t_1' is the time taken for the characteristic line to reach the mean surface level (the boundary separating the two regions of differing sputter yield) and $S'(\theta) = dS/d\theta$.

In the above equations the first term describes erosion within the first bounded region (above the mean surface level) and the second term describes erosion in the bulk. The value of t_1' is calculated initially in order to determine whether the characteristic line reaches the mean surface level in the specified erosion time t. Hence if $t_1' < t$ the resulting equations used to obtain the new point on the profile reduce to ones similar to equations (6.9) and (6.10).

6.3.2. Computer Simulation

For the purposes of the computer simulations only simple surface profiles given by sinusoidal functions were chosen. Each profile is divided into a number of points, and at each one the angle subtended by the ion beam and the normal to the surface at that point is calculated. Using equations (6.9) and (6.10) (or equation (6.11) and (6.12) depending on whether the surface possesses an inhomogenity) the new point (x_1', y_1') may be calculated following erosion, where the sputtering yield S has a dependence on θ, given by (Ducommun et al (1975))

$$\begin{aligned} S(\theta) = {} & 18.73845 \cos\theta - 64.65996 \cos^2\theta + 145.19902 \cos^3\theta \\ & - 206.04493 \cos^4\theta + 147.31778 \cos^5\theta \\ & - 39.389993 \cos^6\theta \end{aligned} \tag{6.13}$$

By performing this operation consecutively on each point a new and eroded profile is obtained. Due to each point having a different value of θ the gradient of the characteristic lines are different and therefore are subject to cross-over. Physically, this effect represents an edge forming on the eroded profile and new points occurring after this profile are meaningless. For an efficient, and immediately recognisable new profile these points are automatically eliminated in the computer simulation by calculating the cross-over time of the characteristic lines, where from equation (6.9) for two consecutive x values (x_1', x_2') on the profile we have: (Tagg (1983))

when $x_1' = x_2'$

$$t_c = \frac{x_1 - x_2}{\cos^2\theta_2 \frac{ds_2}{d\theta_2} - \cos^2\theta \frac{ds_1}{d\theta_1}} \qquad (6.14)$$

Similarly, in the event that a region of the bulk structure is inhomogeneous the time for cross-over of the characteristic lines may be calculated using the following equation:

$$t_c = \frac{(x_1-x_2) + (K_S-S)\cos^2\theta_1 S'(\theta_1)t_1' - (K_S-S)\cos^2\theta_2 S'(\theta_2)t_2'}{S(\cos^2\theta_2 S'(\theta_2) - \cos^2\theta_1 S'(\theta_1))} \qquad (6.15)$$

If the time of cross-over t_c for any two characteristic lines was less than the total erosion time between the initial and final profiles, (i.e. if $t_c < t$), the corresponding points were eliminated accordingly. By a repetition of this process a new eroded profile can be obtained, using equations (6.9) to (6.12), where no crossing of the characteristic lines occurs.

For t = 0 and for subsequent erosion times the current profile could be assessed for its specific value of either average roughness or root mean square (r.m.s.) roughness as depicted in Figure 6.7. This method has been found to be the most appropriate assessment of a surface and has been used by several workers, and also in programmable stylus instruments (Cripps (1975), Kowalski (1983), Whitehouse and Phillips (1982)). Hence, by this computer simulation, the shape of the eroding surface can be monitored and graphical output of the roughness as a function of erosion time easily accessed. In the following sections results are presented illustrating the erosion behaviour of some simple periodic structures. These eroding structures are assessed by evaluating the root mean square roughness as a function of the sputtering time. Further, two types of surfaces will be considered separately for the above assessment, namely homogeneous and inhomogeneous structures, where in the case of the latter enhanced topography growth will be shown to be a result of foreign-body contamination.

6.3.3 Results

6.3.3.1 Surface roughness of an homogeneous bulk under ion erosion

An homogeneous bulk is one that represents material that is of the same composition in all directions. This definition has been adopted for the assessment of the surface roughness of structures following ion erosion, presented in this section. Furthermore, simple structures are considered that possess no inhomogenities such as defect clusters or dislocations, and thus the surface contours erode at a constant

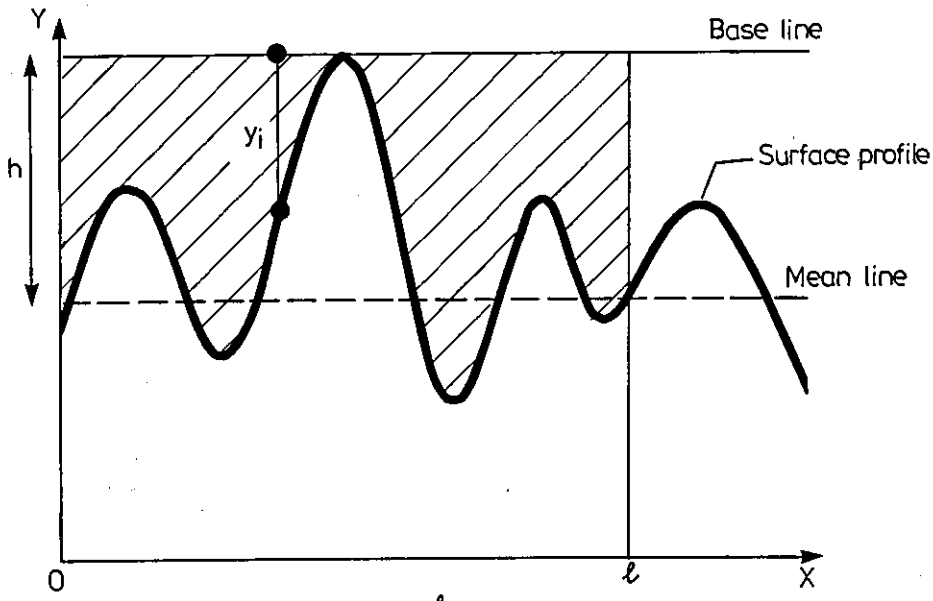

Average roughness $h = \frac{1}{\ell}\int_0^{\ell} y_i \, dx$

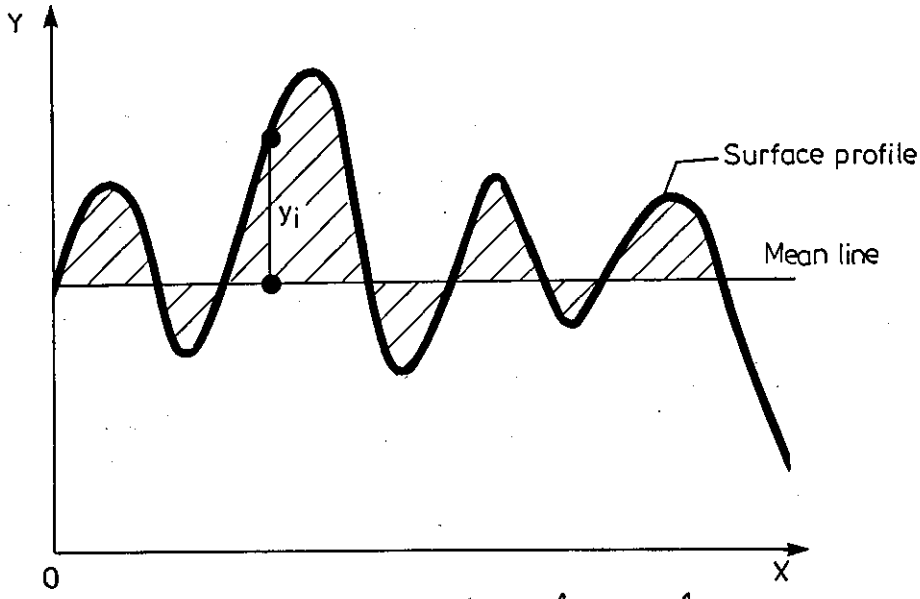

Root mean square roughness $= \left(\frac{1}{\ell}\int_0^{\ell} y_i^2 \, dx\right)^{1/2}$

Figure 6.7: Two diagrams illustrating the method of calculation of the average roughness and the root-mean-square roughness for an undulating surface.

rate everywhere where their velocities are governed totally by the $S(\theta)$ curve.

A simple periodic structure that has been adopted for the presentation of results is a sine curve. By defining the function in the form $y = a\sin bx$ and varying the parameters 'a' and 'b', the effect of amplitude and periodicity of the macroscopic surface can be examined. Figure 6.8 illustrates a family of curves representing the normalised root mean square roughness as a function of erosion time for values of 'a' in the range 0.1 - 1. Note that although the sputter time is shown in seconds this value is not absolute and represents a normalised value of $\frac{\phi t}{N}$ in equations (6.9) and (6.10).

It is evident that during the early stages of erosion the reduction in r.m.s. roughness is relatively rapid compared to later stages of erosion. For example, the r.m.s. roughness is reduced by 75% in the first three seconds of ion bombardment, compared to only a 3% reduction in the last three seconds of erosion, for the curve representing $y = \sin x$ (i.e. $a = 1$, $b = 1$).

This effect, however, is reversed when the initially defined structure prior to erosion has a low amplitude. The curve represented by $y = 0.1 \sin x$ shows a 6% and 13% reduction in r.m.s. roughness respectively for the same time intervals described above. This behaviour can largely be attributed to the absolute angle at the surface that is presented to the ion beam during erosion. Thus the variation in surface roughness is governed by the sputter rate dependence on angle of ion incidence, a relationship which has previously been demonstrated (see Figure 6.2). This process may be

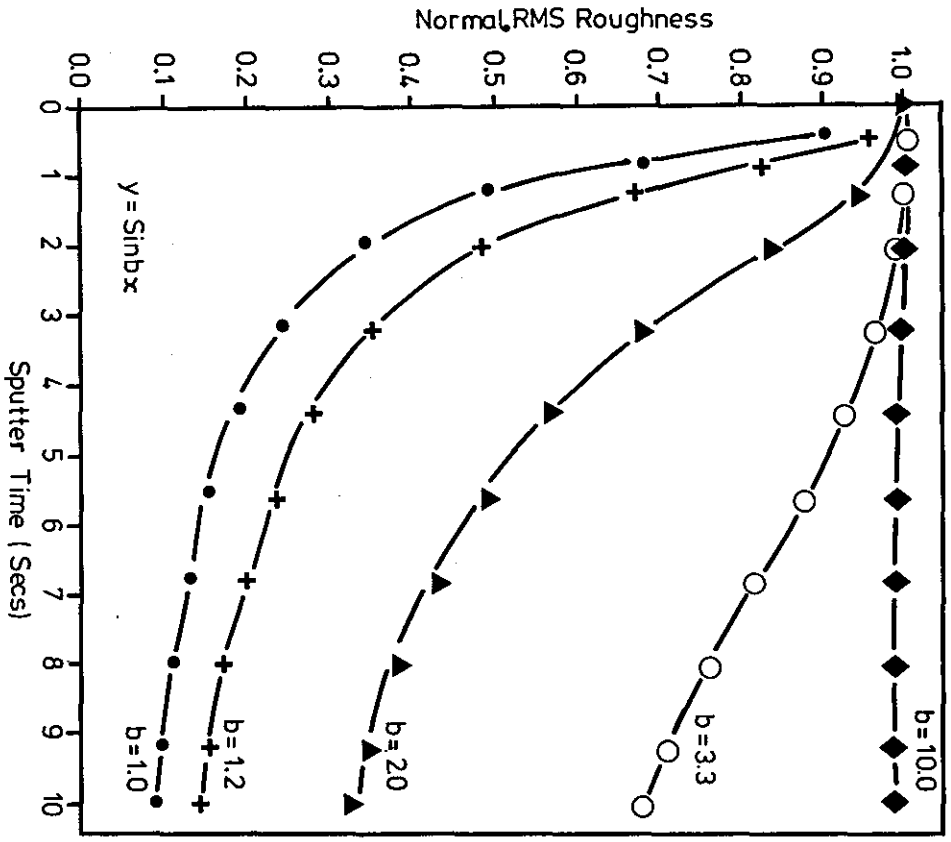

Figure 6.9: Normalised r.m.s. roughness vs sputter time for a surface profile described by y = sin bx.

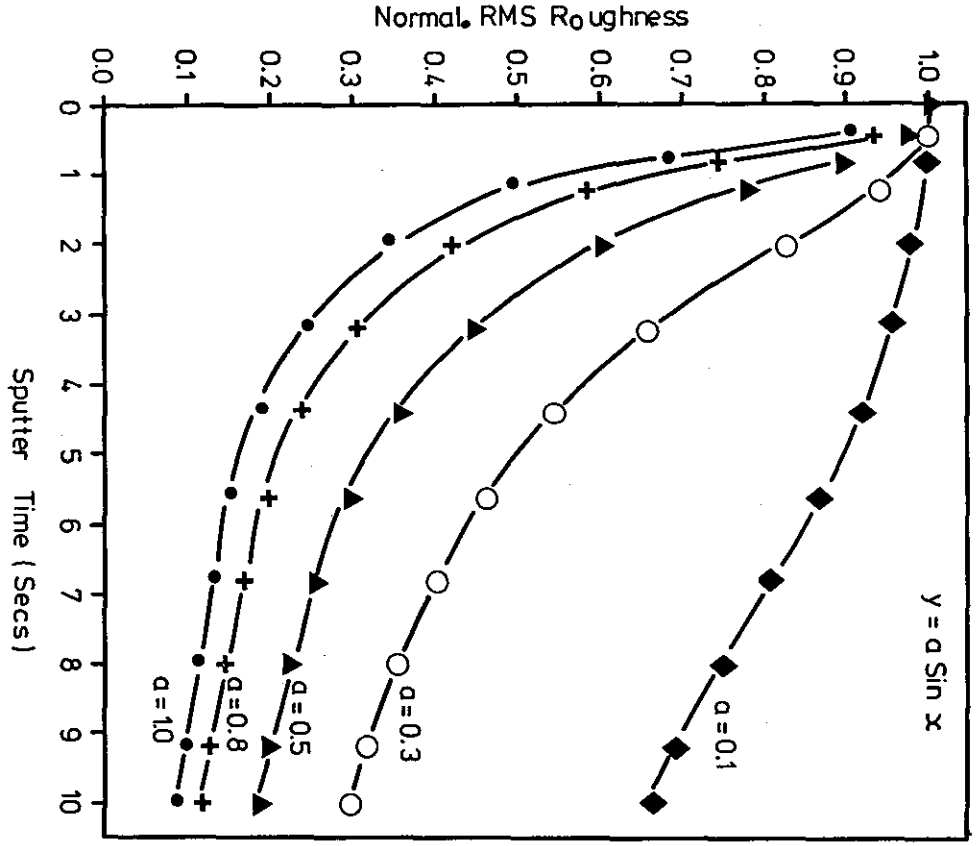

Figure 6.8: Normalised r.m.s. roughness vs sputter time for a surface profile described by y = a sin x.

envisaged physically by considering the angle at the surface presented to the ion beam at a point (0,0) or (π,0) along the profile of a sine curve. These two points represent the centres of the two slopes of the sine function where the gradient is the greatest. Furthermore, the way in which these slopes on the profile erode will greatly influence the nature of the topography forming during ion erosion, since exposure to the ion beam in these regions involves a large percentage of the total area of the whole surface.

For a surface profile described by $y = \sin x$ ($a = 1$, $b = 1$) the angle at this point is 45°, whereas for a profile described by $y = 0.1 \sin x$ ($a = 0.1$, $b = 1$) this angle is 5.7^{o}. In the former case the lateral and vertical erosion will therefore be greater than in the latter as described by the $S(\theta)$ curve, and the resulting cone structure (characteristic of a sine function undergoing ion erosion - Ducommun et al (1974)) will form and erode more quickly.

The most prominent feature associated with the curves in Figure 6.8 is that they asymptote as the time of erosion increases beyond a critical value. This phenomenon, that relates to how an initially rough, homogeneous surface tends towards a flat plane under prolonged ion erosion, has been reported elsewhere (Smith and Walls (1980)). It should be noted, however, that the graphical representations presented here do not illustrate the value of r.m.s. roughness reaching the absolute value of zero which would represent a flat surface. This is due to nature by which the computer program handles individual points along the profile. Initially, the profile is divided into a number of equispaced points each of which are

individually eroded according to equations (6.9) and (6.10). However, during subsequent time intervals of erosion the characteristic lines begin to intersect each other and are thus eliminated, subject to the condition described by equation (6.14). Thus the number of points along the profile available for erosion decrease, thereby introducing possible errors in the calculation of the r.m.s. roughness. Therefore the total interval shown on the graphs represents the stage at which it was considered that the eroded profile of $y = \sin x$ possessed a suitable number of points for the calculation of r.m.s. roughness. The other curves having lower amplitudes (lower 'a' values) will require longer erosion times to reach a 90% reduction in r.m.s. roughness, but have been shown to erode over a specific time interval simply for comparison.

The curves shown in Figure 6.9 represent the behaviour of the r.m.s. roughness as a function of erosion time for the curve $y = \sin bx$ and values of 'b' in the range 1-10. The trends are similar to those shown in Figure 6.8, where an asymptotic quality is evident, signifying that the eroding profile tends towards a flat plane following prolonged ion bombardment. A similar process operates to the one previously described whereby as the periodicity increases the effective angle of the slopes of the profile decrease, thus reducing the sputter rate.

6.3.3.2 Surface roughness of an inhomogeneous bulk under ion erosion

The generation of surface roughness under ion erosion has been discussed in detail in the previous chapters presented in this work. One of the most outstanding features responsible for the growth of surface morphology is the contamination of surfaces by atoms or

molecules foreign to the bulk material. The proceeding mechanism is one by which differential sputtering yields are developed between the two separate materials thus creating local change in sputtering yield. This phenomenon of course can result from a crystal orientation, or a structural defect dependence. The work presented here will confine itself to treating surfaces undergoing erosion having local regions of different sputtering yield than the bulk.

Proceeding to a more realistic interpretation of an eroding surface, particularly for the purpose described above, a simple structure may be constructed representing a foreign body protruding from the flat surface of a bulk specimen. One such structure is illustrated in the inset of Figure 6.10 and for convenience of programming assumes the form of a sine wave over a range of π. The area under the sine function can now be assigned a sputtering yield as some percentage of the sputtering yield of the bulk. The protruding part of the structure will then erode in a similar fashion to that illustrated by Figure 6.4 and described by equations (6.11) and (6.12).

Figure 6.10 illustrates the erosion behaviour of the structure described above, where the differential sputtering yield K_S is varied from 1-1.5. ($K_S = K \times S$, where S is the normalised sputtering yield of the underlying bulk). The normalised r.m.s. roughness falls rapidly in the first 0.5 seconds of ion bombardment to a stable value which represents the point at which the protrusion has eroded completely. The surface then erodes in a similar fashion to that shown in Figures 6.8 and 6.9 and is illustrated in Figure 6.11. It is evident here that as the sputter time increases the r.m.s. roughness

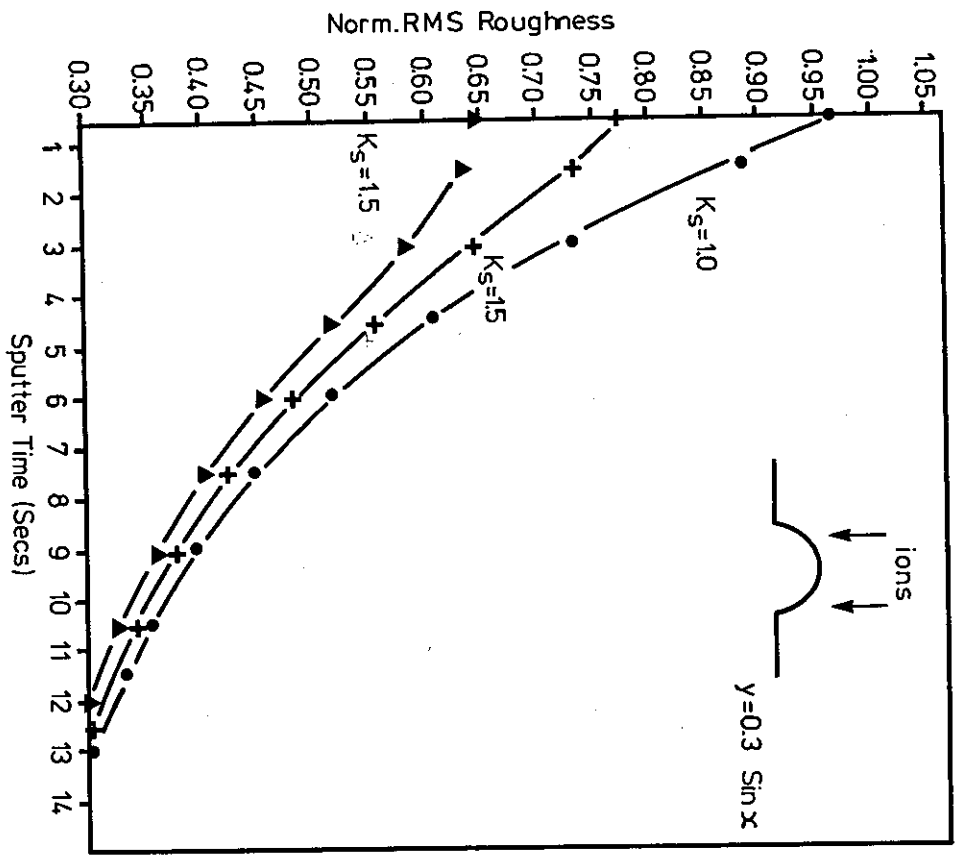

Figure 6.10: Normalised r.m.s. roughness vs sputter time for a surface profile described by y = 0.3 sin x for K_S = 1-1.5 (see inset).

Figure 6.11: Normalised r.m.s. roughness vs sputter time for a surface profile described by y = 0.3 sin x for K_S = 1-1.5 (see inset).

begins to asymptote to a particular value indicating the approach of a flat plane.

In contrast, Figure 6.12 represents the r.m.s. roughness of the surface as a function of sputter time when K_S = 0.2-1. This illustrates the surface morphology of a structure possessing a foreign body of lower sputtering yield than the bulk. Clearly, the increase in the height of the roughness is seen to reach a maximum after a particular sputter time. This optimum structure then begins to erode in the normal way once the foreign body has been completely removed.

Although a measure of the r.m.s. roughness as a function of sputter time describes the behaviour of the eroding surface, it is often of interest to examine the exact shape of the surface profile. This is particularly important on real surfaces where roughness measurements with stylus instruments, for example, do not represent the true shape of the profile. Using an interactive graphics package these eroding shapes can now be observed.

Figure 6.13 illustrates the change in surface shape resulting from the erosion of the structure shown in the insets of Figures 6.10-6.12. It can clearly be seen that if the surface protrusion (represented by the sine function) has a sputtering yield one-tenth of the underlying bulk (K_S = 0.1) the structure develops into the familiar conical shape observed by many previous workers. More importantly, the physical dimension of the structure is greatly increased thus enhancing surface roughness as illustrated by Figure 6.12. This effect would always occur providing that the

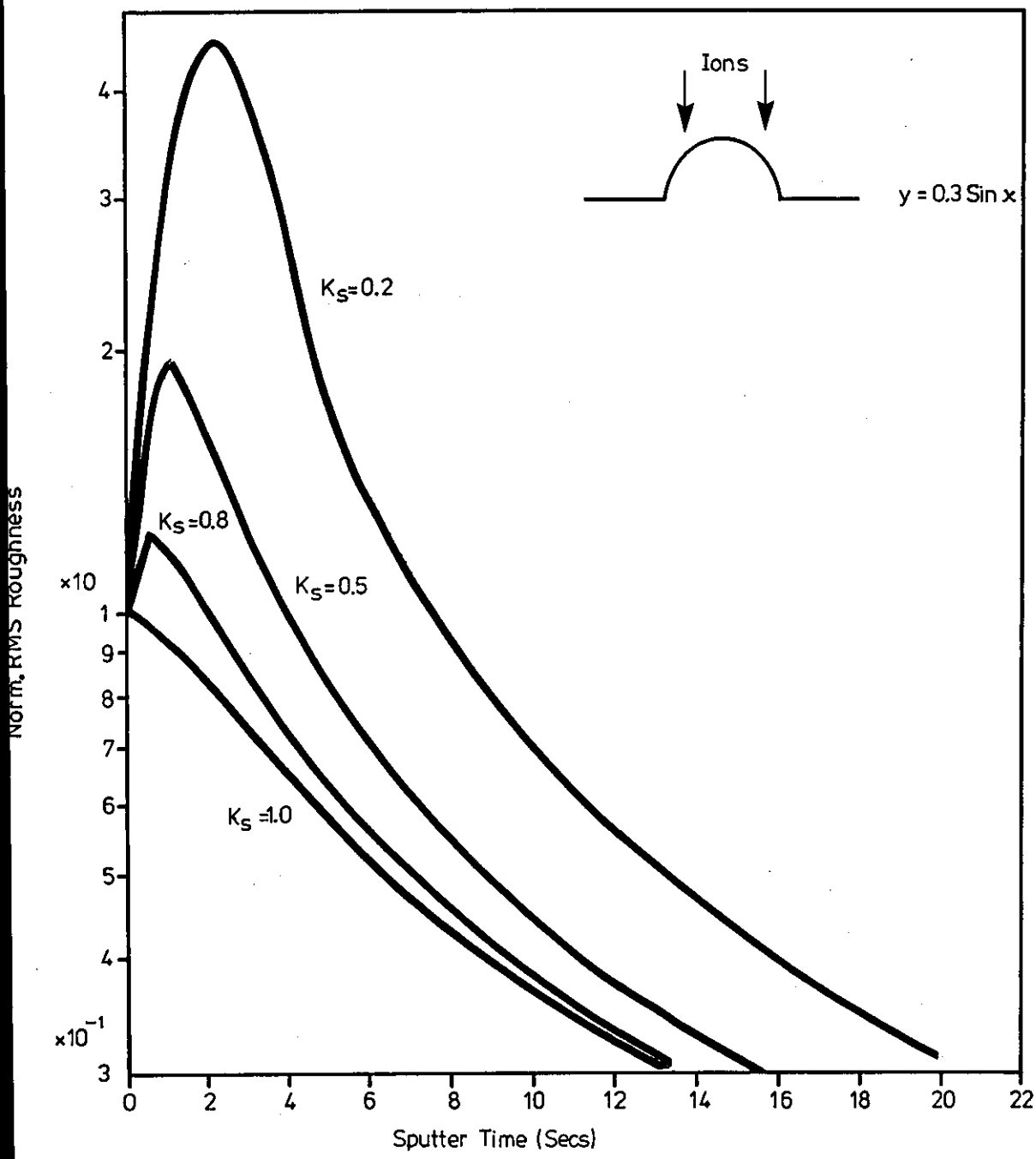

Figure 6.12: Normalised r.m.s. roughness vs sputter time for a surface profile described by y = 0.3 sin x, for K_S = 0.2-1.0 (see inset).

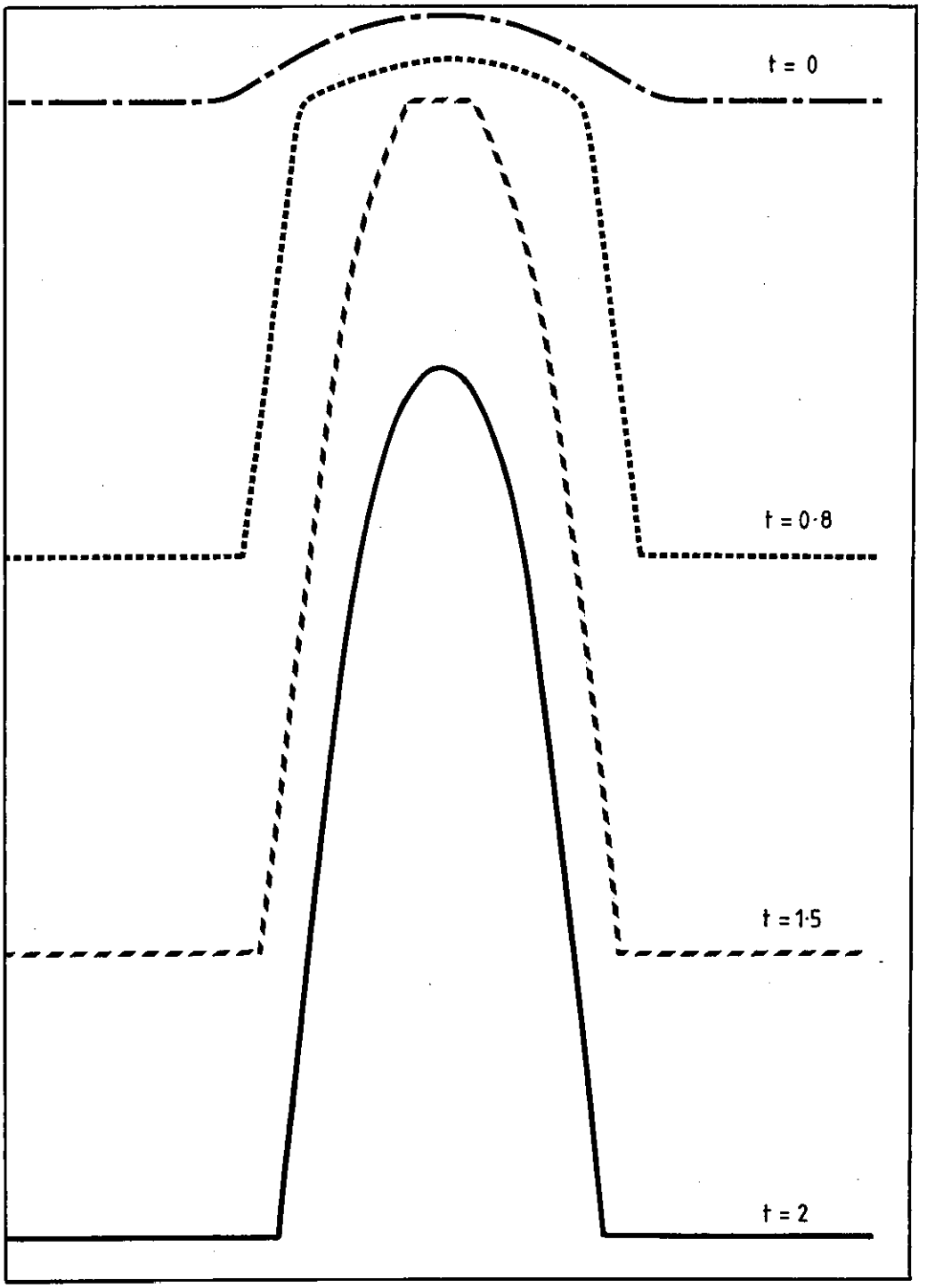

Figure 6.13: Computer generated graphics illustrating the time of erosion of a surface initially perturbed by a body of lower sputtering yield than the bulk (K_S = 0.1). The initial surface profile is partly described by y = 0.1 sin x.

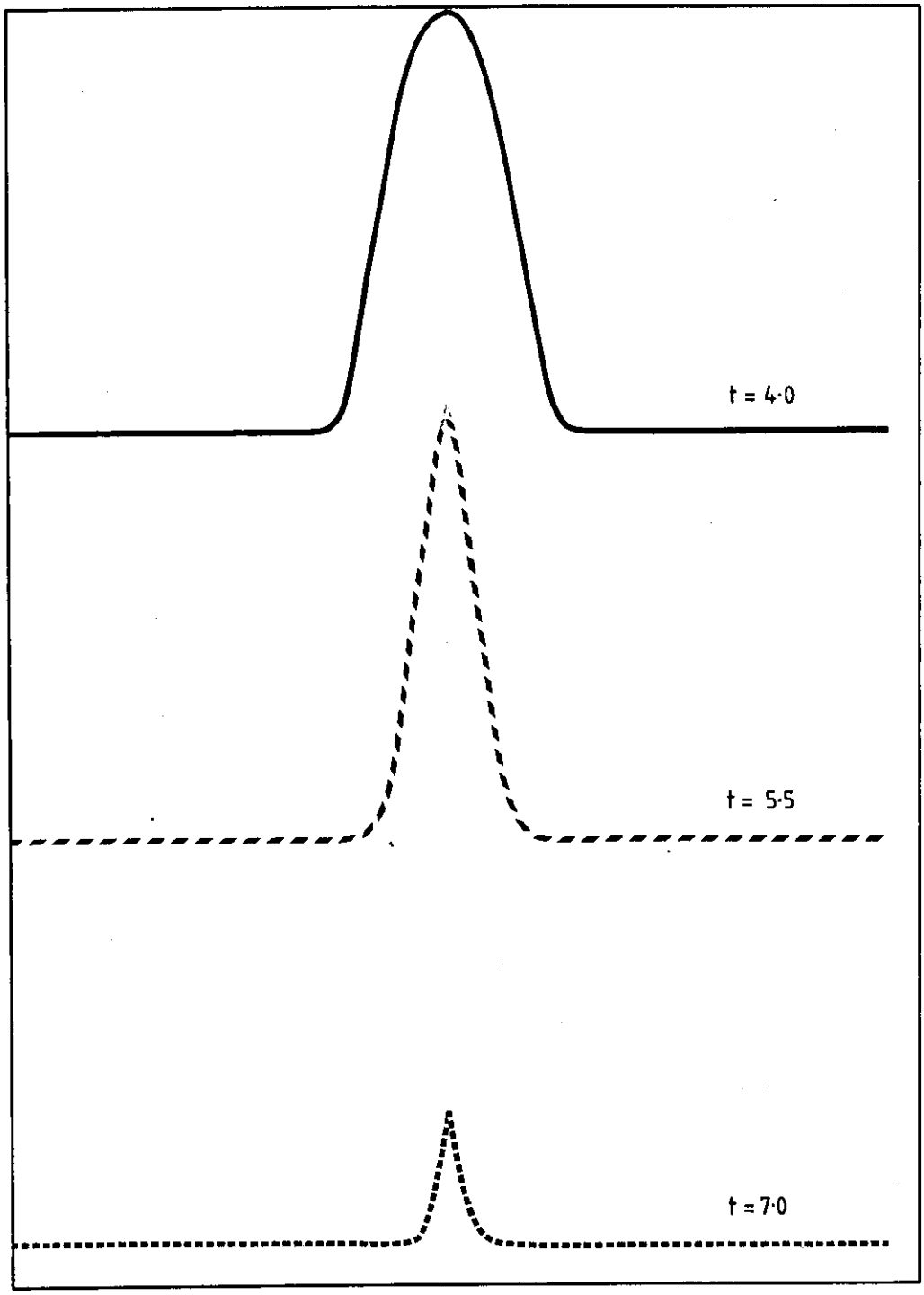

Figure 6.13 continued

protrusion possessed a sputtering yield lower than the bulk.

The viewing of simulated structures such as these undergoing ion erosion can provide qualitative information on the behaviour of real materials during prolonged ion bombardment. For example, Figure 6.14 illustrates a series of micrographs showing a GaAs surface undergoing Ar^+ ion bombardment. Clearly the surface has originally been locally perturbed by a foreign body of low sputtering yield, and conical structures formed during prolonged ion erosion bear a similar resemblance to those simulated in Figure 6.13. The maximum height of the cone will depend on the initial height of the protruding surface and the sputtering yield of foreign material. Further, the width of the pillar structure will vary according to the periodicity of the asperity on the surface (Wilson (1973)).

6.3.3.3 Discussion

Several problems were encountered during the running of the program used to erode specifically designed structures. These were usually related to the way in which the surface profile formed edges during erosion, or where the characteristic lines intersected. The time for this intersection of adjacent points could be automatically calculated using equation (6.14) and (6.15) and the two points related to the characteristic lines responsible for intersection were eliminated prior to final erosion of the profile.

The number of points eliminated during a specified time of erosion depended implicitly on the local variations in the angle at the surface, presented to the ion beam. Thus, situations occurred

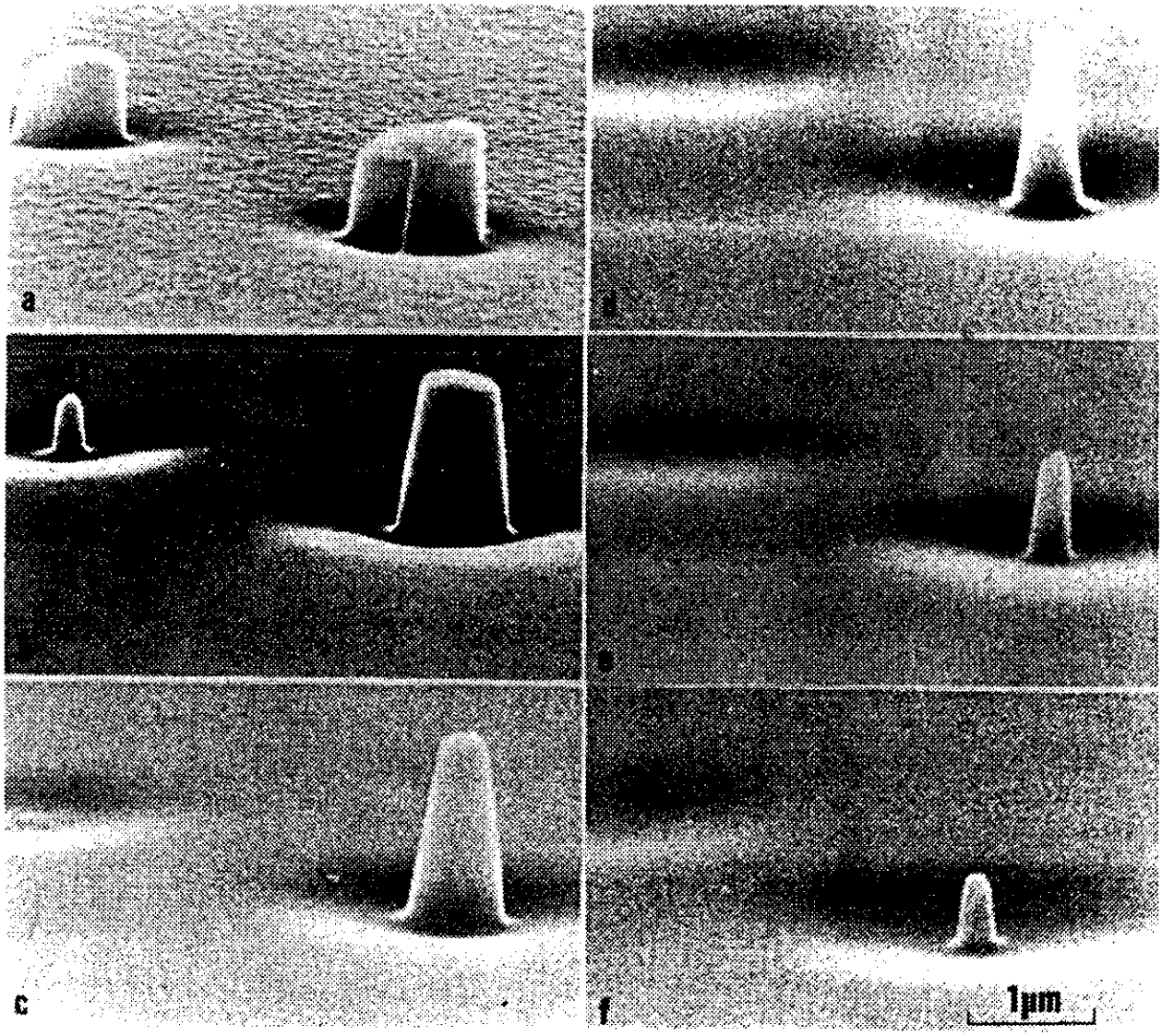

Figure 6.14 Variation of a surface feature on GaAs during Ar^+ ion bombardment (After Wilson 1973)

where many points were eliminated in localised areas of the profile.

Conversely, other regions on the profile existed where, during the specified erosion time, no points were eliminated since no crossing of the characteristic lines occurred. If two of these regions were located adjacent to each other there was often an abundance of points created on the newly eroded profile, which created a false surface shape due to the lack of elimination by characteristic lines normally present from other profile regions.

The structures presented in this work were chosen such that erosion proceeded uniformly over the whole of the surface profile, and there were no discrepancies in the elimination of the characteristics. This problem could be overcome by replacing points in the regions depleted by the abundant crossing of the characteristics using extra sub-routines within the computer program, although this aspect is beyond the scope of the work presented here. Alternatively the eroded points not required on the final profile may be eliminated by editing the data file, although this task is somewhat laborious, and may prove difficult to achieve when sorting through several hundred data points.

A similar problem was encountered when discontinuities were present in the profile. This, however, was only evident for the erosion of surface protrusions as illustrated in Figures 6.10-6.13. The points at which discontinuities would normally occur is where the protrusions boundaries meet the flat surface. To obtain more points in this region a small curvature was produced by fitting a polynomial curve of the form $ax^3 + bx^2 + cx + d$ between the sine

function and the flat surface. By dividing this into a specified number of points and using the normal erosion theory, more points were provided on the eroded profiles between the flat surface eroding in the -y direction, and the adjacent point on the sine curve, eroding at 45° into the bulk. This produced a more accurate representation of the final eroded structure and thus provided a better measurement of surface roughness.

The method of computation of erosion employed in this work relates specifically to the $S(\theta)$ curve as defined by the sputtering behaviour of silica glass (Bach (1970)). Hence the results presented here for inhomogeneous materials rely on those materials having the same characteristic $S(\theta)$ curve as silica glass. It has been shown that several materials possess a similar form of erosion curve (McCracken (1975)) and therefore since the surface protrusion (illustrated in Figures 6.10-6.13) was a specified percentage of the normalised bulk sputtering yield, the results are valid for any combination of materials falling within this ratio. However, due to the versatility of the method of characteristics in erosion theory, the application of differential sputtering yields to simulate eroding structures is not limited to one $S(\theta)$ curve. If the correct data-base is initially determined it is possible to create other fitted $S(\theta)$ curves for materials not possessing the characteristic shape of silica.

6.3.3.4 Conclusions

Erosion theory by the method of characteristics has been used in the measurement of surfaces undergoing ion erosion. Simple

structures have been applied to this problem and the behaviour of their roughness has been assessed as a function of time. This work has served to introduce the concept of monitoring the change in surface roughness as a function of erosion time for both homogeneous and inhomogeneous materials, and has illustrated how a qualitative representation of eroding structures can be produced.

It is envisaged that providing a system is sufficiently described mathematically, a variety of surface features can be observed depending upon the system. For example, an initially flat surface eroding to bulk impurity sites will be of significant interest in the surface analysis of semi-conductor materials. These types of systems are complex and would require substantial computer programming knowledge to initiate. Further, other problems previously mentioned, on the behaviour of the characteristic lines crossing, are largely surmountable with careful manipulation of the computer code.

The theory and results illustrated here have utilised the aspect of ion beams eroding a surface at normal incidence. Extensions of the erosion theory suggest that oblique ion incidence and multiple ion guns can be used to erode and monitor the roughness of surfaces in the manner described here (Makh et al (1982)).

CONCLUSIONS

The work presented is centred on an examination of the phenomenological aspects of ion erosion, both in theory and experiment. The effects of ion erosion of solid surfaces are clearly detrimental to the initial microscopic surface after short bombardment times, or the macroscopic surface after prolonged bombardment. The two regimes, although appearing independent of each other and often may be treated as such, are particularly important in surface analysis where in situ ion bombardment is often performed. The relative effects resulting from ion erosion will ultimately depend on a variety of considerations such as instrumental parameters, initial structure of the surface to be examined, and material-ion species combination. The former of these aspects, of course, holds many explicit conditions relating to the type of surface analytical technique and its optimum mode of operation. Of foremost importance is the sensitivity of the technique in its depth and spatial resolution during sputter-depth profiling and several specific areas have been discussed in this work to assess the effect of ion erosion on these parameters.

The first, and perhaps most widely adopted technique for assessing depth resolution was the use of thin film standards. By varying the thickness of a single film of Cr on a Ni substrate a depth profile by AES could be obtained and the relative broadening at the interface provided a measure of depth resolution. The main object of the work was to compare results from a single layer system to data published by other workers who generally used multilevel thin film systems. Although no significant difference was observed,

the results compared well to criteria formulated by previous workers relating depth resolution to depth. The broad band of data (see Figure 2.4) clearly resulted from the numerous variety of materials and irradiation parameter combinations used in these experiments. These two aspects in conjunction with initial sample preparation will have a significant influence on the sensitivity of a surface analytical technique such as AES.

Further to the above study, an investigation was carried out on the Cr/Ni thin film system to determine whether enhanced depth resolution could be obtained by profiling with two ion guns. These results showed a significant, although small ($\sim 5\%$) improvement in depth resolution as compared to using only one ion gun to depth-profile. It was deduced that the use of two ion guns effectively reduced surface roughening, particularly for the thicker films (2000Å - 4000Å), in accordance with erosion theory (Makh et al (1982)). Future work should incorporate a similar system to the one described in Chapter 2 thus reducing an amplification of atomic mixing and surface roughening effects which are likely to prevail in multilayer systems.

Amongst the influencing factors involved in contributing to either relatively enhanced or degraded depth resolution are the instrumental parameters employed in surface analytical techniques. In particular, ion and electron beams will produce a variety of information from the surface depending on their current densities, angle of incidence to the surface and the material undergoing analysis. It is therefore important particularly in depth resolution studies of thin film systems that the instrumental parameters be kept constant.

Complementary to the experimental studies performed in Chapter 2, a simulated study of events was examined for a depth profile typically used in AES. It was shown in Chapter 3 that varying the angle of the electron and ion beams to the surface of the sample, and the angle between the two beams, revealed significant variation in the relative depth resolution. This, however, was for the case when analysis is performed in a crater produced by a static ion beam thus introducing edge effects. Nevertheless, it is often necessary to reduce the raster size of the ion beam for higher ion currents and thus shorter profiling times. Further, the excitation beam/ion beam ratio may become relatively large if analysis is performed on materials susceptible to excitation beam damage, or if there is no means of focusing the excitation beam, as in ESCA. Thus, this work served to illustrate yet another aspect of surface analytical technique requiring optimisation.

Perhaps the most widely documented topics of investigation relating to ion beam phenomena is the development of surface roughness. The initiation and eventual growth of cones, pyramids, pits and other such structures resulting from ion-induced damage, structural defects or initial surface character has been identified as having a detrimental effect on the sensitivity of several surface analytical techniques. It is therefore imperative that the exact nature and growth process of these phenomena be identified with the prevailing experimental conditions producing them. More importantly, any investigation of this kind should adopt a systematic approach and thus individually assess the effect of the available variable parameters

such as ion species, ion energy, ion angle of incidence, etc. This task was undertaken by performing a series of experiments on three important semiconductor materials (Si, GaAs, InP). By effecting O_2^+ and C_s^+ bombardment at various energies on these materials the development of surface topography could be observed as a function of ion dose. The conditions used were also appropriate to typical SIMS analysis.

At present, there exists a large library of qualitative information on many forms of surface morphology, produced by ion bombardment of a variety of materials. Studies such as these provide a good database for characterisation of surface topography on the macroscopic scale, and help to envisage the processes governing the development of such phenomena on the microscopic scale. The results presented in Chapter 5 of this work have contributed to this library of information. Furthermore, the effects of active gas bombardment have been introduced on materials which allow a direct comparison to other work employing inert ion bombardment (Wilson (1973), Carter et al (1977)).

Qualitatively, there were no significant differences in the topographies on the semiconductor materials, produced by inert or active gas bombardment, which would indicate the domination of purely physical processes prevailing. However, the relative sizes of the surface structures could contain significant information on a minimal chemical dependence, since the topography produced by active gases appeared to be smaller than its counterpart produced by inert gases. This aspect of ion sputtering, particularly for oxygen, would indicate that the shallow amorphous layer existing during bombardment acts as a passivation reducing sputtering rates, and for a nominal ion

dose, reducing the absolute topography size. An enhanced smoothing effect by O_2^+ ion bombardment has been observed elsewhere (Laty et al (1975)).

In general, it was found that topography development on the semiconductor materials did not occur below $\sim 10^{19}$ ions cm^{-2}. This observation, however, was ultimately limited by the resolution in the SEM. Further, more detailed studies of this area of work should adopt higher resolution techniques for the detection of micro-topography. Methods currently in use for this purpose, such as HRTEM (High Resolution Transmission Electron Microscopy) employing methods such as the replica technique and Lattice Imaging Microscopy, are extremely specialised and not always readily available. However, now that the morphological phenomena have been identified on a large scale experimental investigations should be directed towards linking its development to processes occurring on the atomic scale.

The provision of reliable experimental observation, and a qualitative understanding of on-going processes occurring during ion erosion, is a crucial precursory requirement for mathematical descriptions of the same processes. Indeed, in the last decade the theoretical background of eroding homogeneous substrates has become well established (Ducommun et al (1975), Carter et al (1975)) and several secondary effects have also been considered (Smith et al (1983)).

As more data is amassed, so a greater need to mathematically describe the observed phenomena becomes apparent. Recently, workers

have attempted to theoretically assess the behaviour of the facet phenomenon, which has been observed in this work (see Chapter 5) and elsewhere (Carter et al (1977)), and relate the absolute size of facets to depth resolution (Carter et al (1985(a)(b))). The work presented in Chapter 6 has adopted a similar, but more indirect approach, in the assessment of surfaces undergoing ion erosion. By using theory employing the method of characteristics (Smith and Walls (1979)), simple periodic surface structures were eroded, and the intermediate surface profiles monitored as a measure of surface roughness. This work has simply served to introduce a concept, and there is a much wider scope for further development of the computer programs used. The versatility of the method of characteristics and its compatability with computer coding would allow complex systems to be eroded, where several discrete regions could possess differential sputtering properties in relation to the surrounding bulk. Ultimately, this method could provide easily accessible, qualitative information on the nature of surface morphology under particular sputtering conditions (i.e. ion incidence angle, ion flux), and thus determine optimum conditions to suppress surface roughness during ion erosion.

REFERENCES

Almen, O., Bruce, G., Electromagnetic Separation of Radioactive Isotopes, Vienna, 1960, p.227,(Springer-Verlag, Wien).

Almen, O., Bruce, G., Trans. 8th National Symposium, Washington 1, 1961, p.245, (Pergamon Press Inc, New York).

Almen, O., Bruce, G., Nucl. Instr. Meth. 11, 1961, p.257.

Andersen, H.H., Sigmund, P., K. Dan. Vidensk. Selsk. Mat. Fys. Medd., 34, 1966, no.15.

Andersen, H.H, Bay, H.L., Rad. Eff., 13, 1972, p.67.

Andersen, H.H., Bay, H.L., Rad. Eff., 19, 1973, p.139.

Andersen, H.H., Physics on Ionized Gases, Institute of Physics, Univ. Zagreb, 1974, p.361.

Andersen, H.H., Bay, H.L., J. Appl. Phys., 45, 1974, p.953.

Andersen, H.H., Bay, H.L., J. Appl. Phys., 46, 1975, p.2416.

Andersen, H.H., Appl. Phys., 18, 1979, p.131-140.

Arakting, Y.E., Bhacca, N.S., Proctor, W.G., Robinson, J.W., Spectroscop. Letts., 4, 1971, p.365.

Auciello, O., Rad. Eff., 60, 1982, p.1-26.

Bach, H., J. Non-Cryst. Solids, 3, 1970, p.1.

Bader, M., Witteborn, F.C., Snouse, T.W., N.A.S.A. Report no TR-R-105, Washington, 1961.

Baker, B.G., Sexton, B.A., Surf. Sci., 52, 1975, p.353.

Balluffi, R.W., Blakely, J.M., Thin Solid Films, 25, 1975, p.363.

Barber, M., Swift, P., Evans, S.E., Thomas, J., Nature 227, 1970, p.1131.

Bay, L., Bohdansky, J., Hofer, W.O., Roth, J., Appl. Phys., 21, 1980, p.327-333.

Bayly, A.R., J. Mat. Sci., 7, 1972, p.404-412.

Barber, D.J., Frank, F.C., Moss, M., Steeds, J.W., Tsong, I.S.T., J. Mat. Sci., 8, 1973, p.1030.

Belson, J., Wilson, I.H., Phys. Letts., vol 90A, no.3, p.141,1982.

Belson, J., Wilson, I.H., Rad. Eff., 5, 1980, p.27-34.

Belson, J., Wilson, I.H., Nucl. Instr. Meth., 182/183, 1981, p.275-281.

Benninghoven, A., Z. Physik, 230, 1971, p.403.

Benninghoven, A., Thin Solid Films, 39, 1976, p.3-23.

Bernheim, M., Slodzian, G., J. Physique Lett., 381, p.325.

Betz, G., Surf. Sci., 92, 1980, p.283.

Betz, G., Marton, J., Braum, P., Nucl. Instr. Meth. 168, 1980, p.541-545.

Biersack, J.P., Ion Surface Interaction, Sputtering and Related Phenomena, eds. Behrisch, R., Heiland, W., Poschenreider, W., Staib, P., Verbeck, H., Gordon and Breach, London, 1973.

Blattner, R.J., Nadel, S., Evans Jnr, Braundmeier, A.J. Jnr, Magee, C.W., Surf. Int. Anal., 1, 1979, no.1.

Bohdansky, J., J. Nucl. Mat., 93/94, 1980, p.44.

Borgesen, P., Behrisch, R., Scherzer, B.M.U., Appl. Phys. A., 27, 1982, p.183-195.

Brinkman, J.A., H. Appl. Phys., 25, 1954, p.961.

Brown, I.K., Hall, D.D., Walls, J.M., Vacuum, 31, 1981, p.625-629, nos.1-12.

Bykov, M.V., Proc. 4th European Regional Conference on Electron Microscopy, vol.1, p.369, (D.S. Boocciarelli ed), Tipografia Poliglotta Vaticana, Rome, 1968.

Carberry, J.J., Kuczinski, G.C., Chem. Technology, 1973, p.237.

Catana, C., Colligon, J.S., Carter, G., J. Mat. Sci., 7, 1972, p.467.

Carlston, C.E., Magnuson, G.D., Comeaux, A., Mahaderan, P., Phys. Rev. 138, 1965, p.759.

Carriere, B., Lang, B., Surf. Sci., 64, 1977, p.209.

Carter, G., Colligon, J.S., Ion Bombardment of Solids, Heinemann Educational Books Ltd (pubs.), London, 1968.

Carter, G., Colligon, J.S., Nobes, M.J., J. Mat. Sci., 6, 1971, p.115.

Carter, G., Colligon, J.S., Nobes, M.J., J. Mat. Sci., 8, 1973, p.1473.

Carter, G., Colligon, J.S., Nobes, M.J., Rad. Eff., 31, 1977, p.65.

Carter, G.,Nobes, M.J., Paton, F., Williams, J.S., Rad. Eff., 33, 1977, p.65-73.

Carter, G., Webb, R., Rad. Eff. Letts., 43, 1979, p.19-24.

Carter, G., Rad. Eff. Letts., 43, 1979, p.193.

Carter, G., Armour, D.G., Ingram, D.C., Webb, R., Newcombe, R., Rad. Eff. Letts., 43, 1979, p.233-236.

Carter, G., Nobes, M.J., Lewis, G.W., Whitton, J.L., Proc. Symposium on Sputtering, Wien, eds P. Varga, G. Betz and F. Viehbock, 1980, p.604.

Carter, G., Armour, D.G., Donnelly, S.E., Ingram, D.C., Webb, R.P., Rad. Eff., 53, 1980, p.604.

Carter, G., Collins, R., Thompson, D.A., Rad. Eff., 55, 1981, p.99.

Carter, G., Cruz, S.A., Rad. Eff. Letts., 58, 1981, p.125-132.

Carter, G., Nobes, M.J., Webb, R.P., J. Mat. Sci., 16, 1981, p.2091-2102.

Carter, G., Gras-Marti, A., Nobes, M.J., Rad. Eff., 62, 1982, p.119-152.

Carter, G., Nobes, M.J., Lewis, G.W., Nucl. Instr. Meth., 194, 1982, p.509-514.

Carter, G., Nobes, M.J., Lewis, G.W., Brown, C.R., Surf. Int. Anal. 7, 1985, p.35-40, no.1.

Carter, G., Nobes, M.J., Abril, I., Garcia-Molina, R., Surf. Int. Anal. 7, 1985, p.41-48, no.1.

Castaing, R., Slodzian, G., Microanalyse par Emission Ionique Secondaire, Proc. Eur. Reg. Conf. on Electron Microscopy, Delft vol.1, 1960, p.169-172.

Catana, C., Colligon, J.S., Carter, G., J. Mat. Sci. 7, 1972, p.467.

Chang, C.C., J. Vac. Tech. 18, 1981, no.2.

Cheney, K.B., Rogers, E.E., Pitkin, E.T., ARL Report, 1963, p.63-125.

Christie, A.B., Sutherland, I., Walls, J.M., Vacuum 31, 1981, p.513-517, nos.10-12.

Chu, W.K., Howard, J.K., Lever, R.F., J. Appl. Phys. 47, 1976, p.4500.

Chuang, T.J., Wandelt, K., IBM J. Res. Develop. 22, 1978, no.3,

Chuang, T.J., Wandelt, K., Surf. Sci. 81, 1979, p.355-369.

Czanderna, A.W. (ed.), Methods of Surface Analysis, Elsevier, Amsterdam, 1975, p.139.

Davarya, F., Roush, M.L., Fine, J., Andreadis, T.D., Goktepe, O.F., J. Vac. Sci. Tech. A1(2), 1983.

de Broglie, M., Compt. Rend. 172, 1921, p.274.

Ducommun, J.P., Cantagrel, M., Marchal, M., J. Mat. Sci. 9, 1974, p.72.

Ducommun, J.P., Cantagrel, M., Moulin, M., J. Mat. Sci. 10, 1975, p.52-62.

Eckstein, W., Scherger, B.M.U., Verbeek, H., Ion Surface Interaction, Sputtering and Related Phenomena, eds Behrisch, R., Heiland, W., Poschenreider, W., Staib, P., Verbeek, H., London, 1973.

Elich, J.J.Ph., Roosendaal, H.E., Onderdelinden, D., Rad. Eff. 10, 1971, p.175.

Elich, J.J.Ph., Roosendaal, H.E., Onderdelinden, D., Rad. Eff. 14, 1972, p.93-100.

Elich, J.J.Ph., Thesis, University of Amsterdam, 1972.

Eltekov, V.A., Samoilov, V.N., Yurasova, V.E., Poverkhmost (Surface) no. 3, 1982, p.43.

Erents, S.K., McCracken, G.M., Ion Surface Interaction, Sputtering and Related Phenomena, eds Behrisch, R., Heiland, W., Poschenreider, W., Staib, P., Verbeek, H., Gordon and Breach (pubs.), London, 1973, p.239.

Erlewein, J., Hofmann, S., Thin Solid Films 69, 1980, L39-L42.

Etzkorn, H.W., Littmark, U., Kirschner, J., Ibid.

Farrow, R.F.C., Cullis, A.G., Grant, A.J., Pattison, J.E., J. Crystal Growth 45, 1978.

Fetz, H., Z. Phyzik 119, 1942, p.590.

Fine, J., Navinsek, B., Davarya, F., Andreadis, T.D., J. Vac. Sci. Tech. 20, 1982, p.449.

Finnie, I., Kabil, Y.H., Wear 8, 1965, p.60.

Firsov, O.B., Sov. Phys. Doklady 14, 1970, p.1092.

Fischmeister, H., Olejford, I., Montash. Chem. 102, 1971, p.1486.

Formann, E., Viehbock, F.P., Wotke, H., Phys. Lett. 23, 1966, p.558.

Frank, F.C., Growth and Perfection of Crystals, Wiley, New York, 1958, p.411.

Frankenthal, R.P., Siconolfi, D.J., Surf. Sci. 111, 1981, p.317-324, no.2.

Fluit, J.M., Rol, P.K., Kistemaker, J., J. Appl. Phys. 34, 1963, p.690-691.

Gibson, J.B., Goland, A.N., Milgram, M., Vineyard, G.H., Phys. Rev. 120, 1969, p.1229-1253.

Gjostein, N.A., Diffusion, American Society for Metals, Metals Park, Ohio, 1973, p.241.

Gleiter, H., Chalmers, B., Prog. Mat. Sci. 16, 1972, p.77.

Gloersen, D.G., Solid State Tech. 4, 1976, p.68.

Goldstein, E., Verh. Dtsch. Phys. Ges. 4, 228, 237, 1902.

Grove, W.R., Phil. Trans. Roy. Soc. 142, 1852, p.87.

Grove, W.R., Phil. Mag. 5, 1853, p.205.

Grunquist, G., Ofvers. Svenska Vet. Akad. Forh. 54, 1897, p.575; 55, 1898, p.709.

Guntherschulze, A., Tollmein, W., Z. Phyzik 119, 1942, p.685.

Gupta, D., Ho, P.S., Thin Solid Films 72, 1980, p.399-418.

Gust, W., Hintz, M.B., Lodding, A., Odelius, H., Phys. Stat. Sol. (a), 64, 1981, p.187.

Hall, P.M., Morabito, J.M., Surf. Sci. 54, 1976, p.79.

Hall, P.M., Morabito, J.M., Poate, J.M., Thin Solid Films 33, 1976, p.107.

Harris, L.A., Surf. Sci. 15, 1969, p.77.

Harrison, D.A. jnr, Moore, W.L. jnr, Holcombe, H.T., Rad. Eff. 17, 1973, p.167.

Hermanne, N., Rad. Eff. 19, 1973, p.161-169.

Hittorf, W., Ann. Phys. (leipzig) 20, 1883, p.705; 21, 1884, p.90.

Ho, P.S., Lewis, J.E., Wildman, H.S., Howard, J.K., Surf. Sci. 57, 1976, p.393.

Ho, P.S., Lewis, J.E., Howard, J.K., J. Vac. Sci. Tech. 14, 1977, p.332.

Ho, P.S., Lewis, J.E., Chu, W.K., Surf. Sci. 85, 1979, p.19.

Hofer, W.O., Liebl, H., Appl. Phys. 8, 1975, p.359.

Hofer, W.O., Liebl, H., Sputtering in an ion microprobe, Ion Beam Surface Layer Analysis, Plenum Press, New York and London, 1976, p.659-664.

Hofer, W.O., Bay, H.L., Martin, P.J., J. Nucl. Mat. 76/77, 1978, p.156.

Hofer, W.O., Littmark, U., Phys. Letts. A 71, 1979, p.457.

Hofmann, S., Appl. Phys. 9, 1976, p.59.

Hofmann, S., Erelwein, Thin Solid Films 43, 1977, p.275-283.

Hofmann, S., Appl. Phys. 13, 1977, p.205.

Hofmann, S., Zalar, A., Thin Solid Films 56, 1979, p.337-342.

Hofmann, S., Zalar, A., Thin Solid Films 60, 1979, p.201.

Hofmann, S., Surf. Int. Analysis 2, 1980, no.4.

Hofmann, S., Analysis 9, 1981, p.181.

Hoffmann, D.W., Surf. Sci. 50, 1975, p.29.

Hoffmann, D.W., Tsong, I.S.T., Power, G.L., J. Vac. Sci. Tech. 17, 1980, p.613, no.2.

Holloway, P., J. Electron Spec. 7, 1975, p.215.

Holloway, P.H., Bhattacharya, R.S., Surf. Int. Anal. 3, 1981, no.3.

Holmes, D.K., Robinson, M.T., Solid State Division Ann. Prog. Report, Dec. 31st, 1975; U.S. Energy Research and Development Ann. Report, ORNL-5135, 1976, p.16-18.

Honig, R.E., Magee, C.W., Proc. 26th Annual Conf. on Mass Spec., St. Louis, Missouri, U.S.A., 1978, p.207.

Hudson, W.R., J. Vac. Sci. Tech. 14, 1977, p.286, no.1.

Hunt, C.P., Seah, M.P., Surf. Int. Anal. 5, 1983, p.199, no.5.

Hurcules, S.H., Hercules, D.M., Surface Characterisation by Electron Spectroscopy for Chemical Analysis,

Ishitani, T., Kato, M., Shimizu, R., J. Mat. Sci. 9, 1974, p.505.

Joshi, A., Stein, D.F., Metall. Trans. 1, 1970, p.2543.

Joshi, A., Rev. Coatings Corrosion 3, 1980, p.51-57, no.2.

Kaminsky, M., Das, S.K., J. Nucl. Mat. 53, 1974, p.162.

Kaminsky, M., Atomic and Ionic Impact Phenomena on Metal Surfaces, Academic Press, New York, 1975.

Katzschner, W., Steckenhorn, A., Loffler, R., Grote, N., Appl. Phys. Letts. 44, 1984, p.352, no.3.

Kaufman, H.R., Robinson, R.S., J. Vac. Sci. Tech. 16, 1979, no.2.

Keenlyside, M., Stott, F.H., Wood, G.C., Surf. Interface Analysis 5, 1983, p.64, no.2.

Kelly, R., Surf. Sci. 90, 1979, p.280-318.

Kelly, R., Auciello, O.,Surf. Sci. 100, 1980, p.135-153, no.1.

Keywell, F., Phys. Rev. 97, 1955, p.1611.

Kim, K.S., Baitinger, W.E., Amy, J.W., Winograd, N., Proc. Int. Conf. Electron Spectroscopy, Namur, Belgium, 1974 (Elsevier, Amsterdam).

Knotek, M.L., Feibelman, P.J., Phys. Rev. Letts. 40, 1978, p.964.

Kowalski, Z.W., J. Mat. Sci. 17, 1982, p.1627-1631.

Laegreid, N., Wehner, G.K., J. Appl. Phys. 32, 1961, p.365.

Lagally, M.G., Wang, G.C., Lu, T.M., J. Chem. Phys. 69, 1972, p.479.

Laty, P., Seethanen, D., Degreve, F., Surf. Sci. 85, 1979, p.353-364.

Lehmann, C., Sigmund, P., Phys. Stat. Sol. 16, 1966, p.507-511.

Lau, S., Tsauer, B.Y., von Allmen, M., Mayer, J.W., Stritzker, B., White, C.W., Appleton, B., Nucl. Instr. Meth. 182/183, 1981, p.97-105.

Lea, C., Seah, M.P., Surf. Interface Analysis 75, 1981, p.67-86.

Lea, C., Seah, M.P., Thin Solid Films 75, 1981, p.67-86.

Lewis, G.W., Carter, G., Nobes, M.J., Cruz, S.A., Rad. Eff. Letts 58, 1981, p.119-124.

Lewis, G.W., Kiriakides, G., Carter, G., Nobes, M.J., Surf. and Interface Analysis 4, 1982, p.141, no.4.

Lichtman, D., Mat. Sci. and Engineering 53, 1982, p.73-79.

Liebl, H., J. Vac. Sci. Tech. 12, 1975, p.385.

Lighthill, M.J., Whitham, G.B., Proc. Roy. Soc, 229a, 1955, p.281.

Lighthill, M.J., Whitham, G.B., Idem, Ibid 229a, 1955, p.317.

Lindhard, J., Matt. Fys. Medd. 34, 1965, p.14.

Littmark, U., Report IPP 9, 1976, p.21.

Littmark, U., Hofer, W.O., J. Mat. Sci. 13, 1978, p.2577-2586.

Lukaszewicz, M., Kowalski, Z.W., J. Mat. Sci. 16, 1981, p.302-306.

Lundquist, T.R., Byrgner, R.P., Swann, P.R., Tsong, I.S.T., Appl. of Surf. Sci. 7, 1981, nos.1/2.

Madey, T.E., Yates, J.T. jnr, J. Vac. Sci. Tech. 8, 1971, p.525.

Magee, C.W., Botnick, E.M., J. Vac. Sci. Tech. 19, 1981, no.1.

Maisel, L.I., Glang, R. (eds), Handbook of Thin Film Technology, McGraw-Hill, New York, 1970.

Makh, S.S., Smith, R.S., Walls, J.M., Surf. Int. Anal. 2, 1980, p.115, no.3.

Makh, S.S., PhD. Thesis, 1981.

Makh, S.S., Smith, R., Walls, J.M., J. Mat. Sci. 17, 1982, p.1689-1699.

Malherbe, J.B., Sanz, J.M., Hofmann, S., Surf. Interface Analysis 3, 1981, p.235, no.6.

Mathieu, H.J., Mclure, D.E., Landolt, D., Thin Solid Films 38, 1976, p.281.

Mathieu, H.J., Landolt, D., Proc. Spectrometrie Auger, Les Arcs (France), Vide, Num. Spec. 273, Mars 1979.

Mathieu, H.J., Landolt, D., Surf. Interface Analysis 5, 1983, p.77, no.2.

Matsunami, N., Yamamura, Y., Itikawa, Y., Itoh, N., Kazumata, Y., Miyagawa, S., Morita, K., Shimizu, R., Rad. Eff. Letts. 50, 1980, p.39.

Mayer, J.W., Erikson, L., Davies, J.A., Ion Implantation in Semiconductors, Academic Press, New York and London, 1970, p.154.

McCutchen, D.M., J. Appl. Phys. 20, 1949, p.414.

McCutchen, D.M., Pahl, W., Met. Prog. 56, 1949, p.674.

McHugh, J.A., Rad. Eff. 21, 1974, p.209.

Meckel, B.B., Nenadovic, T., Perovic, B., Vlahov, A., J. Mat. Sci. 1, 1975, p.1188-1193.

Menzel, D., Desorption Methods, Topics in Applied Physics, ed. R. Gomer, Vol.4 (Springer-Verlag, Berlin), 1975, p.101.

Meyer, F., Vrakking, J.J., Surf. Sci. 45, 1974, p.409-418.

Millard, M.M., Anal. Chem. 44, 1972, p.828.

Miller, A.C., Czanderna, A.W., J. Vac. Sci. Tech. 12, 1975, p.1086, no.5.

Molchanov, V.A., Tel'kovskii, V.G., Chickerov, V.M., Sov. Phys. Doklady 6, 3, 1961, p.222.

Molchanov, V.A., Tel'kovskii, V.G., English Translation in Bull. Acad. Sci. USSR Phys. Ser. 26, 1963, p.1381.

Morehead, F.F., Crowder, B.L., Rad. Eff. 6, 1970, p.25.

Morgan, A.E., Grefte, H.A.M., Tolle, H.J., Warmholtz, N., Werner, H.W., Proc. 4th Int. Conf. Solid Surfaces, eds D.A. Degras and M. Costa (cont ...)

(soc. Francaise du Vide, Paris), 1980, p.1238.

Mullins, W.W., 'Metal Surfaces', eds N.A. Gjostein and W.D. Robertson (American Soc. for Metals), 1963, p.17.

Navez, M., Sella, C., 5th Int. Cong. for Electron Microscopy (Academic Press Inc, New York), 1962, Paper C5.

Navez, M., Sella, C., Chaperot, D., Le Bombardement Ionique, C.N.R.S. (Bellevue, Paris), 1962, p.233.

Navinsek, B., Prog. Surf. Sci. 1, 1976, p.49.

Nelson, R.S., Phil. Mag. 11, 1965, p.291.

Nelson, R.S., Mazey, D.J., Rad. Eff. 18, 1973, p.127.

Nelson, R.S., Mazey, D.J., Rad. Eff. 19, 1973, p.199.

Nobes, M.J., Colligon, J.S., Carter, G., J. Mat. Sci. 4, 1969, p.730-733.

Nobes, M.J., Webb, R.P., Carter, G., Whitton, J.L., Rad. Eff. Letts. 50, 1980, p.133.

Nobes, M.J., Carter, G., Lewis, G.W., Whitton, J.L., Vacuum 33, 1983, p.381-389, no.7.

Nordling, C., Sokolowski, E., Siegbahn, K., Ark. Fys. 13, 1958, p.483.

Oechsner, H., Thesis, Wurzburg, 1963.

Oechsner, H., Z. Phyzik 261, 1973, p.37.

Oechsner, H., Appl. Phys. 8, 1975, p.185-198.

Okajima, Y., Jap. J. Appl. Phys. 20, 1981, p.2313-2317, no.12.

Onderlinden, D., Can. J. Phys. 46, 1968, p.739.

Onderlinden, D., Thesis, Leiden, 1968.

Orth, H., Zur Anisotropie der Hochfrequenz-Ionenatzung an nichtebenen Polymeroberflachen BEDO5, 1972, p.597-608.

Remy, Munster, 1975.

Padden, T.R., Cain, F.M. jnr, Metal Progress ASM 66, 1964, p.108.

Paine, B.M., Nicolet, M.A., Newcombe, R.G., Thompson, D.A., Nucl. Instr. Meth. 182/183, 1981, p.115-119.

Palmberg, P.W., Appl. Phys. Letts. 13, 1968, p.183.

Pandelisev, K.A., Wang, E.Y., J. Appl. Phys. 53, 1982, no.6.

Panitz, J.K.G., Sharp, D.J., Healey, J.T., J. Vac. Sci. Tech. 18, 1981, p.405, no.2.

Pantano, C.G., Dove, D.B., Onoda, G.Y. jnr, J. Vac. Sci. Tech. 13, 1976, p.414.

Pantano, C.G., Madey, T.E., Applications of Surf. Sci. 7, 1981, p.115-141.

Parson, J.R., Phil. Mag. 12, 1965, p.1159.

Perdereau, M., Compt. Rend. (Paris) C274, 1972, p.448.

Pittway, L.G., British J. Appl. Phys. 15, 1964, p.967.

Plucker, J., Ann. Phys. (Leipzig) 103, 88, 151, 1858; 104, 113, 1958.

Pohl, M., Burchard, W.G., Scanning 3, 1980, p.251-261.

Prival, H.G., Surf. Sci. 76, 1978, p.443-463.

Puluj, J., Sitzungsber d. Weiner Akad. Wiss 81, 1880, p.864.

Rangelow, I.W., J. Vac. Sci. Tech. A 1(2), 1983.

Redhead, P.A., Hobson, J.P., Kornelsen, E.V., The Physical Basis of Ultra High Vacuum, Chapman and Hall, London, 1968.

Rehn, L.E., Wiederisch, H., Thin Solid Films 73, 1980, p.139-143.

Reed, D.A., Ehrlich, G., Surf. Sci. 102, 1981, p.588-609, nos.2/3.

Riggs, W.M., Parker, M.J., Methods of Surface Analysis, ed. Czanderna, A.W., Vol.1, 1975, (Elsevier, Amsterdam).

Robinson, H., Rawlinson, W.F., Phil. Mag. 28, 1914, p.277.

Robinson, M.T., Sputtering by Particle Bombardment, ed R. Behrisch (Springer-Verlag), 1981.

Rol, P.K., Fluit, J.M., Viehbock, F.P., de Jong, M., Proc. 4th Int. Conf. Phen. Ion. Gases, Uppsala, ed N.R. Nilsson (North Holland, Amsterdam), 1959, p.257.

Rol, P.K., Fluit, J.M., Kistemaker, J., Electromagnetic Separation of Radioactive Isotopes, Vienna, (Springer-Verlag, Wien), 1960, p.207.

Roll, K., Losch, W., Achete, C., J. Appl. Phys. 50, 1979, p.4422, no.6.

Roll, K., Wolfgang, L., Achete, C., J. Appl. Phys. 50, 1979, no.6.

Roll, K., Appl. Surf. Sci. 5, 1980, p.388-397.

Roll, K., Reill, W., Thin Solid Films 89, 1982, p.221-224.

Roosendaal, H.E., Proc. Symp. on Sputtering, eds Varga, P., Betz, G., Viehbock, F.P., Vienna, 1980.

Rosenburg, D., Wehner, G.K., J. Appl. Phys. 33, 1962, p.1842.

Rossnagel, S.M., Robinson, R.S., Rad. Eff. Letts. 58, 1981, p.11.

Rossnagel, S.M., Robinson, R.S., J. Vac. Sci. Tech. 20, 1982, p.195, no.2.

Roosendaal, H.E., Sanders, J.B., Rad. Eff. 52, 1980, p.137-144.

Roosendaal, H.E., Sputtering by Particle Bombardment, ed R. Behrisch (Springer-Verlag), 1981.

Schwarz, S.A., Helms, C.R., J. Vac. Sci. Tech. 16, 1979, p.781.

Schwarz, S.A., Helms, C.R., Surf. Sci. 102, 1981, p.578-587.

Schwarz, S.A., Helms, C.R., J. Appl. Phys. 50

Schlaug, R.N., Thesis, University of California, Berkeley, 1965.

Seah, M.P., Sanz, J.M., Hofmann, S., Thin Solid Films 81, 1981, p.239.

Seah, M.P., J. Phys. F3, 1973, p.1538.

Seah, M.P., Lea, C., Thin Solid Films 81, 1981, p.257.

Seah, M.P., Hunt, C.P., Surf. Interface Analysis 5, 1983, p.33, no.1.

Shimizu, H., Ono, M., Nakayama, K., Surf. Sci. 36, 1973, p.817.

Shimizu, H., Kawakatsu, H., Surface Contamination Vol. 1, ed K.L. Mittal, Plenum Press, New York, 1979.

Shimizu, R., Appl. Phys. 18, 1979, p.425.

Shulga, V.I., Thesis, Moscow State University, 1971.

Shulga, V.I., Rad. Eff. 70, 1983, p.425.

Sigmund, P., Physical Review 184, 1969, no.2.

Sigmund, P., Rev. Roum. Phys. 17, 1972, p.823,969,1079.

Sigmund, P., J. Mat. Sci. 8, 1973, p.1545-1553.

Sigmund, P., Appl. Phys. Letts. 25, 1974, p.169.

Sigmund, P., J. Vac. Sci. Tech. 17, 1980, no.1.

Sigmund, P., Claussen, C., Proc. Symp. on Sputtering, Wien, eds P. Varga, G. Betz, and F. Viehbock, 1980, p.113.

Sigmund, P., Gras-Marti, A., Nucl. Instr. Meth. 168, 1980, p.389-394.

Sigmund, P., Sputtering by Particle Bombardment I, Topics in Applied Physics 47, ed. R. Behrisch, pub. Springer-Verlag, Berlin, 1981.

Sigmund, P., Gras-Marti, A., Nucl. Instr. Meth. 182/183, 1981, p.25-41.

Simondet, F., Dolizy, P., Decaesteker, M., Proc. 8th Int. Conf. on Solid Surfaces, eds Abeles, F., Croset, M., Cannes, Vol. 1, 1980.

Skinner, D.K., Swanson, J.G., Haynes, C.V., Surf. and Interface Analysis 5, 1983, p.38, no.1.

Silsbee, R.H., J. Appl. Phys. 28, 1957, p.1246-1250.

Smith, H.I., Etching for Pattern Definition, eds Hughes, H.G., Rand, M.J., (New Jersey Electrochemical Soc.), p.133.

Smith, R., Walls, J.M., Surf. Sci. 80, 1979, p.557-565.

Smith, R., Makh, S.S., Walls, J.M., Proc. 4th Int. Conf. on Solid Surfaces and ECOS 3, Cannes, France, Sept 1980, Vol. 2, eds Degras, D.A., Costa, M.

Smith, R., Valkering, T.P., Walls, J.M., Phil. Mag. A, Vol.44, no.4, 1981, p.879-893.

Smith, R., Makh, S.S., Walls, J.M., Phil. Mag. A, 47, no.4, 1983, p.453-481.

Snouse, T.W., Bader, M., Trans. 8th National Vacuum Symp., Washington, 1961, 1, 271, Pergamon Press Inc, New York (1982).

Southern, A.L., Willis, W.R., Robinson, M.T., J. Appl. Phys. 34, 1963, p.153.

Spivak, G.V., Prilezhaena, I.N., Gruz, E.A., Izv. Akad. Nauk USSR Serf. 15, 1951, p.409.

Stark, J., Die Elektrizitat in Gasen (Barth, Leipzig), 1902.

Stark, J., Wendt, G., Ann. Phys. (Leipzig) 38, 1912, p.921.

Stark, J., Phys. Z. 13, 1913, p.973.

Stein, D.F., Joshi, A., Ann. Rev. Mat. Sci. 11, 1981, p.485-504.

Stewart, A.D.G., Proc. 5th Int. Conf. on Electron Microscopy, Philadelphia (Academic Press, New York) D12, 1962.

Stewart, A.D.G., Thompson, M.W., J. Mat. Sci. 4, 1969, p.56-60.

Swarz, W.E., Holloway, D.M., Appl. Spectroscopy 31, 19 , p.210-213, no.3.

Sykes, D.E., Hall, D.D., Thurstans, R.E., Walls, J.M., Appl. of Surf. Sci. 5, 1980, p.103-106.

Sykes, D.E., Hall, D.D., Thurstans, R.E., Walls, J.M., Appl. of Surf. Sci. 5, 1980, p.103.

Szymonski, M., Bhattacharya, R.S., Overeijnder, H., de Vries, A.E., J. Phys. D 11, 1978, p.751.

Tarng, M.L., Fisher, D.G., J. Vac. Sci. Tech. 15, 1978, p.50.

Taylor, N.J., Johannessen, J.S., Spicer, W.E., Appl. Phys. Letts. 29, 1976, p.497, no.8.

Te-Chang, Chu, Campisano, S.U., Trovato, A., Rad. Eff. Lett. 76, 1983, p.131-134, no.4.

Thompson, M.W., Phil. Mag. 18, 1968, p.377.

Thompson, M.W., Defects and Radiation Damage in Metals, Cambridge University Press, London, 1968, p.113.

Thompson, M.W., Physics Reports 69, 1981, p.335-371, no.4.

Thompson, V., Hintermann, H.E., Chollet, L., Surf. Technology 8, 1979, p.421.

Tognetti, N.P., Webb, R.P., Christodoulides, C.E., Armour, D.G., Carter, G., Nucl. Instr. Meth. 182/183, 1981, p.107-114.

Tsong, I.S.T., Power, G.L., Hoffmann, D.W., Magee, C.W., Nucl. Instr. Meth. 168, 1980, p.399-404.

Tsunoyama, K., Suzuki, T., Ohashi, Y., Jap. J. Appl. Phys. 15, 1976, p.349, no.2.

Turley, D.M., Samuels, L.E., Metallography 14, 1981, p.275-294.

Vossen, J.L., J. Vac. Sci. Tech. 11, 1974, p.875.

Vossen, J.L., Kern, W. (eds), Thin Solid Film Processes, Academic, New York, 1978.

Vossen, J.L., J. Phys. E. 12, 1979, p.159.

Vossen, J.L., Kern, W., Physics Today, 1980, p.26.

Walls, J.M., Martin, A.D., Southworn, H.N., Surf. Sci. 50, 1975, p.360.

Walls, J.M., Hall, D.D., Dykes, D.E., Surf. Interface Analysis 1, 1979, p.204, no.6.

Walls, J.M., Thin Solid Films 80, 1981, p.213.

Webb, R., Carter, G., Collins, R., Rad. Eff. 39, 1978, p.129-139.

Wehner, G.K., Adv. Electronics Electron Phys. 7, 1955, p.239.

Wehner, G.K., J. Appl. Phys. 26, 1955, p.1056-1057.

Wehner, G.K., Phys. Rev. 102, 1956, p.690.

Wehner, G.K., Phys. Rev., 108, 1957, p.35.

Wehner, G.K., J. Appl. Phys. 29, 1958, p.217.

Wehner, G.K., Rosenburg, D., J. Appl. Phys. 31, 1960, p.177.

Wehner, G.K., Hajicek, D.J., J. Appl. Phys. 42, 1971, p.1145.

Wehner, G.K., Methods of Surface Analysis, ed A.W. Czanderna, Elsevier, New York, 1975, p.5.

Weissmann, M.W., Sigmund, P., Rad. Eff. 19, 1973, p.7.

Werner, H.W., Vacuum 24, 1974, p.439.

Werner, H.W., Warmoltz, ., Surface Sci. 57, 1976, p.706-714.

Werner, H.W., Surf. Interface Analysis 4, 1982, p.1.

Whitton, J.L., Tanovic, L., Williams, J.S., Appl. Surf. Sci. 1, 1978, p.408-413.

Whitton, J.L., Grant, W.A., Nucl. Instr. Meth. 182/183, 1981, p.287.

Wildman, H.S., Howard, J.K., Ho, P.S., J. Vac. Sci. Tech. 12, 1975, p.75.

Wilson, I.H., Kidd, M.W., J. Mat. Sci. 6, 1971, p.1362-1366.

Wilson, I.H., Rad. Eff. 18, 1973, p.95-103.

Williams, P., Evans, C.A. jnr, Surf. Sci. 78, 1978, p.324.

Williams, P., Surf. Sci. 90, 1979, p.588-634.

Williams, P., Appl. Phys. Lett. 36, 1980, p.758.

Williams, R.S., Nelson, R.J., Schlier, A.R., Appl. Phys. Letts. 36, 1980, p.827, no.10.

Windawi, H.M., Kayer, J.R., Cooper, C.B., Phys. Lett. A 59, 1976, p.62.

Winterbon, K.B., Ion Implantation Range and Energy Deposition Distrubutions, Vol.II (IF2/Plenum Press, New York), 1975.

Winterbon, K.B., Rad. Eff. 48, 1980, p.97-100.

Winters, H.F., J. Vac. Sci. Tech. 20, 1982, no.3.

Witcomb, M.J., Proc. Electron Microscopists Soc. South Africa 3, 1973, p.93.

Witcomb, M.J., J. Mat. Sci. 9, 1974, p.551-563.

Witcomb, M.J., Rad. Eff. 32, 1977, p.205-211.

Wittmaack, K., Schulz, F., Thin Solid Films 62, 1978, p.259.

Wittmaack, K., Surf. Sci. 89, 1979, p.668-700.

Wittmaack, K., Rad. Eff. 63, 1982, p.205-218.

Wittmaack, K., J. Appl. Phys., 53, 1982, no.7.

Wright, A.W., Am. J. Sci. 13, 1877, p.49; 14, 1877, p.169.

Yurasova, V.E., Kristallografia 2, 1957, p.770.

Yamamura, Y., Nucl. Instr. Meth. 194, 1982, p.515-522.

Yamamura, Y., Matsunami, N., Itoh, N., Rad. Eff. 71, 1983, p.65.

Yu, M.L., Phys. Rev. Letts. 40, 1978, p.574.

Zalar, A., Hofmann, S., Surf. Interface Analysis 2, 1980, p.183.

APPENDED REFERENCES

Bibic N., Wilson I.H., Nenadovic T. - J. Appl. Phys. 53(7)1982

Cong-Xing R., Guo-Ming C., Xin Ding Fu., Jie Y., Hong-Li F., Shih-Chang T.- Rad. Effects 77(1983)177-193

Tagg M., Smith R., Walls J.M.- J. Mat. Sci. vol. 121 1986 p.123-130